Author:
Burt, David John

Title:
Improved Design of Settling Tanks using an Extended Drift Flux model

Improved Design of Settling Tanks using an Extended Drift Flux model

David John Burt

A dissertation submitted to the University of Bristol in accordance with the requirements of the degree of Doctor of Philosophy in the Faculty of Engineering, Department of Mechanical Engineering.

31st January 2010

Word Count 66,000

ABSTRACT

This dissertation investigates the modelling and design of settling final clarifiers for application in the waste water industry. The work begins by establishing the flow scales for clarifiers and introduces the mass flux methods used to size the tank. The problem of influent design is also discussed and alternative influent arrangements are presented.

A model is then developed for the settling of activated sludge within the clarifier based on an extended drift flux CFD method. This model defines the physical properties of activated sludge with constitutive relationships for sludge mixture density, apparent viscosity and settling rate. These properties are investigated and an alternative synthetic latex sludge is proposed for use in laboratory scale experiments. The synthetic latex sludge, real activated sludge and the computational model are all compared in a lock exchange experiment devised to investigate the dynamic behaviour of sludge. From the lock exchange results, a performance comparison is made of various sludge rheology models and two constitutive relationships are selected for future use.

The extended drift flux model is then validated against known data sets in laboratory scale and full scale settling systems. In one system an alternative drift flux model is used to describe the settling of discrete particles as many size classes or multiple drift fluxes. This is found to be a good approach for discrete particle settling where the particle size distribution can be defined. Further comparisons are then made with experimental data for three full scale site trials at the Rye Meads, Witney and Crofton sewage treatment works where the Witney and Crofton trials are new studies performed to support this modelling work. For the model validation trials, alternative influent geometries are also tested and shown to be effective. A new method for assessing the flocculating capacity of the influent stilling well using a G scalar history function to calculate the *Camp number* is developed and this demonstrates that significant orthokinetic flocculation is unlikely to occur in a clarifier.

Finally a connection between mass flux theory and the extended drift flux model is established where the calculated performance parameters for a clarifier may be compared with the mass flux limits. This technique allows the model calculations for sludge bed depth and effluent suspended solids, for all clarifier systems, to be compared with the mass flux limit defined in this work as the *reciprocal of the influent Hazen number.* This design method shows that the theoretical mass flux limit for a clarifier can be approached (but not usually exceeded), with good internal design practice. The design method is applied to influent modifications including the two new designs presented in this work for a counter current energy dissipating influent and a modified McKinney baffle influent. Both of these designs are now installed and in use at the Crofton and Budds farm sewage treatment works and at many other sites throughout the UK.

ACKNOWLEDGEMENTS

The author would like to thank:

My industrial sponsor, Dr Pete Pearce of Thames Water Ltd, my supervisor Dr Mark Gilbertson and my Professor Joe Quarini for introducing me to the subject of waste water settling.

My former colleagues at CFX (now ANSYS), particularly Dr Ian Jones, Dr Nigel Wilkes, Dr Alan Burns, Dr Simon Lo and Ian Hamill who all helped me get to grips with the complexities of multiphase flow.

The many other colleagues at (in no particular order), Thames Water, Severn Trent Water, Yorkshire Water, Wessex Water, Dwr Cymru, United Utilities, Southern Water, Montgomery Watson Harza, Arup, Aquafin, Purac, Pick Everard, Aker Solutions, Meica Process and the many other companies who have directly funded clarifier design projects.

My employers, MMI Engineering Ltd and Geosyntec who have encouraged a continued interest in this subject with particular thanks to my office colleagues Dr Jay Ganeshalingam, Dr Darrell Egarr and Dr Chris Robinson who have all worked with me on clarifier design and the continued development of the ClariSim software.

Finally thanks to my wife Diana and our three children, Harriet, Katie and James without whom none of this would have been possible and to whom this work is dedicated.

AUTHORS DECLARATION

I declare that the work in this dissertation was carried out in accordance with the requirements of the University's Regulations and Code of Practice for Research Degree Programmes and that it has not been submitted for any other academic award. Except where indicated by specific reference in the text, the work is the candidate's own work. Work done in collaboration with, or with the assistance of, others, is indicated as such. Any views expressed in the dissertation are those of the author.

SIGNED: ..... DATE: 24/6/10

David John Burt

31st January 2010

CONTENTS

LIST OF FIGURES

LIST OF TABLES

NOTATION

Symbols

a	Empirical Coefficient	[-]
A_{st}	Surface area of the Clarifier	[m^2]
A_p	Projected area of a particle or floc	[m^2]
b	Empirical Coefficient	[-]
c_{pa}	Fitted coefficient for plastic viscosity	[-]
c_{pl}	Fitted coefficient for plastic viscosity	[(m5/(kg·s^2)]
C_D	Drag coefficient for particle or floc	[-]
C_μ	Empirical constant of the turbulence model (= 0.09)	[-]
C_1	Turbulence model constant	[-]
C_2	Turbulence model constant	[-]
C_3	Constant in ω buoyancy term (0 or 1)	[-]
d	Influent pipe diameter	[m]
d_p	Particle diameter	[m]
D	Clarifier diameter	[m]
$D_{3,2}$	Sauter mean diameter (SMD)	[m]
D_m	Menter function in ω equation.	[-]
Fr'	Densimetric Froude number	[-]
Fr'_{in}	Densimetric Froude number at an influent slot	[-]
f_μ	Empirical constant of the turbulence model	[-]
g	Gravitational constant magnitude (9.81)	[m/s^2]
g or g_i	Gravitational constant vector	[m/s^2]
g'	Reduced gravity	[m/s^2]
G	G scalar (Camp, 1943)	[s^{-1}]
G_b	Buoyancy production term for turbulence	[N/m^2]
$G.T$	Camp Number	[-]
h	Height (of the McKinney Slot) or a length scale	[m]
h_s	Side wall depth	[m]

h_{850}	Depth of the sludge bed contour 850 *mg/l*, (Matko, 1998)	[m]
Ha	Hazen Number	[-]
j_{QF}	Applied solids flux	[kg/m^2.h.]
j_{QF_m}	Maximum solids flux	[kg/m^2.h.]
j_{QH}	Applied hydraulic flux	[kg/m^2.h.]
j_{QH_m}	Maximum hydraulic flux	[kg/m^2.h.]
j_L	Limiting solids flux	[kg/m^2.h.]
j_s	Mass flux	[kg/m^2.h.]
k	Turbulent kinetic energy	[m^2/s^2]
k_c	Consistency coefficient	[Pa.s^n]
K	Head loss coefficient	[-]
l	Length	[m]
m	Stress growth component	[s]
m_p	Mass of a particle	[kg]
m_h	Hydrodynamic added mass of spherical particle	[kg]
n	Consistency index or power index or coefficient	[-]
N	Brunt-Väisälä Frequency	[s^{-1}]
p	Pressure	[Pa]
p'	Fluctuating pressure	[Pa]
P	Mean static pressure	[Pa]
P_{in}	Power from influent	[W]
P'	Modified pressure	[Pa]
P_s	Shear production term for turbulence	[N/m^2]
q_A	Surface overflow rate	[m/h]
q_R	Surface underflow rate	[m/h]
q_{SV}	Volumetric loading rate	[l/m^2.h]
Q	Clarifier flow rate at the effluent weir	[m^3/h]
Q_{in}	Clarifier flow rate at the influent	[m^3/h]
Q_{SV}	Volumetric flow in mass flux criterion III	[l/h]
r_k	Volume fraction of phase k	[-]

r_h	Hindered settling coefficient	[m^3/ kg]
r_p	Colloid of free particle settling coefficient	[m^3/ kg]
R	Recycle ratio	[-]
Re	Reynolds number	[-]
Re_{in}	Influent Reynolds number	[-]
Re_p	Particle or floc Reynolds number	[-]
Re_T	Local turbulent Reynolds number	[-]
Ri'	Densimetric Richardson number	[-]
Sg_k	Specific gravity of phase k	[-]
t	Time	[s]
t_R	Particle or floc relaxation time	[s]
T_R	Particle or floc relaxation time constant	[s]
T	Hydraulic retention time	[s]
T_{10}	Time for 10 % dye trace recovered	[s]
T_{50}	Time for 50 % dye trace recovered	[s]
T_{90}	Time for 90 % dye trace recovered	[s]
SV_{30}	Volume of activated sludge at the end of 30 min SVI test	[ml/l]
u_i, u_j	Instantaneous velocity vector in index directions.	[m/s]
u_i', u_j'	Fluctuating velocity vector in index directions	[m/s]
U_i, U_j	Mean velocity vectors in index directions	[m/s]
$\mathbf{U}_m$	Mean mixture velocity vector	[m/s]
$\mathbf{U}_{sk}$	Mean slip velocity vector of phase k	[m/s]
V	Mean flow velocity	[m/s]
V_o	Terminal Settling velocity of a particle or floc	[m/s] [m/h]
V_{in}	Influent velocity	[m/s]
V_r	A radial or horizontal velocity	[m/s]
V_s	Settling velocity	[m/s]
$V_{s,\max}$	Maximum hindered settling velocity.	[m/s]
V_w	Wave speed in a gravity current	[m/s]
Vol	Volume	[m^3]

x, y, z	Cartesian co-ordinates	[m]
x, r, θ	Cylindrical co-ordinate system in CFX-4	[m]
$\mathbf{x}$	Unit vector in positive x co-ordinate direction	[m]
X	Concentration	[g/l]
X_k	Concentration of phase *k*	[g/l]
X_{ps}	Fitted coefficient for plastic viscosity	[kg/m^3)]
X_{ns}	Concentration of the non settling fraction	[g/l]
X_{23}	Transition from flocculent to hindered settling	[g/l]
X_{34}	Transition from hindered to compression settling	[g/l]
X_E	Effluent concentration or ESS	[g/l]
X_F	Influent or feed solids concentration	[g/l]
X_R	Return activated sludge (RAS) concentration	[g/l]
y^+	Non dimensionalised distance of the near wall node.	[-]
Y_k	Mass fraction of solid phase *k*	[kg/kg]

Greek Letters

β_1	Fitted coefficient for yield stress	[kg/m·s^2]
β_2	Fitted coefficient for yield stress	[m^3/kg]
β_3	Fitted constant for yield stress	[kg/m^3]
Γ_y	Diffusivity of the solid species	[kg/ms]
$\dot{\gamma}$	Shear strain rate magnitude	[1/s]
$\dot{\gamma}_{ij}$	Strain rate tensor	[-]
δ_{ij}	Kronecker delta	[-]
ε	Viscous dissipation rate	[m^2/s^3]
ς	Bulk viscosity	[m^2/s^3]
κ	Von Karmen Constant	[-]
μ	Fluid viscosity	[kg/ms]
μ_{eff}	Effective viscosity	[kg/ms]
μ_m	Mixture viscosity	[kg/ms]

μ_0	Plastic viscosity	[kg/ms]
μ_t	Turbulent viscosity or eddy viscosity	[kg/ms]
ν	Kinematic Viscosity	[m^2/s]
ρ_{in}	Density in the influent pipe	[kg/m^3]
ρ_k	Density of phase k	[kg/m^3]
ρ_m	Density of mixture	[kg/m^3]
ρ_p	Density of a particle	[kg/m^3]
ρ_w	Density of water	[kg/m^3]
σ_{ij}	Total stress	[N/m^2]
σ_k	Prandtl number for k	[-]
σ_p	Constant in buoyancy production term	[-]
σ_ω	Prandtl number for ω	[-]
σ_y	Schmidt Number	[-]
τ	Shear stress	[N/m^2]
τ_0	Yield stress	[N/m^2]
τ_{ij}	Viscous stress	[N/m^2]
ω	Turbulent frequency	[s^{-1}]

Subscripts

i, j	Index for tensor notation
k	Solid phase
m	Mixture
p	Particle or Floc
s	Settling

Superscripts

$\bar{}$	Mean or Average
$'$	Fluctuating or Modified

Abbreviations

1DFT	1D Flux Theory	
ADV	Acoustic Doppler Velocimetry	
ATV	German Association for Water, Wastewater and Waste	
AMP4	Asset Management Plan, 4th period - 2005 to 2010.	
AS	Activated Sludge	
ASM	Algebraic Slip Model	
ASP	Activated Sludge Plant	
BCC	Bristol Colloid Centre, at the University of Bristol	
BOD	Biochemical Oxygen Demand	
CFD	Computational Fluid Dynamics	
CFX	A commercial CFD software package from ANSYS	
CIWEM	Chartered Institute of Water Engineers and Managers	
CSTR	Continuous Stirred Tank Reactor	
DNS	Direct Numerical Simulation	
DSVI	Diluted Sludge Volume Index	
EDF	Extended Drift Flux	
EDI	Energy Dissipating Influent	
ESS	Effluent Suspended Solids	[mg/l]
FST	Final Settlement Tank	
HRT	Hydraulic retention time	[s]
IAWQ	International Association of Water Quality	
IDC	Interfacial Dynamics Corporation	
IWA	International Water Association (formerly IAWQ)	
LES	Large Eddy Simulation	
MDF	Multiple Drift Flux	
MFT	Mass Flux Theory	

MLSS	Mixed Liquor Suspended Solids	[mg/l]
MWH	Montgomery Watson Harza, engineering consultants.	
P	Phosphate or nitrate content	
PSD	Particle Size Distribution	
PST	Primary Settling Tank	
RANS	Reynolds Averaged Navier Stokes	
RAS	Return Activated Sludge	
SAS	Surplus Activated Sludge	
SLS	Synthetic Latex Sludge	
SMD	Sauter Mean Diameter	
SOR	Surface Overflow Rate	[m/h]
SS	Suspended Solids	[mg/l]
SST	Secondary Settling Tank	
SSVI	Stirred Specific Volume Index	[ml/g]
$SSVI_{3.5}$	The SSVI value for a sludge sample at 3.5 g/l	[ml/g]
STW	Sewage Treatment Works	
SVD	Settling Velocity Distribution	
SVI	Sludge Volume Index	[ml/g]
TWL	Top Water Level	
UNSW	University of New South Wales, Australia	
WRc	Water Research Centre based in UK	
WwTW	Wastewater Treatment Works	

CHAPTER 1: Introduction

Summary

This chapter presents the background to the project. The activated sludge process for treating waste water is described and the role of the final settlement tank, or final clarifier, within this process is explained. The flow paths and load distributions within circular clarifiers are discussed and methods for design are introduced. The design limitations and performance difficulties associated with clarifiers are considered and from these considerations, a number of research questions arise. The rest of the thesis is then directed to addressing these fundamental research questions.

1.1 Introduction

In this thesis, methods for modelling the flow and solids settlement in secondary settling tanks (SSTs), also known as final settlement tanks (FSTs) or final clarifiers, are explored and developed and comparisons are made to existing design methods based on the mass flux procedure. The methods are tested and validated at laboratory and industrial scale and the lessons learnt from these studies are applied to new industrial designs. A detailed modeling algorithm has been developed to work with the computational fluid dynamics (CFD) code CFX. This was initially based on the standard model published in the international water association (IWA) scientific and technical report No 6 (Ekama et al, 1997). Extensions have subsequently been included to allow for the significant variations in apparent viscosity throughout the mixing and settling regions of the clarifier through the inclusion of rheological functions used to represent the characteristic non-Newtonian behaviours of activated sludge in the settling bed. This model is referred to in this work as an extended drift

flux (EDF) model. Some of the other ideas that are implemented and explored in this thesis include,

1. The use of multiple drift fluxes (MDF) to represent sludge as a series of size class scalers.
2. The mapping of a stream functions back to the *G* scalar field in order to deduce the likely flocculating capacity of the clarifier stilling well.
3. The development of a lock exchange experiment to compare rheological models for activated sludge.
4. The development and testing of new clarifier influent designs based on a modified McKinney baffle plate and a counter current energy dissipating influent (EDI).

Validation data for the model is provided by comparing CFD simulations with laboratory scale experiments and full industrial scale measurements. Two laboratory experiments are considered: a model system settling tank (Krebs, 1998) and a lock exchange rig built as part of this work. Detailed site measurements are then provided for clarifiers in use at three sewage treatment works (STWs), Rye Meads (Richardson, 1998), Witney (Burt, 2005a) and Crofton (Burt, 2005b). New designs of influent are developed in the course of the work and these have subsequently been implemented at many STWs throughout the UK including the Budds Farm site near Portsmouth (Robinson, 2008).

Before developing a modelling and design strategy, the role of the clarifier is considered with reference to the entire activated sludge sewage treatment plant. The physical and biological processes present within the clarifier are briefly discussed

and a description of activated sludge is presented. These are necessary introductions for the understanding of the hydrodynamic models introduced later to assess the performance of new designs.

1.2 The Activated Sludge Process

The activated sludge process, as a method for treating sewage, was originally developed by G.J. Fowler, E. Ardern and W.T. Lockett of the Manchester Corporation between 1912 and 1914 (Ardern et al, 1914). Their experiments with the aeration of raw sewage led to the installation of the first full scale activated sludge plant at Worcester in 1916. The process involves the treating of sewage by aeration and agitation with an admixture, or culture, of older activated sludge. This induces the growth of organisms that break down the sewage by a series of physical and biochemical processes. The resulting product, the activated sludge, is readily separated from the treated effluent by settlement. The final effluent is water with some trace effluent suspended solids (ESS) which may be further treated by filtration of returned directly to a water course.

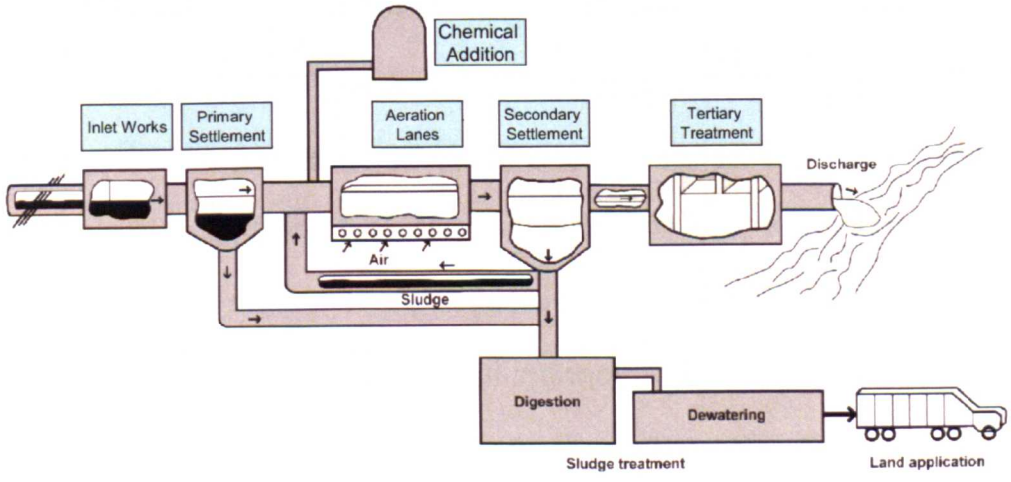

Figure 1.1: Schematic process flow diagram for a typical Activated Sludge Plant (ANSYS, 2007)

Activated sludge plants are responsible for the treatment of about 50% of all sewage treated by biological oxidation in the UK (CIWEM, 1997). These plants are able to produce effluents in compliance with the current legislative requirements for suspended solids (SS), biochemical oxygen demand (BOD) and nitrate content (P). However, changes in European legislation and a move away from generic or blanket standards to catchment-specific standards; that is effluent discharge regulations that are restricted to a particular community or river basin system, is putting additional pressure on the operators of sewage treatment plants to improve the quality of their effluents. As a consequence, there is much interest in the enhancement and improvement of the performance of the final stage of the activated sludge process; the final clarifier.

1.2.1 Inlet Works and Primary Settlement

Crude sewage from the domestic and industrial sewer system undergoes preliminary processing, such as screening and grit removal, in the inlet works before entering a primary settlement tank (PST). Heavy solids settle out in these primary tanks and are removed as primary sludge which is sent to the digester vessels for further treatment. The remaining mixed liquor effluent passes on to a series of aeration lanes where biological treatment occurs. Recycled activated sludge is added to the effluent at the start of the aeration process and adsorption and agglomeration processes occur during aeration which causes the suspended solids to become incorporated into discrete microbial colonies bound together into interconnected structures, or flocs. These flocs combine together to form activated sludge.

1.2.2 The Constituents of Activated Sludge

Definitions of activated sludge are "the flocculent microbial mass of bacteria, protozoa and other micro-organisms with a significant proportion of inert debris" (CIWEM,1997) , or "a complex mixture of inert suspended solids, various micro-organisms and extracellular material" (Örmeci and Vesilind, 2000). The common organisms present in the activated sludge bio-mass, as stated by CIWEM (1997) are,

- Bacteria
- Filamentous bacteria
- Protozoa
- Metazoan and other higher life forms
- Moulds and fungi
- Algae

The most dominant organisms are bacteria which may either be fast growing heterotrophs, with doubling times measured in tens of minutes, or slow growing autotrophs with doubling times of days. The bacteria may adhere to each other in a floc structure, exist as biofilm on solids, or be dispersed in the liquid phase. Dispersed bacteria that remain in the liquid phase will increase turbidity and result in poor effluent quality. Removal of these dispersed bacteria can be achieved by promoting additional flocculation in the aeration lane to the point where the flocs are sufficiently large that they are readily settled. An important point to note is that floc structures are age dependent and most prevalent when the bacterial nutrients are on the point of exhaustion.

1.2.3 Final Settlement

Sufficient residence time in the aeration lanes, typically a period between 3 and 15 days, is required to allow for micro organism development, growth and decay. After this the mixed liquor effluent, containing the floc suspensions, is distributed into the

clarifiers. It is at the final stage, in the clarifier that the activated sludge settles out. The performance of the clarifier is significantly influenced by the hydrodynamic behaviours within the tank. These are the large scale behaviours largely driven by an influent density current (Lyn et al, 1992) and by the smaller scale turbulent eddies that are thought to influence the growth and decay of flocs, (Argaman and Kaufman, 1970).

1.2.4 The role of Flocculation in the Aeration Lane and the Clarifier

The primary particles in activated sludge are the smallest particles which can aggregate. These may be considered to be the smallest biological units, i.e. single bacteria. As the sludge ages and the concentration of primary particles increases, the biomass shows a flocculating tendency. Two mechanisms are thought to be at work; polymer bridging by floc forming bacteria, and the generation of a filament network, by filamentous bacteria. Filaments and floc formers combine together in large (100 to 2000 μm) irregularly shaped strong flocs. In an ideal sludge, the filaments grow largely within the floc length scale providing strength and structure. This process of agglomeration through flocculation within the aeration lane is potentially countered in the clarifier (or in transit to the clarifier) by breakup due to regions of high shear although knowledge of this process is uncertain (Parker et al, 1972).

Studies of particle size distributions for activated sludge show a bimodal relationship with large concentrations in the size range 0.5 to 5 μm and in the range 25-2000 μm (Ekama et al, 1997). Whereas particles in the larger size ranges are readily settled, the smallest particles sizes constitute non settleables and it is these dispersed bacteria which are thought to be significant contributors to the effluent suspended solids (ESS). It is suggested by Wahlberg and others (Wahlberg et al, 1994) that a clarifier

can only function well when the tank hydrodynamics are designed to promote flocculation.

It is known that flocs are constantly forming, breaking and reforming, at many stages from the aeration lanes through to the clarifier influent. In some systems flocculation is promoted in a preliminary stage prior to final settling. Other systems incorporate flocculation zones within the clarifier through the inclusion of an effluent diffusion well and a second flocculator centre well (Parker, 1996). There is continued interest in the development of new clarifier designs which incorporate flocculation zones and in the possibility of retrofitting existing systems with effluent diffusers and flocculating centre wells (IWA, 2008).

1.3 Settling of Activated Sludge

A significant requirement for performing a clarifier design assessment is to understand the sludge properties that influence settling and then provide a method of characterizing them. In the case of activated sludge, it is insufficient to consider only the mechanical or fluid properties as these are directly influenced by the life cycles of the biological organisms that live within the sludge. There are a number of deterministic models which consider the bio-chemical processes of an activated sludge (IWA, 2000); but, for the purposes of this work, the bio-chemical processes are incorporated into averaged physical fluid properties. These properties are in themselves a subject of study and there have been many attempts to construct stable sludge simulants which replicate these properties.

1.3.1 Settling Characteristics

Settlement of the activated sludge occurs entirely under the influence of gravity, however, in addition to hydraulic effects, the rate of settlement can vary considerably

according to the shape and structure of the flocs. Four types of settlement are commonly identified (IWA, 2008).

1) *Free or discrete particle settling*: In the upper reaches of the tank the flocs are thought to be disperse. The flocs do not significantly interact with one another and settle at a free or terminal settling velocity. It is sufficient to construct theoretical models based on a single particle settling in an infinite medium for this part of the tank although these models have to allow for the irregular sizes, shape and porous nature of the floc (Wu and Lee, 1998).
2) *Flocculant settling*: The discrete particles begin to coalesce and form agglomerates or flocs. The growing flocs increase in volume and mass and therefore settle at a faster rate. However, this is not a uniform process and floc size and settling rate can vary considerably leading to preferential settling of some solids. Flocculation is thought to occur when dense particles, falling faster than their neighbours, catch up and combine with smaller slower moving particles. This process is called differential sedimentation (Thomas, 1999).
3) *Hindered or zone settling*: As solids concentration increases, the rate of settlement decreases. The particles begin to interact with one another and there is an increase in the effective viscosity of the mixture. It is possible that some particles may periodically experience less drag than in free settling, due to slip streaming effects; however, the total drag increases as the particles bump into one another and their relative slip velocity with the surrounding liquid decreases. The higher concentration of solids means that the interstitial water is also forced upwards causing even greater drag on the settling particles. The particles also start to bind relative to each other in a loose

matrix and settle as a blanket with a distinct interface developing between the blanket and the supernatant above. This process is referred to as sludge line settling (CIWEM, 1997). Where a solid - liquid system exhibits sludge line settling it is relatively easy to track the progress of the settling interface and thus deduce an aggregate settling velocity.

4) *Transitional and Compression settling*: This is a region where the flocs no longer behave as if settling in a hindered way but the concentration is still not high enough for settlement to stop. Below the transition zone, further settling can only be achieved by displacement of the interstitial liquid by the hydrostatic pressure of the blanket above. In this compression zone the liquid continues to be forced upwards against the flow of solids. A point will be reached where the solids are at their maximum packing and can compress no further. If large growth of filamentous bacteria is present then this packing will be inhibited resulting in a poorly settled low-density sludge sometimes referred to as a bulking sludge (CIWEM, 1997).

Because of the importance of sludge settleability to the performance of an STW, a number of standard tests have been devised to assess this characteristic in activated sludge. In the sludge volume index (SVI) test (Mohlman, 1934), a sample of mixed liquor from the aeration lane at concentration 1500 *mg/l*, is allowed to settle in a 1*l* measuring cylinder. The position of the sludge blanket interface is recorded at specific time intervals. The SVI is then defined as the volume in *ml* occupied by 1*g* of activated sludge after quiescent settling for 30 minutes.

$$SVI = \frac{SV_{30}}{X} \tag{1.1}$$

Where SV_{30} is the specific volume of 1 litre of activated sludge at the end of thirty minutes in *ml/l* and X is the initial concentration of the mixed liquor suspended solids expressed in *g/l*.

Because of bridging or wall effects, thought to occur in the SVI experiment, a later modification by the water research council (White, 1975) was to augment the SVI test with a stirrer rotating at 1 *rev/min* around the peripheral wall of the settling column. This became the stirred specific volume index (SSVI) test and is the standard test for settleability applied in the UK and US.

1.3.2 Synthetic Sludge

The biological content of activated sludge makes it extremely difficult to perform controlled experiments and reproduce test results. The physical characteristics of the sludge are constantly changing with the life cycles of the organisms present. When a sample of sludge is taken from the aeration lanes into the laboratory its properties are inconsistent and after a day or two the characteristics may be appreciably different from a fresh sample. In addition, large amounts of vigorous shearing can have a detrimental effect on the mixed liquor producing something akin to a phase transition from settling sludge into floating, non-flocculating, inert debris (CIWEM, 1997).

Because of the difficulties associated with handling real activated sludge, a number of workers have tried to develop a chemical surrogate for activated sludge so that controlled experiments may be performed in the laboratory. One such surrogate (Örmeci and Vesilind, 2000) is used in this thesis and is compared with real activated sludge in a lock exchange experiment.

1.4 The Final Clarifier

Final settlement is used to separate the heavier solid phase flocs (the biomass) from the lighter liquid phase (effluent) using gravity. The process is carried out in the clarifier which is a large concrete basin. There are many different designs of clarifier throughout the world. Rectangular tanks are common in both the USA and main land Europe, deep hopper bottom tanks (either circular or square) were common in the UK and are still used at some big sites such as Mogden in London. However, the main design, commonly used in the UK, is a shallow circular tank around 20 *m* diameter with a side wall depth of 2.2 to 2.9 *m*. Recent designs put forward as part of the UK asset management plan in the period 2005-2010 (AMP4), have tended to larger diameters; sometimes exceeding 40 *m* (Ganeshalingam, 2006).

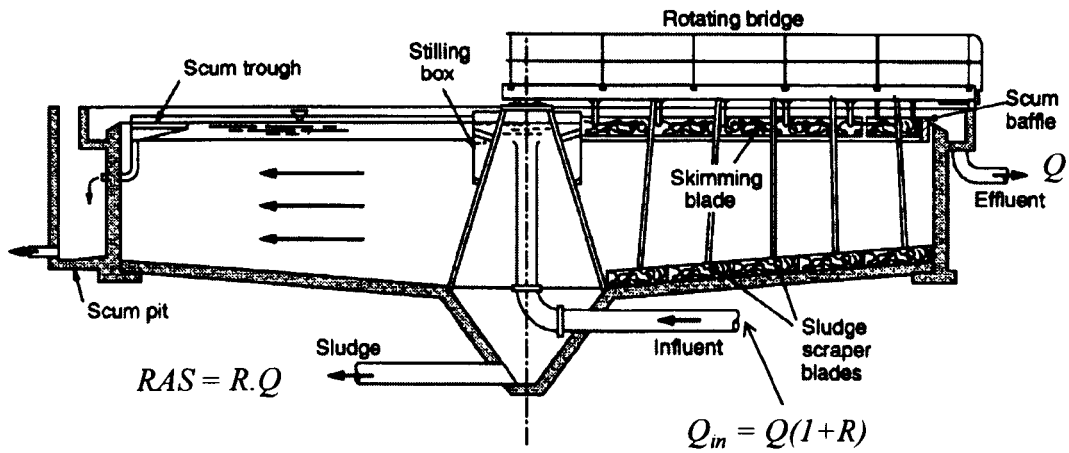

Figure 1.2: Cross section through a typical radial flow final clarifier. Adapted from the Civil Engineering lecture notes of Monash University (2003).

Figure 1.2 shows a cross-sectional view of a typical circular radial flow final clarifier. The mixed liquor is carried from the aeration tanks to the clarifier by a pipe which ends as a vertical riser in the centre of the tank. The flow enters into the tank through either an upturned bell mouth (an expanding opening at the top of the riser) or through vertical inlet slots cut into the riser. The influent flow is then distributed

with the stilling well (drum or box). The flow passes from the stilling zone out into the settling region of the tank where solids form into a settling sludge blanket and the clarified water, or supernatant, passes over the effluent weir. The effluent weir may either sit at the periphery of the tank, as part of an outboard launder, or a channel may be built and suspended within the periphery of the tank to form an inboard launder. There is a slight gradient to the tank floor, 4° to 10° is common, and a scraper blade revolves around the bottom of the tank, with the bridge, at a peripheral speed of between 1.2 and 2.4 *m/min* (ATV-DVWK, 2000).

Note that the exit flow from the clarifier, Q, is augmented at the influent by the recycled flow, $R.Q$. This assumes that all of the RAS is directed back through the aeration lane and into the clarifier. Reference to Figure 1.1 shows that this flow balance is not quite correct as some of the sludge is removed to the digesters. However, the surplus activated sludge (SAS) is usually a very small proportion of the total RAS flow and for analysis studies $Q_{in} = Q(1 + R)$ is always used.

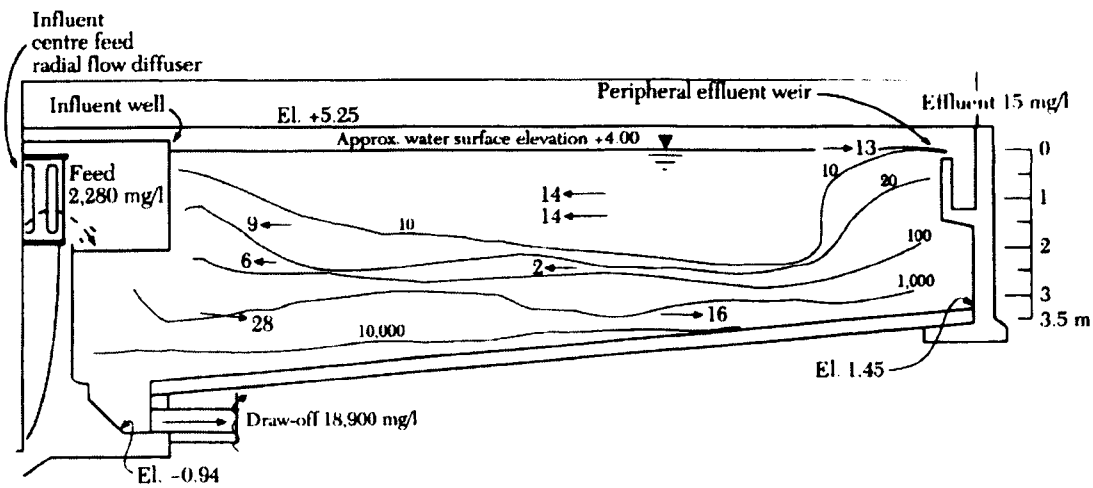

Figure 1.3: Flow patterns and settled solids distribution in a typical circular clarifier shown in radial cross section (taken from Anderson, 1945).
The concentrations are in mgl/l and the velocities are mm/s.

Figure 1.3, shows velocity vectors and solid concentration contours as a radial or axi-symmetric cross section through a circular clarifier of 40 *m* diameter and 3.5 *m* side wall depth. This tank is from Southwest Chicago (Anderson, 1945). The influent shown has an axial riser delivering feed into the tank through a central radial diffuser. Flow rates for this tank are in excess of 1000 m^3/hr giving inlet velocities of order 0.1 *m/s*. A conventional stilling well, arranged as a drum around the influent well, is used to attenuate the turbulent inlet flow.

1.4.1 Clarifier Flow Characteristics

Anderson's (1945) measurements of typical fluid velocities, shown as discrete vectors, and of solids concentration distribution, shown as contours in Figure 1.3, illustrates the density driven current observed in all circular clarifiers. The feed with a concentration of mixed liquor suspended solids (MLSS) typically in the range 2000 to 6000 *mg/l*, falls from the influent where a radial underflow is generated. The sludge thickens into a blanket at lower depths and is drawn off from the central sludge hopper at concentrations up to ten times the feed. A combination of the floor slope, the underflow momentum (driven by a hydraulic gradient) and the action of the rotating scraper blade directs the settled sludge to the central hopper. In order to balance the momentum, the underflow is matched by a significant return flow at higher depths in the tank. The resulting re-circulation is one of the reasons why the sludge blanket appears to lift at the side wall below the effluent weir. The effluent suspended solids (ESS) shown as 15 *mg/l* in Figure 1.3, represents a desirable outcome for the clarification process and typically tanks in the UK are required to meet ESS standards between 20 and 50 *mg/l*, (CIWEM, 1997). Measurements in experimental rigs and on site are usually directed to the understanding of flow velocity and solids concentration distribution. CFD models constructed of the

clarifier system may also be used to obtain similar distributions to those shown in Figure 1.3 for comparison with experimental data.

1.4.2 Shell and Internal Design

There are no fixed standards for the dimensions of circular clarifiers and many designs have been developed independently throughout the world. This is particularly true in the UK where each of the operating companies has evolved their own specific designs. Figure 1.4 shows a parameterised arrangement for the radial cross section of a tank which has become common for new build clarifiers during the AMP4 period (2005 to 2010). In this case the diameter of the stilling well is 20% of the tank diameter and the depth of the stilling is half the distance between the top water level (TWL) and the floor, at the radius of the drum. The floor slope angle is 7.5° and the side wall depth is fixed at 2.5*m* for all tank diameters.

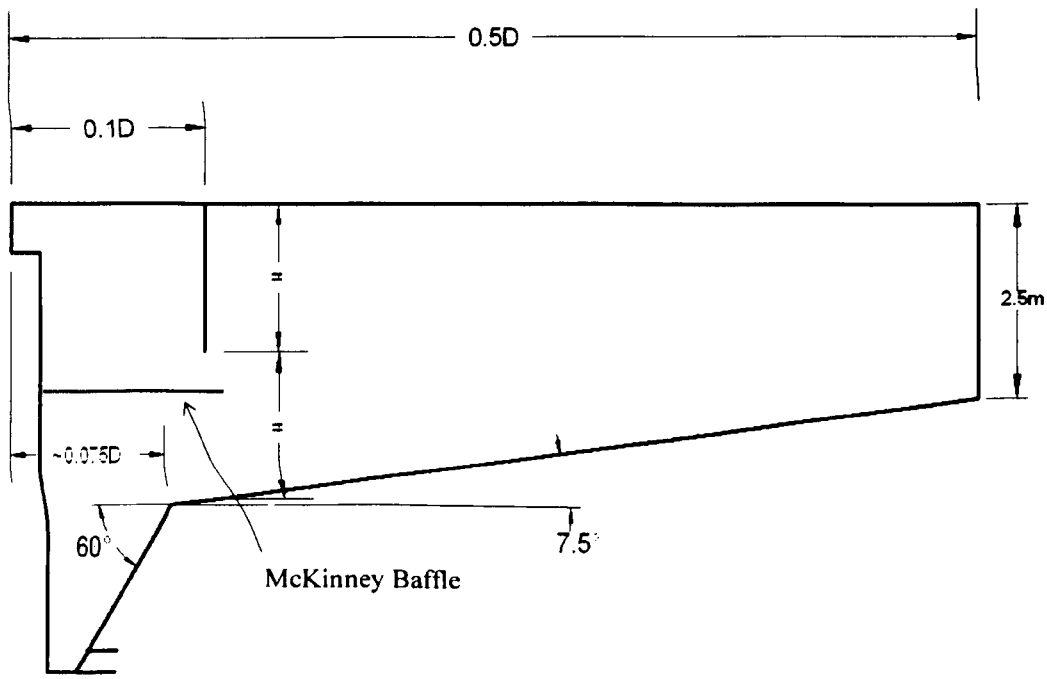

Figure 1.4: A radial cross section for a typical circular clarifier design (Burt et al, 2007), with optional McKinney floor baffle.

1.4.2.1 Influent Modifications

A number of modifications have been suggested to the basic clarifier designs which are thought to improve clarification performance. The McKinney baffle (Ekama et al, 1997), is a simple circular plate which may be positioned horizontally below the stilling drum with a diameter slightly larger than the drum. The plate is intended to break the density current that emanates from the central influent feed and direct the flow out radially into the tank The gap size between the McKinney baffle and the bottom of the stilling well is an important dimension and this may be sized to keep the influent densimetric Froude number between 0.5 and 0.7 so that return flows into the stilling well are prevented (Krebs, 1998),

$$Fr'_{in} = \frac{V_r}{\sqrt{gh\left(\frac{\rho_m - \rho_w}{\rho_w}\right)}} \qquad (1.2)$$

Where V_r is the average radial velocity through the gap under the drum in m/s, h is the height of the gap in m, ρ_m is the mixture density at influent and ρ_w is the density of water both in kg/m^3, g is the gravitational constant in m/s^2. The performance of a flat McKinney baffle design was investigated as part of the site trials at Witney STW described in chapter 6 of this thesis and as part of a modified influent design implemented at the Budds Farm STW discussed in chapter 7 of this thesis.

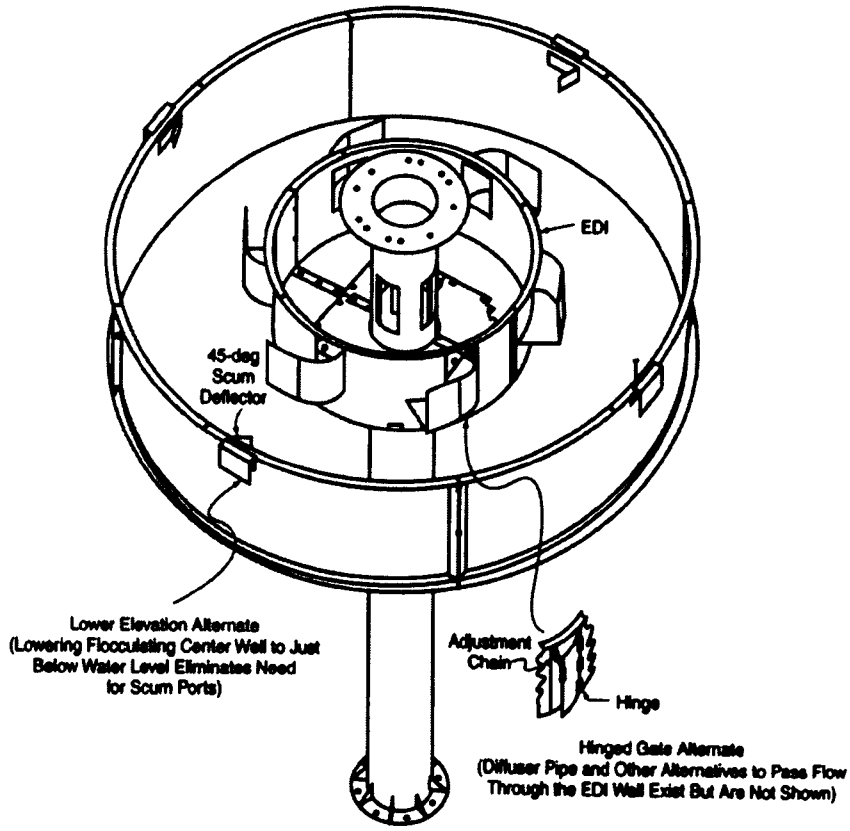

Figure 1.5: An EDI is placed in the centre of the stilling well.
The closed bottom tub surrounds the influent riser and the mixed liquor is directed through swirl vanes into the stilling well (MWH, 2003).

Another influent design idea is to include a flocculating centre well also called an energy dissipating influent (EDI). This consists of a closed bottom tub that sits within the stilling well enclosing the feed influent. The purpose of the EDI is also to break the influent density current and provide fluid velocity gradients that might enhance orthokinetic flocculation (Parker, 1996). A typical EDI is shown in Figure 1.5 where the height and diameter of the closed bottom tub are approximately half that of the stilling well. The performance of a novel counter-current EDI design was investigated as part of the site trials at the Crofton STW also described in Chapter 6 of this thesis.

1.4.2.2 Effluent Modifications

A number of baffle options have been proposed to limit the carryover of effluent solids by redirecting the return flow away from the effluent weir. These baffle arrangements may be attached to the side wall just below the effluent weir or may be cast into the concrete structure of the tank. Figure 1.6 shows some of the typical side wall baffle options that may be applied to circular clarifiers.

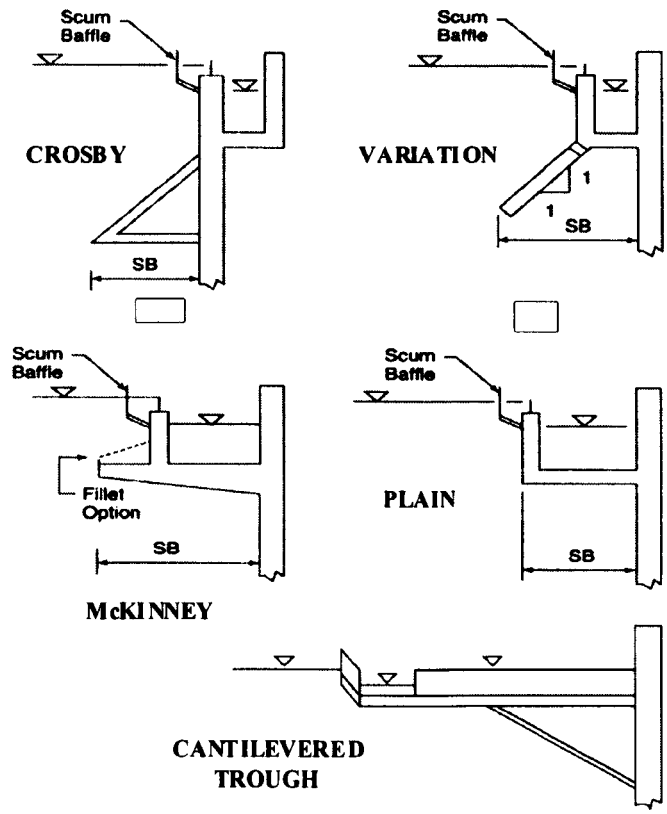

Figure 1.6: Various options for baffling at the side wall below the effluent weir are available.
The Crosby baffle is sometimes called a Stamford baffle. (MWH, 2003).

The performance of a Stamford (or Crosby) baffle was investigated as part of the site trials at the Crofton STW described in chapter 6 of this thesis and a McKinney side wall baffle was investigated as part of the Budds Farm STW study discussed in chapter 7.

1.4.3 Additional Functions of the Clarifier

The clarifier not only serves to clarify the forward flow, it must also thicken the sludge to a sufficiently high concentration for the RAS to be recycled to the aeration lanes and complement the MLSS, or be usefully processed as waste. Current disposal routes involve further de-watering prior to land fill, land spreading or incineration and there is much interest in the possibility of drying sludge to the point where it represents a useful source of fuel.

Finally, the tank must also act as a buffer store, in periods of very wet or very dry weather the flow rates through the tank may differ markedly from the design flow. Under these extreme conditions the tank must be continue to function without serious degradation of the clarification and thickening performance. It is this requirement which makes it very difficult to produce a generalized robust clarifier design for the UK waste water system as, unlike many other countries, the UK still uses a combined sewer system where storm water is channeled through to final treatment. New environmental legislation states that spillage of storm flows from the sewer, through combined sewer overflows, directly into rivers is no longer acceptable. Therefore, more dilute flows must be processed at the treatment works. This generates the requirement to pass higher flows through the clarifier with lower solids loading.

1.5 Hydraulic Models

A model is a tool that can be used to represent the processes occurring in a real system. In this work the model of interest is a mathematical construction of the physical and bio-chemical processes occurring in a clarifier. Mathematical models

are often classified by their dimension. A one dimensional model might be used to describe the sludge concentration profile with depth in a clarifier for a fixed set of process conditions (de Clercq, 2006). Three dimensional models describe the variation of variables in space and time. Such models take the form of systems of non-linear differential equations which are typically solved through the use of numerical methods coded as computer programs. Simplification of the physical processes in a model system requires the use of empirical data or constitutive relationships and it is often necessary to tune a model with constants that fit a particular system. Complex models attempt to represent physical processes explicitly to the point that the reliance on empirical data is reduced or indeed removed. In this work we are concerned with mass flux theory (MFT), which is a 1D model and augmented Computational Fluid Dynamics (CFD) modeling which is a 3D modeling method.

1.5.1 Introduction to Mass Flux Theory

Mass flux theory (MFT) is used to size the required surface area of a clarifier based on the assumption of 1D settling. Mass flux theory may be used to determine the upper bound performance for a tank which, in practice, cannot be achieved. However, through good design of the tank internals the theoretical limit may be approached. There are several mass flux criteria which are applied to clarifiers; the two most significant are; criterion I, the solids mass loading rate and criterion II, the hydraulic loading are described by the WRc method (Ekama, 1997). Criterion III the volumetric loading rate is described in the German ATV guidelines (ATV-DVWK, 2000). These are discussed in greater detail in Chapter 3.

1.5.1.1 State Point Analysis

State point analysis is the basic building block of mass flux theory. It is assumed that sludge settling velocity is a unique function of the solids concentration and the mass flux is the product of settling velocity and the solids concentration,

$$j_s = X.V_s \tag{1.3}$$

Flux can then be plotted against solids concentration to give the mass flux curve..

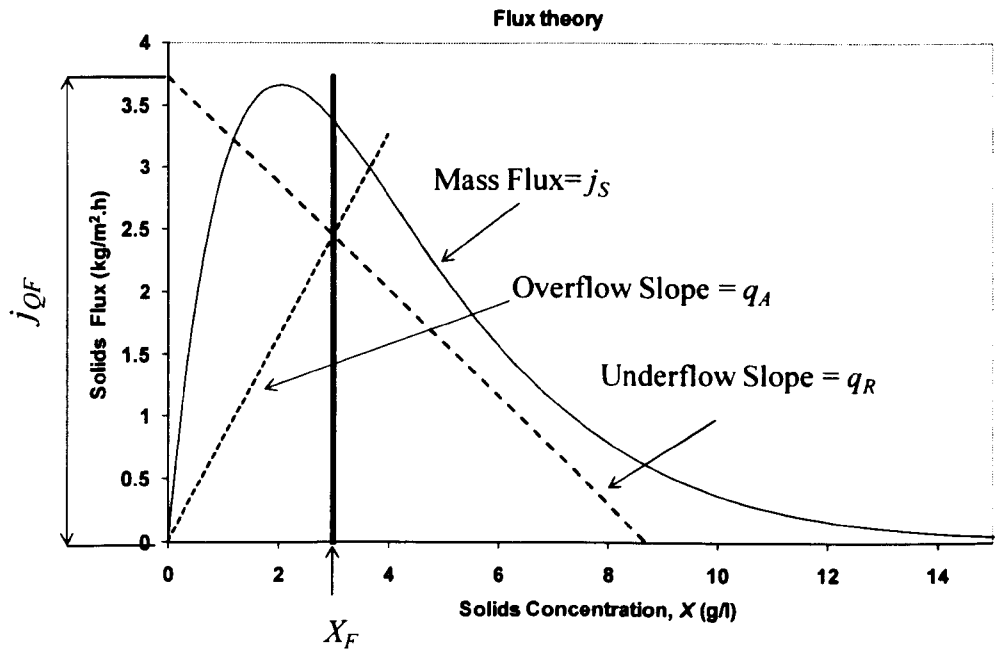

Figure 1.7: Mass flux curve and state point.
The intersection of the overflow and underflow lines is below the flux curve and so the tank is in safe operation.

This generalized flux curve shown in Figure 1.7, can be calculated from any of the standard correlations for settled volume index (SVI) or stirred specific volume index (SSVI), typically the Pitman (1980) and White (1975) correlation is used in the UK. On this same curve two operating lines, the surface over flow and under flow rates, are also plotted where:

The surface overflow rate (SOR), usually expressed in *m/h*, is the ratio of the tank inlet flow over the total tank surface area,

$$q_A = \frac{Q}{A_{st}}. \tag{1.4}$$

and the underflow rate,

$$q_R = -\frac{R.Q}{A_{st}}. \tag{1.5}$$

following the flow rate notation given in Figure 1.2.

If the intersection of these lines is above the flux curve then clarifier failure is predicted. At any state point, the crossing of the underflow and overflow lines must be below the flux curve for safe operation. If the underflow line is below the flux curve, but becomes tangential to it at higher concentrations, then the tank is said to be critically loaded and on the point of failure. There are many other definitions of tank failure obtainable from mass flux theory (IWA, 2008).

The main difficulty in estimating the limiting situation with mass flux theory is a poor correlation between SSVI and flux, this is because the flows in clarifiers are not one dimensional. Therefore, a safe design is not usually based on the generalized flux curve but on only 80 % to 90 % of the value at any point.

The mass flux limits are examined carefully later in this work as the basis for a design method. They are useful bounds and provide a theoretical target against which CFD solutions for new designs may be compared (Ekama and Marais, 2004). It is particularly helpful to characterise the performance a clarifier in terms of the mass flux limit as it provides a normalising function against which all designs may be

compared. A fuller description of mass flux theory and the use of the mass flux limit for design is given in Chapter 3.

1.5.2 Literature for CFD Modelling of Clarifiers

In this work, the emphasis is on progress towards validated and verified models for the processes occurring in clarifiers based around the numerical solution of the conservation equations for mass, momentum and solid species within the tank. This form of modelling fits under the broad heading of Computational Fluid Dynamics (CFD) (Patanker, 1980). Therefore texts that describe the linking of CFD to clarifier design and the subsequent application of techniques are important references for this work.

Hydrodynamic modelling of clarifiers has been developed over many years originally by McCorquadale (1993) and Zhou (1992) from the strip integral method (Abdel-Gawad, 1984) and by co-workers at the University of Karlesruhe under the direction of Rodi including Celik (1988), Stamou (1989), Adams (1990), and Krebs (1991). The developments of these models up to 1997 are very well described in the IWA technical report No 6 (Ekama et al, 1997). Much of the CFD modelling reported by Ekama (1997) uses a form of the Algebraic Slip or Drift Flux (Wallis, 1969) model to represent the two-phase mixture of water and activated sludge. One interesting paper that describes a possible flocculation model for sludge where the flocs are represented by three size group scalars is due to Lyn et al (1992) and this forms the ideas for multiple drift fluxes explored in this thesis.

One thesis that appears to depart from the idea of using a drift flux model is that due to Matko (1998) who proposed the Euler-Euler multiphase frame model

incorporating drag laws for sludge. However, on close inspection it is clear that his work also use the same density and settling models described in Ekama et al (1997). Extensions to the standard model for the inclusion of sludge rheology were first proposed by Lakehal and Krebs (1999). Additional modified rheology models have been described by Armbruster (2003), de Clercq (2003) and most recently by Weiss et al (2007). These models and modifications for the extended drift flux model used in this work are explored in detail in Chapter 2. Following these developments many design studies and papers have been published that use CFD modelling techniques for clarifier design (Ekama and Marais, 2004), (Shaw et al, 2005). The recent book by the IWA (2008) 'Biological Wastewater Treatment', includes some outputs from the work in this thesis.

1.6 Aim and Objectives of the Work.

This PhD thesis sets out to address 5 distinct research questions.

1. What are the correct CFD modelling approaches for calculating the performance of a clarifier and can the model be used to optimise existing and new designs?
2. How do CFD results compare with experimental data?
3. Is it possible to calculate the capacity of different clarifier designs with CFD and compare these calculations with flux procedure predictions.
4. Is it possible to manufacture a simulant for activated sludge and is this simulant useful for experimental validation studies of clarifier systems?
5. Is flocculation an important physical process in the performance of a clarifier and, if so, can it be modelled?

1.7 Methodology

The research was carried out using both computational and experimental methods, which included flow visualisation and measurement. These methods are not described in single chapters but are discussed within the chapters connected with their application. This section summarises all of the methods used in the project.

1.7.1 Computational Methods

Mass flux theory was used throughout the work as a means of assessing the expected operational performance of a clarifier for a particular set of process flow conditions. Computational Fluid Dynamics (CFD) modelling techniques were used to predict the fluid flow and settling processes within a clarifier by solving the Navier-Stokes equations (or governing equation of fluid flows) numerically, in an iterative fashion. A commercial CFD simulation software package, CFX, was used to create the numerical models and calculate the flow and solid distribution fields.

1.7.2 Laboratory Experiments

Experimental work was performed in the laboratory to prepare a synthetic activated sludge and compare the behaviour of this sludge with sludge samples taken from the Swindon sewage treatment works. A lock exchange box was constructed and videos were recorded of the performance of a collapsing sludge column in clear water. Results for real activated sludge, synthetic sludge and a computational model were compared.

1.7.3 Flow visualisation and Site Measurement Techniques

Full scale measurements of velocity and concentration distribution in a clarifier were performed at the Thames Water Witney site (2005). Measurements were made using acoustic doppler velocimetry (ADV) from a bridge mounted rig with a spot sampling

unit for concentration profiling. The data from the experimental work was compared with CFD predictions for a standard tank and for a tank with influent modeifications.

1.8 Outline of the Thesis

This thesis contains nine chapters including this one and is organised in a logical manner rather than a chronological order.

Chapter 2 presents the various theoretical models for implementation in a Computational Fluid Dynamics code. This includes the Euler-Euler, the Euler-Lagrange and Drift Flux frames for multiphase flow. Reasons for using the Drift Flux frame are explained and an extended drift flux model is developed. The model includes a turbulence closure and constitutive relationships for sludge density, settling velocity and fluid mixture rheology.

Chapter 3 examines the constitutive relationships for the model developed in chapter 2 in more detail. A relationship for the Takács (1991) parameters is developed and a method of deducing these parameters from a set of standard settling tests is explained. The various rheological functions are described and the data sources for these functions are presented. Mass flux theory is also explained in much greater detail and the connections between 1D mass flux modelling and 3D CFD modelling are made.

Chapter 4 considers two CFD studies for systems where some limited experimental data was already available, the Krebs (1998) laboratory clarifier and the RyeMeads clarifier site tests performed by Richardson (1998). The model developed in Chapters 2 and 3 is implemented with an extended technical manual of the implementation provided in Appendix B. Details of the application of the model then follow where

sensitivity to computational grid, boundary conditions, fluid properties and other modelling parameters are considered. From these studies, a number of useful guidelines emerge on how to perform numerically stable and accurate CFD solutions. These guidelines are carried forward into the later stages of the work.

Chapter 5 returns to the fundamental characteristics of activated sludge floc. It is proposed that synthetic sludge simulant might be used alongside computational studies to confirm the performance of certain geometric variations in clarifier design. A simulant is developed from the work of Örmeci and Vesilind (2000) and used in a laboratory scale lock exchange experiment. The lock exchange process is examined with synthetic sludge, with real sludge taken from the Swindon STW and with the computational model developed in chapter 2 and verified in chapter 4.

Chapter 6 describes full scale validation experiment performed at Witney (Burt, 2005a) and Crofton (Burt, 2005b), The rig originally proposed by Richardson (1998) for acoustic doppler velocimetry (ADV) and solids profiling measurements was adapted and re-configured for testing at both sites. The measurements were performed over a period of days with the tank conditions modified artificially to represent very high flow and load states. Tests for the sludge in the tanks at Witney revealed a surprising anomally where it was noted that dosing of the sludge affected the choice of correlation that could be applied for deriving the model settling coefficients. The test data was carefully plotted against equivalent CFD modelling results with bands of error defined and validation of the model was obtained for a number of operating conditions.

Chapter 7 looks in detail at the existing and new clarifier designs for the STW at Budds Farm near Havant, Portsmouth in the UK. A McKinney plate influent modification is proposed for application in all ten clarifiers on this site. A program of modelling and testing was carried out and comparisons between mass flux theory and the CFD results are made.

Chapter 8 is a discussion of all of the results contained in the thesis. This includes some comments on the dominant flow mechanism in clarifiers and how these mechanism influence final effluent quality. The limitations of the proposed model are explored and suggestions for improving and extending the model are considered.

Finally, Chapter 9 concludes by returning to the research questions posed in this chapter.

CHAPTER 2: Multiphase Computational Fluid Dynamics, an Extended Drift Flux Model

Summary

In this chapter the flow characteristics for a clarifier are introduced using fundamental equations of fluid mechanics. Various multiphase frameworks are then defined as being possible starting points for constructing a hydrodynamic model for clarifiers including the Eulerian-Eulerian frame, the Eulerian-Lagrangian frame and the drift flux frame. The full Navier Stokes equations for fluid flow are then presented and these are developed, within a drift flux frame, to provide the complete hydrodynamic model. Finally the question of flocculation is considered and the G scalar history function is proposed as a means of assessing the flocculating performance of a clarifier influent.

2.1 Introduction to Clarifier Flows.

The motion of liquid and suspended solids within a clarifier is a multiphase flow. The background fluid is water and this interacts with the activated sludge solids on various length and time scales. Before progressing to a full description of the hydrodynamic models developed in this work, it is worth understanding the various scales in a clarifier that can be obtained from classical fluid mechanics. The following illustration is based on data from a circular clarifier at the Rye Meads sewage treatment works (STW) operating with an average flow and load condition (Richardson, 1998).

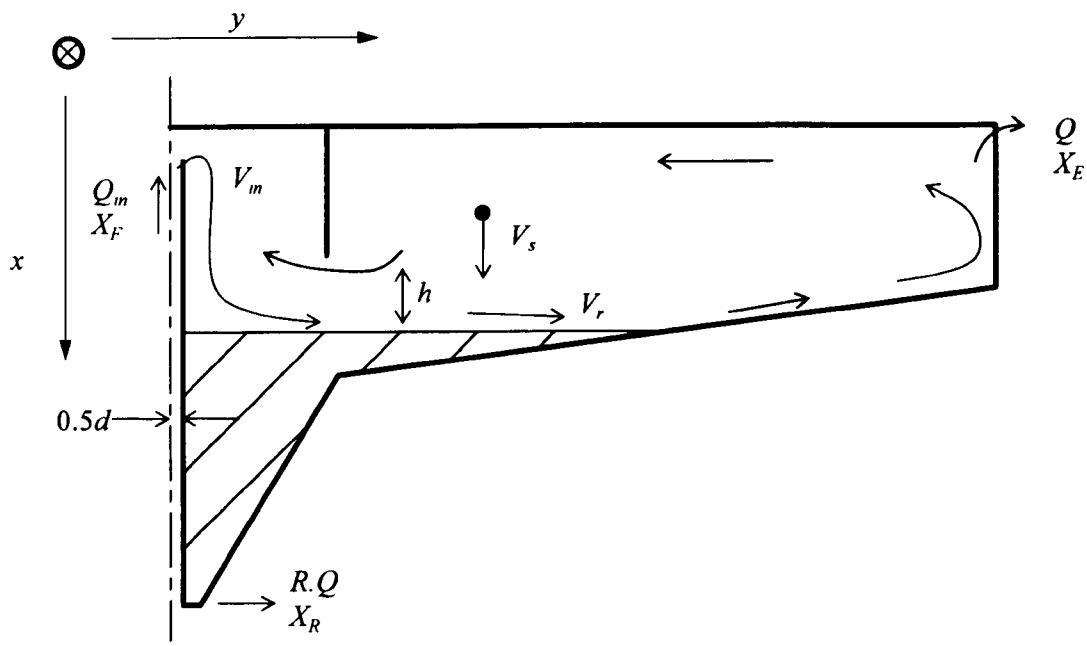

Figure 2.1: Schematic of a radial secondary clarifier showing flow paths and the settling sludge bed. The vertical *x* axis is positive with the depth of the tank in the direction of gravity, the *y* axis is positive with increasing radius.

Figure 2.1 shows a radial or axi-symmetric cross section of a circular clarifier annotated with a hatched region showing the settled sludge bed and the circulating flow path described in chapter 1, (Anderson, 1945). Note that the co-ordinate origin of the system is the central axis at top water level (TWL), the vertical x axis is positive with (rather than against) the direction of gravity and the y axis is positive with increasing radius. This co-ordinate system convention is consistent with the computational model developed later in the work and is retained throughout the thesis.

The example tank at Rye Meads has a diameter, D=28 m, side wall depth, h_s =2.2m, an average forward flow in to the tank, Q_{in} = 720 m^3/hr with a recycle ratio, R =1.0.

The first characteristic of interest is the average amount of time that a parcel of fluid might expect to stay in the tank; the hydraulic residence time,

$$T = \frac{Vol}{Q_{in}}, \approx 2.5\ h \tag{2.1}$$

The flow enters the tank at velocity, $V_{in} = 0.37\ m/s$, from which the turbulence characteristics at the inlet can be calculated giving an inlet Reynolds number,

$$Re_{in} = \frac{\rho_{in} V_{in} d}{\mu_m}, \approx 3.0\ \text{E+05} \tag{2.2}$$

This is much larger than the transition from laminar to turbulent flow which occurs at $Re \approx 2000$ (Acheson, 1990) and indicates that the flow entering into the stilling well is highly turbulent. The concentration of the mixed liquor entering into the tank, $X_F = 2825\ mg/l$, is slightly denser that the fluid within the stilling well. The peak radial velocities attenuate rapidly away from the influent reducing to $V_r \approx 0.04\ m/s$, and therefore a density current is generated. This is demonstrated by balancing the potential energy at the influent against the kinetic energy of the flow with the densimetric Richardson number,

$$Ri' = \frac{g'h}{V_r^2} = \frac{g(\frac{\rho_m - \rho_w}{\rho_w})h}{V_r^2}, \approx 10.0 \tag{2.3}$$

where, the length scale $h = 2.0m$, is the height of the fall from the influent. This is greater than the critical densimetric Richardson number $Ri' = 1.0$ above which buoyancy effects dominate. As the solids build up in the bottom of the tank, the flow from the density current is deflected outwards as a radial flow at a velocity $V_r \approx 0.02$

m/s, which is similar to the Anderson (1945) data, and reducing with radius, therefore the bulk Reynolds number

$$Re = \frac{\rho_m V_r h}{\mu_m}, \approx 2000 \text{ to } 4000, \tag{2.4}$$

indicating that the flow is transitional from turbulent to laminar in the bulk of the tank even where the fluid viscosity is close to that of water. Within the settled sludge bed, where viscosity is increasing with concentration, the flow is likely to be laminar (and non Newtonian).

It is known that where density gradients or stratification occurs, then a time scale arises for a vertically displaced parcel of fluid which can oscillate within a statically stable environment and so for this system, the Brunt-Väisälä Frequency

$$N = \sqrt{\frac{g}{\rho_m}\left(\frac{\partial \rho_m}{\partial x}\right)}, \approx 0.5\ s^{-1} \tag{2.5}$$

This number is useful in that it indicates the likely size of time step that will be required to resolve any transient flows within the numerically solved system of equations.

Finally, it is worth considering the time scales of the sedimenting solids. For this, prior knowledge of floc length scale and density are required. For now, the open flocs are considered to have a typical size of $d_p \approx 200\ \mu m$, (de Clercq, 2003) they are made up of a large amount of interstitial water and so have a particle density $\rho_p \approx 1020\ kg/m^3$ with a terminal settling velocity $V_o \approx 2\ mm/s$, (Li, 1987), This gives a particle Reynolds number

$$Re_p = \frac{\rho_p V_s d_p}{\mu_m}, \approx 0.1 \text{ to } 0.4 \tag{2.6}$$

Therefore, the drag relationship for the floc is in the Stokes regime (Clift, 1978) and the relaxation time scales in the radial flow direction are likely to be so small that it can be assumed that flocs are carried with the flow. The relaxation time constant (Mironer, 1979), can be estimated as

$$T_R = \frac{m_p + m_h}{C_D \rho_m V_s A_p}, \approx 1.6\text{E-}3\ s \tag{2.7}$$

where A_p is the projected are of the particle, m_p is the mass of a spherical particle, m_h is the added hydrodynamic mass of the spherical particle and C_D is the drag coefficient ($24/Re_p$). The time for to reach terminal velocity in a quiescent fluid was found to be close to six time constants (Egarr, 2010), therefore, $t_R \approx 0.01\ s$.

2.2 Multiphase Frameworks

In this thesis, the emphasis is on progress towards validated and verified models for the processes occurring in clarifiers based around the numerical solution of the conservation equations for mass, momentum and solid species. This form of modelling fits under the broad heading of Computational Fluid Dynamics (CFD). In order to use CFD to model the fluid motion and settling behaviour within a clarifier, it is necessary to consider the available modelling frameworks that can be applied to solid settling systems. Broadly, these model frameworks fit under three headings (CFX, 2001);

1. The Eulerian-Eulerian frame, sometimes called the full multi-phase or multi-fluid model.
2. The Eulerian-Lagrangian frame, often called the particle tracking model.
3. The Homogeneous frame, also called the drift flux or mixture model.

These frameworks are available in many CFD codes and potentially, they may all be used as the basis for a model of clarifier performance.

2.2.1 Eulerian-Eulerian Multi-phase Flow

In the Eulerian-Eulerian or multi-fluid framework the phases can be solid, liquid or gas or combinations of multiple solids, liquids and gases. For a clarifier the phases are water, as a continuous background liquid and sludge which can be in the form of freely suspended particulate, semi-continuous hindered floc or continuous compacting slurry enclosing interstitial water. The phases have independent conservation equations for mass, momentum, enthalpy, volume fraction (the marker in cell) and appropriate turbulence quantities. These are coupled through inter-phase exchanges terms defined as sources or sinks to the conservation equations.

In the case of a clarifier, the background liquid and solid particles may move independently of each other whilst exchanging momentum in the form of lift, drag, buoyancy or other sub-grid scale forces. This makes the multi-fluid framework attractive for settling in that a fully deterministic approach may be taken for specifying the momentum exchanges through correlations. For example, the drag force can be determined for a spherical particle across a full range of local particle Reynolds numbers following the correlations of Ishii and Zuber (1979). This approach for computing drag on an idealised sphere may be extended to irregular particles which have a similar volume to surface area ratio. Detailed correlations covering the subcritical drag curve for more irregularly shaped particles are presented in Clift, Grace and Weber (1978)

As solids concentration increases, particles begin to interact with one another which in turn influences the amount of momentum exchanged between the phases. It is

possible to simulate these inter-particle effects as an increase in effective mixture viscosity, as has been done for the fluidization of regular solid particulates (Gidaspow, 1994). There are also semi-empirical drag correlations for regions of densely packed spheres (Ergun, 1952) and compression zone models based on the concept of a solids pressure force (Witt, 1995).

However, all of these correlations rely on the concept of characterising an individual particulate in terms of length scale, density and shape factor, this is a significant limitation for activated sludge in that a single solid phase can only take single values for these properties. The free settling particles that move through clarifiers are flocs of irregularly shaped solids containing significant interstitial water (CIWEM, 1997) and so it is very difficult to define a typical length or a density for such a floc. This makes the deterministic calculation of free settling velocity, based on a local particle Reynolds number correlation difficult. As the flocs begin to interact they grow in size and bridge to form hindered beds finally settling into compression zones. These hindering and compressive processes are difficult to describe through a deterministic model because of the complex collision processes, local deformations and agglomerations that are occuring. Therefore, following these considerations, and attempts to model a settling column with the various multiphase correlations proposed by van-Wachem (1998) for the Eulerian-Eulerian frame, this model framework was ultimately rejected for this work.

2.2.2 Eulerian-Lagrangian or Particle Tracking

In the particle tracking models the continuous flow field is solved in the Eulerian frame and the particle motions are calculated from a force balance along a

representative Lagrangian trajectory. The model allows for one way coupling where particles simply follow the flow or two way coupling where momentum exchanges can occur from the particle back to the flow through drag, lift, buoyancy or other forces. Particles can interact with walls in a number of ways, they either stick, bounce according to a specified coefficient of restitution or saltate, that is continue to flow along the wall at some distance away from the wall. The choice of particle boundary condition can have a significant influence on the final destination of the particle.

This framework has been used by other workers to investigate the capture of solids in waste water systems (Stovin, 1998) and by the author in a detailed study of multiphase flows in combined sewer overflows (CSOs), (Burt et al, 2002). From this work it was determined that there are crucial limitations which make the Lagrangian frame inappropriate for settling tanks of any kind. Numerically, particles that terminate within the system disappear from the calculation, whereas physically they should deposit into a sediment bed or form a body of floating debris. This does not restrict the use of particle tracking as a means of computing separation efficiency in a waste water chamber that does not hold up particulate but it does make it unreliable for sedimenting systems where the retained solids interact with the body of the flow (Burt, 2002). Consequently, particle tracking cannot reliably predict solid retention and this precludes its use in a clarifier where the sludge bed deposition and build up is a crucial element of the hydrodynamics. Following these considerations this model framework was also rejected for this work.

2.2.3 The Homogeneous, Drift Flux or Mixture model

In a settling system, such as a wastewater clarifier, the effects of gravity are significant on the solid phase momentum field but relaxation time for the interphase exchange of momentum through drag is very short. That is the momentum of the activated sludge flocs equalises with the momentum of the background water rapidly in the planar direction whilst continuing to move relative to the background fluid in the gravitational direction at settling (or slip) velocities up to a maximum terminal value V_o, of between 2.0 and 4.6 *mm/s* (Li, 1987).

The assumption that there is little or no interphase momentum exchange in the horizontal plane, whilst the flocs move in the gravitational direction with a relative settling rate, makes it possible to utilise the homogeneous or multiphase mixture model and therefore, most of the cited work on clarifier modelling (Ekama et al, 1997) uses this framework. The homogenous mixture model is also referred to variously as drift flux (Wallis, 1969) and algebraic slip (CFX, 2001). The IWA hydrodynamic model for clarifiers (Ekama et al, 1997), describes a two dimensional system of equations applied to the analysis of settling systems based on the homogeneous model but without a good representation of the settled sludge bed. This model is developed further in this thesis with many modifications and additions. The starting point for the development of the model however, is to return to the fundamentals of turbulent flow, as has been illustrated, the flow in a clarifier is unfortunately (from a modelling perspective) highly turbulent in the stilling zone of the tank but completely laminar, and expected to be non-Newtonian in the slow moving regions of the settling sludge bed

2.3 Conservation Equations for Fluid Flow

The presentation of the governing equations for the flow of activated sludge mixed liquor in a clarifier starts with the Navier-Stokes equations for fluid flow (Acheson, 1990), these are expressed in index (or tensor) notation as the conservation of mass,

$$\underbrace{\frac{\partial \rho}{\partial t}}_{rate} + \underbrace{\frac{\partial (\rho u_i)}{\partial x_i}}_{convection} = 0 \tag{2.8}$$

and the conservation of momentum,

$$\underbrace{\frac{\partial (\rho u_i)}{\partial t}}_{rate} + \underbrace{\frac{\partial}{\partial x_j}(\rho u_i u_j)}_{convection} = \underbrace{\frac{\partial \sigma_{ij}}{\partial x_j}}_{stress} + \underbrace{\rho g_i}_{gravity} \tag{2.9}$$

The total stress exerted on a parcel of fluid consists of both a pressure stress and a viscous stress,

$$\sigma_{ij} = -p\delta_{ij} + \tau_{ij} \tag{2.10}$$

The Kronecker-delta δ_{ij} (see Appendix A), is required to make the pressure force vector act normal to the surface of a fluid packet. For a Newtonian fluid the viscous stress is then related to the strain rate tensor,

$$\dot{\gamma}_{ij} = \frac{\partial u_i}{\partial x_j} + \frac{\partial u_j}{\partial x_i} \tag{2.11}$$

through the Stokes law such that,

$$\sigma_{ij} = -p\delta_{ij} + \mu\left(\dot{\gamma}_{ij} - \frac{2}{3}\frac{\partial u_j}{\partial x_i}\delta_{ij}\right) \tag{2.12}$$

where the additional term in the bracket allows for the deformation or dilation of a fluid parcel.

The substitution of equation (2.12) back into the conservation of momentum equation (2.9) yields the full Navier Stokes equations for a Newtonian fluid. These equations are a closed set and valid for all fluid flow situations as long as they can be solved at an appropriate scale. Analytical solutions of these equations are possible for many classes of flow but for complex industrial problems, where the geometry is not easily simplified, numerical methods are usually employed.

In order to solve the Navier-Stokes equations numerically, using a finite volume based CFD code for example, it is required to discretise the spatial and temporal gradients with length scales to give an equivalent mesh Reynolds number of 1.0 and time scales appropriate to the smallest turbulent eddies in the fluid; these are the Kolmogorov micro scales (Patanker, 1980). This can be done using the techniques of direct numerical simulation (DNS), however, this is not generally practical for many classes of industrial turbulent flows, including flows in clarifiers, because of the large computing resources that would be required to hold and solve the matrix of equations arising from the discretisation (the grid). Therefore it is necessary to convert the variables of interest into mean flow, or time averaged quantities, that can be solved on a realistic computational grid with realistic time scales and use a turbulence model to approximate the smaller scale flow features.

2.3.1 Reynolds Averaged Navier-Stokes Equations

The Reynolds averaged Navier-Stokes equations (RANS) are formed by time-averaging the small scale turbulent velocity fluctuations in a steady turbulent flow. This is illustrated in Figure 2.2 where the dynamic velocity trace for a steady turbulent flow is represented by a flat mean average value and a fluctuating or turbulent component.

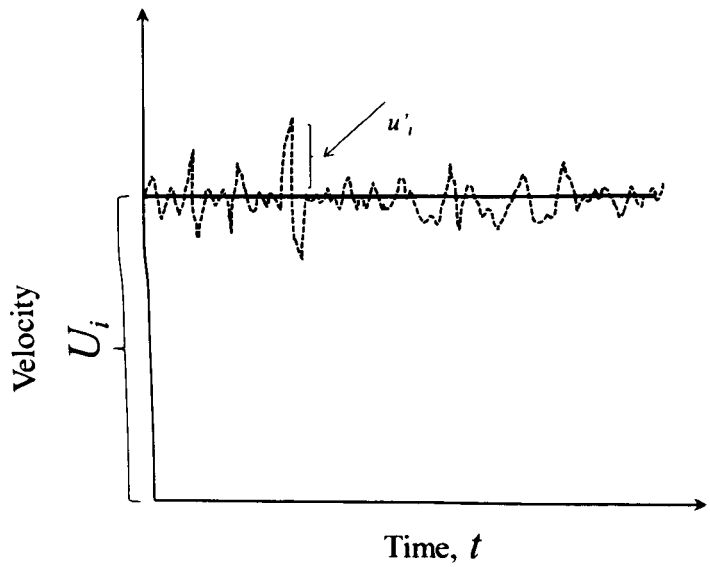

Figure 2.2: A velocity trace for a steady turbulent flow.
The fluctuations in velocity occur at the Kolmogorov time scale.

The dependent variables in the RANS equations are obtained by decomposing the dependent variables from the general equations (2.8) and (2.9) into a mean and a fluctuating part, this is known as the Reynolds decomposition,

$$u_i = U_i + u_i' \tag{2.13}$$

$$p = P + p' \tag{2.14}$$

where,

$$\frac{\partial U_i}{\partial t} = 0 \tag{2.15}$$

Inserting the Reynolds decomposition into equations (2.8) and (2.9) and taking the time average yields the Reynolds time averaged continuity and Navier Stokes equations. The continuity equation remains the same but with the velocity replaced by the mean velocity and the momentum equation gains an additional stress term. The total stress is then made up of the laminar component and the turbulent Reynolds stresses. (the mean components are shown as capitals rather than using an over bar as is sometimes used).

$$\frac{\partial \rho}{\partial t} + \frac{\partial (\rho U_i)}{\partial x_i} = 0 \tag{2.16}$$

$$\frac{\partial (\rho U_i)}{\partial t} + \frac{\partial}{\partial x_j}(\rho U_i U_j) = -\frac{\partial P}{\partial x_j} + \frac{\partial}{\partial x_j}\left[\underbrace{\mu\left(\dot{\gamma}_{ij} - \frac{2}{3}\frac{\partial U_j}{\partial x_i}\delta_{ij}\right)}_{laminar} - \underbrace{\overline{\rho u_i' u_j'}}_{turbulent}\right] + \rho g_i \tag{2.17}$$

The starting point for the turbulence closure problem is the modelling of the Reynolds stresses in terms of the mean flow quantities. A large number of turbulence models are based on Boussinesq's eddy viscosity concept (Tennekes, 1972), which assumes that turbulent stresses are proportional to the mean flow velocity gradients. This relation can be expressed for incompressible flow as:

$$-\rho\overline{u_i' u_j'} = -\rho\frac{2}{3}k\delta_{ij} + \mu_t\left(\frac{\partial U_i}{\partial x_j} + \frac{\partial U_j}{\partial x_i}\right) \tag{2.18}$$

where k is the turbulent kinetic energy, and μ_t is a new quantity called the turbulent or eddy viscosity. Various models are available to determine the unknown variables

k and μ_t, and a suitable model for clarifier flow will be presented in the following sections.

2.4 Mean Flow Equations for Clarifier flows.

To fully represent the flow of mixed liquor in a clarifier it is necessary to augment the Reynolds Averaged Navier Stokes equations with a drift flux sludge mass fraction equation, constitutive relationships for density, rheology and settling velocity and a turbulence closure appropriate for a systems transitioning between high and low Reynolds numbers. This combination of fundamental equations and constitutive relationships makes up the extended drift flux model for clarifiers. In the following sections, the conservation equations for the extended drift flux model are expressed in their averaged forms and the turbulence closure is included. Therefore, the mixture velocity vector $\mathbf{U}_m$ and the pressure scalar, p, are the time averaged quantities.

2.4.1 Conservation of Mass

The conservation of mixed liquor mass or the continuity equation is now,

$$\frac{\partial \rho_m}{\partial t} + \nabla \bullet (\rho_m \mathbf{U}_m) = 0 \tag{2.19}$$

In the drift flux or mixture model, the fluid density varies throughout the domain as a function of concentration. The mixture density is defined in terms of the phase, k, and volume fraction of each phase present r, as,

$$\rho_m = \sum_{k=1}^{n} r_k \rho_k \tag{2.20}$$

2.4.2 Conservation of Momentum

The conservation of mixture momentum is,

$$\frac{\partial}{\partial t}(\rho_m \mathbf{U}_m)+\nabla\bullet(\rho_m \mathbf{U}_m \otimes \mathbf{U}_m)-\nabla\bullet\left(\mu_{eff}(\nabla \mathbf{U}_m+(\nabla \mathbf{U}_m)^T)\right) = -\nabla P'+\mathbf{g}(\rho_m-\rho_w) \tag{2.21}$$

The effective viscosity μ_{eff}, in the diffusive term may be thought of as having two components, an apparent or material dependent viscosity μ_m, which is a physical property and a turbulent viscosity μ_t, which is a model construction that invokes the influence of turbulence on the diffusion of the various fields and is obtained from the turbulence model, and so,

$$\mu_{eff} = \mu_m + \mu_t \tag{2.22}$$

The buoyancy force is included as a source on the right hand side but with a modified pressure incorporating the hydrostatic component. Note that the gravity vector is positive with the x co-ordinate following Figure 2.3.

$$P' = P+\frac{2}{3}\rho_m k+\left(\frac{2}{3}\mu_{eff}-\varsigma\right)\nabla\bullet\mathbf{U}_m+\rho_o(\mathbf{g}\cdot\mathbf{x}) \tag{2.23}$$

2.4.3 Conservation of Solid Species, the Drift Flux Scalar

The conservation of solid species equation is,

$$\frac{\partial}{\partial t}(\rho_m Y_k)+\nabla\bullet(\rho_m(\mathbf{U}_m+\mathbf{U}_{sk})Y_k)-\nabla\bullet\left(\left(\mu_m+\frac{\mu_t}{\sigma_y}\right)\nabla Y_k\right)=0 \tag{2.24}$$

The coefficients for the diffusion of the solids species arise from the Reynolds averaging process which generates a turbulent mass transport term. By direct analogy with the momentum transport equations, a diffusivity is defined, $\Gamma_y = \mu_m + \frac{\mu_t}{\sigma_y}$, where σ_y is Schmidt number and may be varied between 0.5 and 1.0 (Celik and Rodi, 1988). The mass fraction of the solid phase Y_k, is used as the marker for the drift flux or algebraic slip scalar. The subscript k again denotes the possibility of

having multiple mass fractions representing multiple solid phases. Typically, the extension to multiple solid phases may be used to represent multiple drifting solid fluxes within the background fluid. The additional velocity $\mathbf{U}_{sk}$ in the convective term is the slip velocity component representing the local difference between the solid and fluid velocities (CFX, 2001). Either, each solid size group has its own fixed slip velocity, usually based on the terminal settling velocity of a size group, or a single slip scalar is used with $\mathbf{U}_{sk}$ some function of the local variables. For example, where the solids for a primary waste water settling process can be defined as a particle size distribution (PSD), an equivalent settling velocity distribution (SVD) can be defined and applied as a set of conservation equations in the CFD model (Burt and Gilbertson, 2005).

2.4.4 The k-ω Model for Eddy Viscosity.

The closure of the RANS equations is often achieved with the standard k-ε model (Launder and Spalding, 1972). In this case the turbulence field is characterized in terms of two variables, the turbulent kinetic energy k, and the viscous dissipation rate of the turbulent kinetic energy ε. Where, in the standard k-ε model

$$\mu_t = \rho C_\mu \frac{k^2}{\varepsilon} \tag{2.25}$$

$$k = \frac{1}{2}\overline{u_i' u_i'} \tag{2.26}$$

and,

$$\varepsilon = \nu \overline{\frac{\partial u_i'}{\partial x_j}\left(\frac{\partial u_i'}{\partial x_j} + \frac{\partial u_j'}{\partial x_i}\right)} \tag{2.27}$$

In the derivation of the standard $k-\varepsilon$ model the flow was assumed to be fully turbulent, and the effects of molecular viscosity were neglected.

The estimates of Reynolds number in a typical clarifier suggest that the flow is largely quiescent and possibly laminar in some regions away from the influent but is significantly agitated and clearly turbulent within the stilling well. In its original high Reynolds number form, the standard $k-\varepsilon$ model uses logarithmic wall functions to adjust for the turbulence generation or dissipation in the near wall region. The correct application of these wall functions depends on the quality of the grid used for the model and, where very low local Reynolds numbers are encountered, or indeed where large variation in local Reynolds numbers are present throughout the system, it is difficult to correctly apply the standard model with wall functions. For this reason, an alternative low Reynolds number version of the $k-\omega$ turbulence model has been adopted for this work (Wilcox, 1994) where the turbulent eddy frequency is defined as,

$$\omega = \frac{\varepsilon}{k} \tag{2.28}$$

and the turbulence is related back to the momentum through the turbulent contribution to the effective viscosity where,

$$\mu_t = C_\mu f_\mu \rho_m \frac{k}{\omega} \tag{2.29}$$

with C_μ and f_μ being empirical constants of the model.

Although a clarifier is a multiphase system, there is no turbulence within the solid phase; therefore it is appropriate to think about k and ω as single phase scalar fields present as a continuum throughout the domain. Hence k and ω are not subscripted as either mixture or solid phase variables; rather they are the turbulence fields within the background liquid through which the solid phases may move. Two versions of the $k-\omega$ model were used in this work, the Low Reynolds number version of the

Wilcox turbulence model (Wilcox, 1994) and the Menter modified low Reynolds number $k-\omega$ model (Menter, 1994). The transport equations are as follows (CFX, 2001),

$$\frac{\partial}{\partial t}(\rho_m k)+\nabla\bullet(\rho_m \mathbf{U}_m k)-\nabla\bullet\left(\left(\mu_m+\frac{\mu_t}{\sigma_k}\right)\nabla k\right)=P_s+G_b-\rho_m\omega k \qquad (2.30)$$

$$\begin{aligned}&\frac{\partial}{\partial t}(\rho_m\omega)+\nabla\bullet(\rho_m\mathbf{U}_m\omega)-\nabla\bullet\left(\left(\mu_m+\frac{\mu_t}{\sigma_\omega}\right)\nabla\omega\right)\\&=C_1\frac{\omega}{k}(P_s+C_3\max(G_b,0))-C_2\rho_m\omega^2+D_m\end{aligned} \qquad (2.31)$$

where, P_s is the shear production term and G_b is the buoyancy production term for turbulence. C_1, C_2 and C_3 are all empirical constants ranging between 0 and 1, σ_k and σ_ω, are the turbulent Prandtl numbers and D_m is a complex expression, only present in the Menter modification, that forces the turbulence model to revert to a $k-\varepsilon$ form in regions outside of the low Reynolds number regions (CFX, 2001). All of the empirical constants have defined defaults apart from C_3 which is unknown for stratified flows (CFX, 2001).

Table 2.1: Constants used in the $k-\omega$ turbulence models.

Model	κ	C_μ	Re_T	f_μ	C_1	C_2	C_3	σ_k	σ_ω
Wilcox (1994)	0.4187	0.09	$\frac{\rho k}{\mu_m\omega}$	$\frac{-3.4}{e^{\left(1+\frac{Re_T}{50}\right)^2}}$	0.511	0.8333	0 to 1.0	2.0	2.0
Menter (1994)	0.4187	0.09	-	1.0	0.5411 or 1.44	0.8333 or 1.92	0 to 1.0	1.0 or 2.0	$\frac{\kappa^2}{(C_1-C_2)\sqrt{C_\mu}}$

Table 2.1 lists all of the constants used in the two alternative $k-\omega$ formulations, additional constants in the model are, κ, the Von Kármán constant and Re_t, the

local turbulent Reynolds number. The Wilcox model uses natural rather than synthetic wall boundary conditions with a linear approximation between the near wall node and the wall value (the wall value being zero for velocity) this approach requires a good quality grid in the near wall region. This differs from the more widely used $k-\varepsilon$ turbulence model where the log law of the wall is applied for all variables (CFX, 2001). The Menter modification allows the turbulence model to transition between the Wilcox form, where no wall laws are used, in low Reynolds flows into a $k-\varepsilon$ form, with wall functions, in high Reynolds number flows. This is shown in Table 2.1 where, for the Menter model, the empirical constants change according to the local flow conditions. Differences between the two models are explored in Chapter 4.

The shear production and dissipation P_s, is always included in this implementation of this turbulence model. It is also important to include the buoyancy term G_b, in turbulence production and dissipation otherwise the radial shear layer (see chapter 4) becomes diffuse

$$G_b = \frac{\mu_t}{\rho_m \sigma_p} \mathbf{g} \bullet \nabla \rho_m \tag{2.32}$$

A similar model (Lakehal, 1999) refers to the influence of C_3 on this aspect of the flow. However, in testing this idea, by varying the value of the C_3 parameter, it was difficult to observe any significant sensitivity to C_3. This is almost certainly because, in the CFX version of the $k-\omega$ turbulence model, a positive limit on the buoyancy dissipation source is set in equation (2.31) for omega.

2.5 Mixture Equations

At first sight, the equation set for the transport of the solid species through the turbulent background fluid appears to be a one way coupled model. That is the solids are directly convected and diffused by the momentum and turbulent fields but it is not immediately clear how the distribution of the solids species influences the development of the flow field. Unlike the full Eulerian-Eulerian multiphase model, the two way couplings in this model do not occur directly through source term exchanges, rather they occur through the constitutive relationships.

2.5.1 Equation of State

The relationship for mixture density may also be written (Zhou, 1992) as,

$$\rho_m = \rho_w + \sum_{k=1}^{n} X_k \left(1 - \frac{1}{Sg_k}\right) \tag{2.33}$$

where, ρ_w is the density of water and X_k is the solid phase concentration expressed in the same units as density (kg/m^3). This follows from the work of Larsen (1977) who found the specific gravity of dried activated sludge Sg_k, to be 1.445. The relationships between phase concentration X_k, mass fraction Y_k and volume fraction r_k, are particularly useful,

$$X_k = Y_k \rho_m = r_k \rho_k \tag{2.34}$$

so that mass fraction may be directly linked to volume fraction as,

$$Y_k = \frac{r_k \rho_k}{\rho_m} \tag{2.35}$$

Therefore, mixture density can be written in terms of solid phase mass fraction Y_k as,

$$\rho_m = \rho_w + \sum_{k=1}^{n} Y_k \rho_m \left(1 - \frac{1}{Sg_k}\right) \tag{2.36}$$

2.5.2 Hindered Settling

The relative slip velocity for the movement of the activated sludge floc within the background fluid must be calculated from an empirical relationship. For free flocs the slip velocity may be derived from drag relationships but many other model relationships exist for sludge settlement, (some of these are discussed in chapter 3). In this model, following the work of Lakehal (1999), Matko (1998), Armbruster (2003) and de-Clercq (2003), the empirical hindered settling velocity relationship proposed by Takács (1991) is used to represent the settling behaviour of activated sludge across a wide range of mixed liquor concentration. This relationship takes the form of a double exponential,

$$\mathbf{U}_{sk} = \left(V_o e^{-r_h(X_k - X_{ns})} - V_o e^{-r_p(X_k - X_{ns})}\right) \cdot \mathbf{x} \qquad (2.37)$$

where V_o is the free settling, or Stokes velocity, for a single floc in an infinite fluid; X_{ns} is the concentration of non-settleables usually expressed as some small percentage (0.2%) of the total clarifier influent concentration, X_F, (Armbruster. 2003), while r_h and r_p, are the free settling and colloid settling parameters respectively with units *(m^3/kg)*. These Takács parameters may be calculated directly from experimental techniques or by inferring their value from equivalent correlations for the Stirred Settled Volume Index (SSVI). Methods for calculating these Takács parameters will be discussed in detail in chapter 3.

2.5.3 Rheological Properties

By extending the drift flux model to include the rheological properties of sludge it is possible to represent the behaviour of the sludge bed in higher concentration zones. A significant increase in apparent viscosity in the high concentration regions causes the diffusive term of the momentum equation to become dominant and this can, in

the limit, reduce the mixture momentum to simulate thickening to the point where sludge can become stationary. The inclusion of a rheological function in the extended drift flux model also allows prediction of the sludge blanket height, within the clarifier, and the influence of scouring from the top of the settled blanket. However, in order to effectively describe the sludge blanket dynamics a suitable rheology model is required.

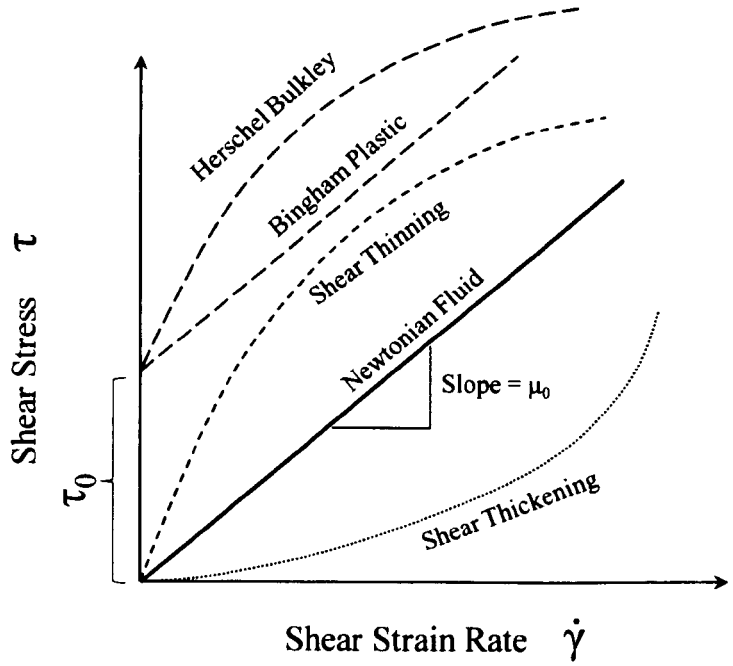

Figure 2.3: Representations of apparent material viscosity.
The viscosity of a Newtonian fluid is a constant with shear stress varying proportionally with shear strain. Activated sludges are usually shear thinning but may also have a yield stress.

Activated sludge exhibits a non-Newtonian behaviour where the magnitude of the shear strain rate $\dot{\gamma}$, does not vary proportionally with shear stress τ, as it does for a Newtonian fluid such as water. The most common non-Newtonian behaviour for activated sludge is shear thinning (Dawson, 2006) where viscosity reduces with increasing shear rate. The sludge apparent viscosity is the absolute ratio of shear stress magnitude to shear strain magnitude at any point on the curve, so for a Newtonian fluid, Figure 2.3,

$$\mu_m = \mu_0 = \frac{\tau}{\dot{\gamma}} \tag{2.38}$$

Where the magnitude of the strain rate tensor is given as,

$$\dot{\gamma} = \sqrt{\frac{1}{2}\dot{\gamma}_{ij}\dot{\gamma}_{ij}} \tag{2.39}$$

All activated sludge appears to exhibit a yield stress which must be exceeded if the sludge is to flow at all. A common model for a fluid exhibiting a yield stress is referred to as a Bingham plastic, figure 2.1,

$$\tau = \mu_0\dot{\gamma} + \tau_0 \tag{2.40}$$

where the gradient of the Bingham curve μ_0, is referred to as the plastic viscosity and the intercept is the yield stress τ_0. This can be rearranged as the apparent viscosity,

$$\mu_m = \frac{\tau_0}{\dot{\gamma}} + \mu_0 \tag{2.41}$$

For fluids that are shear thickening (dilatent) or shear thinning (pseudoplastic) the shear stress to shear strain relationship can be represented by a power law,

$$\tau = k_c\dot{\gamma}^n \tag{2.42}$$

where k_c is known as a consistency coefficient with units, $Pa.s^n$, and n is the dimensionless consistency index that can be rearranged for apparent viscosity as,

$$\mu_m = \mu_0\dot{\gamma}^{n-1} \tag{2.43}$$

where the plastic viscosity is itself some other function of the sludge mixture properties. A completely generalised expression for sludge based on Figure 2.3 is to

extend the Bingham plastic model to include an element of shear thinning (move the shear thinning curve up to intercept at the yield stress τ_0). This becomes the Herschel-Bulkley model,

$$\tau = \tau_0 + k_c \dot{\gamma}^n \tag{2.44}$$

which can be rearranged for apparent viscosity as,

$$\mu_m = \frac{\tau_0}{\dot{\gamma}} + \mu_0 \dot{\gamma}^{n-1} \tag{2.45}$$

The Herschel Bulkley model is the most complete physical representation for activated sludge but it is known that all models which include a yield stress will give a numerical inconsistency when applied in a CFD code. This occurs when near infinite apparent viscosity is calculated as the magnitude of the strain rate evolves to zero (de Clercq, 2003). In order to use any of the relationships for apparent viscosity proposed here it is necessary to define constitutive relationships for the yield stress τ_0 and the plastic viscosity μ_0. It is also required to find a way of avoiding the numerical inconsistencies that can occur with models incorporating a yield stress. These issues are discussed in chapter 3 of this thesis.

2.6 Flocculation Modelling.

The original ideas for modelling flocculation through the use of population balance were described by Smoluchowski (1917). The three modes of flocculation are well described in a review by Thomas (1999) as follows,

1. *Perikinetic*; where random thermal or brownian motion induces particle collisions and thus the opportunity for agglomeration.

2. *Orthokinetic*; in which imposed velocity gradients from the motion of fluid results in mixing across many scales, these turbulent mixing processes promote collision and agglomeration.
3. *Differential sedimentation*; where particles falling under gravity experience velocity gradients which may cause them to move towards each other also promoting collision and agglomeration.

Several possibilities exist for the modelling of flocculation. In the paper of Lyn et al (1992), a first attempt is made to model the activated sludge as separate size groups connected by source terms for orthokinetic flocculation. The thesis of Biggs (2000) gives a formal presentation of a flocculation model for activated sludge in a continuous stirred tank reactor (CSTR). Although it is possible to construct large population balance models with additional drift flux scalars or size groups, it is not clear that this approach can be made directly useful for a clarifier. This is mainly because the laws of coalescence and break up have to be dramatically simplified for the population balance approach to be computationally tractable, even when the system is limited to orthokinetic flocculation only.

In many of the population balance models for activated sludge flocculation (Wahlberg, 1994), an argument is made that the break up or coalescence of a given size group is driven by the local value of a scalar field known as the 'G scalar' (Camp and Stein, 1943) where [1],

$$G = \sqrt{\left(\frac{\partial u}{\partial y}+\frac{\partial v}{\partial x}\right)^2+\left(\frac{\partial u}{\partial z}+\frac{\partial w}{\partial x}\right)^2+\left(\frac{\partial v}{\partial z}+\frac{\partial w}{\partial y}\right)^2} = \sqrt{\frac{\rho_m \varepsilon}{\mu_m}} = \sqrt{\frac{\rho_m k\omega}{f_\mu \mu_m}} \quad (2.46)$$

[1] Note that the expression for G presented on the RHS of equation (2.46) is specific to the CFX-4 code as other CFD codes may have alternative expressions for turbulent viscosity in their implementations of the $k-\omega$ turbulence model

The equation for G appears to resemble $\dot{\gamma}$, the shear strain rate magnitude which is formed from the second invariant rate of strain tensor, a quantity already presented as part of the expression for determining the viscosity in a shear sensitive Non-Newtonian fluid in equation (2.39). Whereas $\dot{\gamma}$ is a valid construct of tensor mathematics, G is based on physical argument. The expressions for the two quantities are similar but G does not contain the higher order terms present in $\dot{\gamma}$ and is clearly not the same quantity. Cleasby (1984) and Clark (1985) have questioned the physical basis of G, in particular the use of apparent viscosity in equation (2.46) for inherently turbulent flows. The G scalar has been used by Argaman and Kaufman (1970) to develop source terms for orthokinetic flocculation and by Parker et al (1972) to develop shearing break up terms..

2.6.1 The G Scalar History Function

In this thesis, population balance modelling with CFD is not investigated, nor is the validity of the G scalar considered. Instead, the shear history of a floc stream line is proposed as a means of assessing whether a particular clarifier design satisfies the requirement to be a good flocculator. The use of G as a marker for flocculation is considered valid because Biggs (2000) provides a numerical bound for G where activated sludge break up and reformation occurs suggesting that G of around 19.4 s^{-1} enhances flocculation and $G > 113$ s^{-1} breaks flocs in an activated sludge systems. If it is accepted that the G-scalar does characterise the flocculation and break-up then a further question is how it should be modelled. The common assumption is that the floc sizes are determined locally by the degree of shearing. In fact, it should also be influenced by the history of the floc: the same value of G will have a different effect on a large floc than on a small one as they pass through the same location, and the

effect of a continuous period of high G will be different from the same total being applied intermittently, Biggs (2000).

It is therefore suggested that the Lagrangian particle tracking method may be used to assess flocculation capacity by following the paths of particles and determining the G scalar histories of those particles. Given an established steady state flow field for the fluid mixture, based on the extended drift flux model above, it is possible to construct an additional scalar field for local shear, or local G at each discrete computational cell. It is then possible to track stream lines (massless particles) through that field for the solids fraction based on the augmented momentum field $\mathbf{U}' = \mathbf{U} + \mathbf{U}_{sk}$. These tracks may be thought of as the motion of a floc convecting along a stream line and passing through a series of mixers (one in each computational cell) thus experiencing a G history. This can be done for a large number of particles and then it is possible to see what proportion of the incoming particles have a desirable G history. This post processing method would then show the shearing processes that take place within a clarifier and provide a useful tool for comparison of designs.

2.7 Conclusion

The flow within a clarifier may be represented by the homogeneous multiphase framework model augmented with experimental correlations and constitutive relationships for density, rheology and settling velocity and an appropriate low Reynolds number turbulence model. This extended drift flux model will yield mixture fluid momentum distribution and solids distribution within a clarifier when implemented in a CFD code. Additional post processing of the numerical solution, using Lagrangian particle tracking, may also be applied to determine the G scalar history which may in turn indicate the flocculating capacity of a system.

CHAPTER 3: Constitutive Relationships, Settling Tests and Mass Flux Theory

Summary

This chapter describes the constitutive relationships appropriate for representing the drift flux settling velocity $\mathbf{U}_{sk}$ and the mixture apparent viscosity μ_m, in the extended drift flux model for clarifiers. It also includes an explanation of the sources for the empirical coefficients required for the models and, for the case of settling, how these coefficients are related to the stirred specific volume index $SSVI_{3.5}$. This is particularly important as it is common to set an acceptable upper bound of $SSVI_{3.5}$ as one of the operational limits for a clarifier design. The work also briefly examines the validity of the Pitman (1980), White (1975), Wahlberg and Keinath (1988) correlations for settling tests performed on samples of activated sludges from the Swindon sewage treatment works (STW) in March and April of 2003. The data obtained from this test was later used in the analysis of a series of lock exchange experiments described in chapter 5 of the thesis. Finally, the mass flux theory (MFT), introduced in chapter 1, is explained in detail and the common links between MFT and CFD are established.

3.1 Introduction

The extended drift flux model for settling presented in chapter 2, includes constitutive relationships, or closures, for mixture density, settling velocity and viscosity. The simplest of these closures is the equation for mixture density,

expressed as a function of solids concentration, equation (2.36). This closure requires only one measured constant, the dried solids specific gravity. This was measured by Larsen (1977) using a lock exchange experiment and was determined as $Sg = 1.445$. However, close inspection of the Larsen data does show considerable spread between the lower and upper bounds of 1.3 and 1.6 (Tchobanoglous, 1991) . This constant is not discussed in further detail here and the standard value of 1.445 was used throughout the rest of this work.

The second closure relationship is required for settling velocity. In chapter 2, this was presented as the double exponential settling function of Takács (1991). The background for this model and the basis for its inclusion as the second constitutive relationship is discussed in detail in this chapter. It is important to note that the parameters for any settling model are based on experimental data and for activated sludge there is a wide body of knowledge on settleability based around the settling index concept presented in chapter 1.

The performance of an activated sludge plant (ASP) is so intrinsically related to the settleability of the sludge produced in the aeration lane that many different settling tests have been devised to assess this quality (Ekama, et al, 1997). Each of these tests has attracted its own index and related naming convention; in the UK the common tests are for the sludge volume index (SVI) or the stirred specific volume index (SSVI). In Europe it is more common to perform a different kind of settleability test which yields diluted sludge volume index (DSVI). All of these tests are intended to provide a standard index which may be used to calibrate the settling performance of a sludge against all other sludges across all waste water treatment works.

The connection between the various settling indices and the hindered settling velocity is made through the use of correlations based on the extensive survey work of Pitman (1980), White (1975), Wahlberg and Keinath (1988) and many others (Ekama et al, 1997). The connection between the settling index and the settling model parameters is particularly important and is explored in this chapter by examining data for the settlement of activated sludge at the Swindon sewage treatment works (STW) taken in March and April of 2003.

The third closure relationship for the extended drift flux model is for sludge viscosity, often referred to as the sludge rheology model. This closure is only used when it is required to represent the sludge bed dynamics. Several rheological functions have been proposed as general models for activated sludge but there is currently no accepted standard. Therefore, several published models have been implemented in this extended drift flux code and are compared throughout the work for their applicability in different situations. The models presented here are based on the experimental data of Bokil and Bewtra (1972), Dick and Ewing (1967), Dahl (1993), Armbruster (2003) and de-Clercq (2003).

Finally, mass flux theory (MFT) is presented at the end of this chapter only after the concepts of the settling model and the related correlations have been presented as these concepts are integral to the development of the mass flux and state point analysis technique.

3.2 Hindered Settling

The settling of suspensions at low solid fraction may be described by Einstein's formula for settling (Kynch, 1952).

$$V_s = V_o\left(1 - a\frac{X}{\rho_p}\right) \tag{3.1}$$

Where V_o is the settling velocity of a single particle in an unbounded flow, X is the solids concentration, ρ_p is particle solids density and a is a factor that incorporates particle shape. Another model, proposed by Richardson and Zaki (1954) for the "sedimentation of uniform particles (> 100.0 μm), sufficiently large for anomalous viscosity effects and flocculation to be negligible", is,

$$V_s = V_o\left(1 - \frac{X}{\rho_p}\right)^n \tag{3.2}$$

These settling functions are commonly used in the chemical process industries to model pneumatic and hydraulic conveying and for the settling of granular solids (Coulson and Richardson, 1968). However, where settlement is dominated by the hindered (Type 3) process (Ekama et al, 1997) or flocculation through differential sedimentation is occurring, then other settling functions are required, many of the functions appropriate for activated sludge have been reviewed by (de Clercq, 2006) and those commonly applied are,

The Vesilind (1968) equation,

$$V_s = V_o e^{-r_h \cdot X} \tag{3.3}$$

two functions proposed by Cho (1993),

$$V_s = a\frac{(1-bX)^4}{X} \tag{3.4}$$

$$V_s = a\frac{e^{-nX}}{X} \tag{3.5}$$

And the Takács (1991) equation,

$$V_s = V_o e^{-r_h(X-X_{ns})} - V_o e^{-r_p(X-X_{ns})} \tag{3.6}$$

where,

X : is the concentration of the mixed liquor, *g/l*

V_o : is the terminal settling velocity of a particle or floc, *m/h*

r_h : is the hindered settling coefficient, m^3/kg

r_p : is the free particle or colloid settling coefficient, m^3/kg

X_{ns} : is the hindered settling coefficient, *g/l*, nominally 0.2% of X_F

and, a b and n are empirical coefficients.

The two constants V_o and r_h are collectively referred to as the Vesilind coefficients while the constants V_o, r_h, r_p and X_{ns} are collectively referred to here as the Takács parameters.

This single exponential (Vesilind, 1968) form is applicable only to the hindered zone or sludge line settling where a discrete interface can be seen between the settling solids and the clear supernatant. The extension of the Vesilind model into a double exponential expression by Takács (1991) is required in order to represent the settling velocity over a large range of concentrations; particularly at low concentrations when the settling velocity is thought to become very small (ultimately becoming zero at X_{ns}). The alternative equations defined by Cho (1993) are similar to the Vesilind form and in a review by Vandershasselt and Vanrolleghem (2000) of the batch settling process for activated sludge, the Takács model was considered to provide the best representation for V_s over the largest range of X. Therefore, in keeping with

many other workers who have applied CFD to clarifier modelling, including Matko (1998), Lakehal (1999), Armbruster (2003) and de-Clercq (2003), the Takács (1991) model, equation (3.6), has been used to determine the drift flux settling velocity throughout this work.

It should be noted that whereas the Vesilind model is almost exclusively used for 1D mass flux theory (Ekama et al, 1997), the Takács model has become an accepted standard for more advanced 1D dynamic models of the activated sludge process (EnviroSim, 2007).

3.2.1 Extending the Settling Model to Low and High Concentrations

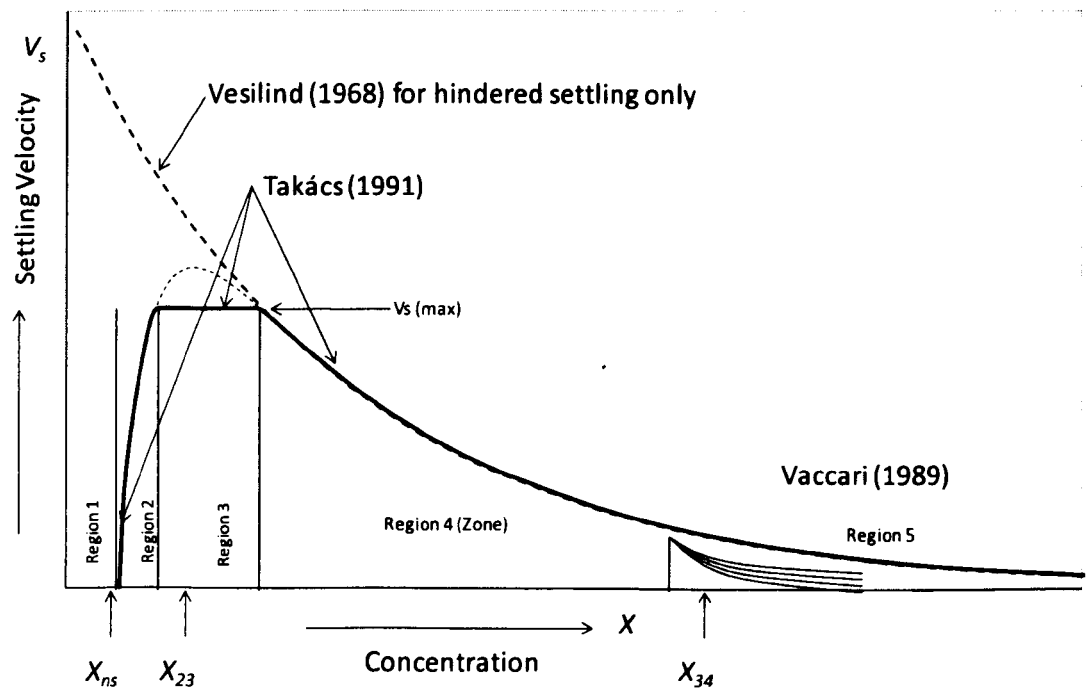

Figure 3.1: The Takács settling model applied across the full concentration range.

The transition from flocculent to hindered settling occurs at X_{23} and from hindered to compression at X_{34}

The extensions proposed by Takács (1991) are presented in greater detail in Figure 3.1, where, instead of describing the settling modes as Types 1 to 4 (Matko, 1998), five regions are defined. In Region 1, the solids concentrations below X_{ns} are so low

that they are deemed to be non settleable. Physically, these are the solids that will inevitably pass through the settler out to effluent. Region 2 is the low concentration range where the particles do start to settle and this includes both discrete (type 1) and flocculent (type 2) settling where the solids of different size classes bind together and form agglomerates which may then settle at differential rates to each other. Region 2 terminates at the fixed maximum settling velocity for a free floc, X_{23}. Region 3 is a transition zone between flocculent and hindered settling. Region 4 is the zone or hindered settling (type 3) region where a clear interface is observed between the settling bed and the clarified supernatant. In Figure 3.1 an additional region 5 is also included which follows the work of Armbruster (2003); this shows that above a certain concentration the settling bed transitions into a compressive mode (type 4) where the Takács model overstates the settling velocity. In this region the settlement velocity dramatically falls and a family of curves is proposed depending on the concentration gradient within the bed (Vaccari, 1989). Although this compression model has been investigated by Armbruster (2003) it was not implemented in this work.

3.2.2 Application of the Hindered Settling Models

In order to apply the Vesilind model for mass flux calculations and the Takács model as a closure for the extended drift flux model, it is necessary to calculate the Takács parameters. Most usefully, these parameters can be directly related to well established correlations for sludge settleability. The following sections explain how this connection is made and illustrates the calculation of the parameters from an experimental method.

3.3 Settling Tests for the Stirred Specific Volume Index, $SSVI_{3.5}$

In the United Kingdom the most commonly applied settlement calibration test is the water research council (WRc) test (White, 1975) and it is used to establish the SSVI of the sludge. This test relies on the assumption that all sludges in the UK have a similar biological make up and exhibit similar sludge line settling characteristics. This assumption was found to be broadly true by Pitman (1980) and White (1975, 1976). For the purposes of generalising for all sites, the SSVI is quoted for a sample with initial mixed liquor concentration of 3500 mg/l, and thus the SSVI value is subscripted as $SSVI_{3.5}$

3.3.1 The WRc Settling Test

The WRc test is performed in a 4 litre column, 100 *mm* diameter and 500 *mm* in height; with a slow speed stirrer (1 *rev/min*) used to prevent the sludge bridging or binding to the wall. Equipment to perform SSVI tests can no longer be obtained directly from the WRc but several suppliers exist[2].

[2] The SSVI equipment used for this work was obtained from Triton Electronics, Bigods Hall, Dunmow, Essex, CM6 3BE; www.tritonel.com/ssvi/index.htm

Figure 3.2: The WRc settling test performed at Swindon STW.
The slowly revolving stirrer prevents the flocs bridging to the wall. The Triton equipment is shown on the right.

Mixed liquour (MLSS) samples are obtained at the site by suspending a bucket at the aeration lane effluent weir. The bucket samples are the baseline MLSS at unknown solids concentration X_F. Once returned to the laboratory, the mixed liquor is stirred to homogenise the samples which are then poured into columns where the process of settling may be observed and characterised. In the WRc test, the interfacial position of the settling sludge blanket is recorded only at the end of a 30 minute period. The ratio of the final settled sludge volume to the initial volume is then used to determine the SSVI which is defined as the volume in *ml* of settled bed containing 1*g* of solids, equation (1.1). Note that the SSVI progresses faster than the equivalent sludge volume index (SVI) experiment where no stirrer is used and therefore the two tests yield different settling indices.

The test is performed at several different initial MLSS concentrations and the resulting range of SSVI data is extrapolated or interpolated for the 3500 *mg/l* value. One complexity of this activity is that concentration can only be measured by drying a filter paper sample over 24 hours and so tests are carried out by either diluting the mixed liquor at X_F with supernatant (decanted from another settled sample) or by mixing concentrated MLSS in known ratios. In this way the same settling test can be readily performed at concentrations from less than $0.5X_F$ up to $> 3X_F$, an additional settlement test with a return activated sludge (RAS) sample is sometimes performed where the RAS concentration is usually between 6 and $10X_F$. It is important to note that the initial MLSS concentration does have a significant impact on whether sludge line settling is observed, that is where the sludge to supernatant interface is clearly visible, as shown in Figure 3.2. At low concentrations, usually with initial MLSS less than 1500 mg/l, the larger sludge flocs tend to settle preferentially and the clear zonal interface is not so easily seen (IWA, 2008).

The settling index is an indicator of the overall performance of the aeration lanes and it is common to group the characteristics of sludge in terms of an SSVI range. Von Sperling (1994) groups sludges as good, fair or poor (Table 3.1) and when designing a new settlement tank it is usually required to ensure that any clarifier will perform adequately for the required site throughput up to an upper bound $SSVI_{3.5}$ of 120 *ml/g*.

Table 3.1: Criteria for sludge settleability following Von Sperling (1994)

SETTLEABILITY	Representative Ranges and Values of the Settleability Indices (*ml/g*)	
	SVI	$SSVI_{3.5}$
Good	50 – 100	40 – 80
Fair	100 – 200	80 – 140
Poor	200 – 300	140 – 200

Another upper bound marker is given by the CIWEM handbook for activated sludge treatment (CIWEM, 1997) which states that an SVI index of above 180 would indicate a bulking condition and therefore the likely loss of significant quantities of solids with the effluent.

3.3.2 Direct Measurement of the Vesilind Coefficients V_o and r_h

The Vesilind coefficients can be determined for a sludge sample by direct measurement using the same test equipment that is applied for the basic WRc thirty minute SSVI test. In order to illustrate the method of direct measurement three settling tests were performed at Swindon STW in March to April 2003 as part of an assessment of the behaviour of a collapsing sludge column in a lock exchange (see chapter 5).

For initial mixed liquor concentrations of X = 4275, 4720 and 5500 *mg/l* and an initial time t = 0.0 s, the falling sludge interface (shown in Figure 3.2) was recorded at regular time intervals, initially at 30 seconds when the interface was fast moving and then at 1 minute intervals thereafter. Plots of the interfacial position with time were recorded for three tests, Figure 3.3a, and the gradients of these curves were measured to give the velocity for the zone settling phase, Figure 3.3b. Finally the settling velocity vs concentration was plotted on a natural-log - linear scale, Figure 3.3c. The gradient and intercept of this curve provided the Vesilind coefficients. It should be emphasized that the final step of fitting a straight line to the data for the Vesilind coefficients is very approximate in this case and normally this experiment is perfomed for eight or more initial concentrations (Ekama, 1997). In addition, the final position of the interface was noted at the end of 30 minutes and the SSVI was determined from equation (1.1) for each initial concentration, the $SSVI_{3.5}$ value was

then extrapolated from these values. The measured Vesilind coefficients, obtained from the graphical method, and the final measured $SSVI_{3.5}$ are shown in Table 3.2.

Table 3.2: Vesilind coefficients and $SSVI_{3.5}$ measured at the Swindon STW, April 2003 based on three samples only.

V_o (m/h)	r_h (m^3/ kg)	$SSVI_{3.5}$ (ml/g)
10.638	0.4125	64

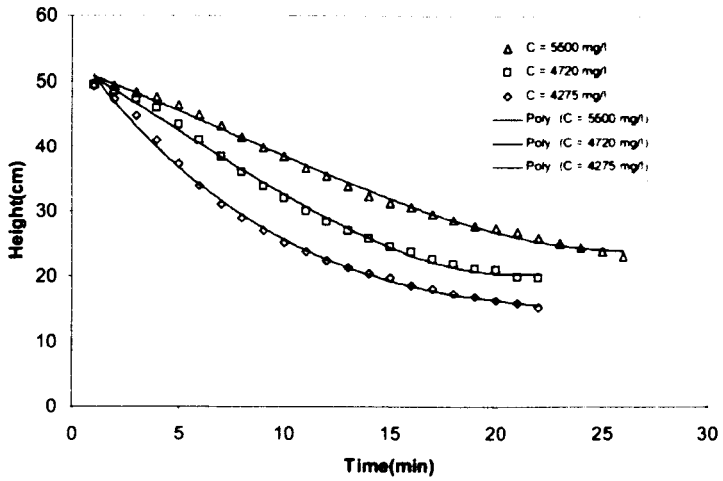

a) Hindered settling curves for three different initial concentration.

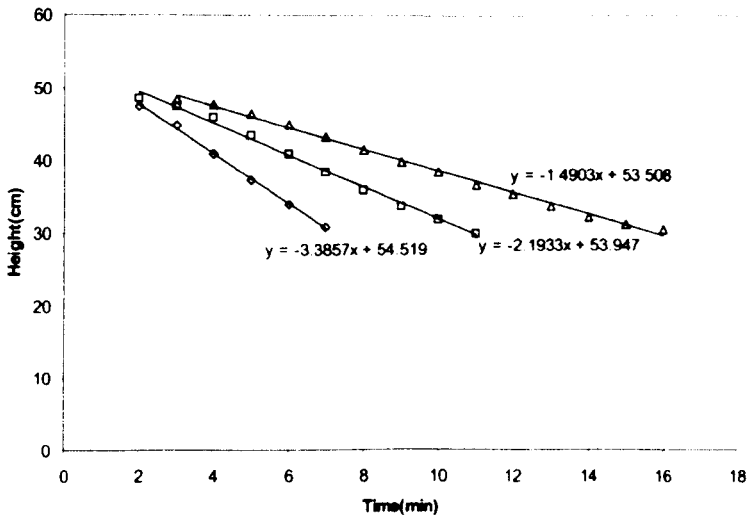

b) Tangents to the curves approximate rate of change with time of the falling interface

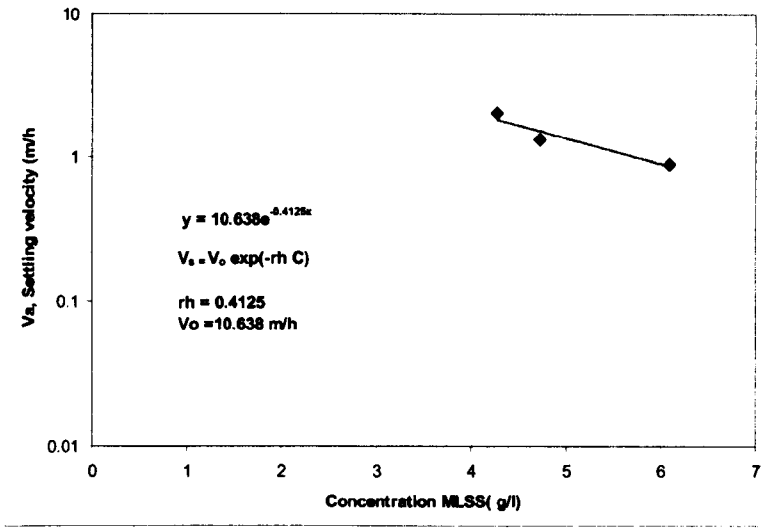

c) Rate of change plotted against initial concentration on log scale

Figure 3.3: Vesilind coefficients calculated from WRC settling tests at the Swindon STW in April 2003.
Performed for three initial concentrations only, 4275, 4720 and 5500 *mg/l.*

3.3.3 Relationship between $SSVI_{3.5}$ and the Vesilind Coefficients.

There are several empirical correlations that relate the Vesilind coefficients to the measured settling indices such as SVI, SSVI and DSVI. A full presentation of this theory and the range of possible empirical correlations are surveyed in Ekama et al (1997). These relationships were obtained by repeatedly performing the settling tests described above at many different sites. The Pitman (1980) data for instance is based on over six years worth of testing from four sites (Ekama et al, 1997) and the White (1975,1976) data is amalgamated from measurements at thirty sites in the UK, (Ekama et al, 1997). The Pitman and White correlations for relating $SSVI_{3.5}$ to the Vesilind coefficients are,

$$\frac{V_o}{r_h} = 67.9 \times e^{(-0.016 SSVI_{3.5})} \tag{3.7}$$

$$r_h = 0.88 - 0.393 \log(V_o / r_h) \tag{3.8}$$

Another commonly used correlation, validated for twenty-one activated sludge plants in the USA, is given by Wahlberg and Keinath (1988) and also relates the Vesilind coefficients to $SSVI_{3.5}$.

$$V_o = 15.3 - 0.0615 \times SSVI_{3.5} \tag{3.9}$$

$$r_h = 0.436 - 0.00384 SSVI_{3.5} + 0.0000543 \times (SSVI_{3.5})^2 \tag{3.10}$$

The Vesilind coefficients may therefore be obtained for a known or specified $SSVI_{3.5}$. However, not all sludges sampled will fit these correlations and, where there is uncertainty, it is more reliable to obtain the Vesilind coefficients directly using the interface tracking test described above.

3.3.4 Comparing Correlations with Direct Measurement of V_o and r_h

It is particularly instructive to compare the two correlations for the Vesilind coefficients with the directly measured $SSVI_{3.5}$ by constructing flux curves.

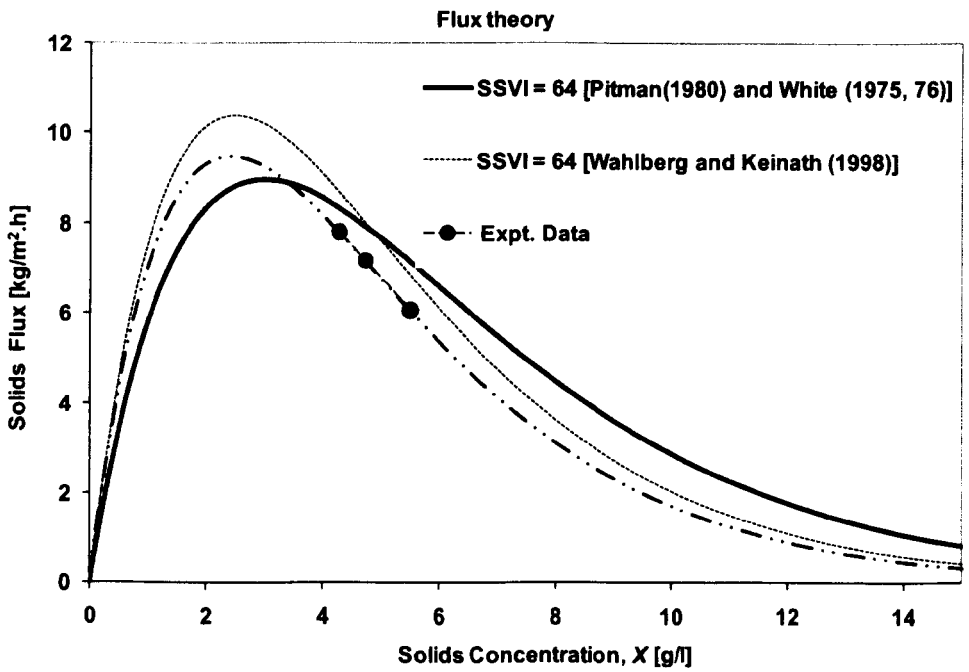

Figure 3.4: Flux curves for the Swindon data comparing the Pitman and White (1975) and Wahlberg and Keinath (1988) correlations for the measured value of $SSVI_{3.5}$=64 *ml/g*

The procedure for doing this is to use the measured Vesilind coefficients from Table 3.2, the Vesilind function, equation (3.3) and the flux equation (1.3) to give the curve marked as experimental data in Figure 3.4 (the three data points are also indicated). Also plotted on the same graph are the flux curves based on calculating the Vesilind coefficients from the Pitman and White equations (3.7) and (3.8) and the Wahlberg and Keinath equations (3.9) and (3.10) using the directly measured value of $SSVI_{3.5}$=64 *ml/g*. What this shows is that the direct measurement of the Vesilind coefficients yields a slightly different answer than the direct measurement of the SSVI and, in this case, it appears that the Swindon sludge is a better fit to the Wahlberg and Keinath correlation; accepting that this observation is based on very limited data.

3.3.5 Fitting the Takács Model to a Known $SSVI_{3.5}$.

The correlations from Pitman, White and others make the connection between SSVI and the hindered settling velocity. This is a very important connection as it allows $SSVI_{3.5}$ to be used as a design parameter as long as the sludge, for a particular STW, is known to follow the correlation selected. When using the extended drift flux model for design it is necessary to convert the single $SSVI_{3.5}$ index into a valid parameter set for the Takács model. The constants used by other workers for the representation of the Takács activated sludge settling relationship are shown in Figure 3.5 and in Table 3.3 for comparison.

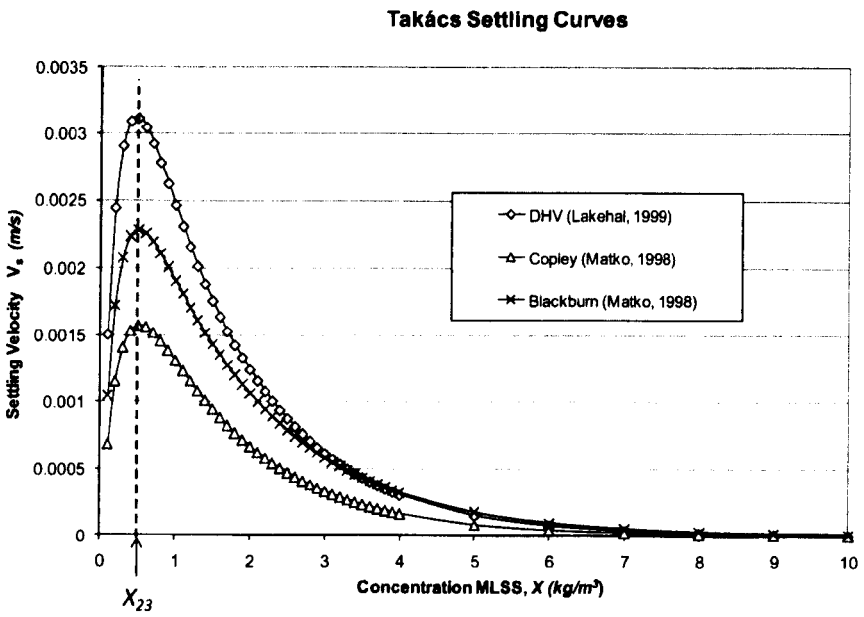

Figure 3.5: Takács settling curves for activated sludges, taken from Lakehal (1999), and Matko (1998).

Table 3.3: Range of Takács constants for settling curves shown in Figure 3.5.

Data Source	V_o (m/hr)	r_h (m^3/kg)	r_p (m^3/kg)	X_{ns} (kg/m^3)
Lakehal (1999)	18	0.7	5.0	0.01
Copley from Matko (1998)	9.73	0.703	4.2	0.01
Blackburn Meadows from Matko (1998)	12.64	0.6	4.8	0.01

These representations show a peak settling velocity at the transition from flocculent to hindered settling, X_{23} , in the region of 500 *mg/l* (Matko, 1998). Further to this Armbruster (2003) states that X_{ns}, the concentration of non-settleables, is typically 0.2% of the MLSS at influent and the colloid settling parameter r_p should vary between 3 and 9.

For the purposes of providing coefficients for design calculations it was found useful to create a family of Takács curves for sludges in the range quoted by Von Sperling (1994) as typical for the UK. To do this, equations (3.7) and (3.8) (or (3.9) and

(3.10)) were used to calculate V_o and r_h. X_{ns} was fixed at 0.01 *mg/l* and the value of the colloid settling parameter r_p was varied between 3 and 9 so that the peak settling velocity occurred at the flocculent to hindered transition concentration, X_{23} = 0.5 kg/m^3, for all $SSVI_{3.5}$ values. The result of this process is shown in Figure 3.6. Particular emphasis should be given to the parameters derived for the curve of $SSVI_{3.5}$ =120 *ml/g*, as this becomes the standard design curve. That is, where a design is required to meet a certain process flow duty for an activated sludge settleability limit of $SSVI_{3.5}$ =120 *ml/g*, it is assumed that the sludge follows the correlation of Pitman (1980) and White (1975) as fitted to the Takács curve in Figure 3.6 following the guidance of Matko (1998) and Armbruster (2003).

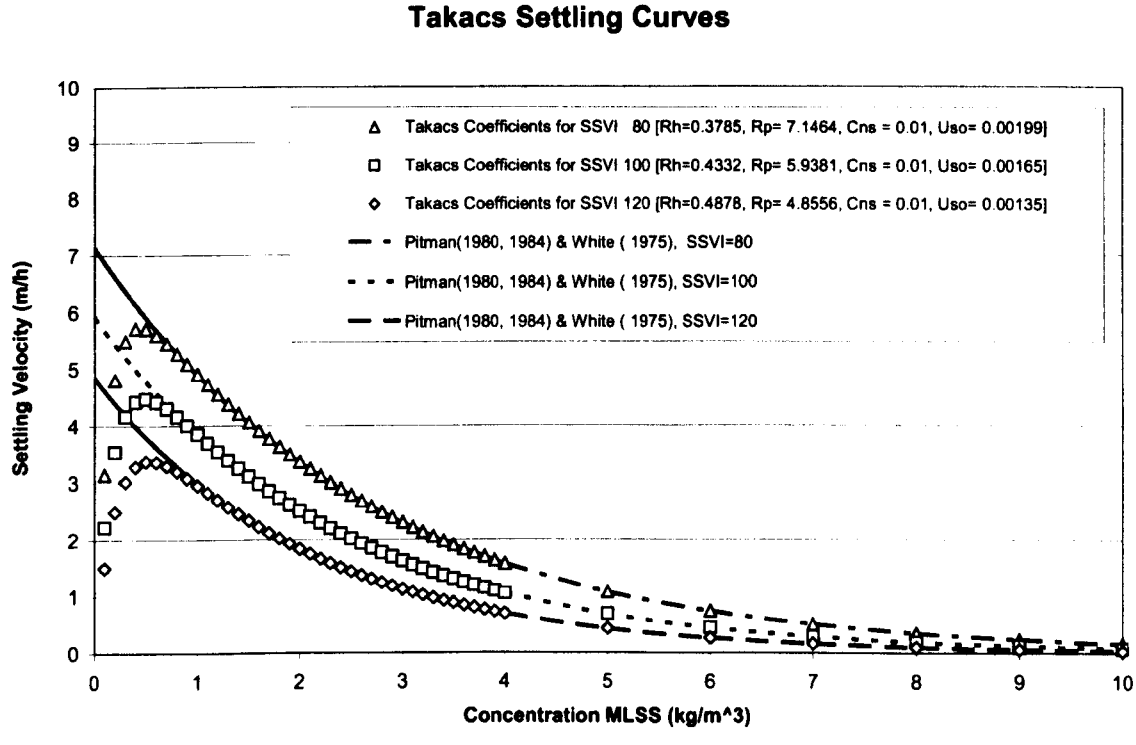

Figure 3.6: Takács settling curves fitted for $SSVI_{3.5}$ = 80 to 120 compared with Vesilind curves for the same range.
Note that the value of r_p is varied between 3 and 9 to give a peak settling velocity at the flocculent to hindered transition, X_{23} =500 *mg/l*.

3.4 Rheology

In chapter 2, activated sludge was described as a non-Newtonian fluid where the magnitude of shear stress does not vary in proportion with shear strain. The apparent viscosity may be made up of a plastic component, being some function of local concentration, and a limiting yield stress / strain rate component where the limiting yield stress must be exceeded before the sludge will move.

3.4.1 The Standard Model (Bokil and Bewtra, 1972).

A first model for rheology is due to Bokil and Bewtra (1972) which makes the apparent viscosity a straight line function of solid phase concentration on a log scale.

$$\mu_m = \frac{\tau}{\dot{\gamma}} = 0.00327 \times 10^{0.132X} \tag{3.11}$$

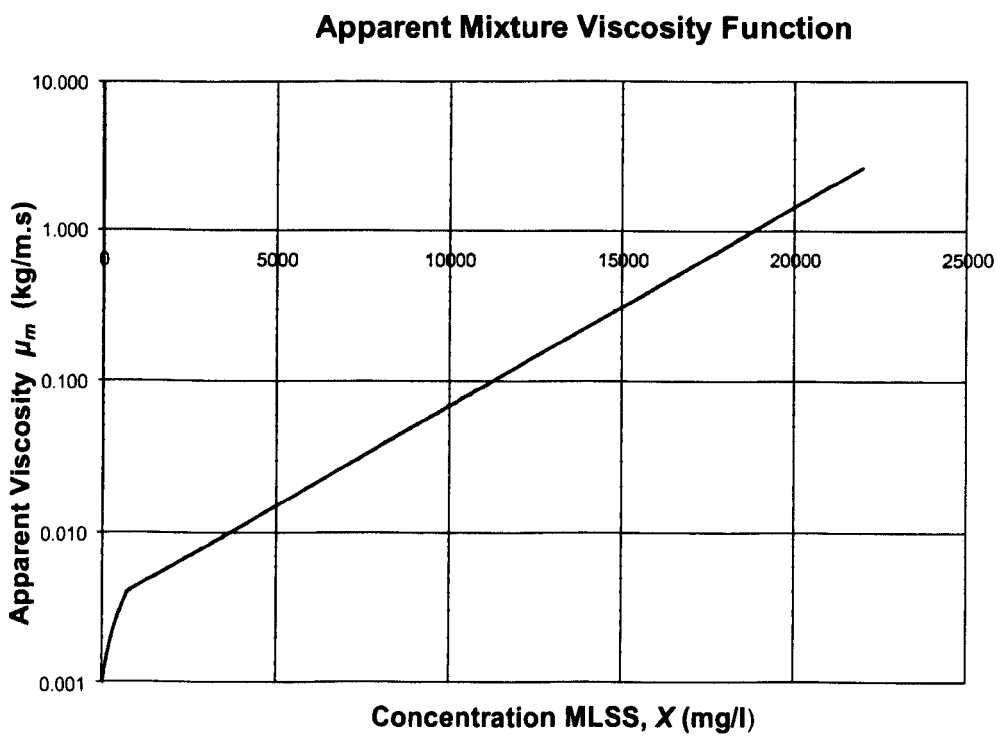

Figure 3.7: Mixture viscosity relationship taken from Bokil and Bewtra (1972) and modified at low concentration (<700 mg/l) by Lakehal (1999).

This simple relationship is based on measurements for sixty five samples but with considerable spread in the data ($R^2 = 0.854$). The data is only valid for concentrations greater than 700 *mg/l* and so Lakehal (1999) compensated for this by introducing a linear fit between the viscosity of clear water and the starting point for the curve of equation (3.11) at 700 *mg/l*. This can be seen in the bottom left of Figure 3.7. Despite the relative simplicity of this model it has been very widely used, particularly by McCorquodale and co-workers (Zhou, 1992).

3.4.2 A Plastic Viscosity Model (Dahl, 1993), (Armbruster, 2003).

An expression for activated sludge plastic viscosity was originally proposed by Dahl (1993) and fitted by Lakehal (1999) as the sum of the water viscosity and a quadratic fit to concentration,

$$\mu_0 = \mu_w + c_{pa} \cdot c_{pl} \cdot (X - X_{ps})^n \qquad (3.12)$$

Armbruster (2003), proposed other coefficients for equation (3.12) to give alternative square or root functions for apparent viscosity as a plastic viscosity only with no yield stress dependent component.

Table 3.4: Fitted coefficients for plastic viscosity in equation (3.12)

Data Source	c_{pa} *[-]*	c_{pl} *[(m5/(kg·s^2)]*	X_{ps} *[kg/m^3)]*	n *[-]*
Lakehal (1999)	1.0	2.473E-4	0.0	2
Armbruster Square Law (2003)	25	2.473E-4	4.5	2
Armbruster Root Law (2003)	450	2.473E-4	4.5	0.5
DeClercq (2003)	1.0	2.49338E-4	0.0	2

3.4.3 A Bingham Plastic Model (Lakehal, 1999)

Lakehal (1999) also proposed that activated sludge could be modelled as a Bingham plastic. This is a reasonable assumption, also discussed in chapter 2, as it is observed in experimental work (see chapter 5) that a sludge bed can remain stationary even

when the fluid above the bed is moving at significant velocity. The apparent mixture viscosity (also equation 2.41) is now expressed with a yield stress component and a plastic component (from equation 3.12)

$$\mu_m = \frac{\tau_0}{\dot{\gamma}} + \mu_0 \tag{3.13}$$

where the constitutive relationship for plastic yield stress τ_0 is given by Dick and Ewing (1967) as,

$$\tau_0 = \beta_1 e^{\beta_2 X} \tag{3.14}$$

The yield stress relationship for activated sludge is an important concept which was originally investigated extensively by Dick and Ewing (1967) for three sites in the United States. Measured plant data is shown in Figure 3.8 with fit parameters to equation (3.14) tabulated according to the different sources in Table 3.5.

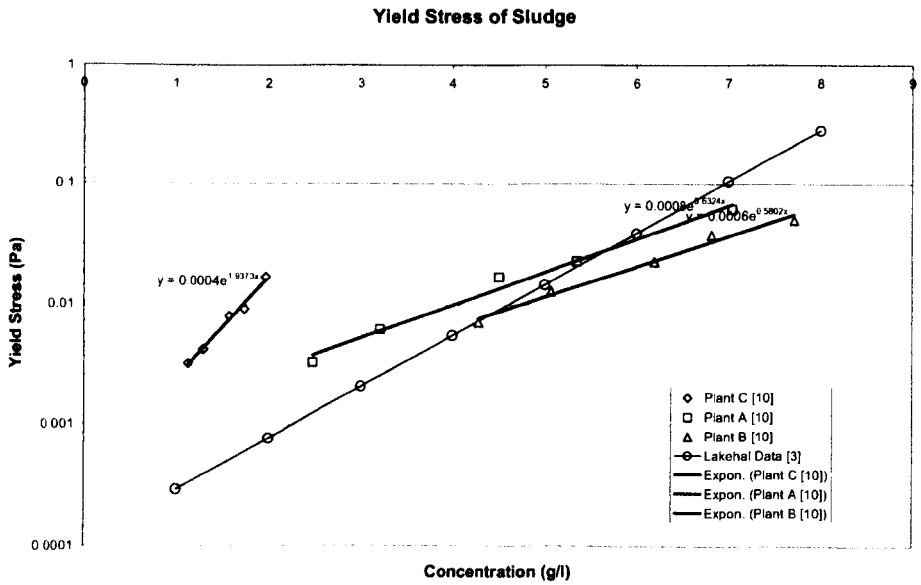

Figure 3.8: Plant data for activated sludge yield stress as a function of concentration, equation (3.14), fitted to data from Dick and Ewing (1967)

Table 3.5: Fitted coefficients for yield stress in equations (3.14)

Data Source	β_1 *[kg/m·s²]*	β_2 *[m³/kg]*
Plant A, Dick (1967)	7.9E-4	0.632
Plant B, Dick (1967)	6.4E-4	0.580
Plant C , Dick (1967)	3.5E-4	1.937
Lakehal (1999)	1.1E-4	0.980

Dick and Ewing (1967) also suggested that activated sludge was thixotropic and observed that for the same three sets of plant data the viscosity reduced with time in the same rheometer test suggesting that "activated sludge possesses some internal structure that is broken down with shear".

3.4.4 A Modified Herschel Bulkley model (de Clercq, 2003)

De-Clercq (2003) proposed modifications to equations (3.13) and (3.14) to give a Herschel Bulkley like relationship,

$$\mu_m = \frac{\tau_0}{\dot{\gamma}}(1 - e^{(-m\dot{\gamma})}) + \mu_0 \dot{\gamma}^{n-1} \tag{3.15}$$

Where m is the stress growth component and has units of time. The term, $(1 - e^{(-m\dot{\gamma})})$ was originally proposed by Papanstasiou (1987), and is a smoothing function which prevents sudden discontinuous rises to very high apparent viscosity when the shear strain rate becomes very low.

The alternative power law function for the yield stress proposed by de-Clercq is,

$$\tau_0 = \beta_1 \left(\frac{X}{\beta_3} \right)^{\beta_2} \tag{3.16}$$

Table 3.6: Experimentally derived constants for (3.15) and yield stress (3.16)

Data Source	m *[s]*	n *[-]*	β_1 *[kg/m·s²]*	β_2 *[-]*	β_3 *[kg/m³]*
de Clercq (2003)	163.4	0.777	9.036E-4	1.12	1.0

The plastic viscosity, μ_0, on the RHS of equation (3.15) still follows the Dahl (1993) expression as given by (3.12). All of coefficients derived by de-Clercq (2003) were

obtained by fitting to data from three sites (Destelbergen, Ossemeersen and Lokeren) in Belgium.

3.5 Mass Flux Theory

The standard method for designing a secondary settlement tank is mass flux theory (MFT), or state point analysis. This technique uses a one dimensional settling model and so cannot take account of any density current flow pattern present in the tank (Anderson, 1945). Mass flux theory allows a designer to investigate the relationship between four main process parameters, waste water flow rate Q, solids at the clarifier influent, X_F, the recycle ratio, R and the sludge settleability, $SSVI_{3.5}$ for a given tank surface area A_{st}; these boundary relationships are shown schematically in Figure 3.9.

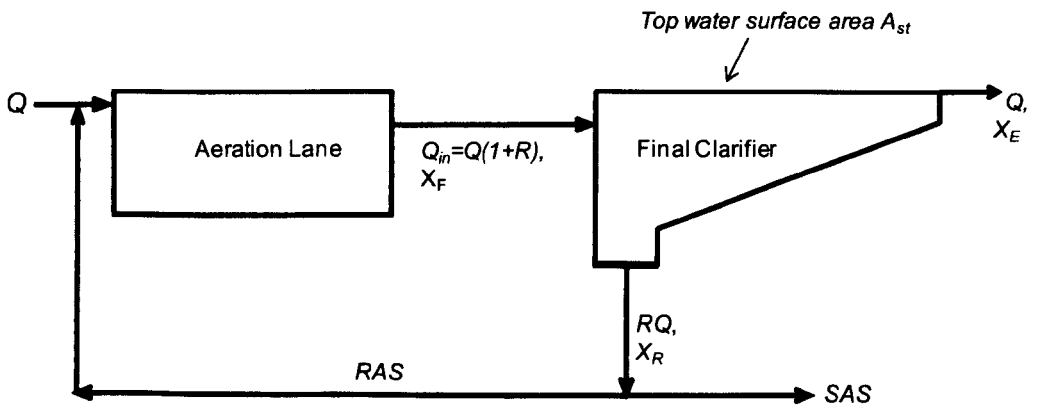

Figure 3.9: Schematic diagram of the activated sludge plant (ASP) showing the boundary values for mass flux theory.
Note that the surplus flow (SAS) is generally ignored in the analysis.

The mass flux method can either be used to check whether a tank of a fixed surface area is able to meet duty for a particular set of process conditions or, the method can be used to design a new tank where the required tank area is calculated to meet the process flow and load requirements.

3.5.1 Limitations

Mass flux is very a useful first pass sizing method but it is not reliable, even if a tank design satisfies the mass flux criteria it may still fail, or perform poorly in reality or when analysed with an equivalent CFD model. Short-circuiting of the influent flow, scouring of solids and re-entrainment of solids into the re-circulating flow pattern can all contribute to a high effluent suspended solids (ESS) concentration or a complete failure with overflow of the sludge blanket. All of these flow features cannot be investigated with mass flux theory.

3.5.2 Definition of Flux

The first concept of the model is that flux due to gravity settling of solids through water is given as the product of the solids concentration and the settling velocity. This was introduced in chapter 1, equations (1.3). By using the Vesilind equation (3.3), for hindered settling the flux becomes

$$j_s = X.V_o e^{-r_h X} \qquad (3.17)$$

where the units of flux are $kg/m^2.h$. The flux curve can therefore be plotted as a function of concentration for any value of $SSVI_{3.5}$ given knowledge of the Vesilind coefficients from equations (3.7 to 3.10) or other correlations (Ekama et al, 1997). This was shown for the Swindon sludge in Figure 3.4.

The following mass flux design method is in fact as a number of criteria all based around the flux concept and all of which must be satisfied for a tank design to be compliant at a given process condition. Elements of the mass flux assessment can also be plotted graphically as a state point graph which provides a visual confirmation of the tank performance.

3.5.3 Criterion Ia: Solids Capacity

The first mass flux criterion states that the clarifier must not be overloaded in thickening; there is a limiting rate of the solids flux that can pass to the bottom of the clarifier j_L, and the solids flux applied to the tank j_{QF}, must always be less than the limiting flux;

$$j_L \geq j_{QF} \tag{3.18}$$

(Sometimes the limiting flux j_L, is referred to as the maximum solids flux, j_{QF_m}). The solids flux applied to the tank is given by:

$$j_{QF} = X_F Q_{in} / A_{st} \tag{3.19}$$

The limiting flux is given by the WRc procedure (White, 1975 and 1976) as derived from equations (3.7) and (3.8),

$$j_L = 8.85(100/SSVI_{3.5})^{0.77}(R.Q/A_{st})^{0.68} \tag{3.20}$$

Where X_F is the feed mixed liquor concentration in kg/m^3, $Q_{in} = Q(1+R)$, is the total flowrate into the clarifier in m^3/h, R is the recycle ratio, Q is the clarifier effluent flow also in m^3/h and A_{st} is the surface area of the clarifier available for settling in m^2. Physically, if this limit is exceeded the flux of the sludge into the tank will be too great, the sludge blanket will build up past the top water level and a sludge blanket spill will occur.

3.5.4 Criterion Ib: Underflow limit

There is also a critical underflow, $R.Q$ for which equation (3.20) is valid and if this value of underflow is exceeded then the basis for the mass flux method (White,

1975) is no longer valid. These critical underflow limits are given by Ekama et al (1997),

$$R.Q \leq 1.612 - 0.00793 \times SSVI_{3.5} \tag{3.21}$$

when $SSVI_{3.5} < 125$ *ml/g* and,

$$R.Q \leq 1.612 - 0.00793 \times SSVI_{3.5} + 0.0015(SSVI_{3.5} - 125)^{1.115} \tag{3.22}$$

for $SSVI_{3.5} > 125$ *ml/g*.

3.5.5 Criterion II: Hydraulic Loading

The second criterion states that the clarifier must not be overloaded in clarification, that is the hydraulic loading rate must not exceed the sludge settling velocity, this concept has its root in the very earliest settling design tank work of Hazen (1904). Assuming sludge settling velocity is a unique function of the solids concentration;

$$\frac{Q}{A_{st}} \leq V_0 e^{(-r_h.X)} \tag{3.23}$$

where V_0 and r_h are the Vesilind coefficients. This ratio is also known as the surface over flow rate, $q_A = Q / A_{st}$. Physically, if this limit is exceeded the sludge will be convected through the clarifier at too fast a rate and will have insufficient residence time to settle effectively. Therefore, the sludge blanket will be driven to the top water level and a sludge blanket spill will occur.

3.5.6 Criterion III: Volumetric Loading Rate

This criterion is set as part of the German ATV131 (ATV-DWK, 2000) guidelines: it is the product of the solids loading rate and the sludge SSVI. The volumetric loading rate, $q_{SV} = Q_{SV} / A_{st}$, should be less than 500 $l/m^2.h$

$$\frac{Q_{SV}}{A_{st}} = X_F . \frac{Q_{in}}{A_{st}} . \left(\frac{4}{3} SSVI_{3.5} \right) \tag{3.24}$$

Physically, the concept behind this criterion is that the total amount of sludge in the volume of the tank should be kept to a level which will limit the amount of solids escaping to the effluent weir. If this limit is exceeded the tank may not necessarily fail with a blanket spill but the effluent suspended solids (ESS) may be too high to meet regulatory requirements (ATV, DVWK, 2000).

3.5.7 Criterion IV: Weir loading Rate

This is the effluent flow rate per length of overflow weir and provides a guide to the flow velocities in the vicinity of the weir. Typically, the value of weir loading rate is kept below 10 $m^3/h.m$; however, for light or diffuse sludges this is sometimes reduced to 5 $m^3/h.m$ (Ekama et al, 1997). Weir loading rate is of secondary importance to criteria I, II and III.

3.5.8 State Point Analysis

The requirements for Criteria Ia and II can also be checked visually by plotting the operational state point on the axes of concentration and flux as follows.

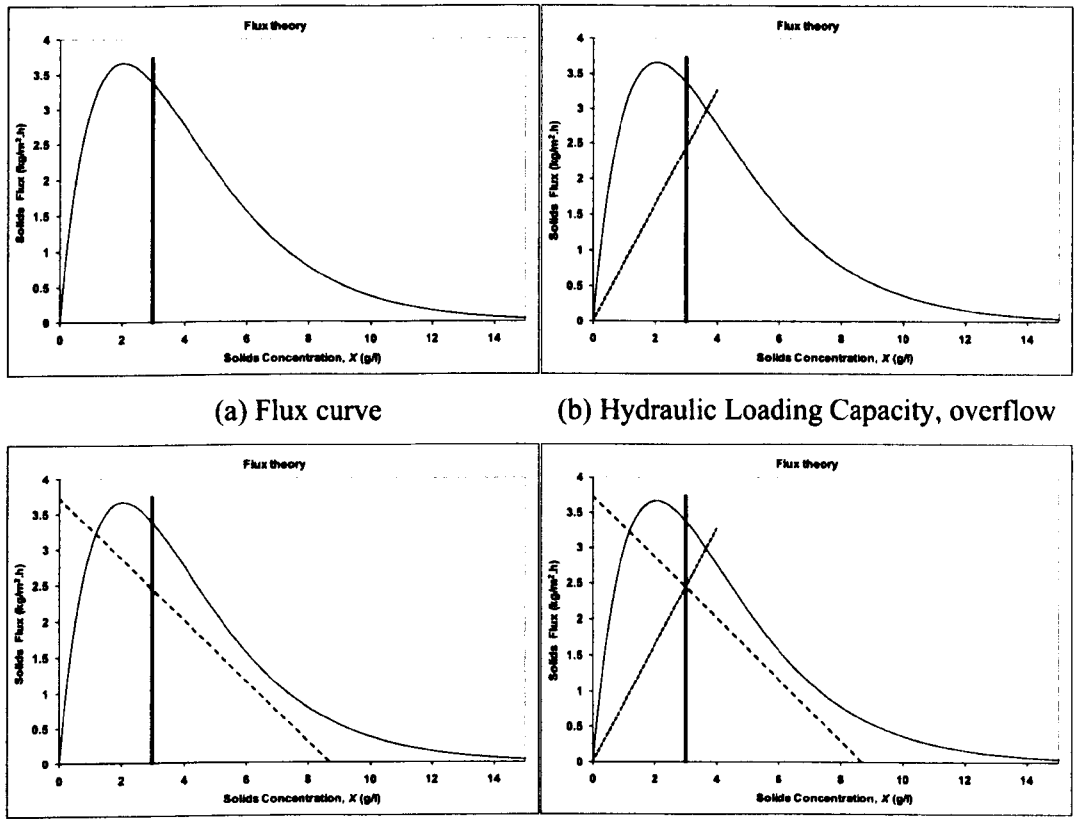

(a) Flux curve (b) Hydraulic Loading Capacity, overflow

c) Solids loading Capacity, underflow d) Solids and Hydraulic loading Capacity

Figure 3.10: Graphical method showing the progression of steps for state point analysis.

In Figure 3.10a, the flux curve is plotted from equation (3.17) with a vertical line placed at the feed concentration X_F . The overflow line may then be plotted starting at the origin with a slope equal to the surface overflow rate $q_A = Q / A_{st}$, as shown in Figure 3.10b. The point at which the overflow and influent concentration line intersect is called the state point.

The under flow line shown in Figure 3.10c describes the amount of solids the tank is required to settle and remove via the RAS. This line is drawn through the state point at the gradient $q_R = -R.Q / A_{st}$ and the intercept point of this line at the x = 0.0 axis gives j_{QF} (also shown in Figure 1.7). The intercept of the underflow line with the concentration axis is an indication of the expected RAS solids concentration. The

final state point of the clarifier is determined by the intersection of the influent concentration underflow and overflow lines.

Preliminary sizing of most tanks in the UK is based on the settleability of $SSVI_{3.5}$ =120 *ml/g*. Provided that the underflow line crosses the solids flux line only once, and remains below the falling leg of the flux line at all points, then the tank will not be overloaded in solids capacity for sludge with this settling index.

Often the ratio j_{QF} / j_L is used as a design measure with a 20% safety factor in solids load. In the graphical method, this usually ensures that the state point lies well below the solids flux curve. It has been suggested by Ekama and Marais (2004) that maximum solids mass loading rate should be 85% for deep tanks (15% safety factor) and 75% for shallow tanks (25% safety factor) but this may be conservative.

Another attractive comparison proposed here is to define a limiting hydraulic flux as

$$j_{QH_m} = X_F . V_0 e^{-r_h X_F} \tag{3.25}$$

And to compare this with the actual hydraulic flux.

$$j_{QH} = X_F . Q / A_{st} \tag{3.26}$$

The relative ratio of the state point compared with the best possible hydraulic performance (intercept of the flux curve with the influent concentration line) at this concentration is then,

$$\frac{j_{QH}}{j_{QH_m}} = \frac{Q}{A_{st} V_0 e^{-r_h X_F}} \tag{3.27}$$

or simply the ratio of surface overflow velocity to settling velocity at the influent concentration. This is a useful normalizing quantity for comparing designs and is proposed here as the limiting 1DFT (1D Flux Theory) parameter, where the unity ratio may be thought of as 100% of the available 1DFT.

The main difficulty in estimating the limiting situation with mass flux theory is a poor correlation between SSVI and flux, largely due to the flow patterns and physical processes previously discussed. Therefore the state point for a safe design must sit well below the flux curve. For solids loading the ratio of j_{QF} / j_L may be used to define the limit of Criterion I. For hydraulic loading a new ratio is proposed j_{QH} / j_{QH_m} in equation (3.27) as %1DFT. Typically, it is expected that a tank is likely to operate up to a limiting value of 80 to 90% of 1DFT but this may be tested with CFD simulation.

3.6 Conclusions

Both mass flux theory and 3D CFD modelling rely on the use of experimental data to provide the constant coefficients in the constitutive relationships. The common link between CFD and mass flux is in the settling function attributed to Vesilind (1968) which in turn may be connected to the $SSVI_{3.5}$ index through correlations. The Vesilind equation has been expanded by Takács to cover a wider range of settling regions in the CFD model than can be addressed by the mass flux model. However, there is only limited data available for the low and high concentration regions.

CFD modeling also includes a dynamic model for the thickening of activated sludge in the form of a rheology function. The origins of the standard Bokil and Bewtra

(1972) model have been explored and a number of newer, yield stress based, rheological functions have been presented. Whereas the Takács double exponential function has become a preferred model for hindered settling, there is no preferred model for rheology. Therefore, the various rheological functions available will be investigated further in the rest of the thesis.

The mass flux method has been illustrated as a means for checking the compliance of a tank for a given process condition. The first two mass flux criteria may be checked graphically using state point analysis. Any state point that falls below the mass flux curve should be achievable in a real system but it is known that tanks can fail well below the limits of Criteria I and II (Ekama and Marais, 2004). An index, based on hydraulic loading, is defined for future comparison between CFD and mass flux, this is called 1DFT. It is anticipated that any given SST design will fail when the process condition exceeds 100% of 1DFT.

CHAPTER 4: First Applications of CFD Modelling to Settling Flows

Summary

This chapter describes the application of a CFD model for calculating flow and solids settlement in a final clarifier with initial verification and validation test cases; these compare model results with the laboratory data of Krebs (1998) and with site measurement data for the Rye Meads clarifier acquired by Scriven and Richardson (1998). The models described in Chapter 2 were implemented in the CFD code CFX at versions 4.2 and 4.4 through Fortran extensions and by making direct modification to the original source code routines; these extensions are listed in Appendix B.

4.1 Introduction

Flow in an industrial scale clarifier is characterised by regions of mixing in the stilling well near the influent and quiescent settling regions where sludge thickens in to a blanket on the tank floor. Therefore the effective viscosity of the mixture, (equation 2.22) is dominated by the turbulent viscosity component near the influent and by the non-Newtonian or apparent viscosity component in the settling bed. The CFD code originally chosen for the implementation of the model, CFX 4.2 did not support a turbulence closure which allowed both apparent and turbulent viscosity to vary simultaneously in space and time. Therefore, for this implementation, extensions were coded into the Wilcox (1994) low Reynolds number turbulence model (CFX, 1997). For a later implementation in CFX4.4, additional object code was obtained from CFX for the Menter (1994) modified low Reynolds number

$k-\omega$ turbulence model. This automatically allowed modification to the apparent viscosity in a turbulent flow (CFX, 2001).

The standard algebraic slip model available in CFX 4.2 and 4.4 (CFX,2001), was used to represent the drift flux scalars for settling solids and the constitutive relationships for density, settling velocity and rheology discussed in chapter 3, were implemented through the appropriate Fortran extension routines. A full description of the model implementation is presented in Appendix B with examples of source code and command file fragments. The results obtained with this model for two test cases are discussed here.

4.1.1 The CFD Test Cases

Several verification and validation studies were considered as part of the model development exercise. These studies were performed to get a thorough understanding of the model and to demonstrate the ability of the model to calculate settling flows accurately. The two cases discussed here are,

1. A model based on the laboratory clarifier of Krebs (1998). This study compares the Euler-Euler multiphase frame, using a single particle/floc size class, against a single averaged drift flux scalar model and the multiple drift flux (MDF) model. This is not a definitive validation exercise; but a test of the alternative Eulerian-Eulerian multiphase frames.
2. A model for comparison with the experimental measurements of the full scale RyeMeads clarifiers by Richardson (1998). This model uses the full range of density, settling and rheology functions described as the extended drift flux model (EDF) in Chapter 2. The sensitivity to grid, rheological function and the floor boundary condition are tested. This allowed full scale validation of the CFD results against site measurements.

4.2 The Laboratory Scale Clarifier of Krebs (1998)

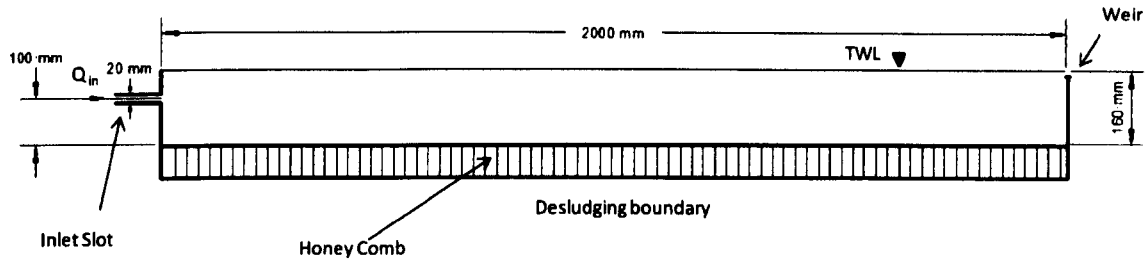

Figure 4.1: Schematic diagram of the Laboratory clarifier of Krebs (1998), case 4. The flow carrying the glass bead suspension enters at the inlet slot on the left. Solids fall out into the honeycomb array and the clarified flow exit at the weir on the right.

In the work of Krebs (1998), a laboratory rig was designed and built to represent an idealised waste water clarifier, Figure 4.1. The tank was $2m$ long, $0.5m$ wide and with a water depth set at $0.16m$. The experimental work was carried out in order to understand the influence of the densimetric Froude number on the settling performance of the tank where,

$$Fr' = \frac{V}{\sqrt{gh\left(\frac{\rho_m - \rho_w}{\rho_w}\right)}} \tag{4.1}$$

The densimetric Froude number Fr', is the ratio of the fluid velocity to the "internal wave speed at a density interface" (Ekama et, 1997) or the ratio of momentum to buoyancy. For the Krebs laboratory clarifier experiment illustrated in Figure 4.1, it can either be scaled to the tank, where V is the average horizontal velocity and h is the depth of the tank or to the influent slot where V is the average influent velocity and h is the height of the influent slot (as mentioned in the introductory note on the McKinney baffle in chapter 1). In either case this number is critical to the processes occurring in this tank as small values of $Fr' < 1.0$ mean that buoyancy effects, or gravity currents will dominate the flow.

4.2.1 Particle Size Distribution

In the experiment, the influent was dosed with a range of glass bead diameters representing characteristic settling rates for wastewater sludge, the cumulative particle size distribution (PSD) for the glass beads is shown in Figure 4.2. The mixture flowed over a honeycomb structure, which acted as a sink for the solid phase and approximated a rough wall to the liquid phase. The honeycomb was made sufficiently deep to capture all solids over the sustained period of the experimental measurements. The model discussed here relates to the system where the inlet slot at the left of the tank was $20mm$ high and centred $100mm$ from the bottom of the tank, Figure 4.1, (case 4 in the original work). The effluent weir was located at the top right of the tank. The water entered at 1.0 l/s carrying glass beads at concentration 18.9 g/l. So, in this case, $Fr' = 0.09$ and $Fr'_{in} = 2.1$.

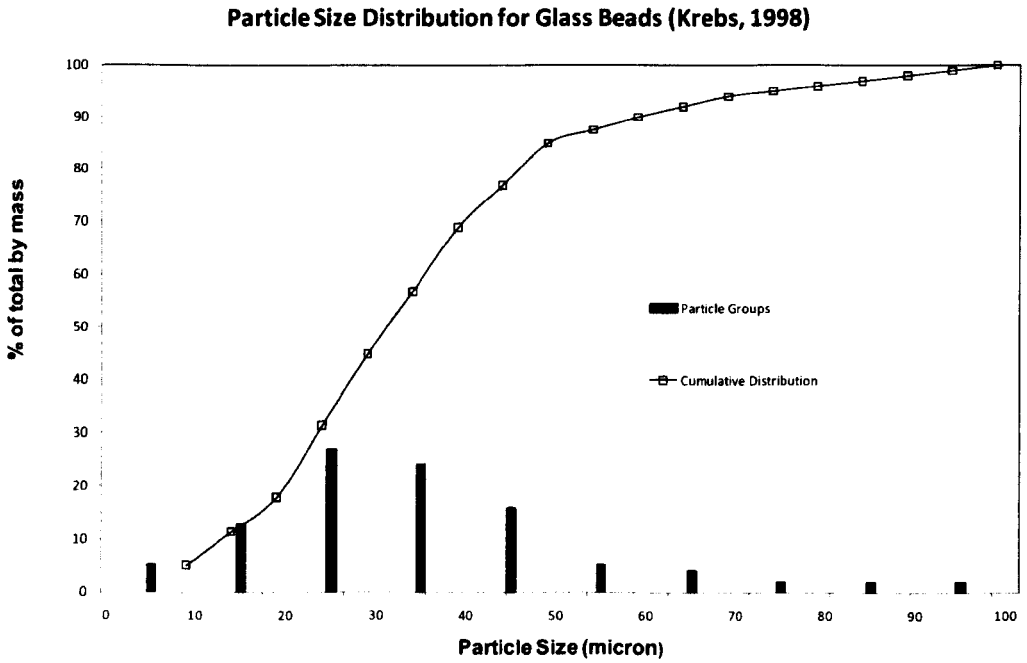

Figure 4.2: Cumulative particle size distribution (PSD) for glass beads at the influent for the laboratory clarifier experiment from Krebs (1998).
The distribution is discretised into ten size classes for the MDF model.

In order to represent this system in a computational model some attention had to be given to the representation of the solids PSD. In a system where the settling is believed to be dominated by discrete settling only then the terminal settling velocity for the spherical glass beads at low particle Reynolds number ($Re_p < 1.0$) may be calculated from the Stokes law,

$$V_o = \frac{g}{18\mu}(\rho_p - \rho_w)d_p^2 \qquad (4.2)$$

Either, the settling velocity may be calculated for a single average size class or the PSD may be discretised in some way to represent a range of size classes. In this case, the mean particle diameter is d_p = 40 μm and the terminal settling velocity from equation (4.2) is V_o= 1.3 *mm/s*. A possible discretisation is shown in figure 4.2, where 10 size classes have been used to represent the PSD.

4.2.2 CFD, Physical Models and Boundary Conditions

The computational model domain was defined with a two dimensional grid of 80x50 hexahedral cells. The multiphase flow was represented in three different ways for comparison.

1. A full Eulerian-Eulerian multiphase model, (as described in section 2.2.1) with the solid phase defined as single spherical glass particle of d_p=40 μm.
2. A single drift flux scalar model, equivalent to model 1 but ignoring interphase drag, with the settling velocity fixed as the average settling velocity of V_o= 1.3 *mm/s*.
3. A multiple drift flux (MDF) model with a distribution of ten additional algebraic slip scalars, each scalar representing one size class for the sludge with each size class having a discrete settling velocity. This discretisation is

shown graphically in Figure 4.2 as a histogram plot and the data for the size classes is shown in Table 4.1

Table 4.1: Particle size range, settling velocity and influent mass fraction for a disretisation of ten drift flux scalars based on the data of Krebs (1998).

d_p (μm)	Cumulative (%)	Group (%)	V_o (m/s)	Y_k (kg/kg)
5		5	2.04E-05	9.344E-04
15	11.5	13	1.84E-04	2.429E-03
25	31.5	27	5.11E-04	5.046E-03
35	57	24	1.00E-03	4.485E-03
45	77	16	1.66E-03	2.990E-03
55	87.5	5	2.47E-03	9.344E-04
65	92	4	3.45E-03	7.475E-04
75	95	2	4.60E-03	3.738E-04
85	97	2	5.91E-03	3.738E-04
95	100	2	7.38E-03	3.738E-04

For the drift flux models, (2 and 3) , the flow was defined with a density function for concentration following equation (2.36). Turbulence was modelled with the Menter modified k-ω model (section 2.4.4). The outlet was modelled as a pressure boundary, the top surface as a free slip wall and the bottom boundary was modelled as a sludge removing (or desludging) boundary following Figure 4.1. That is the bottom floor acted as a sink to the solid phase but did not allow the liquid phase to pass through.

For the multiphase model and the single drift flux model the influent concentration of sludge was defined as either the total sludge volume fraction or the total sludge mass fraction. For the MDF model the influent solids were represented as a series of size groups with a defined mass fraction and settling velocity for each group. The sum of all of the mass fraction components in model 3 was equal to the total solids mass fraction in model 1 or model 2. Table 4.1 also gives the influent mass fractions for each of the ten discrete size groups.

4.2.3 Model Solutions

All calculations were calculated steady state using 2nd order differencing for the momentum equations. Under relaxation factors or false time steps were used to control the rate of convergence for each of the variables in the segregated solver algorithm used by CFX. A maximum of 10,000 iterations of the solver was required to achieve stable steady state solutions for all three models.

4.2.4 Results of the Analyses

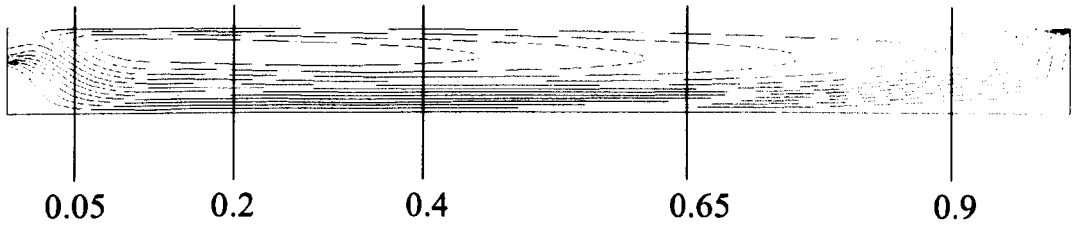

Figure 4.3: Streamline plot for the Multiple Drift Flux Solution with Fr' = 0.09, showing the density current at the influent and the positions where the solids concentration profiles are measured. This streamline plot was produced using additional code for a stream function in CFX4, see USRTRN in Appendix B.

The streamline plot in Figure 4.3 shows that the momentum is strong enough at the influent (Fr'_{in} = 2.1) for the mixture to travel a few influent lengths before the density current begins to dominate. At x/l = 0.02 the shape of the density current is apparent. From x/l = 0.1 and onwards a shear layer occurs through the settling bed where the streamlines are closest together (Lyn, 1992). The main characteristic of the flow is a large re-circulation with the surface flow returning to the influent with a flow split at length x/l = 0.9. These flow features, illustrated in this simple system, are the dominant characteristics of all settler flows and will be seen many more times in later analyses of industrial clarifier systems.

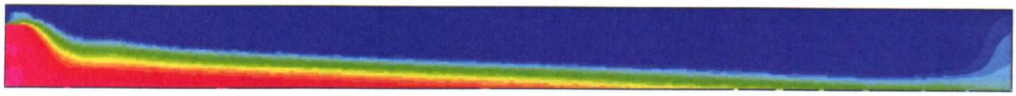

1) Multi-phase single particle size (40 μm)

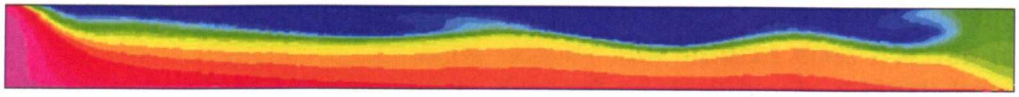

2) Single drift flux (V_o = -1.3 *mm/s*)

3) Multiple drift flux (10 scalars V_o = -0.02 to -7.4 *mm/s*)

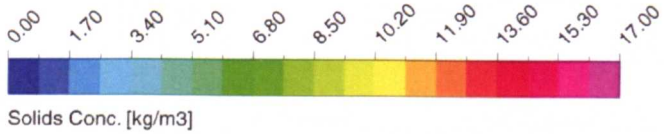

Figure 4.4: Concentration distribution on a linear scale 0.0 to 17 g/l for the three multiphase approaches for modelling the Krebs (1998) laboratory clarifier.
Using a single average size class does not give a good representation of the solids distribution.

Although the flow patterns were broadly similar for the three multiphase modelling approaches, Figure 4.4 shows significant differences in concentration distribution. The Eulerian multiphase solution, based on a single average particle size of d_p = 40 μm, shows only limited solids carry over to effluent; the solids are largely exiting the tank at the floor into the hopper. The single drift flux solution based on a fixed terminal settling velocity of V_o = 1.3 *mm/s* shows a different solution to the multiphase model. The solids bed does not fully settle and there is some solid carry over to effluent. This solution also shows an unstable shear layer, which caused convergence difficulties for a steady state solution. The final plot shows the concentration field for the MDF model based on the algebraic sum of all of the size group concentrations in each computational cell. This shows significantly less settling than either of the averaged particle size models with significant solid carry-over to effluent.

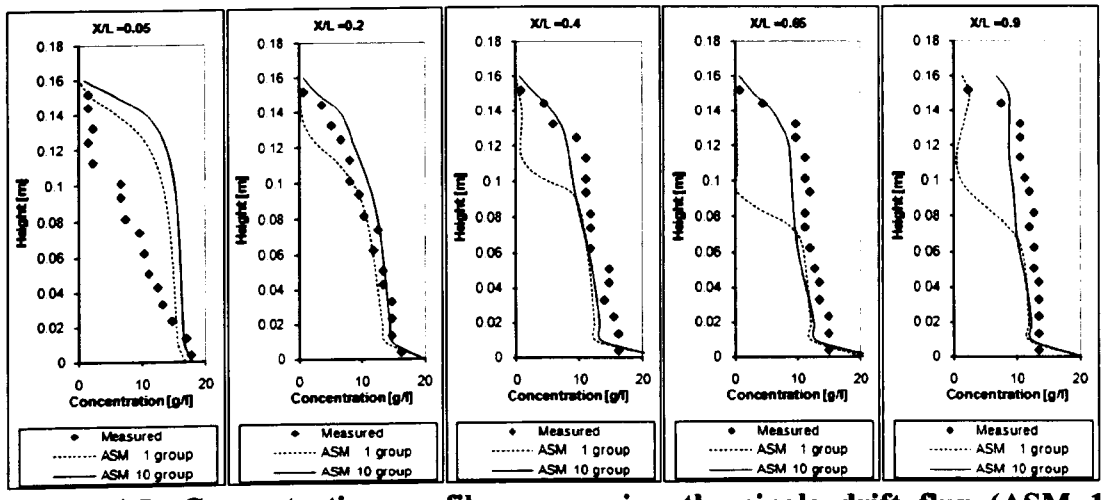

Figure 4.5: Concentration profiles comparing the single drift flux (ASM 1 group) solution and the multiple drift flux (ASM 10 group) solution with the experimental data of Krebs (1998).
From X/L =0.2 the ASM 10 group solution matches the experimental data well.

The concentration profiles in Figure 4.5 show a comparison between the CFD models 2 and 3 and the experimental data. There is a significant deviation in the profiles closest to influent, it may be that the density water fall is stronger than the model is predicting at this grid resolution. However, at the later profiles the MDF model solution shows the best agreement with experimental data.

4.2.5 Conclusions for the Laboratory Clarifier Results

These models all show the dominant density driven current typical of flow in a clarifier. There is little difference at the influent for the three model cases but the stream line plots, Figure 4.3, for the loaded system is significantly different to an equivalent single phase solution with no particle loads. Hence, the influence of the solid settlement and density variation on the momentum field is seen to be particularly significant in setting up the characteristic re-circulatory flow. The use of an average slip velocity, in the single drift flux case, or an average particle size for the multiphase case does not predict the correct solids distribution. The Eulerian multiphase model includes interphase drag in both the horizontal and vertical components of the momentum equations. However, having only a single length scale

representing a complex PSD appears to be a severe limitation for this model and the calculated sludge bed solids distribution and effluent solids concentration is unsatisfactory. These results show that it is not appropriate to model a settling system with significant particle size variation with an average size class or an average settling velocity and the best approximation to the experimental data is obtained with the MDF model. The MDF model is therefore a good starting point for any settling system where the solids distribution can be characterised and where particle hindering is insignificant; in the context of waste water systems then it is a good candidate model for Primary Sedimentation Tanks (PSTs) or Humus tanks. It may also be useful for modelling type 1 and even type 2 settling in a clarifier but would need to transition to a hindered settling model as the sludge concentration increased, as shown in Figure 3.1.

4.3 The Rye Meads Final Settlement Tanks

In 1998, the Rye Meads sewage treatment works had 3 stages of activated sludge plant with a total of 16 final clarifiers. The tanks were circular of diameter, D=28m and side wall depth of h_s = 2.2m and with a floor inclined at 8° to the horizontal. They were equipped with a central feed well, perimeter weir and bridge driven scrapers. The conventional centre well was a 9m diameter, open bottomed, circular baffle arrangement, 1.5m deep (of which 1.3m was submerged).

This arrangement is a typical circular clarifier for the United Kingdom and the scales of this particular system were discussed at the start of Chapter 2. The one significant point to note about the geometry is that the stilling well diameter is 32% of the total tank diameter. This is therefore a flocculating stilling well design (Ekama et al, 1997).

Experimental data in the form of solids distributions and point velocimetry measurements were obtained by Scriven and Richardson (1998) at average and high flow rates representative of the bounds of operation for the tanks. Table 4.2, adapted from Richardson (1998), shows a summary of the average and high flow conditions. The $SSVI_{3.5}$ was estimated as being defined only as a 'good settling sludge' at approximately 80 *ml/g* (von-Sperling, 1994). This is the best available settling data for the site as no attempt was made to measure the Vesilind coefficient V_o and r_h, for the sludge at this site directly as discussed in Chapter 3.

Table 4.2: Flow conditions for the Rye Meads validation study.

Run	Flow Rate	Q *(m^3/hr)*	R	X_F *(mg/l)*	$SSVI_{3.5}$ *(ml/g)*
1	Average	360	1.0	2825	80
2	High	720	1.0	3725	80

The experimental work of Richardson (1998) provided information on effluent quality, fluoride tracer break through curves, approximate blanket depth and acoustic doppler velocimetry (ADV) data. An ADV probe was mounted on the stationary clarifier bridge and instantaneous velocity was recorded for five depths at five radial locations (Figure 4.8) at low and high flow. Solids concentration was only recorded at the sludge blanket depth. The ADV data is useful for providing a first comparison with CFD results. Sensitivity studies were performed on the CFD model of this system in order to investigate the influence of changes in grid resolution, scraper model boundary conditions and the sludge rheology function all compared back to the Richardson (1998) data. The method used by Richardson (1998) to obtain point velocities within the clarifier flow are discussed in detail in Chapter 6.

4.3.1 Mass Flux Theory

The process diagram for mass flux theory was introduced in Chapter 3. A single clarifier at Rye Meads recieves a total flow Q_{in}, and this is split equally to effluent and return activated sludge (RAS), the recycle ratio R is 1.0. The state point graph in Figure 4.6 shows that the average flow operating condition falls well below the flux curve for activated sludge at 80 *ml/g* $SSVI_{3.5}$ using two of the common correlations discussed in Chapter 3. Therefore the size of the tank is more than sufficient for the low flow rate.

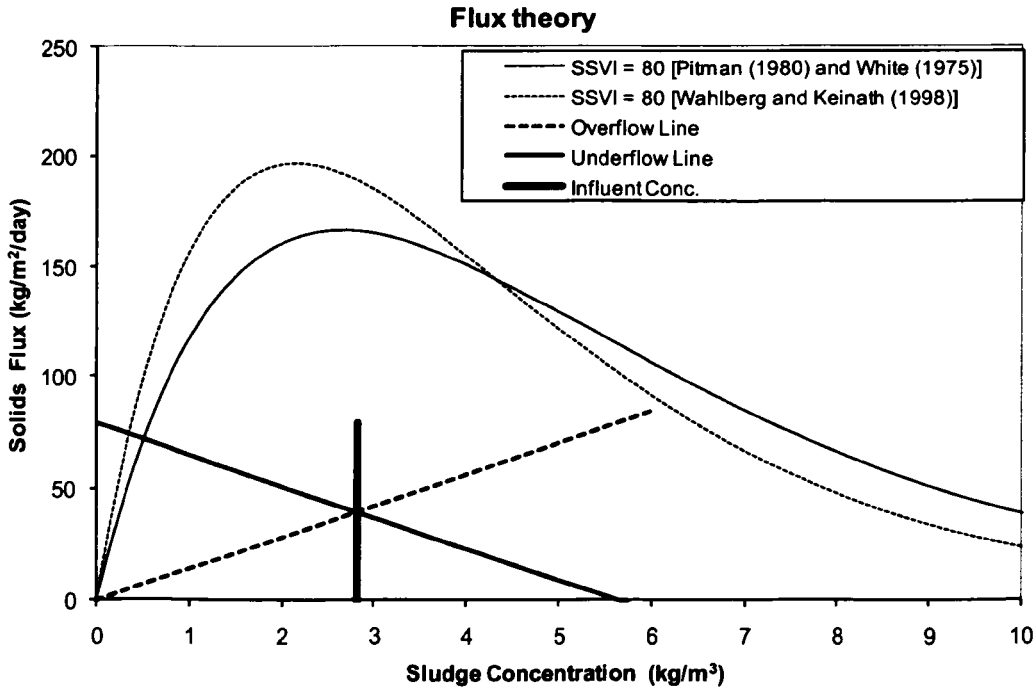

Figure 4.6: Mass flux state point graph for the Rye Meads clarifier at average flow with an $SSVI_{3.5}$ of 80 *ml/g*.
The correlations discussed in chapter 3 have been used to form two flux curves. The state point is well below the flux curves and good performance from the clarifier is expected.

4.3.2 CFD Analysis for the Rye Meads Clarifier

The first stage of the CFD study was to perform a series of analyses based on the average flow condition, run 1 from Table 4.2, using the base models described in Chapter 2 and following the solution sequence outlined in Appendix B.

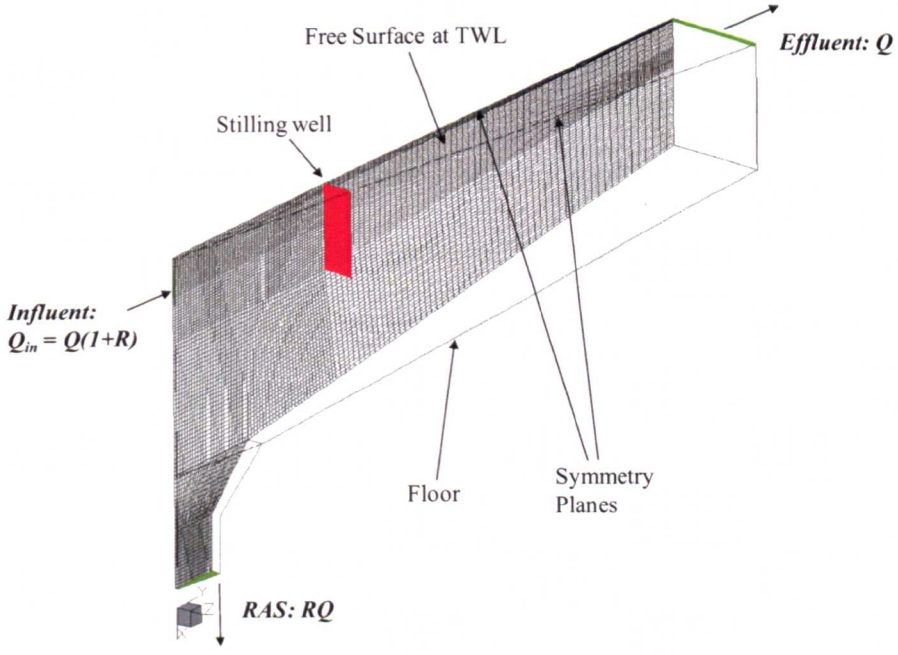

Figure 4.7: Outline geometry and 2D axisymmetric hexahedral mesh for the Rye Meads clarifier CFD model. The coordinate system is x, r, θ mapping to x, y, z.

4.3.2.1 Physical Models and Boundary Conditions

Figure 4.7 shows the computational domain, initially defined with a 2D axisymmetric grid of 8542 hexahedral cells. The co-ordinate system that CFX4 uses for 2D axisymmetric models is slightly unusual and, as for Figure 2.1, the vertical x axis is positive with the depth of the tank in the direction of gravity and the y axis is positive in radial velocity. The θ direction maps to the z co-ordinate in the figure but this is only used for swirling flow calculations (when an energy dissipating influent (EDI) is included for example).

The multiphase flow was represented with the extended drift flux model presented in Chapter 2. Using a single drift flux scalar but with the settling velocity a function of concentration following the Takács (1991) equation (3.6) with settling parameters initially following those defined by Lakehal (1999), shown in table 3.3. These equate approximately to a good settling sludge of $SSVI_{3.5} = 80$.

The flow was defined in the CFX command structure as *weakly compressible* that is with mixture density a function of concentration according to equation (2.36) such that the mass of the system may change with time. (N.B. Some texts refer to the difficulties experienced with convergence when the buoyancy term is invoked (Zhou, 1992). In fact it is apparent that the inclusion of varying density will inevitably mean that the mass of the system will change as the CFD calculation progresses if the tank volume is invariant; hence, the system is mathematically compressible even if the fluids themselves are not and the CFD code must be allowed to express this compressibility or the model will not converge). Turbulence was modelled with the Menter (1994) modified k-ω model. The sludge rheology was initially approximated with the standard Bokil and Bewtra (1972) model relationship equation (3.11) discussed in Chapter 3 and later extended to test a range of rheology models.

The boundary condition logic is common to all clarifier modelling in this thesis and the explicit values for this model were calculated using a standard spreadsheet described in Appendix B (Table B.3). The ***influent*** was defined as a constant velocity inlet with sludge drift flux scalar in units of mass fraction. The ***effluent*** was set as a pressure boundary condition with reference pressure = 0.0 *Pa*. Flow should not enter through this boundary so ambient conditions were also set with sludge mass fraction $Y_k = 0.0$. The ***RAS*** boundary was initially defined as a constant volume flow boundary, not a constant mass flow. This was achieved in CFX by updating the mass

flow at each time step according to the local density above the boundary, this method was eventually rejected in favour of setting the ***effluent*** and ***RAS*** boundaries as percentages of the total exit mass flow and just specifying the mass flow split. The ***free surface*** was set as a slipping wall with zero shear stress. The ***floor*** was initially modelled as a zero shear stress slipping wall following the arguments of Deininger (1998). Sensitivity to the floor boundary condition is considered in the next sections. General guidance on the application of CFD model boundary conditions for Clarifier flows is given in Appendix B.3.

4.3.2.2 Solution Procedure

In order to obtain accurate 2nd order converged solutions for this model the procedure described in Appendix B was followed. A typical final calculation required to achieve a time invariant solution is presented in the command file at the end of Appendix B. Under relaxation factors were used to control the rate of convergence for each of the variables in the segregated solver algorithm used by CFX4 (2001) and a transient approach was followed using physical time stepping between 1 and 10 *s*. (Armbruster (2001) used up to 15.0 *s* with the Fast2D code).

It was found that the computing time to achieve a converged solution for a completely new clarifier model at an individual process state point, could be accelerated by introducing the physical models in stages. The model was initially solved as a steady state ***laminar*** flow with the full inlet and outlet flow boundary conditions. The laminar solution was then used as an initial guess for a second ***transient laminar*** calculation where the slip scalar equation for the activated sludge model was also solved with the density equation (2.36) and the settling model equation (3.6) invoked. The solids bed height was initialized at the start of this

calculation in order to speed up the process of filling the tank with sludge. In the user manual for ClariSim (Appendix B), this stage is referred to as "Run 2, making the sludge blanket".

A ***transient turbulent*** model was then set up as, Run 3, using the previous converged solution for the laminar sludge blanket as an initial guess. In order to aid convergence only ***first order differencing*** was used at this stage and the fluid viscosity was maintained at a constant value throughout the model. Finally, all of the constitutive models were invoked at Run 4 as a ***transient turbulent non-Newtonian*** model with 2^{nd} ***order accurate differencing*** (higher upwind in CFX4) for the velocity field variables and the sludge drift flux scalar only. The density equation and the turbulence quantities were highly under relaxed throughout (Appendix B) to maintain good convergence on each transient time step.

4.3.2.3 Varying the Process Conditions

Although this initialisation procedure may appear unwieldy, it was found to be completely robust for all clarifier simulations and is easily automated as a series of batch calculations on a computer. Once these calculations are set up, they require no further intervention and only take a few hours to achieve a non varying transient solution on a modern personal computer. The results of the fourth run may be used as an initial guess for investigating the more complex non-Newtonian models or as a starting point for a new state point. In this way it becomes possible to quickly investigate the relationships between the four main process parameters, waste water flow rate Q, solids at the clarifier influent, X_F, the recycle ratio, R and the sludge settleability, $SSVI_{3.5}$ in exactly the same way as mass flux theory is used.

4.3.2.4 Using a Transient to achieve a Steady State

The need for a transient solution strategy appears to be related to the shear layer behaviour above the settling bed. A clarifier model with a stably stratified shear layer can be made to converge as a steady state; particularly if it is diffused by use of a coarse grid or a first order convection scheme. As the grid resolution is improved, the time step reduced and higher order convection schemes used (in order to better capture the flow features) then physical instabilities, waves, form above the settled bed with a characteristic time scale. A false time stepping approach in CFX can sometimes be used to diffuse these instabilities into a pseudo steady state solution but ultimately time steps based on the Brunt-Väisälä Frequency (equation 2.5) of between 1 and 5 seconds are needed to get fully converged transient solution on typical grids of 10,000 hexahedral cells. The model must run for several hydraulic retention times T, before complete stability is observed in the monitor points. A good way to monitor convergence is to write the exit concentration (ESS) to a file and to monitor all variables just outside of the stilling well.

4.3.2.5 Results of the Initial Analysis for the Rye Meads Clarifier

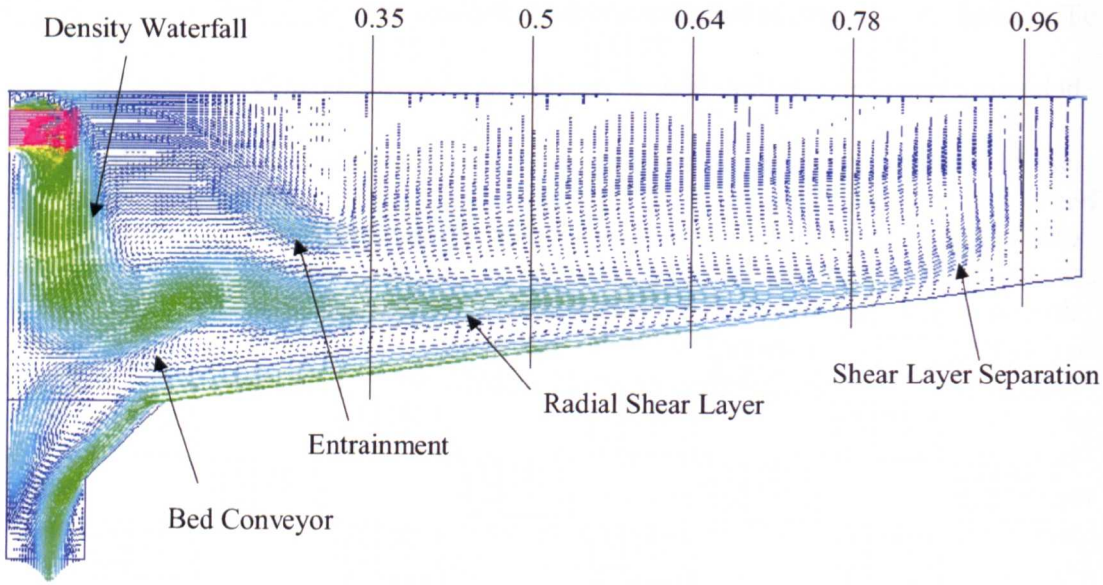

Figure 4.8: Velocity vectors for the Rye Meads clarifier CFD solution at average flow,
$Q = 360 (m^3/hr)$, solids at the clarifier influent $X_F = 2825$ *(mg/l)*, the recycle ratio R = 1.0 and the sludge settleability $SSVI_{3.5} = 80$ *(ml/g)*, $Fr' \approx 0.15$. This result is for the mass flux state point shown in Figure 4.6. The figure also shows the radial locations used for the experimental measurements of velocity.

The results for the CFD analysis are shown as a velocity vector plot in Figure 4.8. Some key flow features are observed in these results which are common to similar design. These are as follows;

The ***influent density waterfall***: at this flow rate and for this size of stilling well, the flow entering at influent does not spread throughout the stilling zone. Rather it spreads locally from influent and then falls into the sludge blanket before forming a radial jet. In this case the densimetric Richardson number Ri', equation (2.3), was estimated in Chapter 2 as $\approx$ 10.0 and from equation (4.1), the densimetric Froude number, $Fr' \approx 0.15$.

The ***radial shear layer***: all circular clarifiers show a strong radial shear layer immediately above the settled sludge bed. This feature was originally reported by

Anderson (1945) and is clearly visible in this simulation. The shear layer will be constantly depositing and re-suspending solids from the settling sludge bed and it is this mechanism which is largely responsible for determining the effluent solids loading.

The ***shear layer separation***: at some point the radial flow breaks away from the settling bed and heads upwards before returning back along the surface towards the central stilling well. The flow upwards at the side wall and the point of separation both influence the process of solids re-suspension and carry over to the effluent weir.

The ***stilling well re-entrainment***: In this model the return flow is not sufficiently separated from the influent stilling well and there is re-entrainment of clarified water back into the mixed liquor or stilling zone. This augments the influence of the density current and may be contributing to a higher ESS values than could be achieved for this tank. The effect of this re-entrainment phenomenon on the energy balance of the system is discussed by Armbruster (2003).

The ***bed conveyor***; solids that enter into the sludge bed are carried back to the RAS return by flowing down the sloping floor. It is not clear whether this return mechanism is influenced by the action of the rotating scraper. However, it is noticeable that some of the flow returning to RAS can be re-entrained by the influent density waterfall resulting in several recycles and increased residence for solids in the bed.

4.3.3 CFD Sensitivity Studies.

The process of comparing experimental velocity measurements with CFD prediction is now reported for various sensitivity studies for the Rye Meads clarifier CFD solution at average flow $Q = 360(m^3/hr)$, with solids at the clarifier influent $X_F =$

2825 *(mg/l)*, recycle ratio R = 1.0 and the sludge settleability $SSVI_{3.5}$.= 80 *(ml/g)*, as follows;

- Sensitivity to grid.
- Sensitivity to the floor boundary condition.
- Sensitivity to rheological model.
- Sensitivity to the turbulence model.

4.3.3.1 Sensitivity to Computational Grid

Three grid resolutions were considered, coarse (4,480 cells), medium (10,080 cells) and fine (17,920 cells).

Table 4.3: Summary results of the grid sensitivity study.

Model	Cells	RAS, X_R *(mg/l)*	ESS X_E *(mg/l)*	Bed Depth h_{850} *(m)*
Experiment		8613	16	2.4
Coarse	4480	5623	17.48	2.31
Medium	10080	5632	16.00	2.4
Fine	17920	5593	16.27	2.47

Table 4.3 compares the CFD predictions for RAS concentration X_R, effluent suspended solids (ESS), X_E and the bed depth h_{850} , at different grid resolutions with the experimental results (Richardson, 1998). The bed depth is taken to be the position of the 850 *mg/l* contour relative to the free surface, following Matko (1998). The effluent concentration (ESS) is the solids concentration recorded at the effluent weir for both the CFD models and the physical system. There is reasonable agreement between CFD prediction and the experimental measurement of these parameters for all grid resolutions.

4.3.3.2 Measurement Profiles

In order to compare the CFD results with the experimental velocity measured by Scriven and Richardson (1998), results for point measurements within the tank are compared as a series of five velocity profiles. Each profile has a normalised radial position which is shown in Figure 4.8. At each radial position, the depth at which the measurement is recorded is normalised to the total depth at that position. For radial velocimetry the experimental data was extracted as the radial component of the velocity vector reading from the ADV probe, the time averaging of this data is explained in Chapter 6. At each data point, the average value of the component was calculated and normalised to the influent flow velocity V_{in}. The normalised radial velocity profile is then plotted against normalised height for all 5 radial locations.

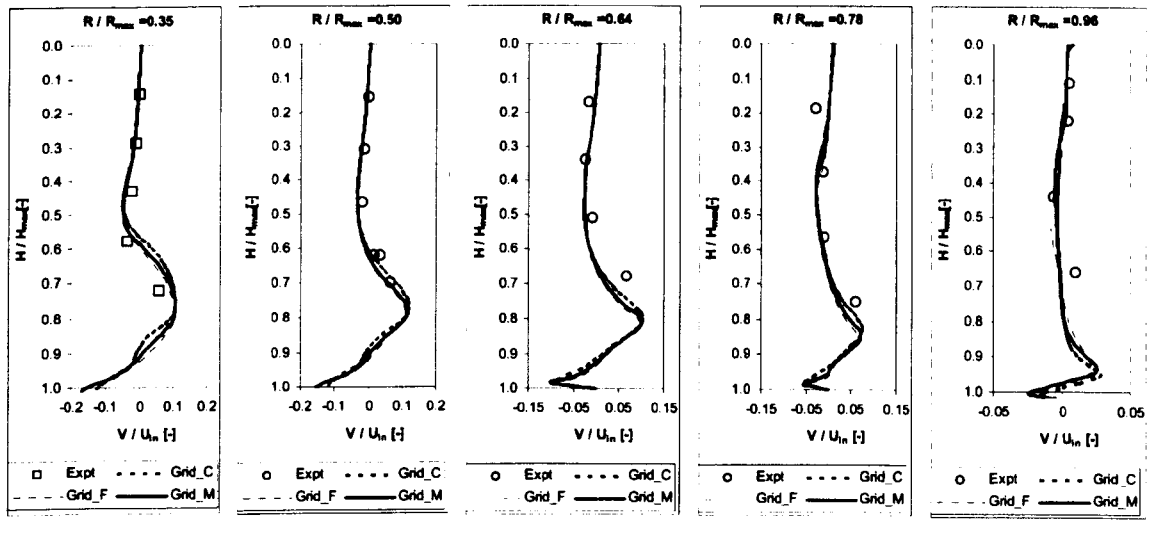

Figure 4.9: Radial flow velocity profiles for grid sensitivity study comparing the coarse, medium and fine grids with the experimental data of Scriven and Richardson (1998).

Figure 4.9 shows the normalised velocity profile shapes at each radial position; the broad shape of the flow is captured and the peak velocity occurs in the shear layer region above the settled bed. There is also evidence of radial flow reversal where the normalised velocity is less than 0.0. The extent of this reversal at the peak negative

radial velocity is shown by the CFD solution. There is little difference in the velocity profile shapes for the three grids considered.

4.3.3.3 Sensitivity to the Floor Boundary Condition

The purpose of this next comparison was to determine an appropriate floor boundary that might be representative of the scraping action in the real secondary clarifier. Modelling the dynamic action of the blade is not impossible to do in CFD, it can be achieved through the use of sliding meshes and multiple frame of reference simulations, (Winkler, 1999) but it is largely impractical for design assessments. Three options for the floor boundary were considered,

1. A no slip wall which is a stationary boundary with fluid velocity zero at the wall. In this case the CFD code may apply a log law of the wall depending on the local value of y^+ (CFX, 2001).
2. A slip wall which is a stationary boundary with zero shear stress at the wall allowing the fluid to move adjacent to the wall with no frictional effects (Deininnger, 1998).
3. A rotating wall applying an angular (w velocity or swirl in axisymmetric co-ordinates) velocity to the floor surface at the speed of the rotating scraper with a radial velocity component directed towards the hopper and determined by the inclined angle of the scraper blade (de-Clerq, 2003).

The last boundary condition replicates the action of the scraper as a solid body rotation where the whole of the clarifier floor is moving. This is an idealization of the real situation as it is not possible to represent the intermittency of the scraper action in a 2D axi-symmetric model.

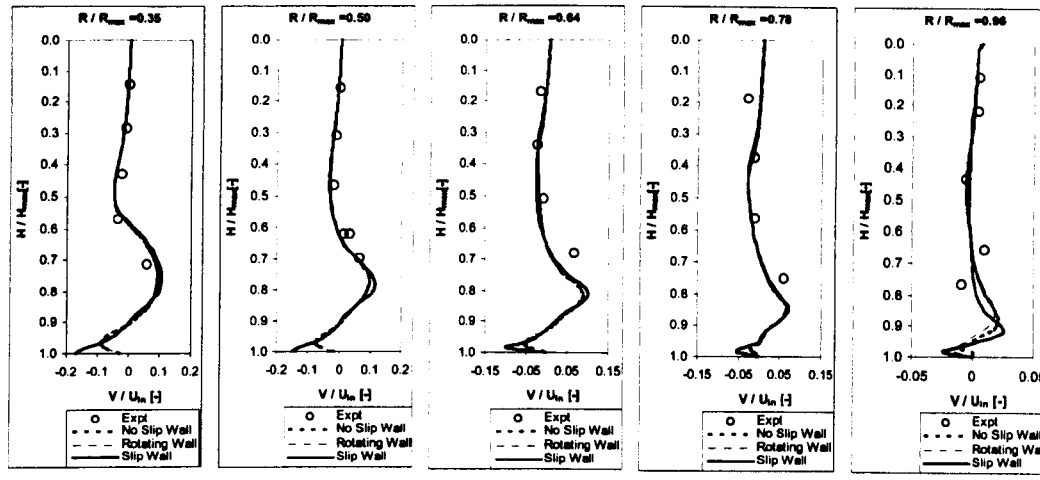

Figure 4.10: Radial flow velocity profiles for the floor boundary study comparing stationary walls, slip walls and rotating walls with the experimental data of Scriven and Richardson (1998).

Figure 4.10 shows that in the bulk flow it is difficult to discern notable differences between the CFD solutions. However, in the near wall region, there is an obvious increase in the near wall velocity for the no-slip wall condition tending towards the centre line axis. Given that there is a significant lack of data for flow in the near wall region it can only be said that all of these approaches may be valid ways of representing the tank floor. An appealing model, is to argue that the scraper simply separates the compressed sludge from the floor and therefore allows it to fall in sympathy with the exit momentum, driven by the differential head between the RAS bell mouth and the water free surface. This is the idea originally proposed by Deininger (1998) and confirmed in numerical studies by Armbruster (2001). Therefore the slip wall model is used for all of the model results presented in the later chapters of this thesis.

4.3.3.4 Sensitivity to Rheological Properties.

In this study, two of the non-Newtonian models, the Bokil and Bewtra (1972), equation (3.11) model and the Lakehal (1999) Bingham plastic model, equation (3.13) are compared with CFD results for constant apparent viscosity and the

experimental data. Figure 4.11 shows the velocity and sludge concentration profiles at the different radial location. The concentration profiles are normalised to the influent concentration X_F, and compared with a single experimental data point recording the sludge blanket depth h_{850}, taken to be the 850 *mg/l* concentration contour. There is a significant variation in these results; the constant viscosity model predicts a sludge blanket above the measured position while the Bingham model shows the lowest bed depth below the measured position.

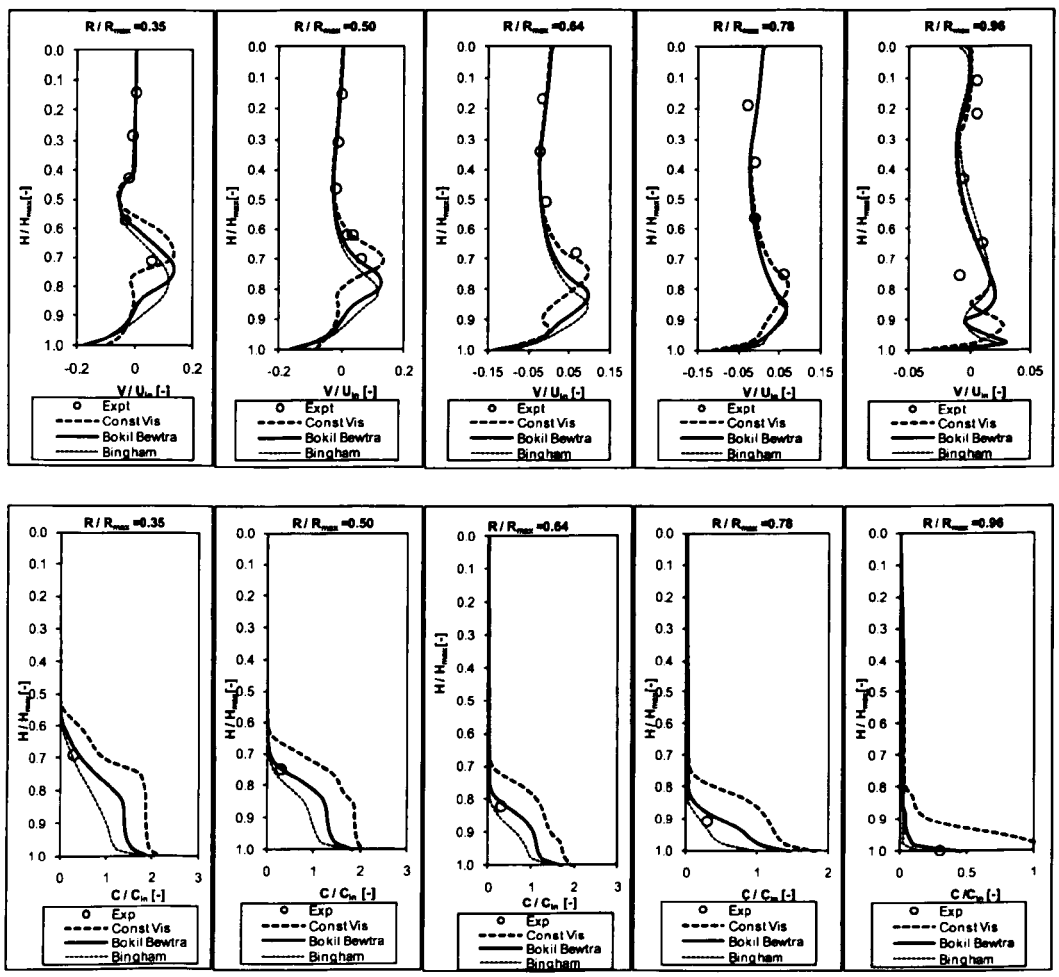

Figure 4.11: Radial flow velocity and concentration profiles at normalized radial positions for the medium grid with alternative rheology models, compared with constant viscosity and the experimental data of Scriven and Richardson (1998).

4.3.3.5 Sensitivity to the Turbulence Model.

In this work both the standard Low Reynolds number version of the Wilcox turbulence model (Wilcox, 1994) and the Menter modified low Reynolds number $k-\omega$ model (Menter, 1994) were used.

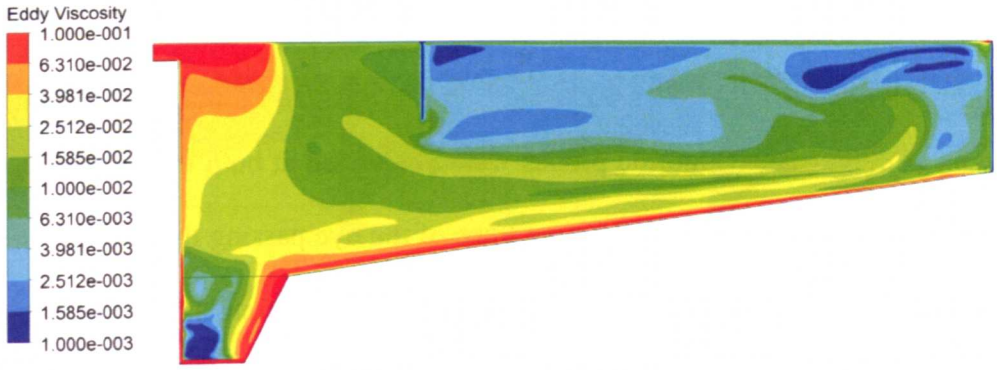

a) Eddy viscosity with the Wilcox (1994) low Reynolds number $k-\omega$ model.

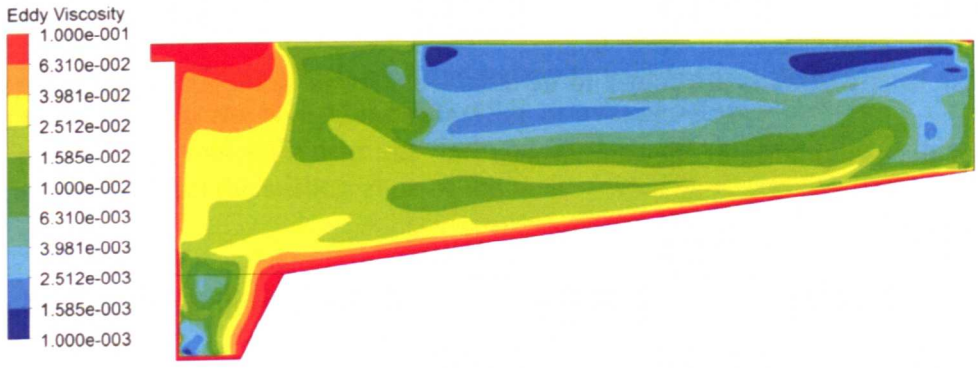

b) Eddy viscosity with the Menter (1994) modified low Reynolds number $k-\omega$ model.

Figure 4.12: Comparison of the turbulent eddy viscosity field μ_t, for the Wilcox (1994) model and the Menter (1994) model in using the fine CFD mesh.
A log scale is used from 0.001 to 0.1 *kg/ms*. There are only marginal differences in the two results.

In Figure 4.12, the turbulent eddy viscosity μ_t is compared for both of the turbulence models used in the Rye Meads clarifier study at average flow conditions with a fine mesh (17920 hexahedral cells). It can be seen that there are only marginal differences between the two results. There is significant turbulence in the influent regions, and there is also turbulence near the floor of the tank. The high turbulent

viscosity near the floor is produced by the velocity gradients in the sludge bed near the floor (Figure 4.8). In the settling zone of the tank there is very little turbulence predicted.

4.3.4 A Transient Tracer Study

An experimental test using a sodium fluoride dye test is discussed by Richardson (1998). In the test, 40 l of sodium fluoride solution at 1g F/m^3 was introduced into the tank at the influent. Fluoride probes were positioned at both the RAS and at the effluent weir in order to record the time trace of the dye passing the probes. Several key times were recorded from the experiment. T_{Peak} is the time at which the highest fluorine concentration exits the tank and T_{50} is the time at which 50% of the dye tracer has exited the tank. T_{10} is the time taken for 10% of the tracer to exit the tank, if these time constants are found to be small relative to the total hydraulic retention time it shows evidence of short circuiting.

A similar experiment was performed with the CFD model with a simple scalar field representing the dye tracer. Initially a pulse of dye at unit value was introduced at the influent for five seconds only. At the end of five seconds the pulse was switched off and the progress of the convection and diffusion of the dyed water was tracked through the tank with time; Figure 4.13 shows this process.

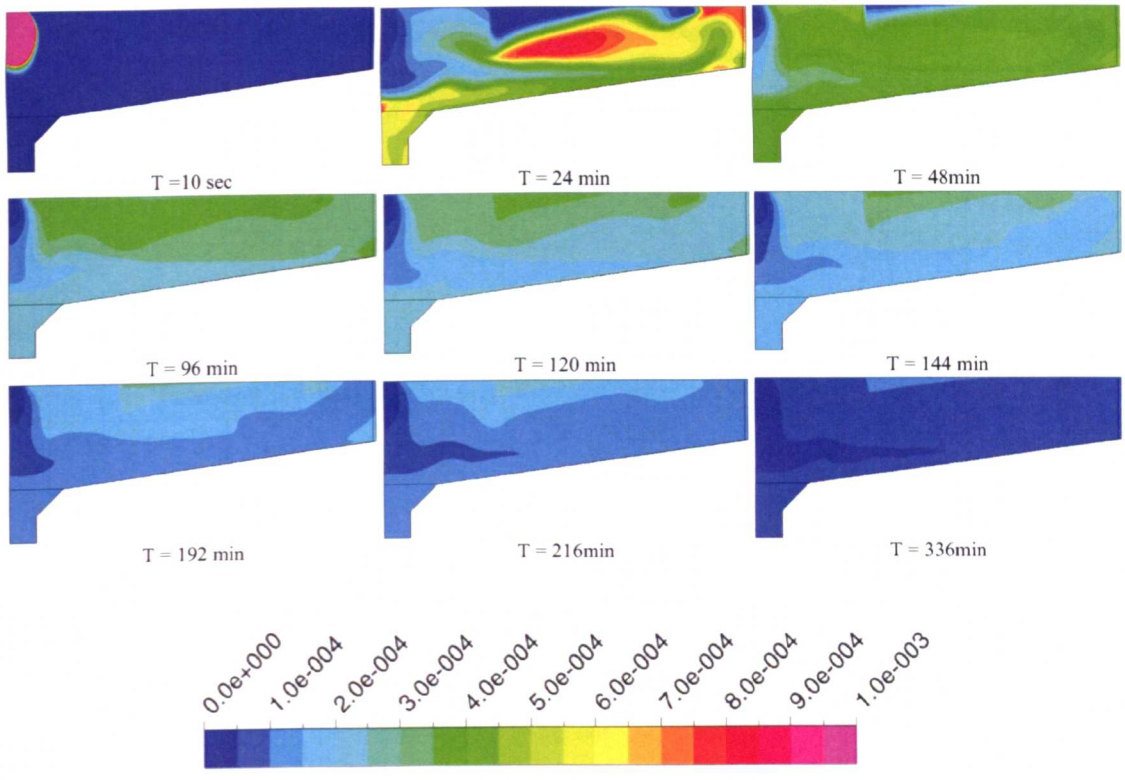

Figure 4.13: A CFD prediction of dye tracer concentration distribution convected with time through the Rye Meads clarifier at average flow.
The pulse of dye is still near the influent at 10s. At 24 min, the dye is largely concentrated within the stilling zone of the tank.

For the RyeMeads tank at average flow the hydraulic retention time (HRT), T, (equation 2.1), was calculated to be approximately 157 minutes (9400 seconds). Figure 4.13 shows the dye being convected and diffused through the tank with some tracer still present in the tank after $2T$. The concentration with time was recorded by the model at discrete positions, or monitor points as shown in Figure 4.14. These monitor points corresponded with the experimental probe positions.

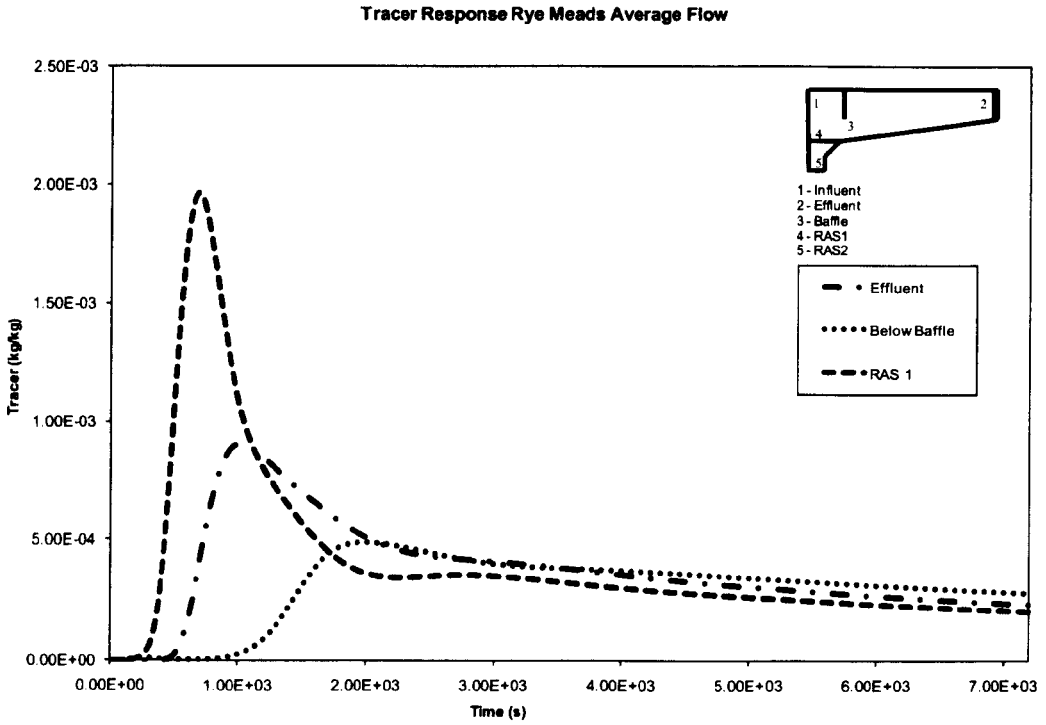

Figure 4.14: CFD predictions of the dye tracer history.
Traces are plotted at the experimental probe locations 2) for the effluent, 3) below the stilling well and 4) near the RAS hopper.

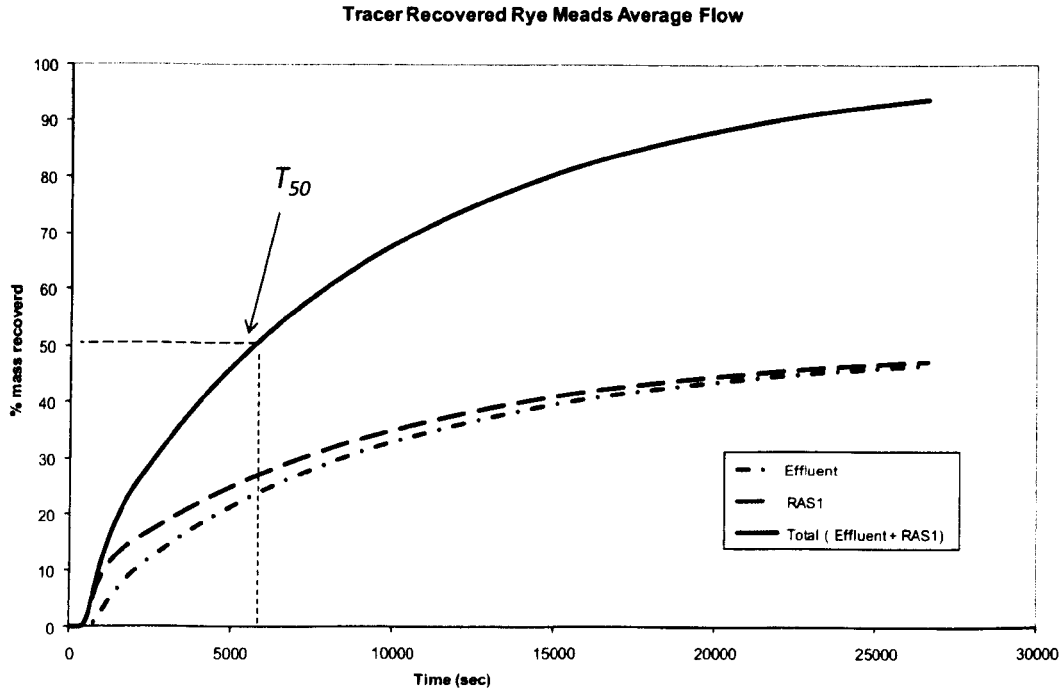

Figure 4.15: Cumulative dye tracer history at RAS and Effluent.
The time to recover 50% of the dye T_{50}. is shown on the graph.

Figure 4.15 shows the tracer recovery at effluent and RAS with time, T_{10} is around 1000 s, and it is noticeable that nearly all of the tracer that has exited the tank at this time has appeared at RAS, T_{90} is around 2.2T The experimental peak arrival times and tracer recovery times for the average flow condition are compared with CFD prediction in Table 4.4

Table 4.4: Tracer test results for the Rye Meads clarifier at average flow

Results	Experiment *(s)*	CFD *(s)*
T_{Peak} at effluent	900 - 2820	1020
T_{Peak} at RAS	540-720	690
Time to recover 50% T_{50}	6120	5890

4.3.5 The G Scalar History Function for Rye Meads

A final post processing step for the Rye Meads tank was to track streamlines that follow the augmented solids velocity field as discussed in Appendix B.5. Figure 4.16 shows the G field, equation (2.46), around the influent on the right hand side of the influent riser and stream lines passing though the stilling pond G field on the left hand side of the influent riser. The G field itself only exceeds a value of 35 s^{-1} in a small local region adjacent to the influent slot. In the left hand figure there are 14 streamlines equi-spaced vertically entering the stilling well from the influent slot. These streamlines follow the path of the flocs falling with the density current into the re-circulating and settling bed. The streamlines are tracked and coloured with time.

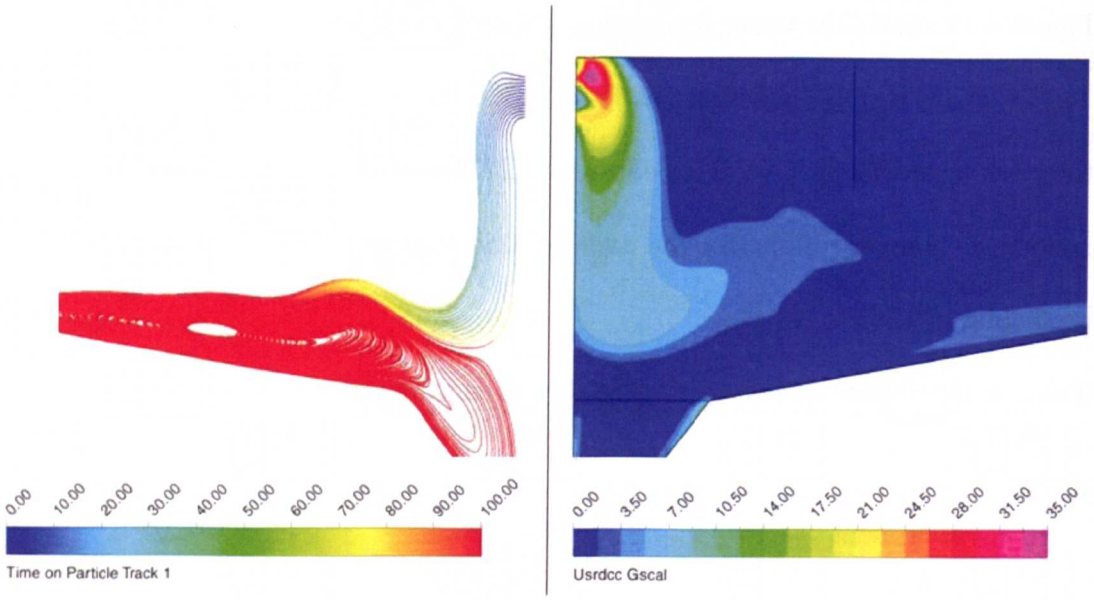

Figure 4.16: *G* scalar field (right) and streamlines following the solid velocity field coloured with time (left).
The magnitude of G only exceeds 35 s^{-1} very close to the influent. The solids stream lines fall rapidly into the settling bed.

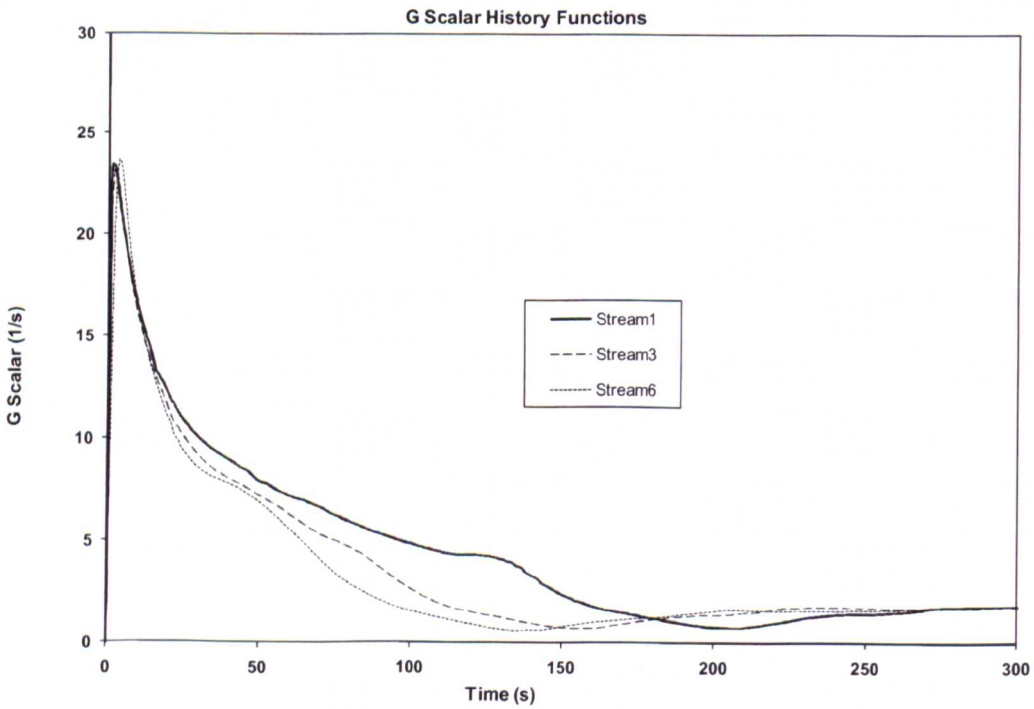

Figure 4.17: Individual stream *G* histories for tracks 1, 3 and 6. .

From the stream lines and the *G* field it is possible to deduce the *G* scalar history for each of the streams, Figure 4.17 shows the *G* history plots for streams 1, 3 and 6. It

can be seen from these plots that a typical G history does not exceed 25 s^{-1} and that G only remains above 10 for the first 25 to 30 seconds of the time period. These values are much lower than might be expected and G only exceeds the levels high enough to promote orthokinetic flocculation of activated sludge, as defined by Biggs (2000), in the first few seconds following entry into the stilling pond. The G history tracks were performed for over one hundred particles with and without turbulent dispersion applied. All of the tracks produced similar plots to Figure 4.17.

4.3.6 The Camp Number *G.T* for Rye Meads.

Camp (1953) proposed that the performance of a flocculating zone may be correlated to $G.T$; where the average G value may be obtained from knowledge of the power dissipated from the influent flow, P_{in}, (or a local mixer) into the flocculating zone (Twort et al, 2000).

$$G = \sqrt{\frac{P_{in}}{\mu_m . Vol}} = \sqrt{\frac{K Q_{in}^{\ 3} \rho_m g}{\mu_m . Vol}} \qquad (4.3)$$

and the hydraulic retention time is given by equation (2.1), $T = Vol / Q_{in}$, where, Vol is the enclosed volume of the stilling well, Q_{in} is the flow through the influent riser and K is a loss coefficient through the influent bellmouth or slot ($K \approx 0.5$).

For a flocculator to work well, it is generally found that the mean G values should be in the range of 20 to 100 s^{-1} (Twort et al, 2000), or specifically between 30 to 70 s^{-1} for the flocculation of activated sludge (Parker, 1972). The solids must also be retained within the mixing zone for long enough to allow sufficient collisions to occur so that $G.T$ is in the range 20,000 to 200,000. (Twort, et al).

From equations (2.1) and (4.3) the flocculating parameters for the Rye Meads centre well at average flow were calculated to be $G \approx 22\ s^{-1}$ and $G.T \approx 9000$. The

equivalent mean flocculating parameters were obtained from the CFD results by volume averaging G within the stilling zone, this gave $G \approx 3.0\ s^{-1}$ and then $G.T$ was approximated as the numerical integration of the floc G history, plotted in Figure 4.17, for the time that the stream line was resident within the stilling zone ($< 13\ s$) which gave an average $G.T \approx 200$.

4.3.7 Conclusions for the Rye Meads Results

The Rye Meads study is the basis for much of the further work on industrial design. The following observations are made from these results:

- The mass flux prediction, which shows that the tank should be performing well within its maximum capacity, is confirmed by the CFD prediction.
- A first analysis on an average density grid shows a velocity distribution with flow features similar to those described by Anderson (1945). The main features of the flow are named and some new ones, such as the bed conveyor, are identified.
- The differences between the coarse, medium and fine grids are marginal but it cannot be said that the solution has achieved full grid independence. It was decided to pursue further simulations with grids of around 10,000 hexahedral cells in a single axi-symmetric plane.
- An investigation of the floor boundary condition, with some regard to approximating the action of a scraper was explored. There were certainly differences between the methodologies tested but these were all in the near wall regions and the bulk flow behaviour seemed to be largely unaffected by the floor boundary condition. For future working the arguments of Deininger (1998) and Armbruster (2001) were followed in approximating the action of

the scraper as a mechanism for breaking the frictional link between the compressing sludge blanket and the floor without imparting significant radial and rotational momentum to the fluid mixture.

- The comparison between different rheological models for sludge shows a similar trend to that observed by Lakehal (1999), that is the more complex Bingham plastic relationship (equations 3.13 and 3.14) predicted a lower settled bed than the Bokil Bewtra (1972) empirical function.
- Comparisons of the two different turbulence models used in this work showed no significant differences between the Wilcox (1994) turbulence model and the Menter (1994) modified low Reynolds number $k-\omega$ model for this class of flow.
- The transient tracer work gave short circuit times and residence time distribution in close agreement with the site experiments.
- The G scalar plots and G scalar history function indicate that the magnitude of G in the clarifier is very low and only exceeds the levels high enough to promote orthokinetic flocculation of activated sludge, as defined by Biggs (2000), in the first few seconds following entry into the stilling pond. The Camp number for the stilling well, calculated by the use of the G scalar history function, was two orders of magnitude lower than might be expected for good flocculating function, (Twort, 2000)

The results for the Rye Meads study were sufficiently convincing to consider an extended validation programme for the model and future use in design studies.

CHAPTER 5: Laboratory Scale Experiments

Summary

This chapter describes the production of synthetic latex sludge (SLS) and its use in laboratory experiments. A lock exchange experiment is described and comparisons of the dynamic behaviour of SLS and real activated sludge are made. Finally, CFD results for the same lock exchange experiment are presented where alternative rheological functions are used to model the apparent viscosity of the sludge mixture as discussed in Chapter 3. The transient CFD results are compared with the experimental data for the activated sludge and the SLS in order to see which rheological function best describes the dynamic behaviour of sludge in the lock exchange in the CFD model.

5.1 Introduction

The accurate modelling of final settling tanks requires the use of constitutive relationships to represent the particle interactions and hydrodynamics of the activated sludge flocs. These relationships are difficult to determine in a laboratory situation because of the sensitivity that sludge exhibits to external factors such as heat, shearing and oxygen supply. Therefore, experiments with real activated sludge have to be carried out at the sewage treatment works or within short periods of sampling accepting that the sludge is potentially changing its characteristics through the course of the experiment as biological populations grow and die. A surrogate sludge that has similar constitutive relationships for density, settling velocity and viscosity to that of activated sludge but does not have such sensitivity to external factors would be a useful tool for the physical modelling of settling systems and the subsequent validation of the computational models discussed in this thesis.

In order to gain a fundamental understanding of the motion of sludge in a controlled laboratory environment, an activated sludge surrogate or Synthetic Latex Sludge (SLS) was manufactured following the work of Örmeci and Vesilind (2000) and a number of tests were devised to compare this surrogate with real activated sludge. Further to this, a lock exchange rig was built at the University of Bristol and experiments were performed with, SLS and real activated sludge, at the Swindon STW, for comparison with CFD predictions. Lock exchange tests with simulant were performed in September 2002 and a campaign of tests with real activated sludge was performed at the Swindon STW in March and April of 2003.

This chapter describes the SLS characterisation tests and results for sludge volume index (SVI), floc density and particle size distribution (PSD). Additionally, the lock exchange experiment was used to estimate the specific gravity of SLS following an analysis similar to that performed by Larsen (1977). Comparisons are made between SLS and activated sludge characteristics and these observations are used to interpret the lock exchange results for SLS and activated sludge. Finally, the experimental results are compared with computational predictions using the Bokil and Bewtra (1972) and Herschel Bulkley (de-Clercq, 2003) model representations for sludge mixture apparent viscosity (additional results for other rheology models are included in Appendix C).

5.1.1 Acknowledgements

The manufacture of SLS was a relatively complex procedure and could initially only be performed in small, 100 *ml*, samples primarily because of the prohibitive cost of the monodisperse latex microspheres[3] provided by the Interfacial Dynamics

[3] In 2001 a 50 *ml* solution of 1200 *nm* latex microspheres cost £240.00 (ex VAT) from Interfacial Dynamics Corporation, www.idclatex.com

Corporation (IDC). For 0.5 *l* batch production of SLS, as used in the later lock exchange experiments, polydisperse latex microspheres were provided in large quantities by Dr Tim Obey at the Bristol Colloid Centre (BCC).

The SLS discussed here was manufactured by the author using the facilities of the BCC while the work on Particle Size Distributions for SLS was performed in collaboration with Dr May Lim at the Centre for Particle and Catalyst Technologies at the University of New South Wales (UNSW), Sydney Australia. Assistance in the experiments with the lock exchange rig using activated sludge samples from the Swindon STW site was provided by Dr Peter Pearce.

5.2 The Manufacture and Characterisation of Synthetic Latex Sludge (SLS)

A simulant for activated sludge referred to here as SLS was manufactured using materials and methods originally proposed by Örmeci and Vesilind (2000). The SLS was manufactured in various forms with idealised monodisperse latex (IDC) or a polydisperse latex (BCC) used alternately with three lengths of cellulose. Settlement tests were performed with 100 *ml* batch samples in a simple glass measuring cylinder and particle size distributions were obtained with a Malvern master-sizer. The density of an individual floc was approximated by a relatively simple bed weight analysis. The purposes of this characterization was to determine whether SLS could be used as a surrogate for activated sludge in lab scale experiments in order to provide data sets which could in turn be used for the validation of computational settling models.

5.2.1 The Constituents of Activated Sludge

Activated sludge flocs are aggregates of suspended soft solids with groups of microorganisms embedded in a polymeric network referred to as extra-cellular material. It is thought that alginate, which occurs naturally in the cell walls of brown algae, is a likely constituent of the extra cellular material. It is known that alginate changes its properties in the presence of various cations. In particular, calcium-alginate gel is formed when alginate is combined with Ca^{+2} ions. The primary particles in an activated sludge are the smallest particles that can aggregate. These may be considered to be the smallest biological units, i.e. a single bacterium. As activated sludge ages, or is exposed to low shear environments, the concentration of primary particles increases and the sludge shows a flocculating tendency (CIWEM, 1997). Two mechanisms are thought to be at work;

- Polymer bridging by floc formers. The overall floc structure is negatively charged and therefore multivalent cations act to form bonds between the extra cellular material and the bacteria. Ca^{+2} is known to be the most important cation in this bridging process.
- Formation of a filamentous bacteria backbone. As the floc grows it is given strength and structure by the presence of fibrous filamentous bacteria.

Filaments and floc formers combine together in large, 100 μm – 2000 μm, irregularly shaped strong flocs. In an ideal sludge, the filaments grow largely within the floc length scale providing strength and structure. Bulking sludges, however, have larger concentrations of filamentous bacteria that protrude from the floc. These settle poorly and also break more easily in a high shear environment.

5.2.2 The Constituents of Synthetic Latex Sludge (SLS)

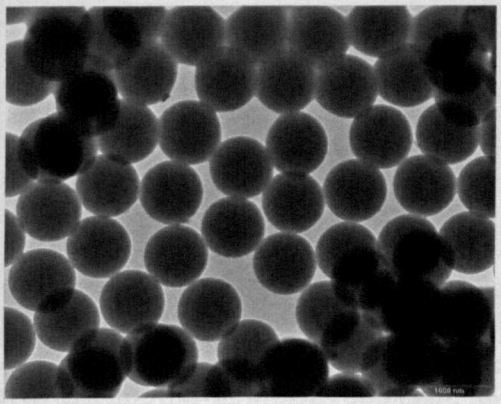

Figure 5.1a: Latex microspheres Polydisperse wih the majority at 850 *nm* diameter supplied by the Bristol Colloid Center. Photo T. Obey BCC.

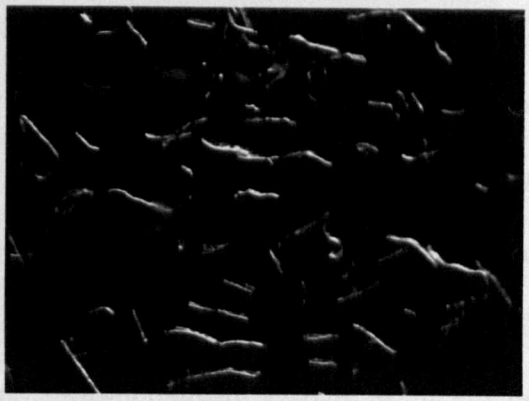

Figure 5.1b: Long cellulose fibres 125-400 *μm* fibres used to represent filamentous bacteria colonies. Photo M. Lim UNSW.

In this SLS, originally proposed for use in dewatering experiments, negatively charged latex polystyrene microspheres were used to simulate the smallest individual bacterium. Alginate was used to simulate the extra cellular material and a calcium chloride solution was used to provide the bridging cations. The filamentous bacteria were represented by fibrous cellulose with different cellulose length scales, short, medium and long, used to influence the strength and bulking characteristics of the sludge. The base materials used are listed in Table 5.1

Table 5.1: Materials used for the manufacture of SLS following Örmeci and Vesilind (2000).

Material	Dimensions	Supplier
White monodisperse polystyrene latex microspheres in de-ionized distilled water suspension, 8% by mass	1200 *nm* diameter micro spheres	Interfacial Dynamics
Sodium chloride		Sigma Aldrich
Calcium chloride dehydrate		Sigma Aldrich
Alginic acid, sodium low viscosity, from macrocystis pyrifa (Kelp)		Sigma Aldrich
Cellulose, long fibrous	125-400 *μm*	Sigma Aldrich
Cellulose, medium fibrous	50-350 *μm*	Sigma Aldrich
Cellulose, micro granular	25-75 *μm*	Sigma Aldrich

5.2.3 Manufacturing Method for SLS

Three stock solutions of 0.085 *M* sodium chloride in distilled water (NaCl), 0.5 *M* calcium chloride ($CaCl_2$) and 5 *g/l* Alginate (alginic acid) were made up. The flocs were made in batches as follows; 100 *ml* of 0.085 *M* NaCl solution was poured into a conical flask and dosed, using a 2*ml* pipette, with 2.5 *ml* of recently manufactured alginic acid (5 *g/l*) to approximate a 125 *mg/l* alginate solution. The conical flask was set on an IKAMAG magnetic stirrer and a magnetic flea was introduced to the mixture; the sample was stirred at around 100 *rpm.*

The sludge was produced following a similar method to Örmeci and Vesilind (2000). The cellulose was weighed to 0.06*g* using a Precisa 125A balance and introduced to the sample slowly to obtain good mixing. Three samples were prepared one for each cellulose type, long, medium and micro-granular. Samples were dosed, using a 2*ml* pipette, with 1.25 *ml* of the latex bead solution (taken from the 50 *ml* IDC solution at 8% solids) to give the required 0.1% latex particles. The samples were left to stir at 60 *rpm* and 21°C overnight for 15 hours in order to allow adsorption of the alginic acid onto the solids. Flocculation was achieved by dosing the next day with a pipette up to 4 *ml* of 0.5 *M* $CaCl_2$ solution, Figure 5.2 shows the flocs forming immediately after this dosing process. A further 1 *ml* of $CaCl_2$ solution was added after flocculation had occurred to give 25 *mM* Ca (II). The resulting SLS was a readily settling floc with irregular size and shape as shown in Figure 5.3.

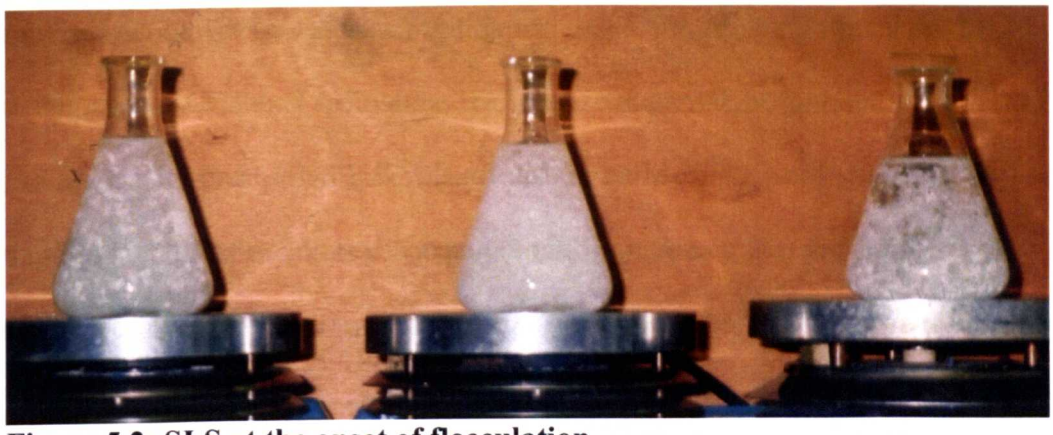

Figure 5.2: SLS at the onset of flocculation.
Microgranular cellulose to the left, medium fibrous in the middle and long fibrous to the right. Flocs are forming in the stirred solution immediately after dosing with . $CaCl_2$ solution. The microgranular cellulose forms a clumping floc while the long fibrous cellulose forms long strands of floc.

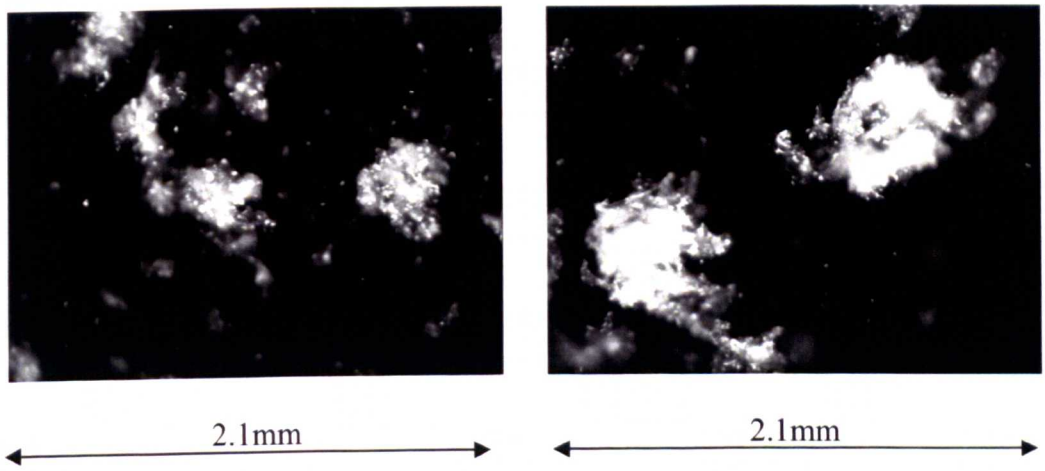

Figure 5.3: Micrographs of SLS.
Flocs formed with microgranular cellulose are on the left and medium fibrous cellulose on the right. Typical floc length scales are 200 to 1000 μm.
Photo M. Lim UNSW.

5.2.4 Characterisation of SLS

Characterisation is required to determine the necessary data for the calculation of model coefficients to be used in settlement models. For the drift flux model of settling a sludge volume index (SVI) measurement may be used to approximate the Vesilind settling constants (see Chapter 3).

For analysis using multiple drift fluxes it is necessary to describe a particle size distribution (PSD), and individual floc density. If the SLS is to be used to validate

models of flocculation then it must have the ability to break and then coalesce again in the correct shearing environment. Therefore, settlement and PSD measurements were performed to obtain representative data for the SLS before and after a shearing event. In all cases it is required to understand the concentration of solid held up in the mixed liquor suspension the MLSS (*mg/l*) and to determine the density of the dried solid for use in equation (2.36).

5.2.4.1 Mixed liquor suspended solids for SLS.

The constituents of SLS are summarised in Table 5.2 in the proportions recommended by Örmeci and Vesilind (2000).

Table 5.2: Review of sample volumes and solids content for SLS.

	Sample Volume (*ml*)	Concentration	Solids (*mg*)
NaCl Solution	100	0.085 M	497
Alginate	2.5	5 g/l (0.5%)	12.5
Cellulose			60
Latex spheres	1.25	80 g/l (8%)	100 (0.1%)
$CaCl_2$ Solution	5	0.5 M	367
Total	108.75		1036.5

In order to use the properties of SLS for further analytical study it is necessary to understand the proportion of the total mass, summarised in Table 5.2, that is taken up by the solid flocs. This becomes the SLS analogue for the mixed liquor suspended solids (MLSS) or the initial solids concentration. Just drying the SLS gives the same solids content as applied (0.95%) but this is clearly a significant over estimate for MLSS as a large amount of the solid remains in the supernatant as dissolved salt. If it is assumed that the settling bed was formed only from the binding of the alginate, cellulose and latex, a solids concentration of 172.5 *mg* in the SLS sample would equate to a mixed liquor concentration of 1586 *mg/l*. However, this would be an under estimate as it is known that the Calcium ions play an important part in the floc binding process. Therefore, in order to estimate the MLSS, a measure of the calcium

uptake into the floc is required. The approximation used to determine the MLSS was to measure the residual solids dissolved in the supernatant by a dry weight analysis and assume that only $CaCl_2$ took part in the floc binding process. In this way it was found that 11% of the total calcium salt mass was taken into the floc giving an SLS sample solids concentration of 212.9 *mg* or equivalent MLSS of 1965 *mg/l*.

5.2.4.2 Settlement Characteristics

A total of 9 x 100 *ml* samples were made and allowed to settle in a 100 *ml* measuring cylinder for 30 minutes before the settled volumes were noted. The MLSS and settled volume data could then be used to calculate Sludge Volume Index (SVI) values following equation (1.1) as shown in Table 5.3. These SVI values are low in comparison to the range expected for real activated sludge of between 50 and 120.

Table 5.3: Settled volume of SLS and the SVI index. The SVI values are low when compared to real activated sludge.

Samples	Cellulose Used	Average Settled Volume		Variation	Average SVI
		(ml)	*(%)*	*(min - max %)*	*(ml/g)*
1,2,3	Microgranular (25-75 μm)	6.8	6.2	5.5 – 6.8	31.7
4,5,6	Medium Fibrous (50-350 μm)	7.5	6.9	5.9 – 7.8	35.2
7,8,9	Long Fibrous (125-400 μm)	7.8	7.2	6.8 – 7.8	36.5

5.2.4.3 Floc Density

In order to estimate the floc density, the settled floc beds for three samples, one sample for each cellulose size, were decanted into a 10 ml settling column with the remaining supernatant carefully extracted from above the bed with a pipette. The settled wet sludge beds were then weighed and found to have an average mass of 6.92 *mg*. By approximating the flocs in the settled beds as spheres, with a maximum

packing factor of 0.62 (this is highly approximate as the flocs are packed in an irregular manor with deformation of the floc shapes), the individual floc specific gravity was estimated to be 1.016. It has been suggested by other workers that an individual activated sludge floc specific gravity may vary between 1.01 and 1.02 (ASF, 2003). Although this estimate is a useful indicator that free SLS flocs may settle at a similar rate to free activated sludge flocs, it is not at all easy to calculate the specific gravity of dried SLS by direct measurement. Therefore, the method of Larsen (1977) was followed to estimate this from the lock exchange test data as discussed in section 5.3.

5.2.4.4 Particle Size Distribution (PSD)

This study was performed by Dr May Lim of UNSW and is discussed in more detail in a separate paper (Burt and Lim, 2003). Only the results are presented here in order to allow comparison with activated sludge.

Small angle light scattering was used to measure the particle size distribution (PSD) of synthetic latex sludge (SLS) with a Malvern Master-sizer before and after a shearing event.

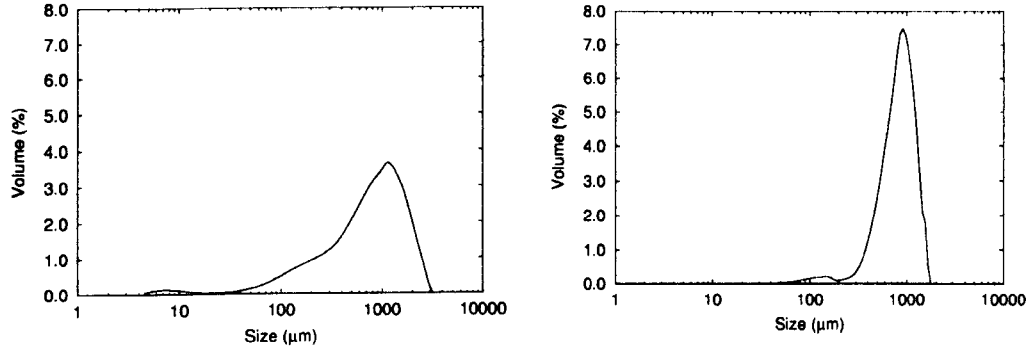

a) SLS made with microgranular cellulose.

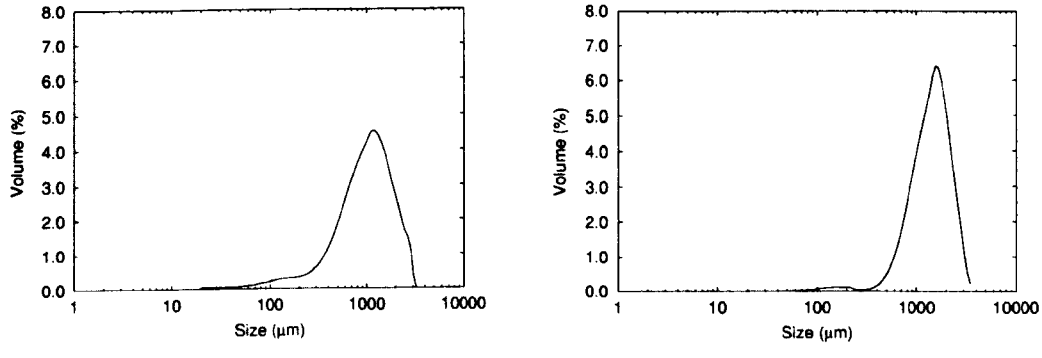

b) SLS made with medium cellulose

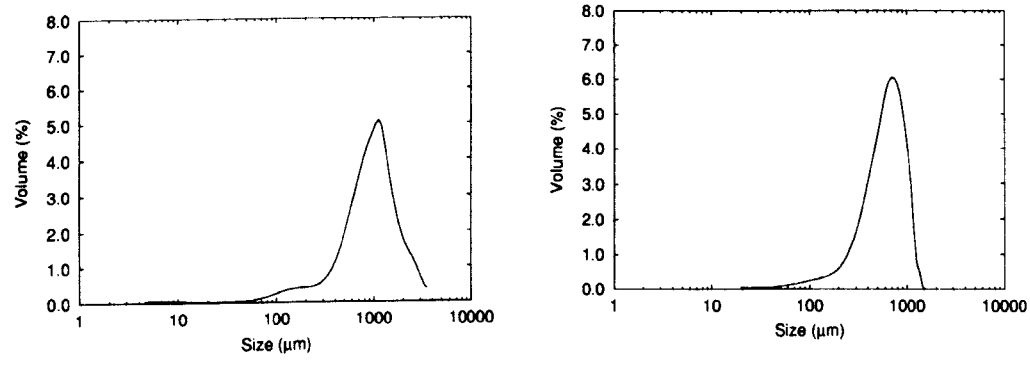

c) SLS made with long cellulose.

Figure 5.4: PSD of SLS before and after resuspension.
Plots on the left are for the SLS immediately after production. The plots on the right are for the same floc samples resuspended after 24 hours. Measurements taken by M. Lim UNSW, (Burt and Lim, 2003).

In Figure 5.4, The most common floc size values for SLS are in the range of 1 *mm* with Sauter Mean Diamater (SMD or $D_{3,2}$) between 260 and 540 μm for this data. These results are different to the on line PSD measurements for activated sludges in

the stilling zone of a settlement tank as reported by de-Clercq (2003) which showed peaks between 100 and 300 μm and an SMD of 100 μm. The PSD for microgranular and long fibrous cellulose show a small peak in the distribution curve between 5 μm and 10 μm. This is particularly evident for SLS made from microgranular cellulose. This feature is common in PSD data for real activated sludge and is of significant interest because it is material in this size range which must be flocculated to the large particles in order for a settlement tank to work well as a clarifier (Ekama et al, 1997).

After 24 hours of settling, the SLS was resuspended and the PSD measured again. For SLS produced from micro-granular and medium fibrous cellulose, the PSD became narrower after the flocs were resuspensed. The peak in the distribution curve is shifted slightly to the right, indicating an increase in floc size. On the other hand, the PSD for resuspended long fibrous cellulose SLS showed a shift to the left. This indicates that the long fibrous sludge actually decrease in size after settling and resuspension. This confirms laboratory observation that long fibrous cellulose SLS flocs are weak and can be broken easily by shear and therefore this version of SLS would not be useful for repeat use in a test rig.

5.3 The Lock Exchange Experiment

The use of lock exchanges to examine fluid properties and dynamic behaviour of activated sludge systems was originally proposed by Larsen (1977). The lock exchange test rig used in this work was designed and built according to the engineering drawings included in Appendix C where the bulk of the rig was constructed in transparent perspex. The purpose of the rig was to investigate the hydrodynamic behaviour of activated sludge mixtures and to observe similarities and

differences between real activated sludge, SLS and provide validation data for a CFD model of the experiment. The rig was also used to visualise the dynamic behaviour of the sludge gravity current and examine the interactions between moving sludge and stationary surfaces.

The principle of the lock exchange is to generate a controlled release of dense fluid into a lighter fluid in order to observe a gravity current (Härtel, et al, 2000). In this case, the dense fluid is concentrated mixed liquor and so the lobed front of the gravity current will contain disperse flocculated solids while the lighter fluid is sludge supernatant. In this work the dynamics of the gravity current were observed by taking videos and photographs of the lock exchange release event and the distribution of solids concentration with time provided transient data for comparison with CFD modelling.

Of particular concern, is the influence of rheology on the dynamic behaviour of the gravity current. It is known that the rheological properties influence the consistency of the sludge mixture under shearing, that is, where an increasing apparent viscosity makes the fluid harder to shear, there is a damping of momentum. This is a very important aspect of flow in a settlement tank as it is the sludge thickening process that influences the dynamic response of the fluid mixture in the lower depths of a clarifier and these are known to be particularly difficult to model with CFD. This was identified by Ekama et al (1997) as a key research area which has been investigated in turn by Lakehal (1999), de Clercq (2003), Armbruster (2003) and most recently Weiss (2007). All of these workers have proposed variations on rheological models for activated sludge, but they made only limited efforts at validation. Therefore, it was intended to use the results from the Lock Exchange rig

to compare CFD predictions for some of the proposed rheological model as presented in section 3.4.

5.3.1 The Lock Exchange Apparatus

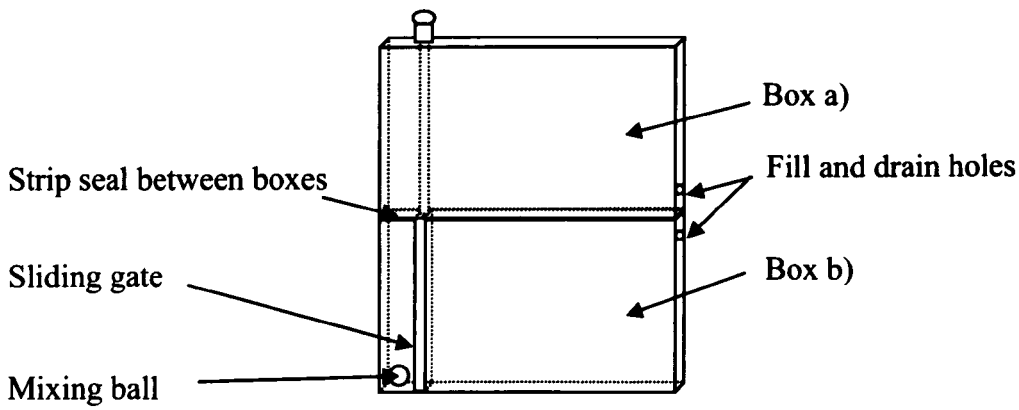

Figure 5.5: Schematic of the lock exchange apparatus.
Sludge is trapped at high concentration behind the closed sliding gate. When the gate is lifted the column of retained sludge falls into box b). The fluid zone in box a) is used only to maintain the fluid seal for the sliding gate.

The apparatus is arranged as two fluid boxes or zones. The top box is passive in the experiment providing only a fluid seal for the sliding gate to move into. The bottom box is the active zone in which the lock exchange experiment may be observed. The active zone is 300 x 300 x 25 *mm* (2250 *ml*) while the passive zone is slightly taller to accommodate the gate in the fully open position. The rig rotates on a pivot from a horizontal attitude, in which the rig is primed, into a vertical attitude immediately prior to lock release.

Figure 5.6: Lock exchange apparatus being tilted from vertical to horizontal. This photograph also shows the sliding of a dense cohesive activated sludge bed down the tilted floor of the apparatus.

The brass lock gate may be opened or closed by pulling or pushing the steel tie bar up and down; the tie bar is sealed to atmosphere with circular 'o' rings in an aluminium bush and the gate is sealed to retain flocs at the connection between the upper and lower boxes with a rubber strip. In the closed position, the lock gate traps settled flocs in a volume which is 10% of the active zone. This becomes the initial sludge volume for release at the start of the experiment.

The apparatus was originally conceived as a sealed unit for repeat experiments with SLS but it was also found to be well suited for experiments with activated sludge. When using real activated sludge it was necessary to limit the experimental time to a few hours and, when not in use, the apparatus was left in a horizontal attitude with air periodically sparged through the fill and drain holes to prevent the sludge denitrifying.

5.3.2 Experimental Procedure for the Lock Exchange Experiment

In order to begin an experiment the correct amount of homogenised mixed liquor, at known solids concentration, had to be distributed evenly behind the sliding lock gate. This distribution was achieved in a number of steps.

1) An SSVI test was performed, at unknown initial sludge concentration, in order to establish the settleability of the sludge. A sludge line settling test was also performed to determine the Vesilind coefficients for comparison and later use in CFD modelling. These tests and the settling data produced at Swindon were discussed in Chapter 3.
2) A drying test was performed to calculate the solids content of the MLSS samples.
3) Based on knowledge of the SSVI at 30 minutes, an estimate of the amount of supernatant was made so that, once settled in the lock rig, the sludge bed would sit behind the lock gate line.

Tests were perfumed with SLS and activated sludge varying the initial concentration of the mixed liquor retained behind the lock gate with each event recorded on to a digital video camera as follows:

Table 5.4: Initial conditions and indices for the Lock Exchange Tests.

Tests	Matl	MLSS *(mg/l)*	SSVI or SVI *(ml/g)*	Vol_{ML} *(ml)*	Vol_S *(ml)*	X *(mg/l)*
1	SLS	1965	35	2250	0	19650
2,3,4	AS	4700	70.2	480	1770	10027
5,6	AS	3820	70.2	750	1500	12733
7,8	AS	5500	73	480	1770	11733

Table 5.4 summarises the initial data for each test. The MLSS is the solids content of the sludge in its sampled form; either, as directly retrieved from the aeration lane, or in the case of SLS, the calculated quantity discussed in this chapter (section 5.2.4.1).

The SVI or SSVI are the settlement indices, Vol_{ML} and Vol_S are the volumes of mixed liquor and supernatant combined together to give the active zone volume of 2250 *ml*. The SLS, with SVI around 30, settles to less than 10% of its original volume so it is not required to dilute the original mixture down before adding it to the lock active zone. This means that the concentration of settled sludge behind the lock gate is 10 times the original MLSS. However, for the activated sludge, the SSVI values indicated that dilution was required to allow the settled sludge bed in the active zone to collect behind the lock. Therefore, various mixture dilutions were tested giving initial column concentration between 10,000 and 12,700 *mg/l*. Notice that the solids density of the activated sludge mixed liquor is significantly less than for the SLS because of the requirement to maintain equal lock volume in all tests.

In order to prime the apparatus, it was seated in a horizontal attitude with the fill / drain holes located at the top of the tank. Supernatant was added to the top box, (a, in Figure 5.5) and the MLSS mixture was added to the bottom box (b) with the lock exchange gate fully open. Each box was filled progressively in order to minimize the cross over of flocs through the gate seal from the active to passive zones. Once both boxes were full, the mixed liquor in the active zone was allowed to settle and occupy the lock region. Note that during this process a buoyant mixing ball was retained behind a protruding portion of the lock gate, as shown in Figure 5.7. Once the sludge had fully settled the lock gate was closed. Before starting the test, the rig was raised and lowered several times about the pivot in order to homogenise the mixed liquor behind the gate through the action of the buoyant mixing ball. Finally the rig was placed in vertical attitude and the gate raised.

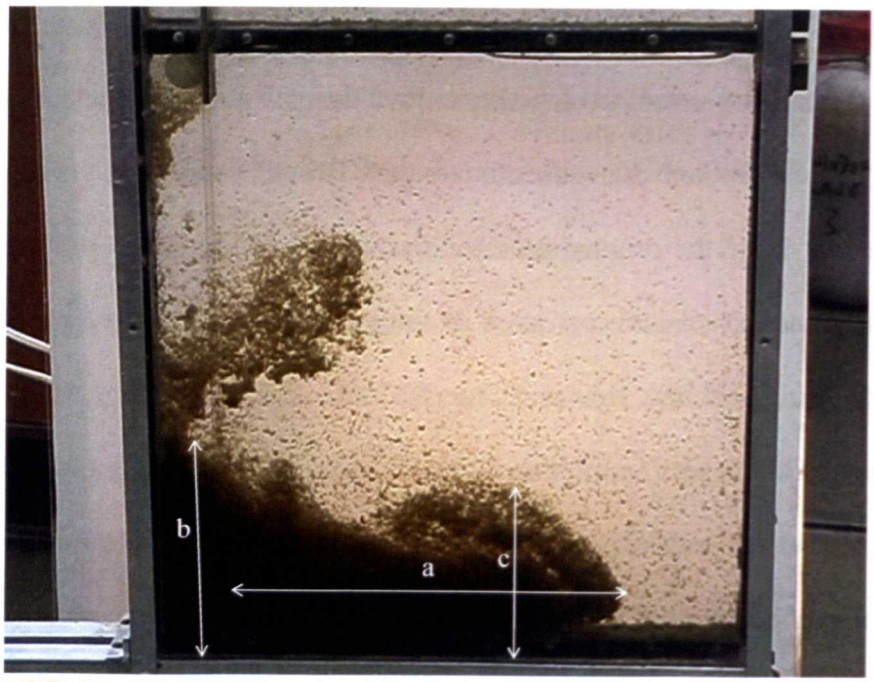

Figure 5.7: Lock Exchange for test 2 shortly after release.
The characteristic dimensions are a) the distance travelled by the nose, b) the height of the collapsing column and c) the height of the lobed front.

The resulting flow, shown in Figure 5.7, is a strong gravity-current (Simpson, 1992) with a lobed front of dispersed flocculated material followed by a slower moving (slumping) cohesive bed. In order to compare the results for this flow with activated sludge, SLS and computational models, some characteristic flow dimensions were identified with the intention of monitoring these with time for all test cases. These are indicated in Figure 5.7 as follows:

a) Distance travelled by the nose of the lobed front.

b) Height of the collapsing column.

c) Height of lobed front.

Each of these features can be measured from still frames extracted from the video sequence recorded on the digital camera. The distance travelled by the nose is a sharp interface and is easily discernible in the film images, the height of the lobed front is also relatively easy to distinguish, accepting that there is a degree of dispersion and

the concentration is lower in this zone. The height of the collapsing column is measured 15*mm* from the left hand wall (half of the original column width) and there is the potential for considerable error (+/-20%) in this reading.

5.3.3 Results for the Lock Exchange Experiment

The dynamics of the collapsing column are compared for SLS, test 1, and the real activated sludge, test 2, in Figure 5.8. These pictures show the motion of the collapsing column at time intervals after the lock release. The initial sludge bed volumes were similar and the beds were fully homogenised before release. The results for the SLS test 1 and the activated sludge tests 2 to 8 are summarised in graphs normalised to a characteristic time. This is the time taken for the nose of the lobed front to cross the floor and was found to be in the range of T=15 to 18 seconds for all tests. The progression of the lobed fronts crossing the floor of the rig is shown in the graph of Figure 5.9. The rate for the falling column with time is shown in Figure 5.10 and the variation in the height of the lobed front with time is shown in Figure 5.11.

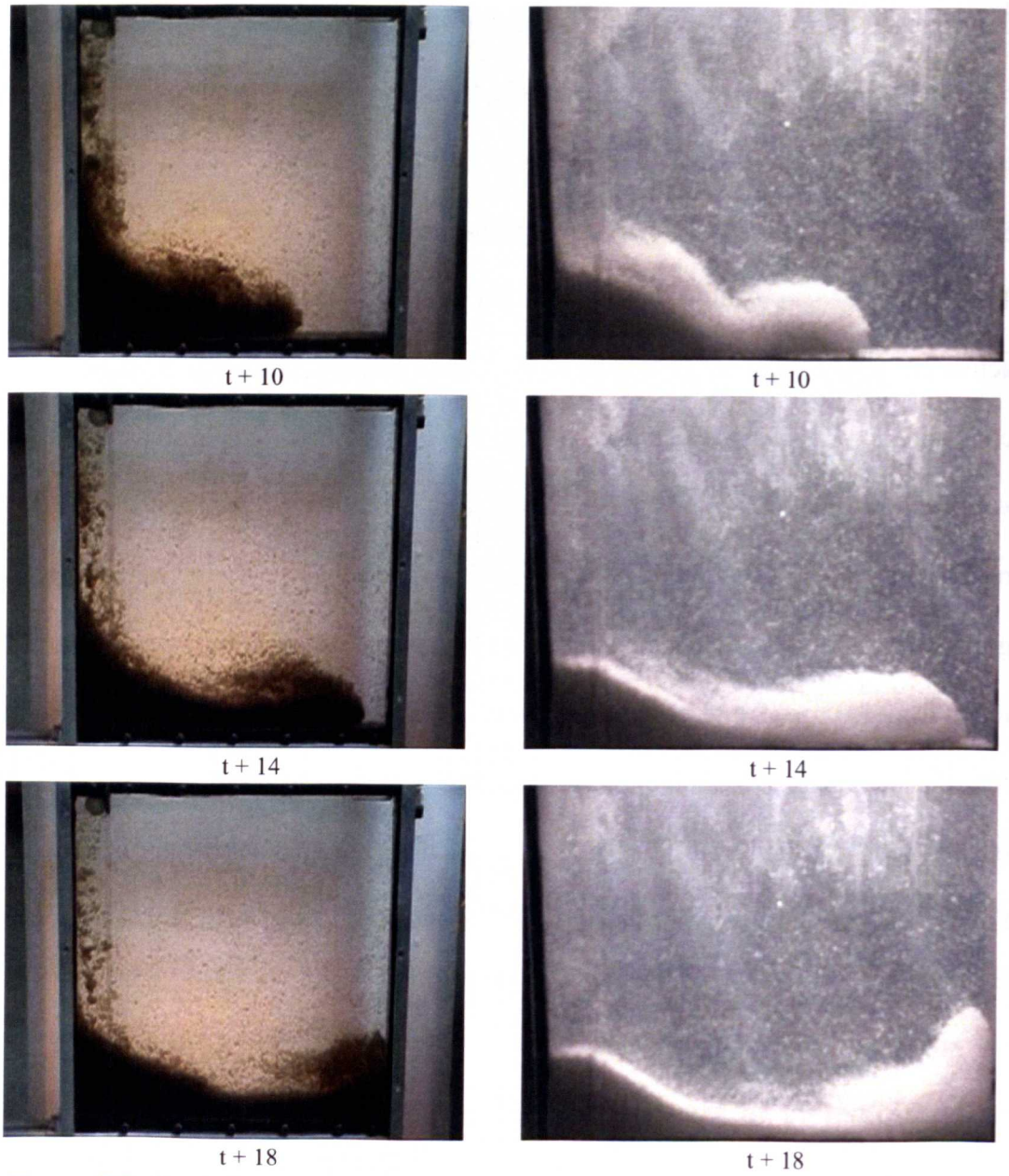

Figure 5.8: Lock Exchange experiment comparison of activated sludge and SLS. The figures in the left column are for activated sludge moving across the base of the active zone with time from test 2. The figures in the right column are at equivalent time for the equivalent test with SLS from test 1.

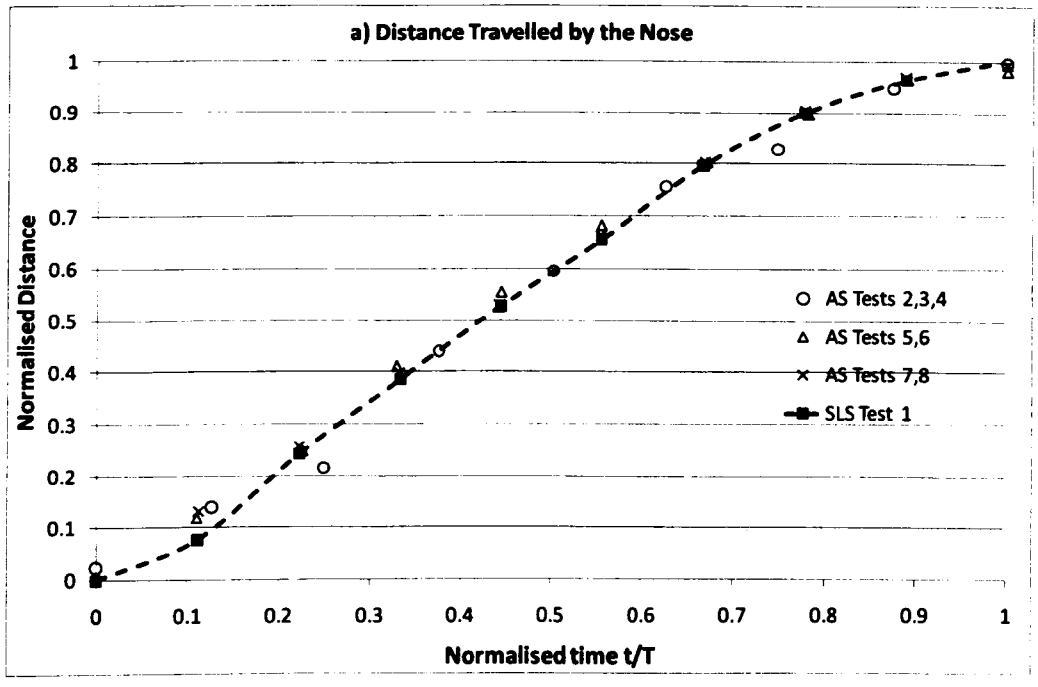

Figure 5.9: Measurements for normalised distance travelled (a) with time comparing SLS with the various activated sludge tests.

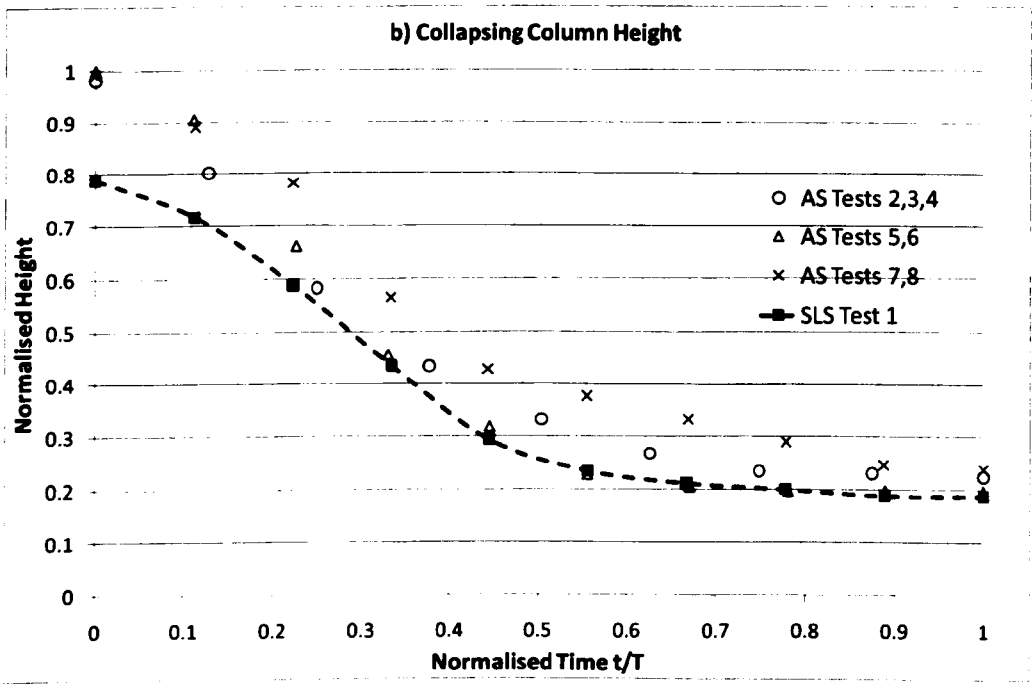

Figure 5.10: Measurements for the sludge collapsing column height (b) with time comparing SLS with the various activated sludge tests.

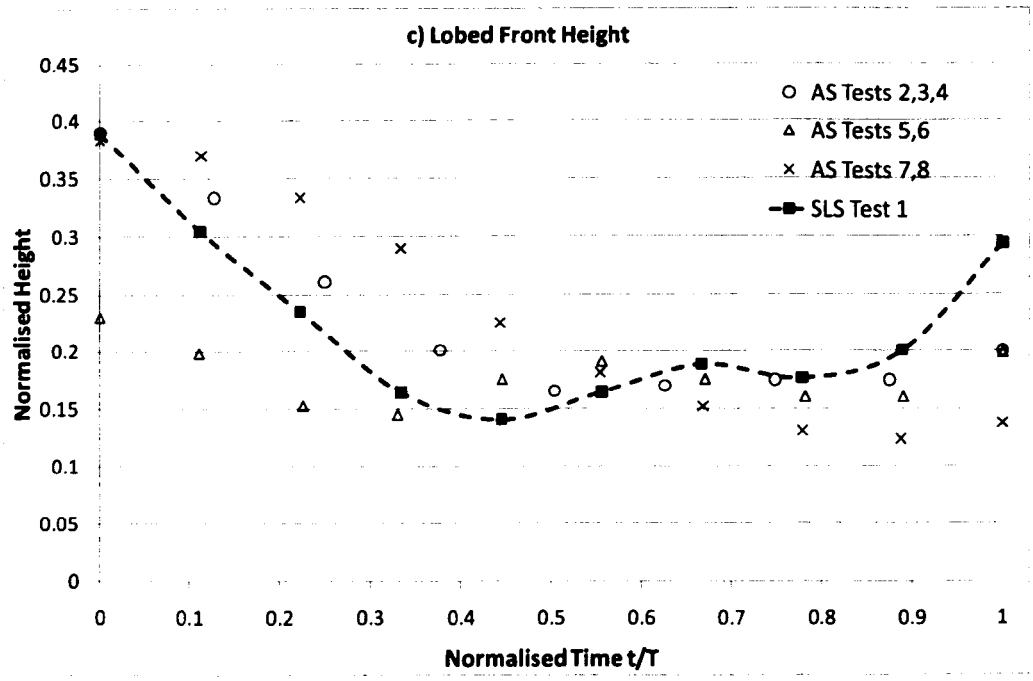

Figure 5.11: Measurements for the normalised lobed front height (c) varying with time comparing SLS with the various activated sludge tests.

In Figure 5.9 it can be seen that the rates at which the fronts of the different sludges approached the far wall were broadly similar, however, in Figure 5.8, the SLS appears to be more disperse. It is important to note that the initial sludge bed volumes were similar but the initial mixed liquor concentrations for SLS and activated sludge, shown in Table 5.4, were considerably different. In Figure 5.10, the SLS initial column starts lower (is less well homogenised) than the activated sludge but falls to the same depth as activated sludge tests 5 and. In Figure 5.11, the SLS data for the lobed front follows the activated sludge trends but is more disperse than the activated sludge approaching the right hand wall.

5.3.4 Discussion of the Lock Exchange Results

Larsen (1977) used an open flume lock exchange experiment to estimate the specific gravity of dried activated sludge. He used the theoretical speed of wave propagation in a gravity current, assuming frictionless flow and small differences between

densities, to calculate the mixture density assuming that the wave speed velocity V_w is the velocity at the lobed front, 10 seconds after the lock release has occurred,

$$V_w = 0.5\sqrt{\left(\frac{\rho_m - \rho_w}{\rho_w}\right)gh} \qquad (5.1)$$

This equation taken directly from Larsen (1977) is a re-arrangement of the expression for densimetric Froude number with Fr' = 0.5. This same expression is discussed in Simpson (1992) who quotes Fr' = 0.47 for constant speed of the front for a general gravity current in a long tank[4].

From knowledge of the mixture density and the concentration of the mixed liquor in the initial column the solid specific gravity may be determined from equation (2.36). The characteristic length scale, h, in the Larsen experiment was the total depth of fluid or twice the height of the lobed front for an open flume. The flows in this lock exchange experiment are confined and re-circulating, so h is not so easily defined.

Table 5.5: Results for the lock exchange tests. Solid density for SLS is calculated from equation (5.1) with the length scale h=50*mm*

Test	Date	Matl	X *(mg/l)*	V_w (mm/s)	T *(s)*	ρ_m *(kg/m^3)*	ρ_s *(kg/m^3)*
1	2/09/02	SLS	19650	18.2	18.00	***1002.5***	***1150***
2,3,4	1/04/03	AS	10027	17.4	16.06	1003.1	1445
5,6	1/04/03	AS	12733	15.9	17.92	1003.95	1445
7,8	9/04/03	AS	11733	18.3	17.98	1003.64	1445

Table 5.5 shows the measured characteristic time T for each test and the measured instantaneous wave speed velocity V_w at 10 seconds into each test, derived from the gradients of Figure 5.8. The characteristic time was found to be similar for all tests and promotes the observation that although the SLS solids concentration behind the

[4] Careful inspection of the Larsen (1977) data reveals he actually used that Fr' = 0.45 to calculate dried activated sludge density in the open flume rig. Not 0.5 as indicated in equation 5.1.

lock in test 1 is much higher than for all other tests, it is this test that has the longest characteristic time.

Given that the specific gravity for dried activated sludge is known to be in the region of 1.445 (Larsen, 1977), it was possible to determine an approximate characteristic length scale of $50mm$ for this experiment from equation (5.1), for tests 2 to 8, which is twice the depth of the rig. Further manipulation of equations (5.1) and (2.36) for the SLS test 1, following the same method as Larsen and assuming that the same length scale applied for all tests, allowed the specific gravity for SLS to be calculated at being between 1.1 and 1.2. This then confirmed that the density of the SLS initial column was lower than for the equivalent activated sludge test even though the solids concentration was much higher. This is a crucial observation and explains why the dynamic results for SLS closely match the other tests with real activated sludge. This is confirmed in Figures 5.9 and 5.10 which both show the SLS following the trend of the other tests.

5.3.5 Summary of SLS Properties.

Visually the SLS appears similar to activated sludge and is equally shear sensitive. At high concentration it is cohesive but it does not exhibit the clear interfaces seen for sludge when it is settling (sludge line settling). The performance in the lock exchange rig also suggests that its dynamic behaviour is at least similar to real sludge. The SVI tests show that simulant can be modified to hold increased amounts of interstitial water by increasing the length of the cellulose used. However, this is at the expense of making the sludge more shear sensitive. In all cases the SVI values for SLS are much lower than normally recorded for activated sludge in the UK.

Table 5.6: Characteristics of SLS compared with Activated Sludge.

	SLS	Activated Sludge
Typical SVI (*ml/g*)	32 – 36	80-100 (Von Sperling, 1994)
SMD $D_{3,2}$ (μm)	260-540	100 (de Clercq, 2003)
Dried Solids Density (*kg/m3*)	1150	1445 (Larsen, 1977)
Open Floc Density (*kg/m3*)	1.016	1.01-1.02 (ASF, 2003)

In addition to SVI, the key model parameters of interest, are particle size distribution, solids density and rheology.

- The PSD measurements show shape distributions very like real sludges with significant amount of non-settleables at around the 5 μm to 10 μm range. However, the Sauter mean diameter for SLS is high.
- The open floc density approximation for SLS appears to be in line with expectations for real activated sludge suggesting that all sludge floc may be thought of as a loose solids matrix containing interstitial water.
- The dried solids density is significantly lower for SLS but this proved to be particularly advantageous in the case of the lock exchange experiment as the combination of low SVI with low density enabled a ratio of equal mass and equal volume for SLS and activated sludge to be tested in the same rig.

5.4 Computational Predictions for the Lock Exchange Experiment.

It was shown in Chapter 4 that a rheology model was required in order to calculate the bed depth correctly inside the Rye Meads clarifier model. This CFD study of the lock exchange experiment was performed as a further attempt to validate the various constitutive relationships for sludge rheology discussed in Chapter 3. Simulations and experiment were compared using the same dynamic markers shown in Figure 5.7 where the position of the sludge to supernatant interface in the CFD model was taken

to be at around the 1000 mg/l contour (thought to be at 850 mg/l following Matko (1998)).

5.4.1 CFD Method

A CFD model of the lock exchange apparatus was constructed with a computational grid of 80 x 80 cells. The sludge column was initialised at 10,027 mg/l following the data for tests 2,3 and 4 in Table 5.4. The dynamic simulation proceeded with 500 time steps of 0.1 s. A high order differencing scheme was used for the spatial discretisation and convergence was achieved within 40 iterations on each time step for the segregated CFD solver CFX4.4. Three model representations of the apparent viscosity were considered

1. A constant viscosity set to be that of water only.
2. The Bokil Bewtra (1972) model
3. The modified Herschel Bulkley model of de Clecrq (2003)

Additional results for the Power law model (Armbruster, 2003), the Root law model (Armbruster, 2003) and the Bingham Plastic model (Lakehal, 1999) were also produced and are included in Appendix C for comparison.

5.4.2 CFD Results

A comparison between experiment and the Herschel Bulkley model is shown in Figure 5.12. The progression of the lobed fronts crossing the floor of the rig is shown in the graph of Figure 5.13. The rate for the falling column with time is shown in Figure 5.14 and the variation in the height of the lobed front with time is shown in Figure 5.15. The CFD results are not normalised to a characteristic time as it is useful to see the dynamic differences that result from using different rheology models.

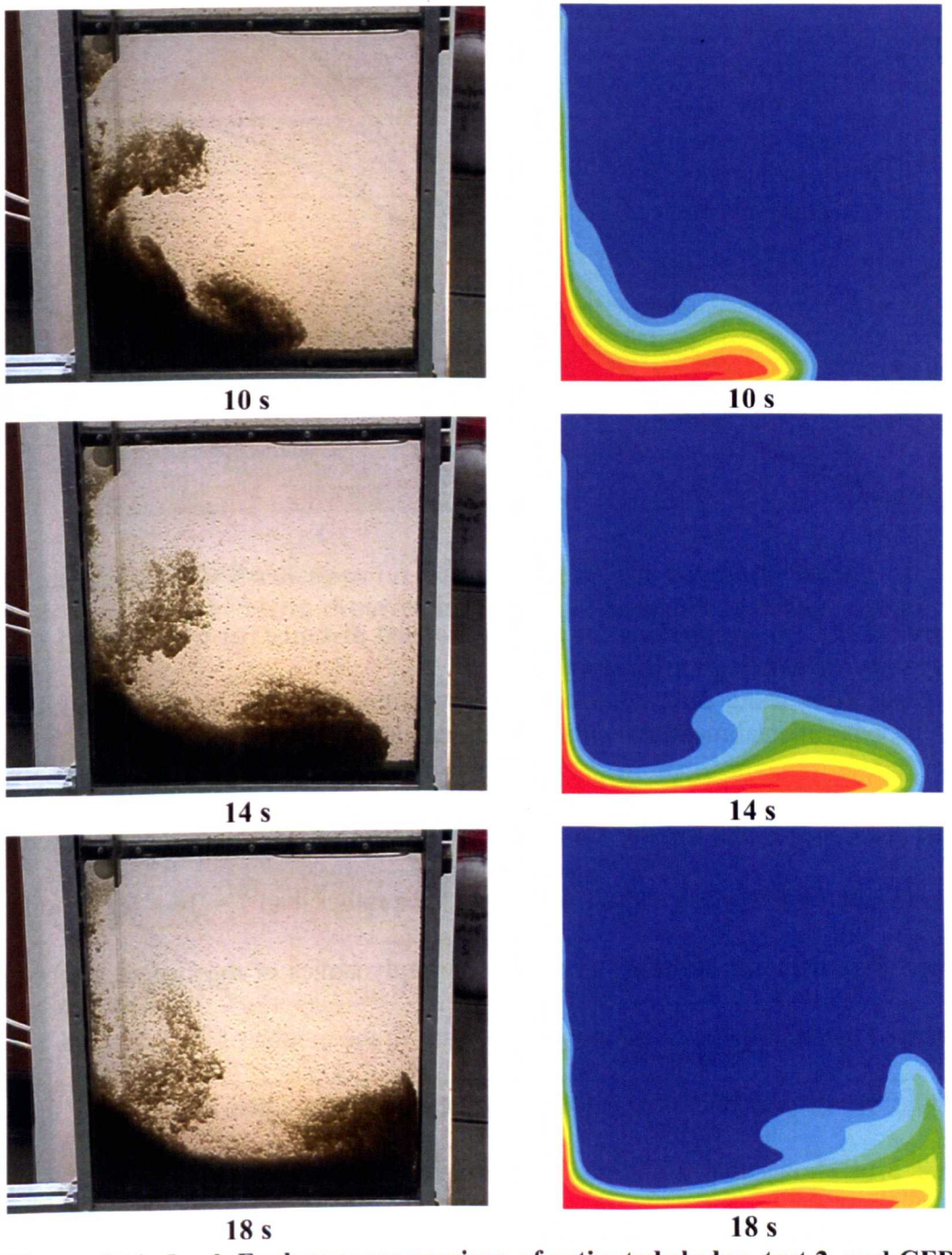

Figure 5.12: Lock Exchange comparison of activated sludge, test 2, and CFD. The CFD predictions are for the Herschel Bulkley rheology model with the sludge column initialised at 10,027 mg/l. The concentration scale is linear between 0 and 10,000 mg/l.

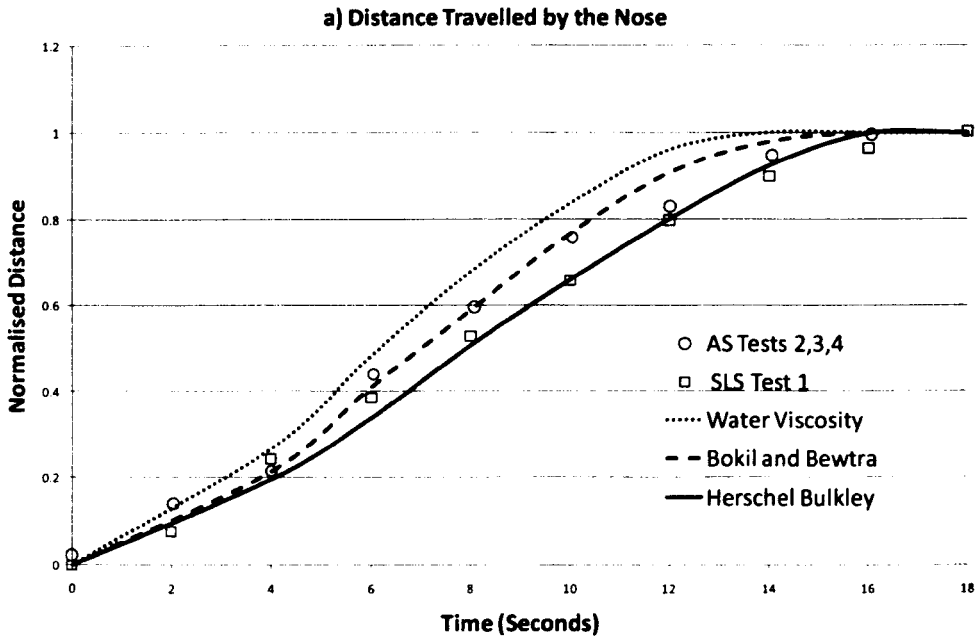

Figure 5.13: CFD predictions for the normalised distance (a) travelled by the gravity current nose with time.
The predictions using different models for apparent viscosity are compared with the experimental measurements for activated sludge and SLS.

Figure 5.13 shows that for the simplest representation with constant viscosity, the characteristic time is much shorter with T = 13.5 s rather than T = 16 s for the other models. This demonstrates that, as expected, the dynamics of the system are being influenced by the rheological properties. In terms of the motion of the front with time the Bokil Bewtra (1972) model is following the experimental data better.

Figure 5.14 shows that all of the CFD models have difficulty representing the collapsing column element of the system. This can be seen in Figure 5.12, where the real sludge appears to be falling as a cohesive body but the concentration gradients in the CFD model show solids adhering to the side wall. The interaction between the stationary wall and falling sludge appears to be a problem for the Bokil and Bewtra (1972) model that is better resolved for the Herschel Bulkley model of de Clercq (2003) which includes the Papanstasiou (1987) modification.

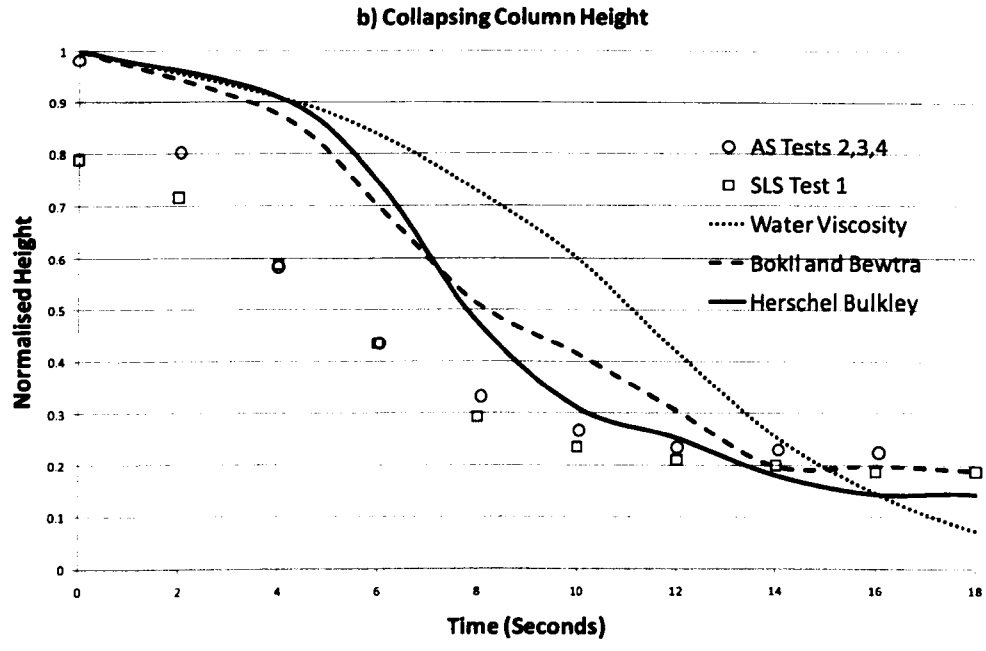

Figure 5.14: CFD Predictions for normalised column height (b) falling with time compared with experimental measurements for activated sludge and SLS.

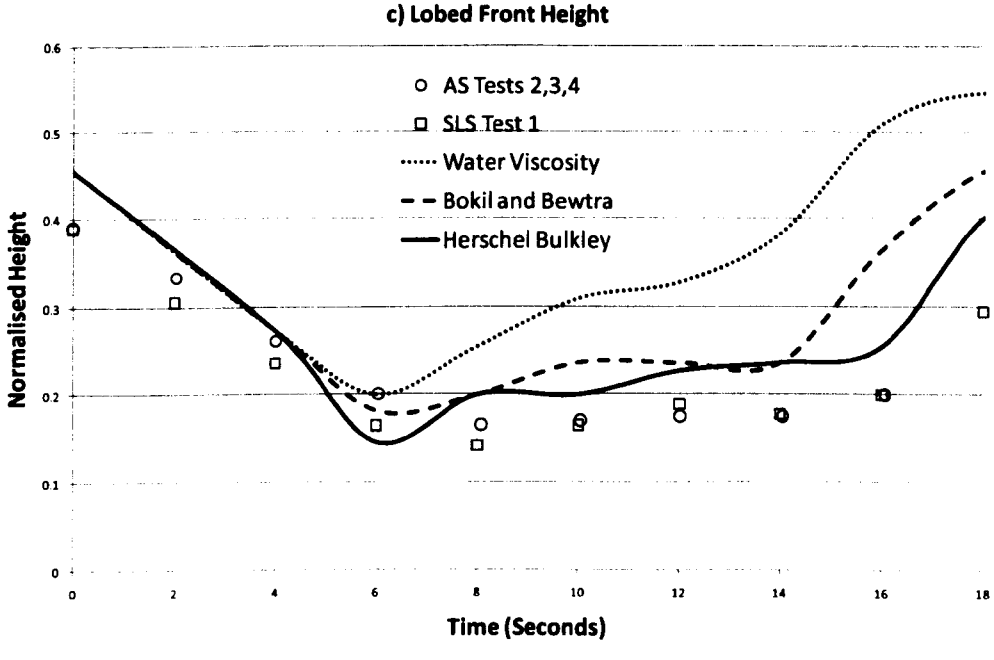

Figure 5.15: CFD Predictions for normalised lobed front height (c) varying with time compared with experimental measurements for activated sludge and SLS.

Figure 5.14 is of particular interest in that it appears to show that the Herschel Bulkley model is providing a better representation of the lobed front dynamics. This is also seen in Figure 5.12, particularly at 18 *s* after impingement on the far wall.

5.5 Conclusions

At first sight, the differences between SLS and real activated sludge shown in Table 5.4 contradict the apparent similarity that is observed in the lock exchange tests for these two materials. The useful point here is that dynamic similarity can be achieved by maintaining equal mass and volume such that the driving gravitational force on the system is equivalent. As, in all gravity current flows, the non-dimensional scaling parameter of interest is the densimetric Froude number (equation 4.1), (Simpson, 1982). In order to maintain similar velocities in laboratory scale systems with SLS the mixture density for the MLSS must be kept in the same range as real activated sludge even when the concentrations and settling indices are markedly different.

For the CFD results it is particularly interesting to note that dynamic behaviour is strongly influenced by rheology (the experimental data does not explore this and it can only be assumed that the cohesive behaviour of SLS is at least similar to that of activated sludge). Of the models tested, both the Bokil and Bewtra (1972) and the Herschel Bulkley (de Clercq, 2003) model gave the best predictions with the latter model giving a better representation of the lobed front dynamics. The standard Bingham Plastic model (Lakehal, 1999) performed extremely badly and, as can be seen in Appendix C, a large amount of the sludge remained adhered to the side wall throughout the transient which is completely inconsistent with the experimental data.

This is a known problem for yield stress based rheology models that is resolved by the Papanstasiou (1987) modification applied by de-Clercq (2003). This is an important conclusion for the later modelling work and therefore, for later studies, the standard model of Bokil and Bewtra (1972) and the Herschel Bulkley model of de Clercq (2003) are considered further.

CHAPTER 6: Full Scale Model Validation and Testing of New Settling Tank Influent Designs

Summary

This chapter describes two full scale trials and the associated CFD studies that were performed at the Witney sewage treatment works (STW) in Oxfordshire in the summer of 2004 and at the Crofton STW in Yorkshire during the spring of 2005. The trials were used to provide validation of the extended drift flux model developed in Chapter 2 and to test two candidate influent modifications.

6.1 Introduction

Two trial studies were performed in order to validate the CFD models proposed in Chapters 2 and 3 and to test two possible influent modifications. These influent designs were a McKinney baffle, similar to Figure 1.4, placed below the stilling drum at Witney and a new design for a counter current energy dissipating influent (EDI), similar to Figure 1.5, proposed by the author for installation at Crofton. The influent modifications were both expected to offer similar performance improvements by limiting the interaction between the influent density current and the settled bed. The measurements presented here provided much higher resolution data sets than were previously available from the experimental work of Richardson (1998). In particular, concentration profiles were recorded throughout the settling basin at the same resolution as the velocity data.

For the original Rye Meads velocity measurements (Scriven and Richardson, 1998), a mast rig was assembled that could be attached to the bridge of a clarifier and lowered or raised within the stilling or settling zones to place an acoustic Doppler

velocity meter (ADV) into the clarifier flow with a reasonable degree of locational accuracy (+/- 10.0 *mm*) for the scale of the tank. This rig was extensively modified for these trials in order to allow point solids sampling and velocimetry data to occur during the same test campaign. Care was also taken to calibrate the models to the site activated sludge by testing the settlement characteristics and directly measuring the Vesilind coefficients for the sludge by the methods discussed in detail in Chapter 3. All of the experimental methods described here relate to the Witney site trials in which the author was directly involved. The second trial at the Crofton-Walton STW was performed in the spring of 2005 independently using the same methods under guidance from the author.

6.1.1 Acknowledgements

For the Witney trials the rig set up and much of the data gathering was performed by Dr Pete Pearce, Dr Yasmin Jaffer and Mr Dan Strange of Thames Water. For the Crofton trial the measurements were co-ordinated by Dr Yanmin Zhang of Yorkshire Water. The CFD modelling work and data analysis was performed by the author, but many of the graphs and figures in this chapter were produced by Dr Jay Ganeshalingam under guidance from the author both as employees of MMI Engineering Ltd.

6.2 The Witney Trials

In June 2004, the Witney wastewater treatment works had six final settling tanks, each of 18.3*m* diameter with side-water depth of 1.8*m*. Five of the tanks were equipped with standard 4*m* diameter stilling wells whilst one tank had already been modified with a 6*m* diameter stilling well.

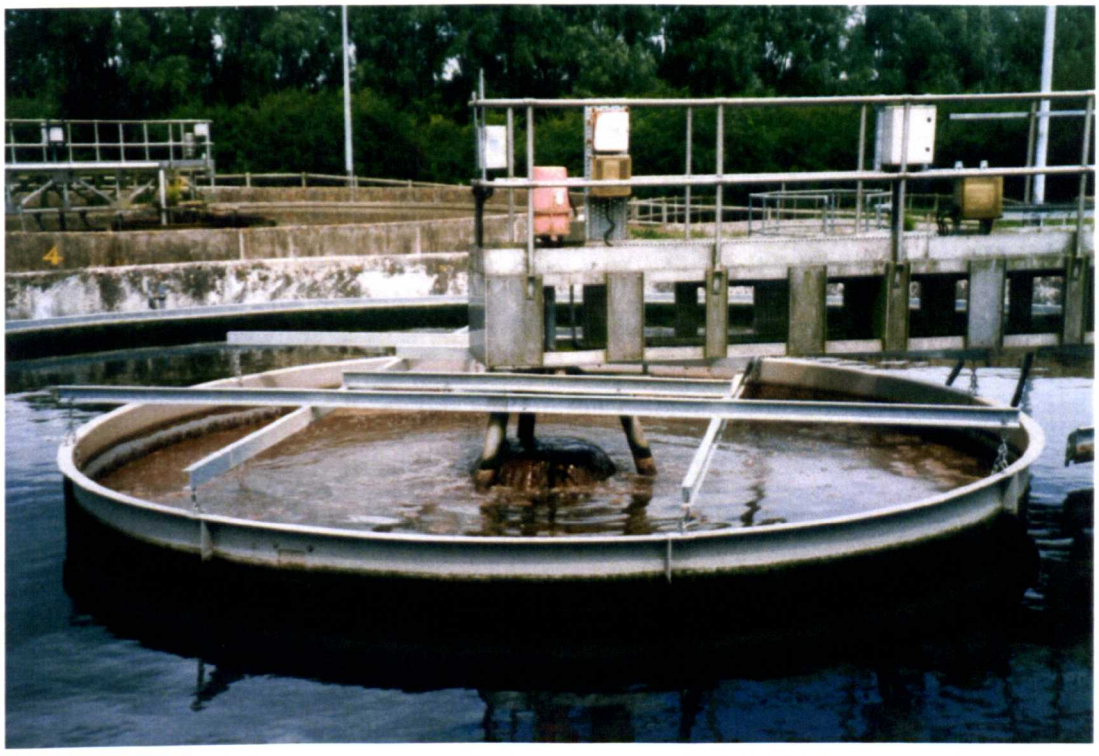

Figure 6.1: The large 6*m* diameter stilling well on the modified tank at Witney. The photograph shows the activated sludge welling up into the stilling well from the submerged bell mouth influent (Burt, 2005a).

All tanks were of a standard UK design with a tank floor slope inclined at 7.5° to the horizontal and a hopper floor slope inclined at 60° to the horizontal (Figure 6.2). It was proposed to trial the addition of a McKinney baffle in one of the standard tanks located below the stilling well at the side water depth of 1.8*m*. The gap between the McKinney plate and the drum was designed to prevent re-entrainment of clarified supernatant back into the stilling pond. This study was intended to compare the performance of this design against the large influent drum design and provide detailed comparisons of CFD predictions with experimental measurements. Therefore, measurements and modelling were carried out for the two tank arrangements as follows:

a) The tank with a large stilling well of 30% D (or 10% A_{st}), 0.8m below top water level.

b) A modified tank with the stilling well at 20% D and 1.65 m below top water level incorporating a McKinney baffle below the stilling well at depth 1.8 m.

An axisymmetric cross section of the modified tank b) is shown in Figure 6.2 with key geometric features and boundary conditions shown.

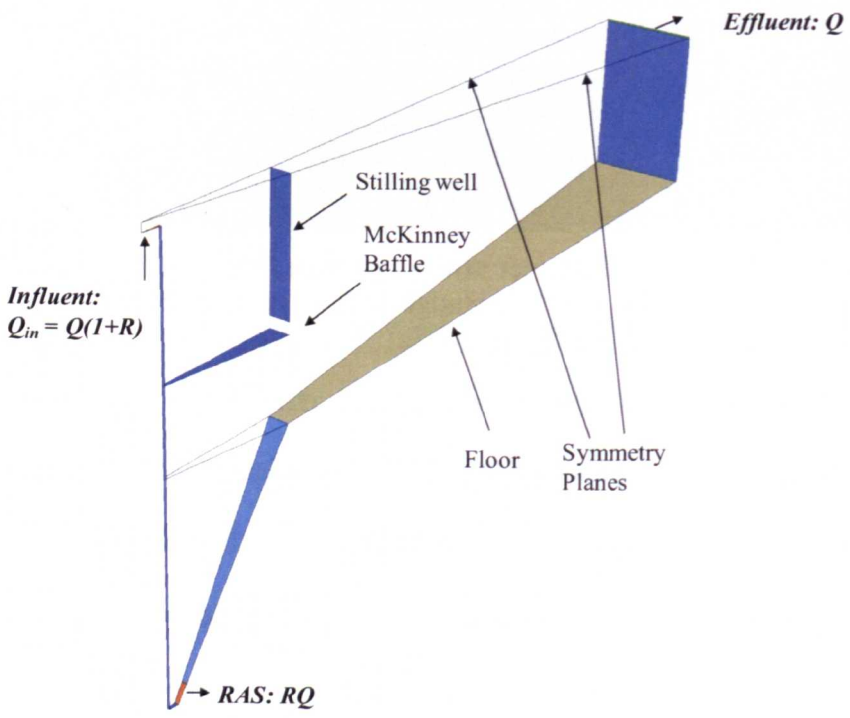

Figure 6.2: Geometry and modified influent arrangements for the Witney trial tank b).
The smaller diffuser drum incorporates a McKinney baffle below the influent. The gap between the drum and the baffle of 150 *mm* was sized for 0.5 > Frd > 0.7. The figure is a 15° axisymmetric segment of the full 360° circular tank.

These tanks were configured at site to receive different combinations of flows and loads as shown in Table 6.1. Trials 1 and 2 were used to test the differences between the alternative influent arrangements for the same flow rates; trials 2 and 3 were intended to contrast different flows in the same tank geometry.

Table 6.1: Flow and load conditions for the Witney site trials. Trial 1 was performed on tank a), trials 2 and 3 on tank b).

Trial	Tank	Dates	Q	RAS	R	X_F	$SSVI_{3.5}$
		2004	*(m3/hr)*	*(m3/hr)*		*(mg/l)*	*(ml/g)*
1	a)	28/06 –02/07	87.16	95.0	1.09	4187	50
2	b)	02/08 –06/08	87.16	95.0	1.09	3384	61
3	b)	09/08 –13/08	177.0	146.9	0.83	2904	61

Note that for trials 1 and 2, the upstream variability in mixed liquor suspended solids (MLSS) and the sludge settleability (SSVI) made it impossible to maintain the same feed concentration X_F into the tanks.

The settlement characteristics of the sludge were assessed using the water research council (WRc) direct method, discussed in Chapter 3, and found to be in the range of 50 to 61 *ml/g* which is a very good settling sludge (Table 3.1). The sludge characteristics were controlled upstream of the aeration lanes by dosing with the coagulant, ferric chloride. This is added to improve the flocculating capacity of the activated sludge and improve settleability which accounts for the very low $SSVI_{3.5}$ values. Further analysis of the settlement data revealed that the sludge interface settlement curves did not correlate well with the Pitman (19880) and White (1976) equations (3.7) and (3.8) for the directly measured $SSVI_{3.5}$. Therefore the Vesilind coefficients V_o and r_h were calculated using the method described in section 3.3.2, in order to provide inputs for the hindered settling model. All of the trial flow and load conditions were well within the performance capacity of the tank, as shown on the mass flux plot for trial 3, Figure 6.3.

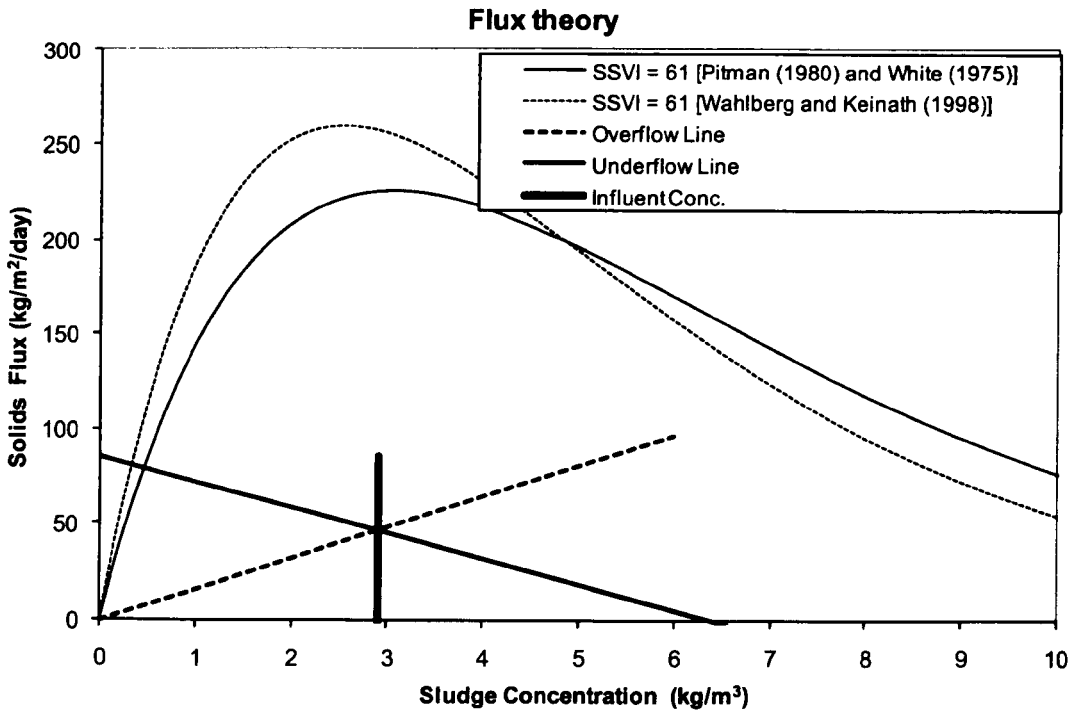

Figure 6.3: Mass Flux graph for Witney trial 3.
Even at the highest flow condition the tank is operating well below the mass flux limit because the dosing with ferric chloride which reduces the $SSVI_{3.5}$ of the activated sludge.

6.2.1 Obtaining the Vesilind Coefficients from Tests

The CFD model requires the input of settling coefficients as parameters for the Takács equation. The method for obtaining these parameters from settling tests is described in Ekama et al (1997) and discussed in detail in Chapter 3 with reference to sample sludges from Swindon STW. This method is now applied to the Witney experiment to determine the settling coefficients for the CFD model. For trial 1, the sludge was sampled from the aeration lanes at concentration X (g/l) over a period of two days, 29th and 30th June 2004. For phases 2 and 3, similar samples were taken on August 10th 2004. The sludge was decanted into measuring cylinders and several initial mixed liquor batches were made up at different concentrations relative to the sampled sludge. Dilution with decanted supernatant was used to achieve initial concentrations less than X. For concentrations greater than X it was necessary to

retain the settled beds from previous settling experiments and then combine them, in known ratios, with other settled sludges. In this way, thickening of the original mixed liquor up to $2X$ was readily achieved.

The settling test procedure described in Chapter 3 was then performed for different initial sludge concentrations and the resulting data is plotted in figure 6.4.

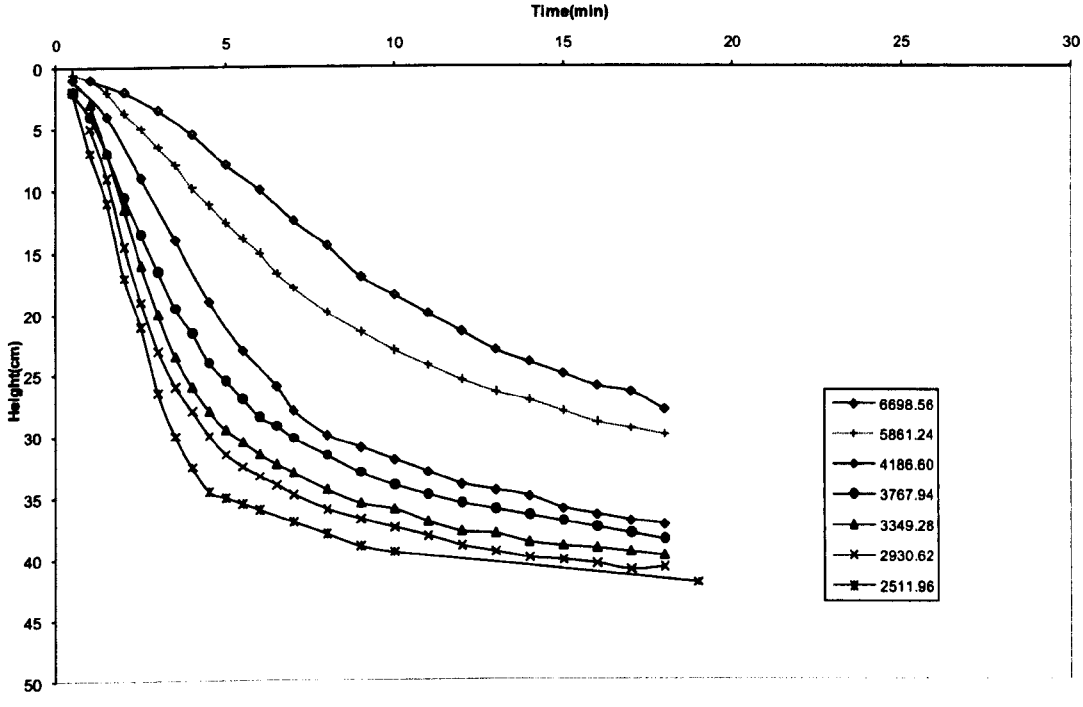

Figure 6.4: Falling sludge line tests for different initial MLSS concentrations at the Witney STW, 29th June 2004.

The gradient of the curves in Figure 6.4 were measured through the zone settling concentrations to give the settling velocity for the zone or hindered settling phase; usually using only the first 8 to 10 data points to describe a tangential straight line to the settling curve. The derived hindered settling velocity against concentration data was plotted on a natural log to linear scale. The gradient and intercept of this curve provided the Vesilind coefficients. In these experiments the settlement tests were performed for up to seven different initial mixed liquor concentrations which gave the reliable straight line plots in Figures 6.5 and 6.6.

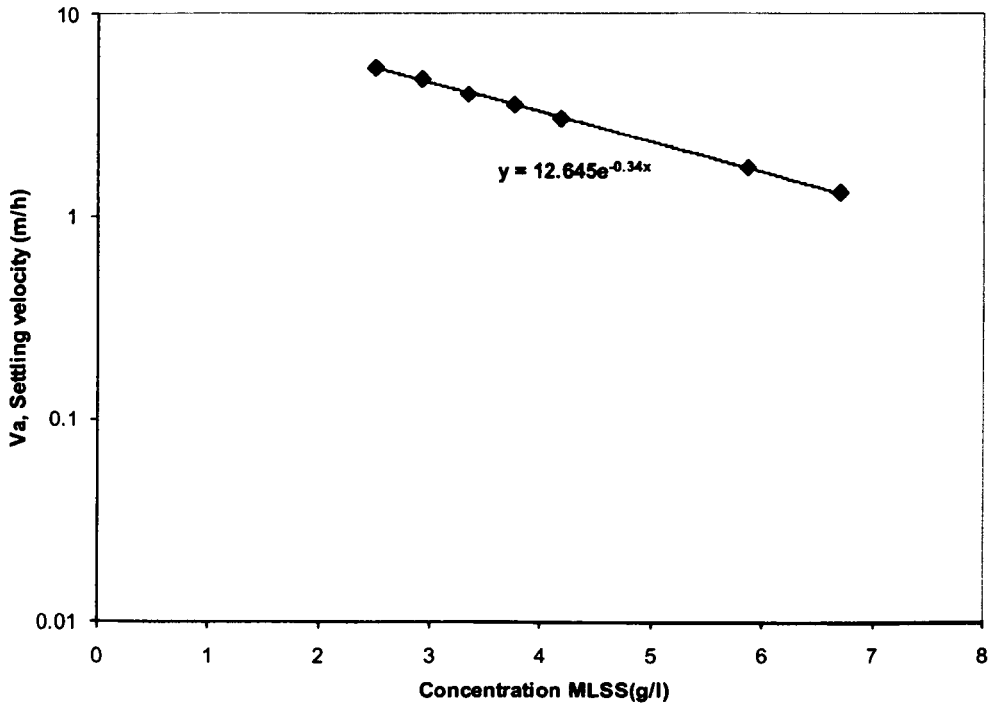

Figure 6.5: Experimentally derived hindered settling or Vesilind coefficients obtained for activated sludge from the Witney STW, 29/6/04. Where $V_s = V_o e^{-r_h X}$, r_h= 0.34 m^3/kg; V_o=12.64 *m/h*; $SSVI_{3.5}$ Pitman and White equivalent = 37.6 *ml/g*

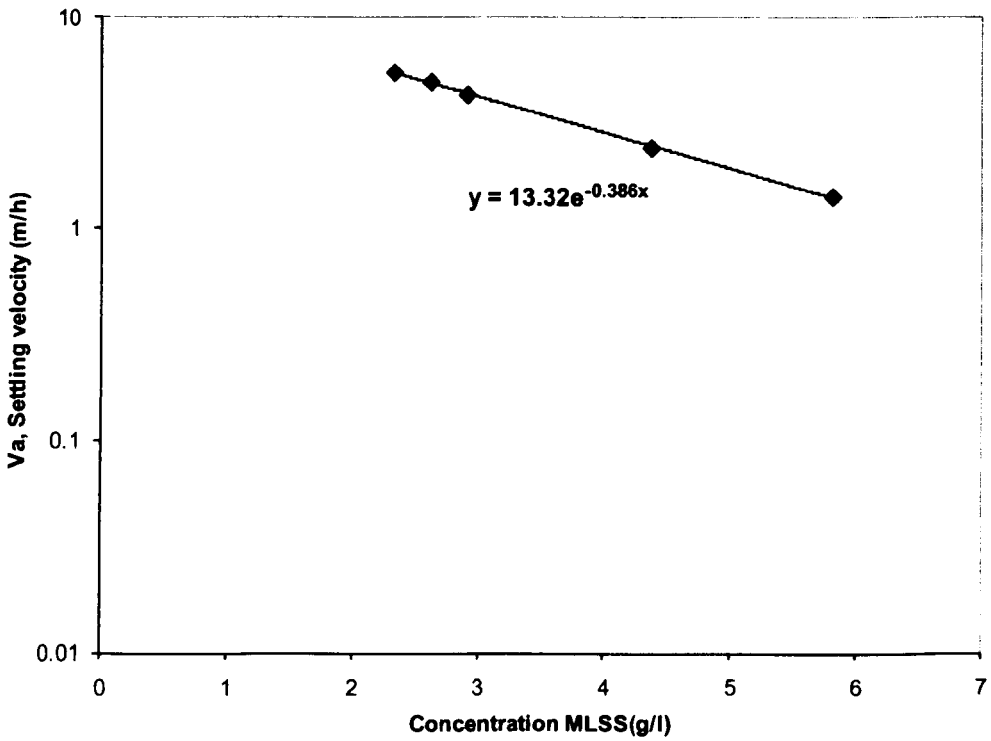

Figure 6.6: Experimentally derived hindered settling or Vesilind coefficients obtained for activated sludge from the Witney STW, 10/08/04. Where $V_s = V_o e^{-r_h X}$, r_h= 0.386 m^3/kg; V_o=13.32 *m/h*; $SSVI_{3.5}$ Pitman and White equivalent = 42.3 *ml/g*

Table 6.2: Takács parameters derived from settling tests for use in the Witney CFD models.

Trial	$SSVI_{3.5}$ Measured *(ml/g)*	$SSVI_{3.5}$ P&W Equiv *(ml/g)*	$SSVI_{3.5}$ W&K Equiv *(ml/g)*	V_o *(m/h)*	r_h *(m^3/kg)*	r_p *(m^3/kg)*	X_{ns} *(g/l)*
1	50	37.6	30	12.64	0.34	12.25	0.01
2,3	61	42.3	45	13.32	0.386	13.0	0.01

Finally, the colloid settling parameter and concentration of non-settleables required for extending the Vesilind function into the Takács equation for use in the CFD model were approximated according to the method described in Chapter 3. The final set of Takács parameters determined for trials 1,2 and 3 are given in Table 6.2. Note also in Table 6.2 that equivalent $SSVI_{3.5}$ values have been calculated by inserting the derived Vesilind coefficients back into the Pitman (1980), White (1975) and Wahlberg (1988) correlations equations (3.7) to (3.10), and these differ from the values measured by direct settlement over 30 minutes reported in Table 6.1. This highlights the fact that the sludge settling characteristics have been altered by the addition of ferric chloride into the system.

6.2.2 Controlling the Clarifier Flows

The tank of interest was isolated from the site flow by a pair of Selwood pumps each with a diesel generator pack. At influent, the penstock controlling the flow to the tank was completely closed and a 6" hose was connected from the penstock sump to the first pump. The return hose from the pump delivered flow to the other side of the closed penstock via a valve and flow meter. At the exit bellmouth for the return activated sludge (RAS), a 4" hose was pushed down the pipe and connected to the second pump. The return line from the second pump passed through a valve and flow meter and delivered sludge back to the RAS sump. The bellmouth was raised as high

as possible so that the RAS flow was entirely maintained by the pump. For both the influent and the RAS return, the function of the pump, hose, valve and flow-meter was to over-ride the existing flow control arrangements and provide a measure of the flow rate. A schematic of the arrangement is shown in Figure 6.7.

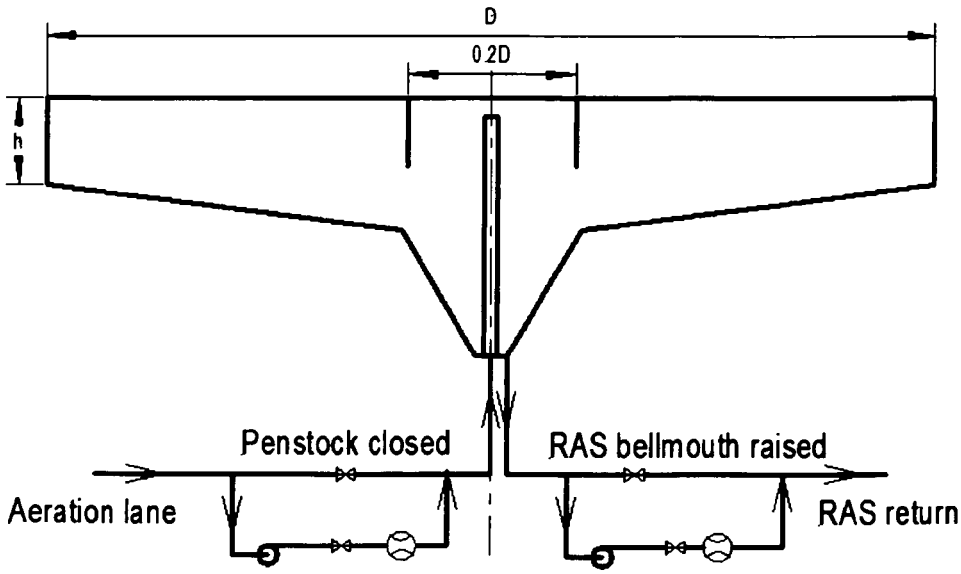

Figure 6.7: Schematic for the Witney trial showing how the tank was isolated from the site flows.
This was achieved by closing the influent penstock and the RAS return bellmouth and diverting flows directly through pumps and flowmeters.

The influent pump and 6" hose was operated at an average of $Q_{in} = Q(1+R) = 182$ m^3/hr and the maximum flow achievable was found to be 270 m^3/hr. Hence, for the high flow test where $Q_{in} = 324$ m^3/hr, a much larger pump was required with an 8" hose. The RAS pump and 4" hose operated at 95 m^3/hr for the average flow test and 146 m^3/hr for the high flow test.

6.2.3 Acoustic Doppler Velocimetry and Solids Profiling

Both Richardson (1998) and deClercq (2003) discuss the use of Acoustic Doppler Velocimetry (ADV) devices to measure radial velocity profiles of mixed liquors in

final settlement tanks. The ADV probe used in these trials was provided by Nortek AS and had one transmit and two receive arms as shown in Figure 6.8. The probe works by sending out a short acoustic pulse from the transmit element. When the pulse travels through the focus point for the receiver beams (located about 10 cm from the tip of the transmitter), an echo is recorded in each of the acoustic receiver elements. The echo is then processed to find the Doppler shift, the scaling is adjusted with the measured speed of sound in the liquid, and the calculated velocity resultant is transmitted to an attached data capture PC at a rapid rate

Figure 6.8: The ADV Field probe from Nortek AS attached to the bridge mounted measurement rig.
The solids sampling hose is to the left of the ADV probe attached to the stop leg which prevents the probe from hitting the floor of the tank.

The ADV data of Scriven and Richardson (1998) for the Rye Meads site was compared with CFD modeling results in Chapter 4. However, Richardson only measured a limited data set at 25 locations for velocimetry inside the tank and the only concentration data recorded was the blanket depth. In this work, the data was taken at 6 radial positions and between 10 and 15 axial locations in depth for both

point velocity and solids concentration. The main modification to the rig for this work was to include a solids sample point, in the form of a hose linked to a peristaltic sludge sample pump, attached to the ADV probe support structure as shown in Figure 6.8.

6.2.4 Measuring from the Clarifier Bridge

The rig was bolted to rails on the bridge with 35mm brackets and a winch arrangement was used to allow the operator to locate the ADV probe and peristaltic pump sample hose at discrete locations within the tank. The bridge had to be stationary whilst measurements were being taken to facilitate interpretation of velocity vector data and to prevent hoses becoming entangled in the bridge supports. Therefore the measurements were performed in brief campaigns with the bridge operating between each campaign. The ADV field probe from Nortek AS was mounted at the base of the rig so that the legs at the base of the rig protected the probe when the rig bottomed out. The end of the griflex sampling hose can be seen in Figure 6.8 attached to the nearer of the two supporting legs.

Radial positions were marked out on the bridge at 5 locations outside of the stilling well and 1 position inside. The probe was set at datum to the water surface and dropped down initially at 200*mm* intervals. Velocity component data from the ADV probe was recorded on to a laptop computer at a frequency of 4 samples per second for a total of 3 minutes representing 720 discrete samples with time. At the end of the 3 minutes a 1 litre sample of liquor was drawn up by operating the sample pump into a sample bottle and discarded, this was followed by a second litre representing the final sample which was kept for solids analysis. Radial measurement locations for all of the trials are shown in Figure 6.9.

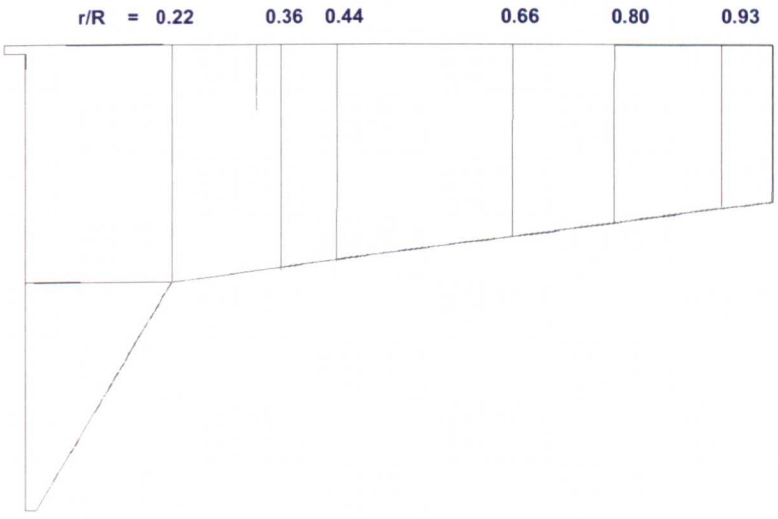

		Stilling	A	B	C	D	E
Radius	(m)	2.0 or 1.4	3.3	3.97	6.06	7.27	8.55
r/R		0.22	0.36	0.44	0.66	0.8	0.93

Figure 6.9: Radial positions for measurement of point velocity and solids profiling for the Witney site trial.

For radial velocity the experimental data was extracted as a single component of the velocity vector reading from the ADV probe. At each data point, the average value and the standard deviation of the radial velocity component was calculated.

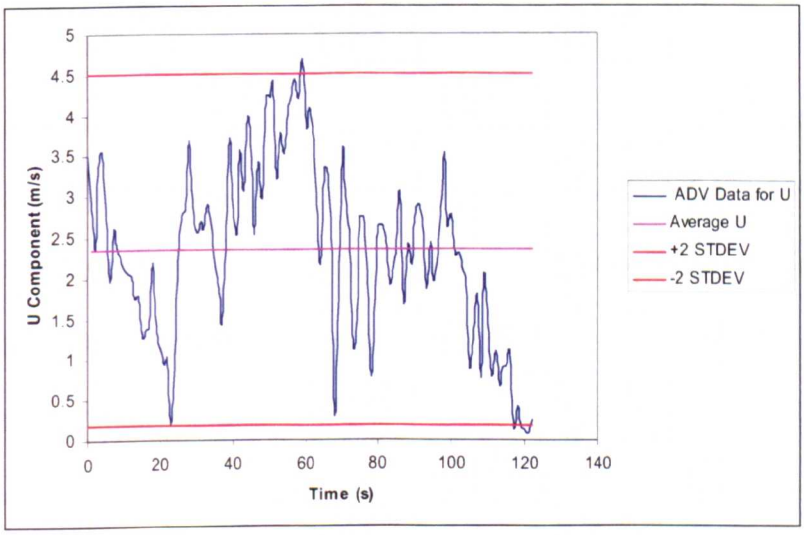

Figure 6.10: An ADV data trace for radial velocity component. Trial 1, profile A at 2000mm depth

Figure 6.10 shows an ADV velocity trace for the radial velocity component, for profile A, from the first trial, at 2000mm depth over a period of 2 minutes. Overlaid onto the trace is the mean value and bars of variation in the mean flow at ± 2 standard deviations. In this case there is significant variation in the radial component. This variation is not really an error; rather it is a record of the time dependent fluctuations at this point in the flow field reflecting the fact that the flow field is continuously unsteady. At high depths in the tank the variation in the mean value of radial velocity was relatively small but in the highly turbulent stilling pond, at the transition into the shear layer, and in the higher concentration regions of the sludge these variations were large sometimes showing flow reversal over a two minute period. The full measurement data sets for radial velocity are tabulated in Appendix D for trials 1, 2 and 3.

For solids profiling the concentration at the discrete points within the tanks was recorded from drying out and weighing the mixed liquor samples. These direct measurements of the solids at discrete positions within the tank are also presented as tables of data in Appendix D for trials 1, 2 and 3.

6.2.5 The CFD Models

The model geometries are as described for the physical systems in the introduction and shown in Figure 6.2. All of the models in this work used a grid of 11,385 hexahedral cells. The geometric features for tanks a) and b) were incorporated into the same computational grid as shown in Figure 6.11.

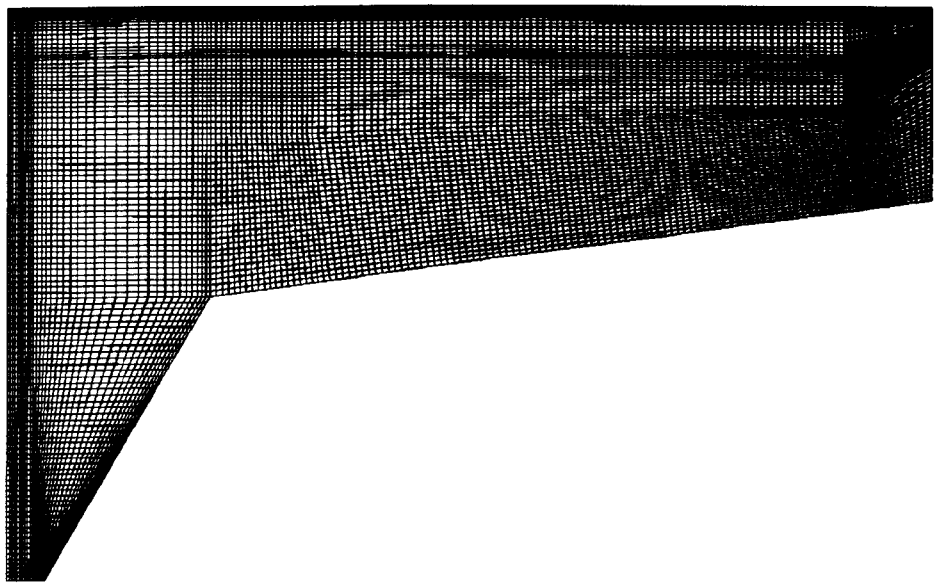

Figure 6.11: A computational mesh of 11,385 hexahedral cells was used for all of the Witney CFD model studies.

The boundary conditions for this model were defined according to the definitions in Figure 6.2 and Table 6.1. The Takács (1991) parameters required for the settling model, equation (3.6), were based on those derived from the settling experiments shown in Table 6.2. The first analyses used the simple rheology function following Bokil and Bewtra (1972) with the empirically derived constants for apparent viscosity shown in equation (3.11) and Figure 3.7. The methods used to obtain converged CFD solutions for the three trial conditions were exactly equivalent to those described in Chapter 4 and Appendix B for the Rye Meads study. That is the initial model was converged by applying different elements of the physical models in stages and a transient solution method was applied in the final runs. The other modelling details follow the command file structure for the Rye Meads clarifier study discussed in Appendix B, as follows,

- The calculations were performed in CFX4.4 using the Menter (1994) modified Low Reynolds number k-ω model, equations (2.30) and (2.31). Extensions to this model were provided by CFX (2001) to allow modification

to the apparent viscosity as part of this turbulence model as discussed in Appendix B.

- The additional user routines for the constitutive relationships for density, settling velocity and apparent viscosity discussed in chapter 3 were applied and a drift flux scalar was used to represent the activated sludge (equation 2.24).
- The model was two dimensional axisymmetric in cylindrical co-ordinates (x, r, θ mapping to x, y, z).
- Buoyancy was invoked with the gravity vector acting in the positive x direction and the fluid was made compressible (weakly compressible using the CFX4 definitions) to allow for variation in density and changes in the total mass of the system as sludge accumulates in the tank.
- Higher Upwind differencing was used in the final transient calculations for the velocity components and the drift flux scalars.
- Under relaxation factors were used for the momentum and turbulence equations.
- The scraper at the floor was approximated by the use of a slipping wall.
- The final models used a transient convergence strategy with time steps of order 5 to 10 seconds for a total duration of up to 12 hydraulic retention times.

6.2.6 Comparing CFD Results with Measurements

The comparisons between CFD and experimental results for point measurements within the tank are presented as a series of 6 profiles for each of the trials. Each profile has a normalised radial position which is shown visually in Figure 6.9. At

each radial position, the depth at which the measurement is recorded is normalised to the total depth at that position; in this way radial position profiles can be compared for different tanks with varying degrees of slope. The average radial velocity component and the standard deviation of the radial velocity component were normalised to the influent velocity V_{in} and the solids concentration values at each depth position were normalised to the influent feed concentration X_F. Finally, the normalised velocities and normalised concentrations were plotted against normalised depth for all 6 radial locations and all 3 trials. These results are shown in Figures 6.12, 6.13 and 6.14.

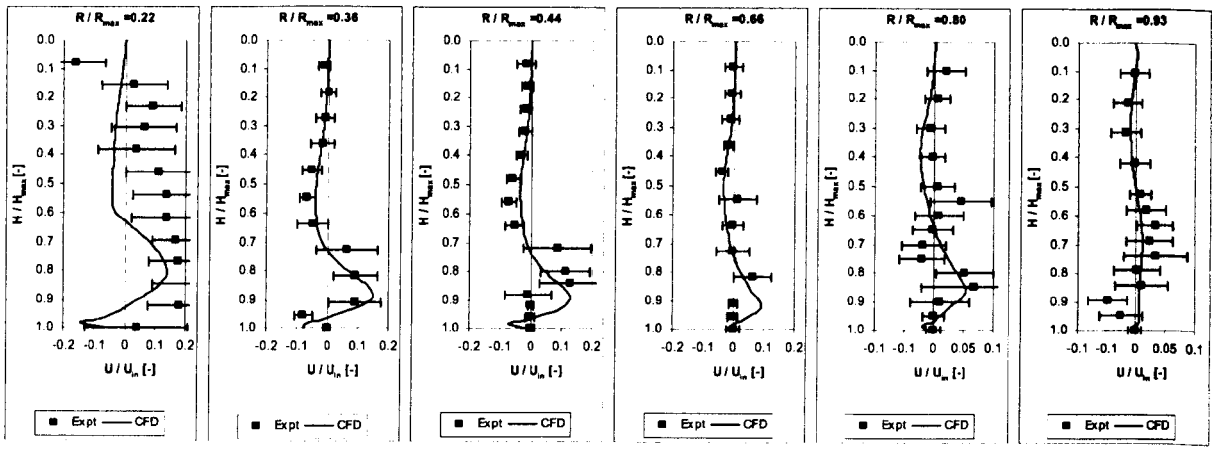

a) Trial 1: Low flow with large stilling well.

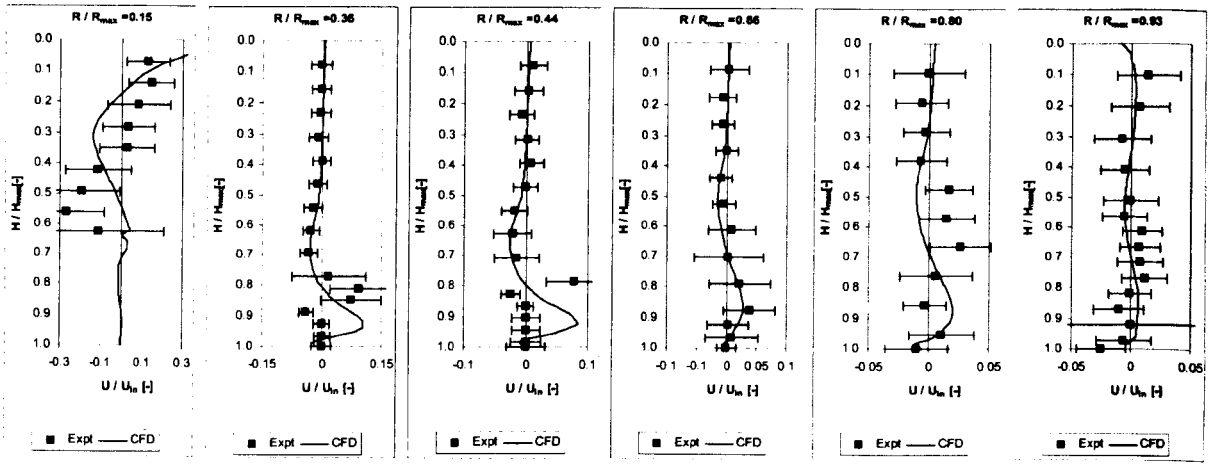

b) Trial 2: Low flow with McKinney baffle

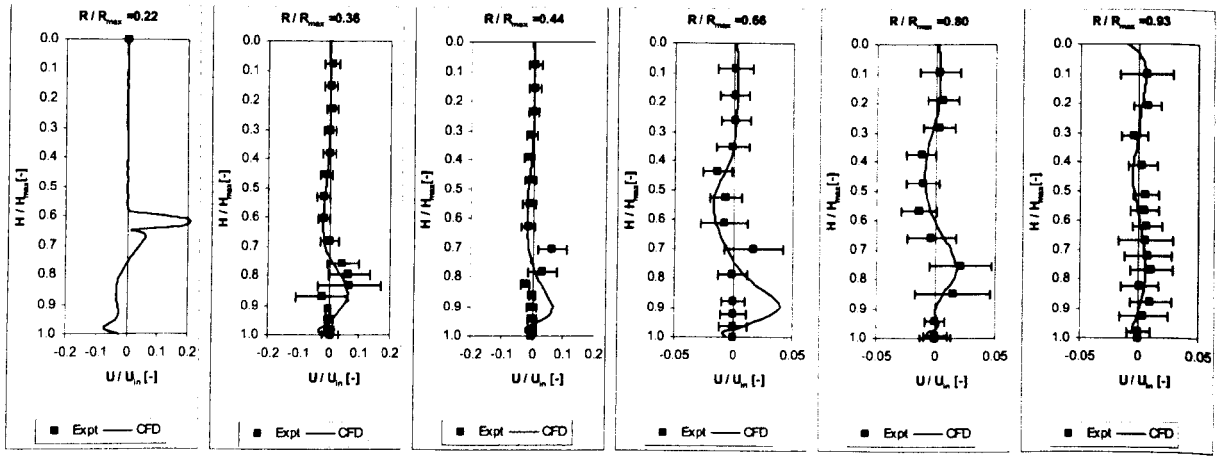

c) Trial 3: High flow with McKinney baffle

Figure 6.12: Comparison of radial velocity profiles for CFD and experimental data for the three trial conditions at 6 radial locations.
Bars of variation are provided for the experimental measurement at +/- 2 standard deviations.

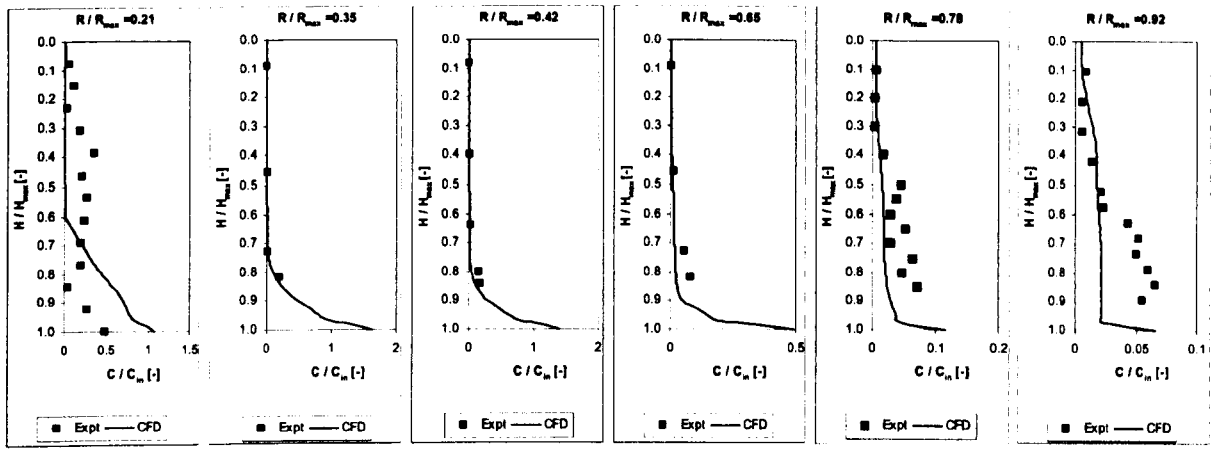

a) Trial 1: Low flow with large stilling well.

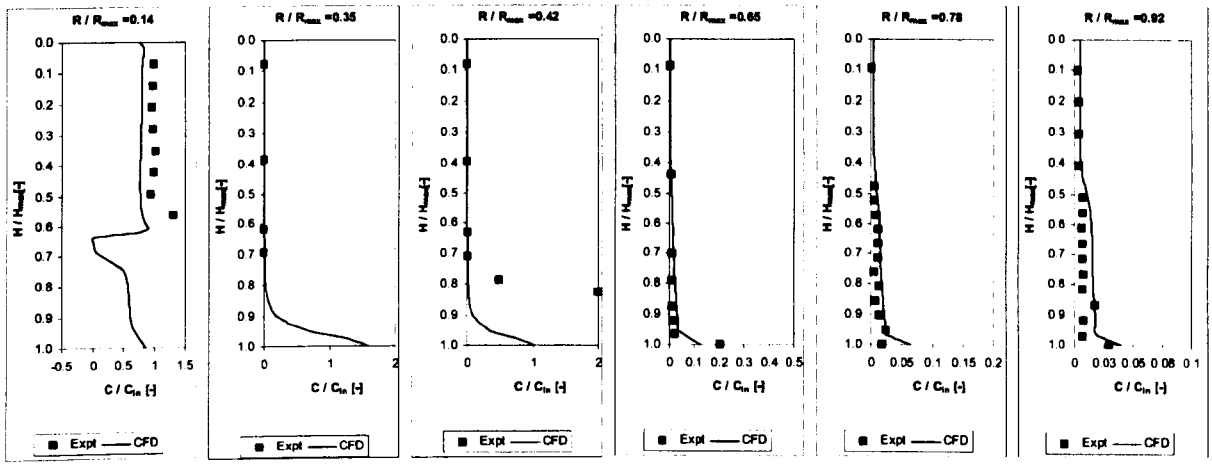

b) Trial 2: Low flow with McKinney baffle

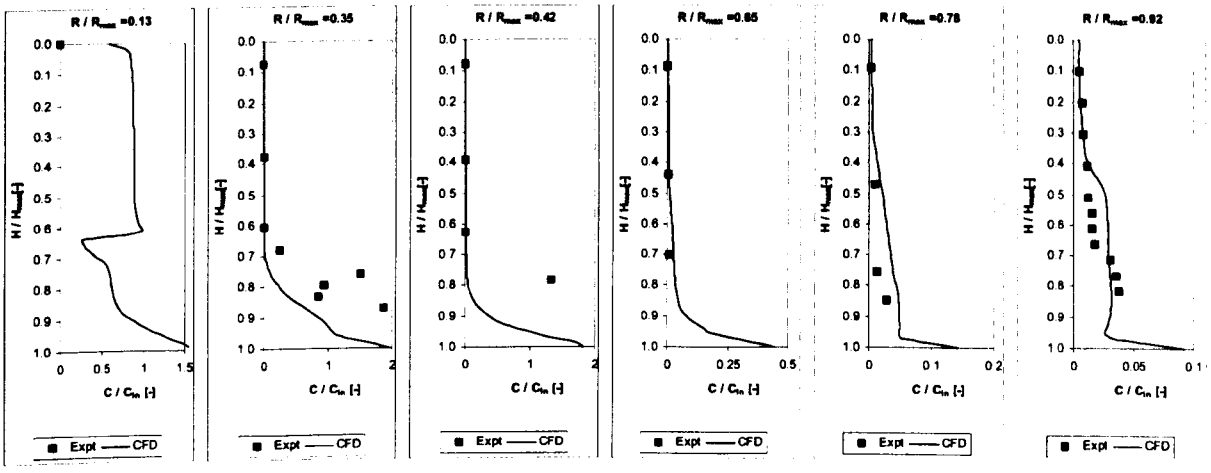

c) Trial 3: High flow with McKinney baffle

Figure 6.13: Comparison of concentration profiles for CFD and experimental data for the three trial conditions at 6 radial locations.

The concentrations are normalised to the influent concentration X_F on a limited scale.

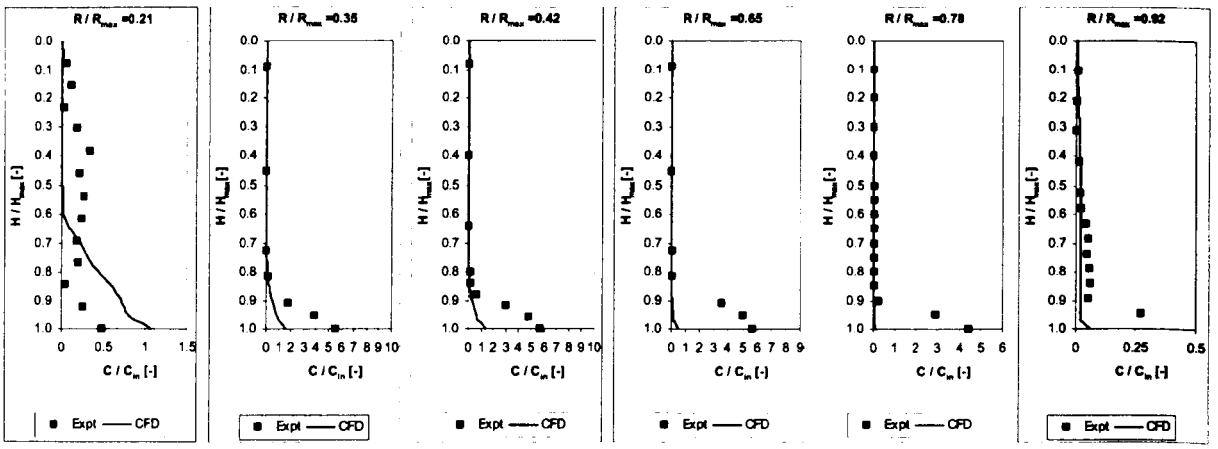

a) Trial 1: Low flow with large stilling well.

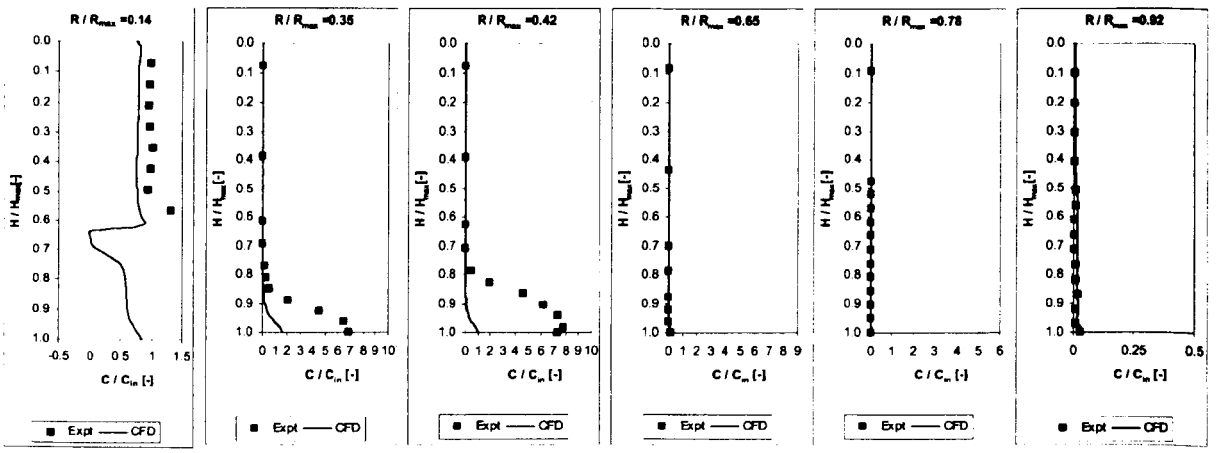

b) Trial 2: Low flow with McKinney baffle

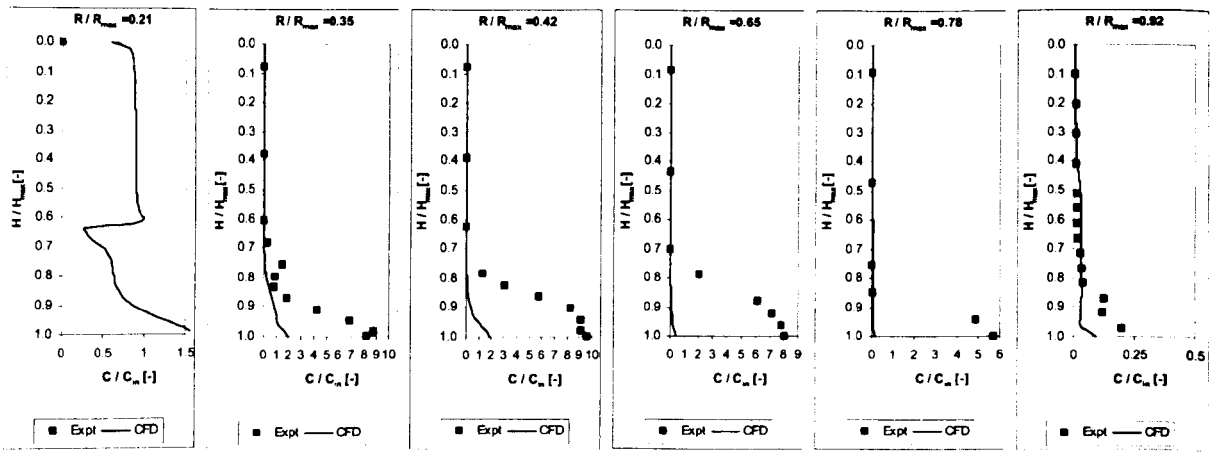

c) Trial 3: High flow with McKinney baffle

Figure 6.14: Comparison of concentration profiles for CFD and experimental data for the three trial conditions at 6 radial locations.

The concentrations are normalised to the influent MLSS on a large scale to show the experimental evidence for thickening approaching ten times (9.5 in trial 3) the inlet concentration that is not captured by the model.

6.2.6.1 Radial Velocity Profiles

Figure 6.12, shows comparisons between CFD and experiment for the radial velocity profiles. Both CFD and experiment show the classical radial shear layer developing above the sludge bed and radial flow reversal from the side wall back to the centre stilling well. The profile in the stilling well suggests that there may be some eccentricity to the flow where the experimental results are displaced from the CFD prediction.

Figure 6.12b shows reasonable agreement for velocity data above the solids bed but the predictions inside the bed show that the model is predicting a lower bed than is observed on the site trial. This is also seen in the higher flow rate result, Figure 6.12c.

6.2.6.2 Concentration Profiles

Figures 6.13 and 6.14, a to c, show comparisons between CFD and experiment for concentration profiles. Figures 6.13a and 6.14a show the concentration profiles at different scales for trial 1. Figure 6.13a indicates that the CFD model is picking up the bed transition (arbitrarily the 850 mg/l contour) reasonably well but bed thickening is not well predicted. The experimental data shows that sludge in the bed can reach concentration approaching ten times the inlet value but the CFD predictions based on the simplest viscosity law do not match this. Figures 6.13b, 6.14b, 6.13c and 6.14c also show that for trials 2 and 3, the solids profiling is reasonably well predicted above the settled bed but poorly predicted within the bed.

6.2.6.3 Performance Parameters

Table 6.3 shows results for the trial comparing global data for bed height and ESS with the CFD prediction. Differences between influent conditions and the $SSVI_{3.5}$ data are again shown in the same table noting that direct measurement of the Vesilind parameters and the use of the parameters to calculate an expected $SSVI_{3.5}$ did not yield the same result as the direct measurement of $SSVI_{3.5}$. The results for trials 1 and 2 show reasonable agreement between CFD and experiment for ESS whereas the trial 3 result is not as good. The CFD results are also consistently showing the sludge bed to be slightly lower in the tank than is measured.

Table 6.3: Comparison of performance parameters for experimental measurement and CFD for the Witney site trials.

Trial	Q *(m3/hr)*	X_F, *(mg/l)*	$SSVI_{3.5}$			Bed Depth h_{850} *(m)*		X_E, (ESS) *(mg/l)*	
			Expt (WRc)	Equiv (P&W)	Equiv (W&K)	Expt	CFD	Expt	CFD
1	87.16	4187	50	37.6	30	1.850	2.180	24	21.85
2	87.16	3384	61	42.3	45	2.100	2.425	15	16.63
3	177.0	2094	61	42.3	45	1.800	2.250	22	15.66

It is important to note that, although the bed thickening process does not seem to have been well captured by the model for these results, concentrations in the upper reaches of the tank are well represented by the model and therefore, the prediction of the effluent suspended solids (ESS) is in reasonable agreement. This is also seen when examining all profiles at r/R = 0.92 in Figure 6.13 where there is good prediction of the solids distributions near the side wall.

As with the Rye Meads study, the fundamental flow patterns are well captured by the model and the flow reversal, back towards the stilling well (between 0.3 and 0.7 of non dimensional depth) correlates well between CFD and experiment. It is disappointing that, in these models, the radial shear layer, and the top of the

consolidating bed (the 850 mg/l contour) sits between 10 and 20% lower in the tank than is predicted by experiment however, the relative position of the shear layer and the peak radial velocities with respect to the sludge bed do appear to be well captured.

6.2.7 Testing sensitivity to the Rheological Model

Because of the disappointing results observed for bed thickening, using a simplified rheology model, particularly for the trial 3 concentration profiles shown in Figure 6.14, a further investigative study was carried out with modifications to the CFD model. This study compared the experimental results from trial 1 for alternative sludge rheology models as discussed in Chapter 3 and previously compared for the lock exchange experiment in Chapter 5.

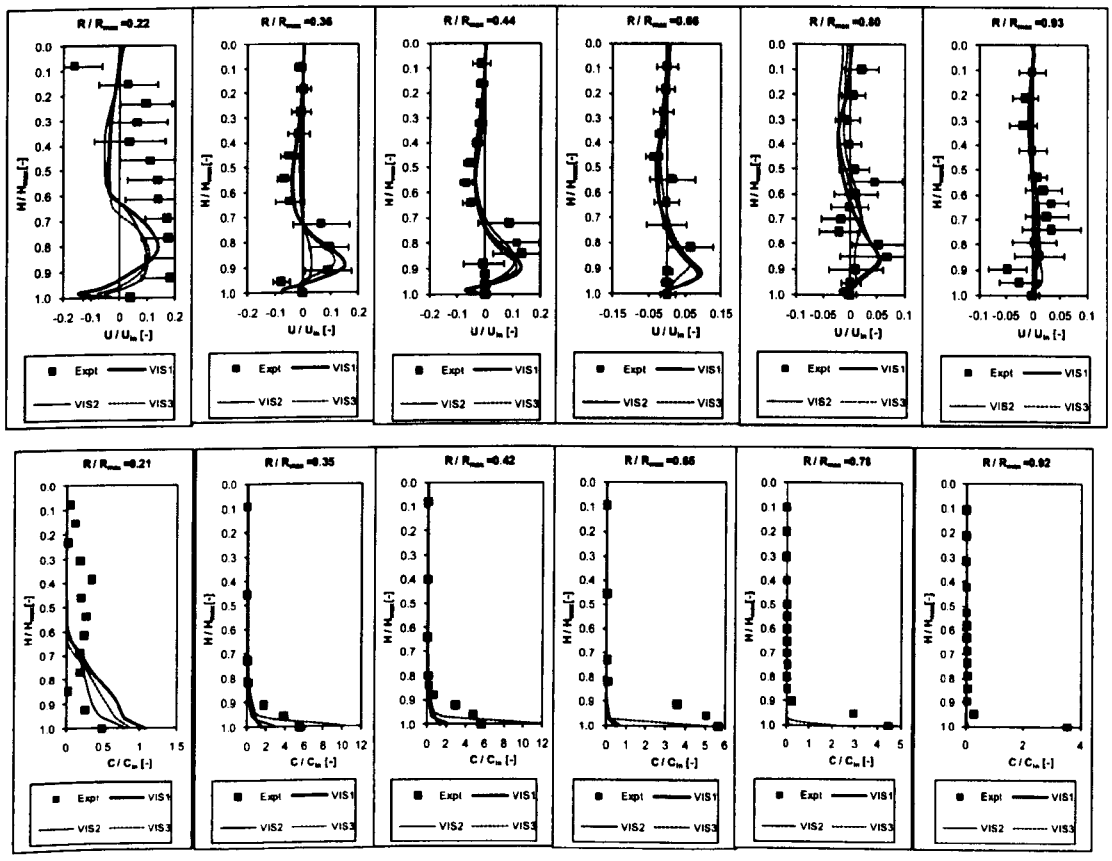

Figure 6.15: Radial flow velocity and concentration profiles at normalized radial positions for trial 1 with alternative rheology models.
Where Vis 1 is the Bokil and Bewtra (1972) model, Vis 2 is the Armbruster (2003) Square Law, and Vis 3 is the de Clercq (2003) variant of Herschel Bulkley model.

Figure 6.15 shows that there is not much variation on the velocity profile data except for VIS2, the Armbruster square law, which tends to flatten the velocity profiles within the bed and produces a less credible result. Only, VIS3, the deClerq variant of Herschel Bulkley, predicts solids concentrations near the floor approaching the experimentally measured values. All of the rheology models show sludge bed transition at a position lower than experimentally measured, there is little difference between the rheology models in this respect. This issue is discussed in detail in Chapter 8.

6.2.8 Discussion of the Witney Settling Parameters

It is useful to compare the data from this experiment to known settling coefficients based on the standard correlations for $SSVI_{3.5}$. Ekama (1997) lists many different correlations for the Vesilind coefficients as a function of $SSVI_{3.5}$. Two of these correlations due to Pitman (1980), White (1975) and Wahlberg and Keinath (1988) were discussed in chapter 3. The variation between the directly measured value of $SSVI_{3.5}$ and the equivalents derived from the Vesilind coefficient and correlations, equations (3.7) to (3.10) are shown in Table 6.2; the difference warranted further investigation.

The hindered settling velocities determined by experiment were plotted as a function of concentration on the same graph as the Pitman and White correlation for *SSVI* 30 and *SSVI* 50 *ml/g*, see figure Figure 6.16. This showed the data deviating between the two characteristic curves. Plotting the same data onto a family of sludge characteristic curves based on the Wahlberg and Keinath correlations showed an exact match at *SSVI* = 45 *ml/g*, see Figure 6.17.

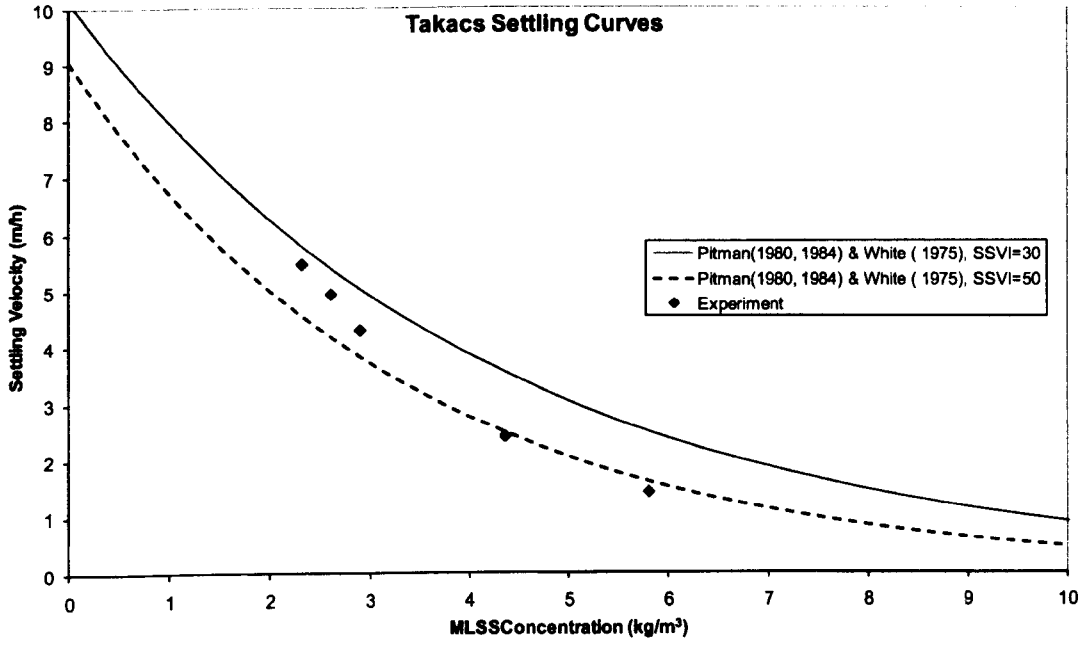

Figure 6.16: Experimental data points for the SSVI experiment of 10th August 2004 compared to Pitman (1980) and White (1975).

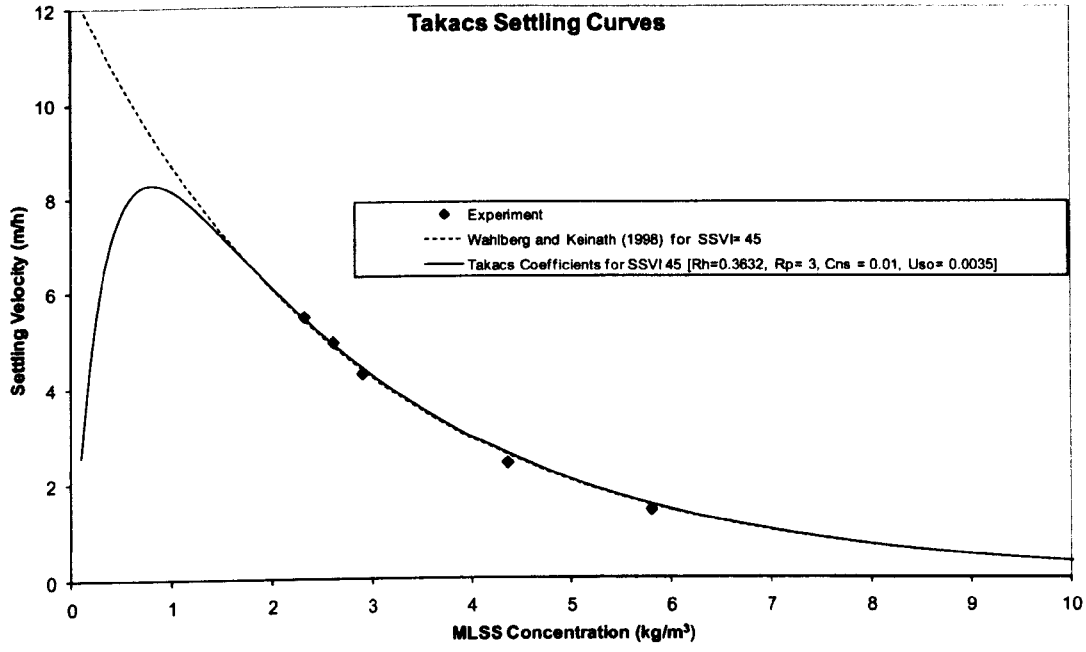

Figure 6.17: Experimental data points for the SSVI experiment 10th August 2004 compared to the Wahlberg and Keinath (1988) correlation.

It should be noted that the tests for hindered settling velocity at different concentrations, Figure 6.4, were based on gradients plotted from the first 10 or so measurement points where a clear linear relationship is seen. At much higher concentrations the relationship is no longer linear and this data is not used, at lower

concentrations it is not clear what represents the zone of hindered settling as there are continuous changes in the gradient and so this data is not used either. Of particular note was a marked reduction in the settling velocity at the higher concentration. The hindered settling velocity was only measured up to 6000 mg/l with SSVI tests but point measurements in the tank show concentrations approaching 30,000 mg/l. The CFD model is therefore relying on extrapolation of the data based on the settling coefficients for higher concentrations. This is possibly the biggest weakness in the model and may be one of the reasons why the sludge bed height predictions are consistently lower than those measured.

6.3 The Crofton Trials

In February 2005, the Crofton and Walton sewerage treatment works operated with two final settling tanks each of 16.76 *m* diameter and 2.438 *m* side water depth. The original tanks were equipped with an undersized 2*m* diameter stilling wells of depth 1.5*m*. All tanks were of a standard UK design with a tank floor slope inclined at 7.5° to the horizontal and a hopper floor slope inclined at 60° to the horizontal. One of the tanks was modified for the trial to incorporate

- A stilling well of 3.5m diameter (close to 20% D) at 1.5 m depth below top water level (TWL).
- An EDI with two rows of 6 ports (12 in all) each with cross section 0.25 (width) x 0.3 (height) giving a maximum port area of 0.9 m^2 following the design of the author. Figure 6.18.
- A side wall Stamford baffle of 1m length inclined at 30° to the horizontal with the root of the baffle 350mm below the TWL. Figure 6.19.

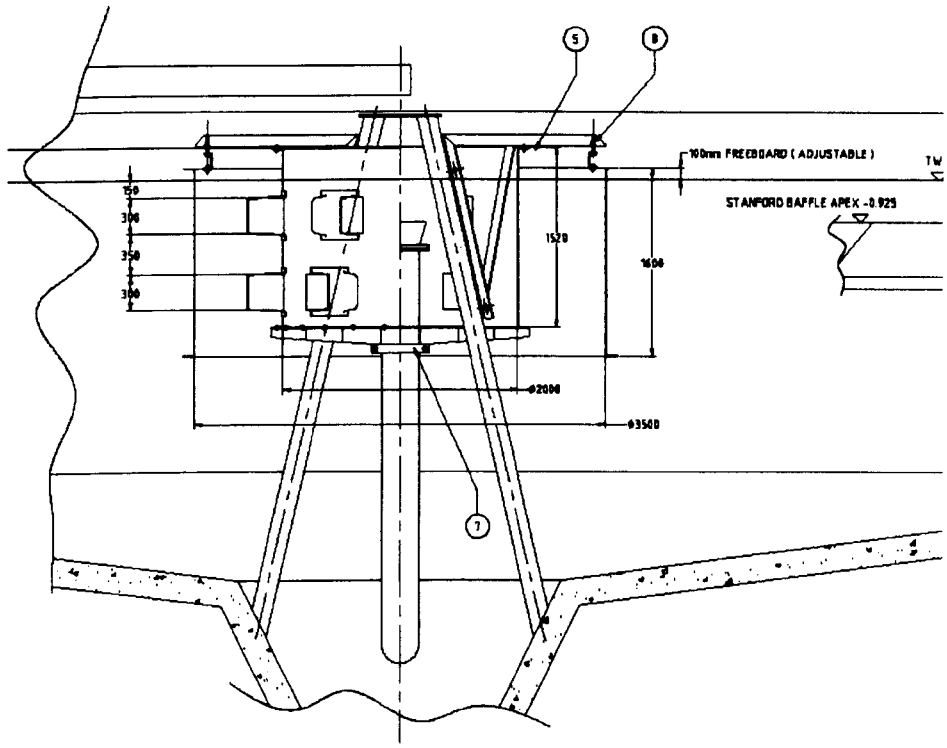

Figure 6.18: Influent arrangements for the Crofton trial.
The tank was modified to include a counter current EDI within the stilling well following the authors own design (Burt, 2004a). Note that there are 12 ports (300 x 300 *mm*) arranged in two rows which rotate the flow in opposite swirl directions.

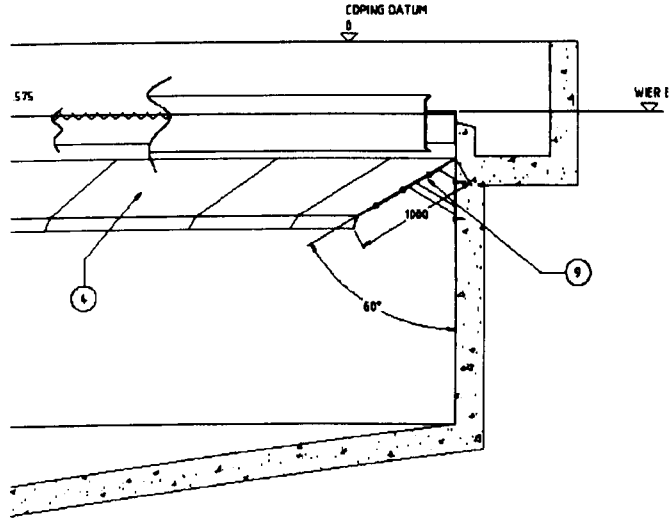

Figure 6.19: Effluent arrangements for the Crofton trial.
A Stamford wall baffle was constructed below the effluent weir, 1m long and inclined at 60° to the vertical.

This tank was trialled at only one process condition known to be close to the limit of operation. The SSVI value for the trial was estimated by measuring the height of a settled sludge bed at the end of a 30 minute settling test in a standard WRc settling column. This was recorded as 122.92 *ml/g* for a sludge column of initial concentration 1383 mg/l and 148.63 *ml/g* for a sludge column of initial concentration 2920 mg/l. From these two numbers the $SSVI_{3.5}$ was extrapolated to be 159 *ml/g*. Although these numbers are a reasonable estimate for the sludge settleability they were not obtained by direct measurement of the Vesilind settling parameters as required for use in the CFD model as discussed in detail for the Witney trial. Therefore, the Vesilind parameters had to be calculated from the Pitman and White correlation and sensitivity to $SSVI_{3.5}$ was tested between values of 140 and 159 *ml/g*. This means that the model validation exercise was less reliable than for the Witney study.

Table 6.4: Flow and load condition for the Crofton site trial.

Trial	Dates	Q	RAS	R	MLSS	X_F	$SSVI_{3.5}$ (ml/g)		
	2005	*(m3/hr)*	*(m3/hr)*		*(mg/l)*	*(mg/l)*	*Expt (WRc)*	*CFD1 (P&W)*	*CFD2 (P&W)*
1	16/03 21/03	126.0	126.0	1	2920	2920	122.9 159	140	159

At this flow condition and with a bulking sludge the tank is operating right on the mass flux limit as shown in Figure 6.20. From this analysis it might be expected that the tank would fail in operation by blanket spill, that is the blanket would be so high in the tank that effluent solids would be in excess of the acceptable limit set arbitrarily at 50 *mg/l*.

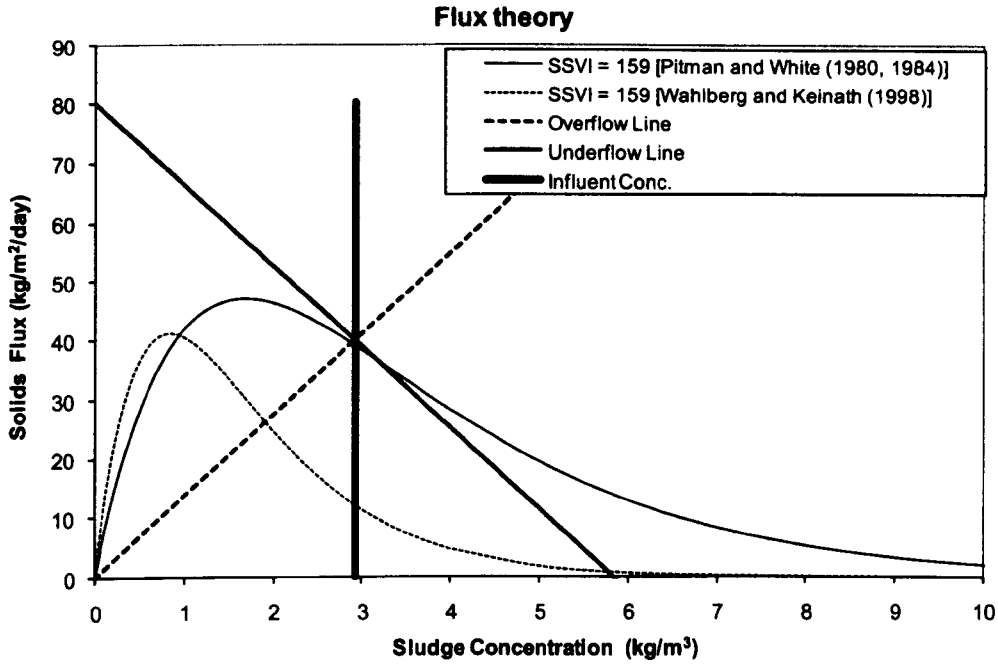

Figure 6.20: Mass Flux graph for the Crofton trial.
At this flow condition the tank is operating right at the mass flux limit and is therefore on the brink of failure.

6.3.1 Experimental Method

As with the Witney trial, the trial tank at Crofton was isolated from the main works flow with a single pump. This allowed direct measurement of the influent and RAS flow rate. Activated sludge samples from the aeration lane were dried to determine the influent mixed liquors (MLSS), X_F and a limited number of settling tests were undertaken to establish the $SSVI_{3.5}$. The experimental programme was carried out over a period of several days between, March 16th and 21st 2005. The data used for comparing experimental measurements with CFD predictions is for the process conditions defined in Table 6.4 which was recorded at 6 radial locations as shown in Figure 6.22 .

6.3.2 The CFD Model

The outline model geometry, CFD grid and boundary conditions are shown in Figure 6.21, the model used a grid of 13,100 hexahedral cells. All of the simulations

were performed in 2D axi-symmetric co-ordinate systems with the addition of a swirling velocity component to account for the influence of adding an EDI.

The boundary conditions for this model were defined according to the definitions in Table 6.4. The Takács (1991) parameters required for the settling model, equation (3.6), were based on those derived from the settling experiments for $SSVI_{3.5}$ between 140 and 159 *ml/g*. The analysis was limited to the use of a simple rheology function following Bokil and Bewtra (1972). The methods used to obtain converged CFD solutions for the trial condition were exactly equivalent to those described in Chapter 4 and Appendix B for the Rye Meads study.

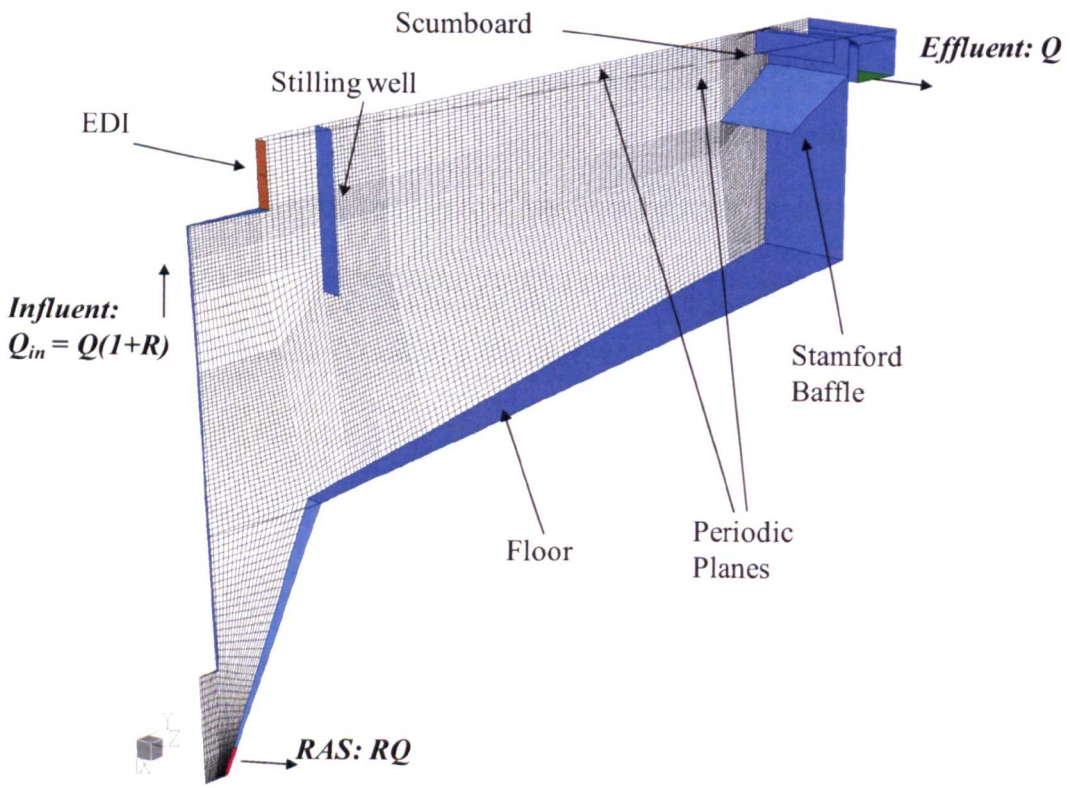

Figure 6.21: Geometry and modified internals for the Crofton trial.
The diffuser drum incorporates an EDI with ports sized to give an exit velocity at each port of 0.1 *m/s*. The figure is a 15° axi-symmetric segment of the full 360° circular tank. The high and low 'k' planes are periodic to allow for rotational swirl. The computational mesh has 13,100 hexahedral cells. Note the addition of a Stamford baffle following the dimensions in Figure 6.19.

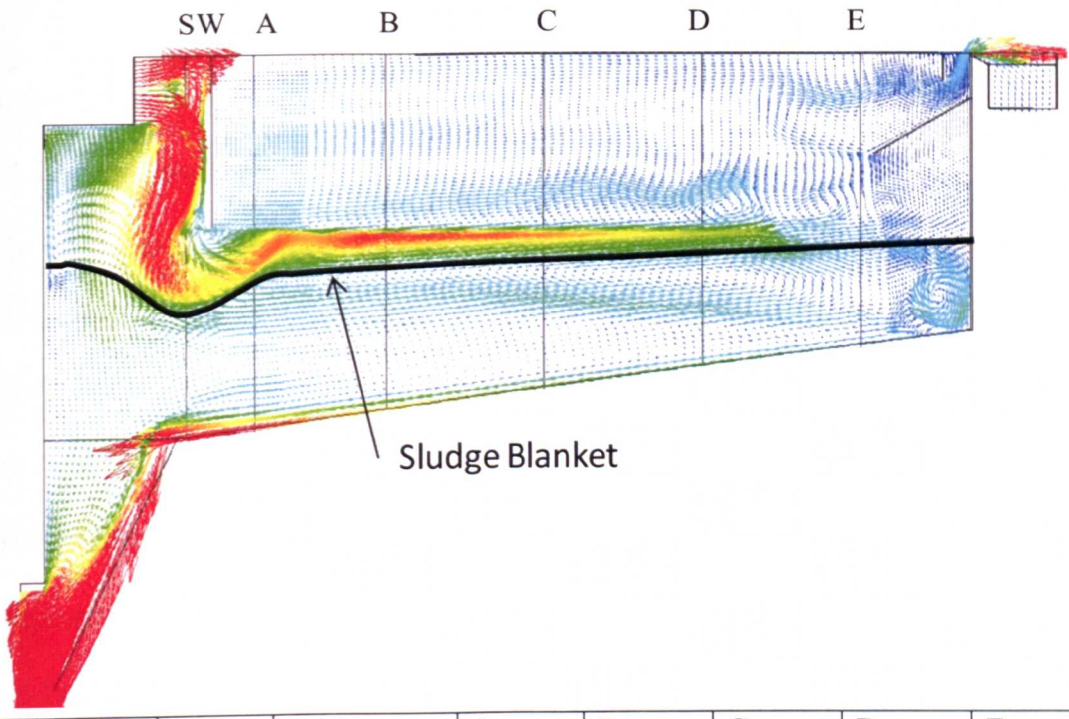

		Stilling	A	B	C	D	E
Radius	(m)	1.45	2.05	3.21	4.61	6.01	7.41
r/R		0.17	0.24	0.38	0.55	0.72	0.88

Figure 6.22: Velocity vectors in the Crofton Clarifier for the trial with $SSVI_{3.5}$ = 159 *ml/g* also showing the radial locations for the measurements of point velocity and solids concentration.

The blanket and radial shear layer are very high in the tank at this state point.

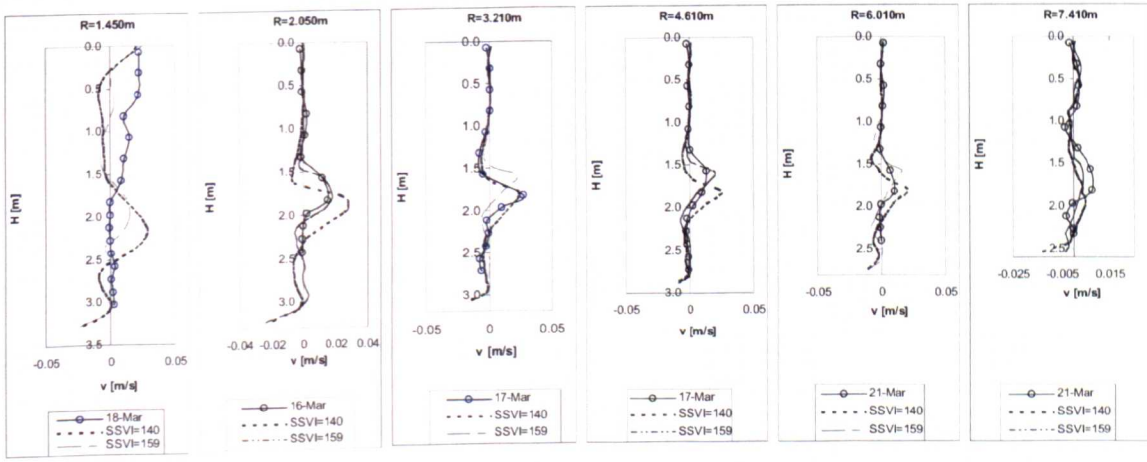

Figure 6.23: Comparison of radial flow velocity profiles for CFD predictions with $SSVI_{3.5}$ = 140 or 159 *ml/g* and the experimental data at 6 radial locations.

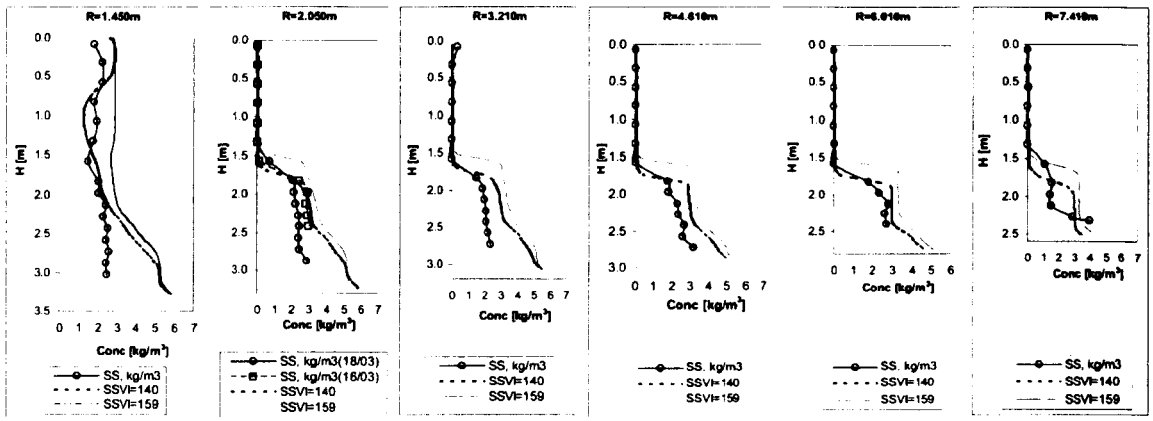

Figure 6.24: Comparison of concentration profiles for CFD predictions with $SSVI_{3.5}$ = 140 or 159 *ml/g* and the experimental data at 6 radial locations.

6.3.2.1 Radial Velocity Profiles

Figure 6.23 shows comparisons between CFD and experiment for the radial velocity profiles. This figure should be viewed in conjunction with the vector plot shown in Figure 6.22. Both CFD and experiment show the classical radial shear layer developing above the sludge bed and radial flow reversal from the sidewall back to the centre stilling well. The shear layer development of the experimental data sits between the CFD predictions at 140 and 159 SSVI. The profile in the stilling well suggests that there may be some eccentricity to the flow where the experimental results are displaced from the CFD prediction.

6.3.2.2 Concentration Profiles

Figure 6.24 shows comparison between CFD and experiment for concentration profiles. The experimental data sits between the CFD predictions at 140 and 159 SSVI up to 3 kg/m^3 solids concentration. It indicates that the CFD model is picking up the bed transition (arbitrarily the 850 mg/l contour) very well and the bed thickening is much better predicted than for the Witney study. It should be noted that

the measurement were not carried out close to the tank floor where solids concentration are thought to be much higher

6.3.2.3 Performance Parameters

The CFD calculation for the flow in the tank with SSVI at 159 *ml/g* produced a successful result with the process condition right on the mass flux limit of 100% 1DFT. The bed is stable at 1.54 *m* below the TWL and effluent suspended solids (ESS) is calculated to be 24 *mg/l*. Appendix D shows a sensitivity test performed to determine the influence of $SSVI_{3.5}$ being increased from 80 up to 159 *ml/g* in increments of 20 to approach the expected tank failure. The effluent concentration and bed depth predictions fall within the bounds of experiment for $SSVI_{3.5}$ = 140 *ml/g* and this suggests that the value approximated at 159 *ml/g* may be a little high.

Table 6.5: Comparison of performance parameters for experimental measurement and two CFD predictions for the Crofton site trial.

Trial	Q *(m3/hr)*	X_F *(mg/l)*	$SSVI_{3.5}$			Bed Depth h_{850} *(m)*		X_E, (ESS) *(mg/l)*	
			Expt (WRc)	Expt (P&W)	CFD (P&W)	Expt	CFD	Expt	CFD
1a	126	2920	159	159	140	1.75	1.75	12.5 - 24.9	18.57
1b	126	2920	159	159	159	1.75	1.54	12.5 - 24.9	23.86

For the Crofton trial, the bed thickening process does seem to have been well captured by the model for these CFD results and the prediction of the bed height and the effluent suspended solids (ESS) is within the bounds of the measured values. Of particular note is the prediction of blanket height and the associated shear layer above the blanket. This has been completely captured by the model to a high level of accuracy as shown in Figure 6.23. In this case the sludge bed only thickens up to $3X_F$ and so the CFD and mass flux model (where the underflow line crosses the

concentration axis in Figure 6.20) are in better agreement with the experimental concentration predictions.

6.3.2.4 Other Internal Design Features

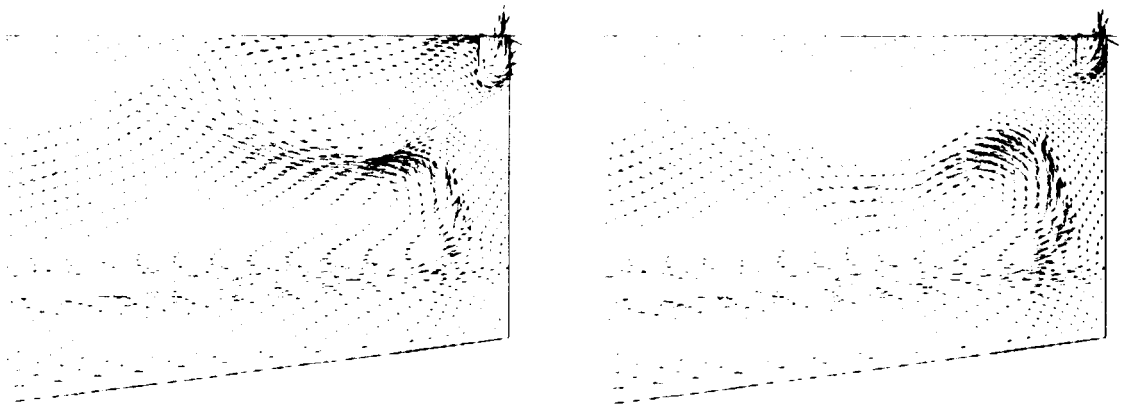

Figure 6.25: Velocity Vectors at the effluent Weir with and without the Stamford Baffle (Burt, 2005c).
These CFD results are for the Crofton clarifier boundary condition Trial 1a).

Additional calculations were performed for the Crofton study in order to answer questions about the quality of the design. For the trial 1a) boundary conditions, results were produced with and without a Stamford baffle, as shown in Figure 6.25. This demonstrated that although the flow patterns near the effluent were redirected by the baffle, there was no significant difference in the effluent quality. The G field was also calculated and, as for the Rye Meads study, the bulk G value within the stilling well was very low; from equations (2.1) and (4.3) the flocculating parameters for the Crofton clarifier were calculated to be $G. \approx 28\ s^{-1}$ and $G.T \approx 5200$. From the CFD results, the equivalent mean flocculating parameters were obtained by volume averaging G within the stilling zone, this gives $G. \approx 0.9\ s^{-1}$. $G.T$ was then approximated as the numerical integration of the floc G history plotted in Figure 6.26 which gave $G.T \approx 220$. This number was similar to the Rye Meads value but again, a long way short of the $G.T$ required for enhancing the flocculation process in activated sludge.

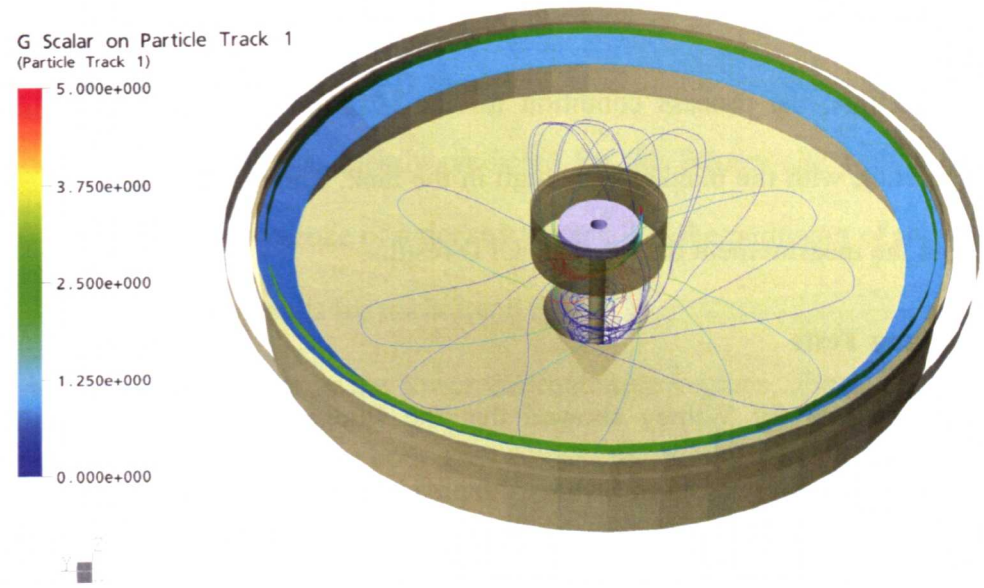

Figure 6.26: Tracking the G Scalar field in the Crofton Clarifier.
A massless particle is released from the EDI port and is tracked following the sludge velocity field $\mathbf{U}' = \mathbf{U} + \mathbf{U}_{sk}$. $G.T \approx 220$ was calculated for this track (within the stilling well) following the method described in Chapter 4. The plot also shows the effect of the swirling EDI and the use of periodic boundaries for a 2D swirling flow calculation.

6.4 Conclusions for the Site Trials

The two trials were performed on tanks of similar dimensions but operating at different extremes of normal operation. The Witney trial was carried out well within the mass flux limits at low flow and with extremely low SSVI. In contrast, the Crofton trial was performed on the mass flux limit at very high flow and with a poor settling (or bulking) sludge. It is useful to contrast the performance of the CFD model and the behaviour of the influent modifications for these two sites. These observations are considered further for the different aspects of the study as follows;

6.4.1 Mass Flux Theory

- Mass flux theory for the Witney site showed the tank was under-loaded for all of the process conditions considered. This is reflected in the solids profiling

data, Appendix D, and the CFD results which show a very low blanket in all cases.

- In contrast, the process condition for the Crofton tank is on the limit of operation with the blanket very high in the tank. This can be clearly seen in both the measurement data and the CFD results.

6.4.2 Settling Tests

- Settling data for Witney showed that the sludge had very good settling qualities but the measured $SSVI_{3.5}$, obtained from the standard WRc settling test, did not match with the measured Vesilind parameters, (probably because of iron dosing). The activated sludge at the Witney site appeared to follow the Wahlberg and Keinath correlation not the Pitman and White correlation.
- For the Crofton site the sludge had a particularly high SSVI and might be described as bulking, in line with the definition given in Chapter 1, which is the main reason why the tank was seen to be operating so close to the failure limit.
- It cannot be assumed that SSVI based on the standard 30 minute test will always give the correct Vesilind parameters for the CFD model. Therefore, direct measurement of the interface falling with time as a function of sludge concentration, as discussed in Chapter 3, is a more reliable method for obtaining parameters for the Vesilind (and thereafter the Takács) model. However this experiment must be performed across a range of sludge concentrations and is time consuming to perform.
- Where there is uncertainty in the measurements, and this was apparent at both sites, it is appropriate to perform CFD modelling for a range of $SSVI_{3.5}$ values to test the sensitivity of the tank to this parameter. This was

particularly useful for the Crofton study and, in retrospect, should have been done for the Witney study.

6.4.3 Performance of the CFD Model

- Under-loading was clearly predicted for the Witney site with a low sludge bed and the presence of a density waterfall at the perimeter of the McKinney baffle in the results for trials 2 and 3.
- Velocity profiles in the lower concentration regions, above the settled bed, were well predicted at both sites.
- Velocity profiles and solids distributions within the settled bed were not as well predicted for the Witney site trials.
- The concentration results may be highlighting a weakness in the Bokil and Bewtra (1972) viscosity model which never shows thickening greater than 2 or 3 times influent. This suggests that the CFD model may need to be extended to include a thickening function, similar to that proposed by Vaccari (1989) and as discussed by Armbruster (2003).
- CFD predictions of the effluent solids are close to experimental data for both trials and re-suspension of solids at the side wall is clearly seen in both the CFD and the experimental data.

6.4.4 Alternative Rheology Models

- Experiments to measure sludge viscosity were not performed, only known correlations with parameters derived by other workers were used in the CFD predictions.
- In Chapter 4 it was noted that changes in the rheological function can influence blanket depth significantly. However, for the Witney study, where

the tank is in a highly underloaded condition, the blanket (850 *mg/l* contour) remained close to the same depth for all rheology models.

- For the Witney trial number 3 the sludge at the floor was measured as high as 27,840 *mg/l* ($9.5\,X_F$). Only the modified Herschel Bulkley model of de Clerq (2003) predicts values close to this. All other rheology models predicted maximum concentrations < 10,000 mg/l.
- The square law rheology model of Armbruster (2003) flattens some of the velocity profiles and appears to give the least physical results.

6.4.5 Comments on the Influent Designs

- Results for the Witney trial showed a lower ESS than for equivalent flow rate for the tank with McKinney baffle influent. This might imply that the McKinney baffle is performing significantly better than the large stilling well. However, the results from the trial are not a direct comparison as the solids loading differ, see Table 6.3.
- Results for Witney trial number 3 also showed good performance in ESS but significant turbidity was observed in the effluent during this phase of the experiment. It is possible that this turbidity may have come from the shearing action of the centrifugal pump directly upstream of the tank.
- There is evidence of bed scouring for the Witney McKinney baffle solution. Particularly when comparing solids profiling results from trials 1 and 2. This implies the jet from the McKinney slot is not entirely radial. This angled jet may be avoided by extending the baffle to a diameter 20% greater than the stilling drum. This is recommended design change for all McKinney baffle installations.

- The EDI influent arrangement for the Crofton site appears to have been particularly effective at maintaining the operation of the tank at the mass flux limit.

The observations made from these two trials provided significant confidence that the extended drift flux model was able to predict many of the salient features observed for sedimenting flows in settling tanks. The trials also highlighted the weaknesses of the model in dealing with unusual settling parameters and compacting sludges. The performance of the McKinney baffle was encouraging and the results provided various pointers on how the baffle design might be improved. The EDI performance was particularly encouraging for the Crofton site. As a result of these trials, both the EDI and McKinney influent designs were explored further in tank performance studies for other waste water treatment sites. It was also noted that the stilling well and EDI combination applied at Crofton did not increase the Camp number $G.T$ beyond the values observed for the Rye Meads stilling well.

6.4.6 Comments on the Extended Drift Flux Model

For the rheology models investigated, the modified Herschel Bulkley model of de-Clercq (2003) appears to be both robust and more able to predict the near wall thickening observed in the Witney trials. The settling model of Takács (1991) has to be used with care and where only SSVI data is available, as for the Crofton trial, then sensitivity to the Takács parameters has to be explored as part of the CFD modeling activity.

CHAPTER 7: CFD and Mass Flux Analysis for Clarifier Process Design

Summary

In this chapter the McKinney plate influent design previously presented as part of the Witney trial is developed further for application in the clarifiers at the Budds Farm sewage treatment works (STW) near Portsmouth in Southern England. This study compares existing and new clarifier designs for the site operating both with and without a McKinney baffle influent modification. Different designs for the Budds Farm clarifiers were assessed by contrasting the CFD predictions for effluent suspended solids (ESS) and sludge bed depth against the mass flux parameter 1DFT, introduced in Chapter 3. This new method of presenting the CFD results allows the process performance of a clarifier design to be contrasted against the performance of all clarifiers.

7.1 Introduction

Whenever a town or city is subject to continued growth and expansion there is pressure of the receiving sewage treatment works (STW) to safely and efficiently treat the additional effluents that arise from that expansion. This requirement is compounded in the United Kingdom by the fact that most sewage systems are combined and so the industrial and domestic waste streams are mixed with large amounts of storm water during periods of excess rainfall. To a certain extent, these hydraulic surges can be compensated for at the STW through the use of storm overflow tanks but ultimately, the capacity of a site to treat the waste water is limited by the surface overflow rate and mass flux capacity of the final clarifiers.

It is usual for water companies engaged in the management of their infrastructure to plan ahead for expected population increases in areas where they provide treatment services. This was the case at the Budds Farm STW, where in 2006, as part of Southern Water asset management plan four (AMP4), two new, large, circular (35m diameter), clarifiers were to be built alongside the eight existing clarifiers already in service. In this case the projected increases in flow during the AMP4 period were not the greatest concern as the maximum storm flows were to be managed close to earlier levels. However, the solids loading in the aeration lanes through to the clarifiers were projected to increase significantly from 2000 mg/l up to a maximum of 4000 mg/l. It was realised that, in order to meet the flow and load requirements with the available clarifier surface area, all of the clarifiers, existing and new, would need to perform very close to their mass flux limit and therefore good influent design would be required.

In this process design study, CFD and mass flux predictions were used to demonstrate the effectiveness of alternative influent designs for the eight existing and two new clarifiers at the Budds Farm STW. The original proposals for standard stilling well influent designs were compared with a McKinney influent modification using fifty two separate CFD analyses with supporting mass flux calculations.

7.1.1 Acknowledgements

This study was sponsored by Dr Ajay Nair of 4Delivery Ltd, a consortium including United Utilities, Costain and Montgomery Watson Harza (MWH) responsible for environmental improvement schemes across Sussex, Kent, Hampshire and the Isle of Wight on behalf of Southern Water in the UK during the AMP4 period (between

2005 and 2010). The CFD calculations were performed by Dr Andrew Grand and Dr Jay Ganeshalingam both as employees of MMI Engineering Ltd (Burt et al, 2006).

7.2 The Budds Farm Clarifiers

In the summer of 2006, the STW at Budds Farm operated with eight clarifiers. Each one had a 35*m* internal diameter with a 2.77*m* sidewall depth and a 5° floor slope. The average works settled sewage flow rate was 1200 *l/s*, rising to a maximum value of 2400 *l/s* in very wet weather conditions and the return activated sludge (RAS) rate for the site was typically in the range of 480 to 950 *l/s*.

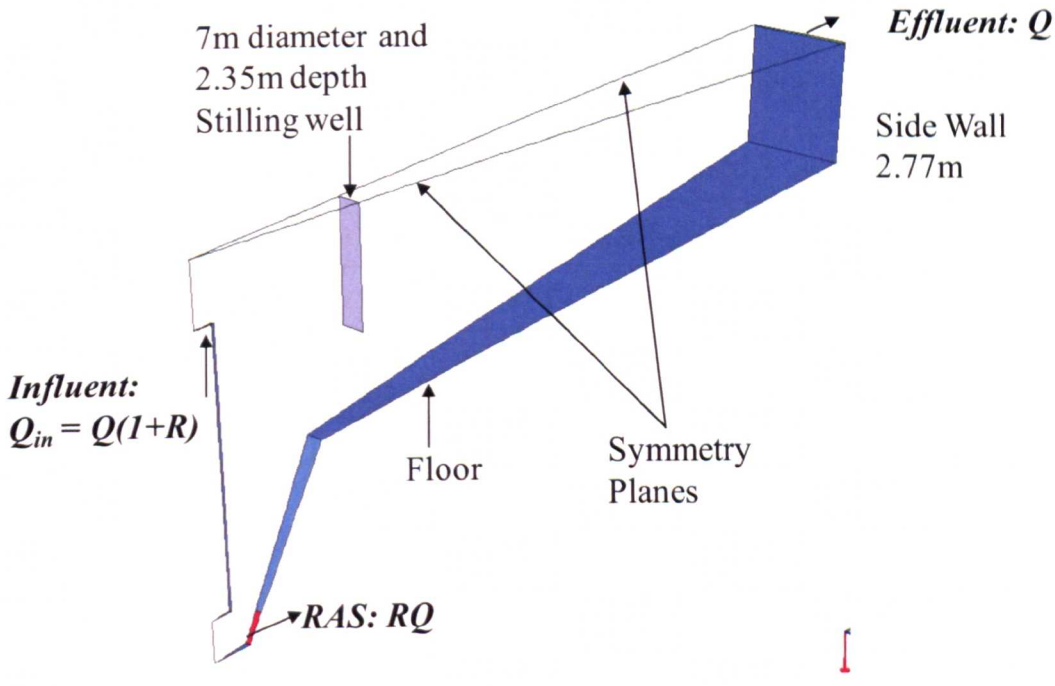

Figure 7.1: An axisymmetric cross section of one of the existing Budds farm clarifiers operational in early 2006.

The future site design flows projected for the AMP4 period were for an average of 1158 *l/s* rising to a maximum of 2531 *l/s* during wet weather, with RAS flows projected to increase to between 1000 and 1158 *l/s*. These flow changes were also subject to a substantial increase in the mixed liquor suspended solids (MLSS) rising

from 2000 up to a maximum of 4000 *mg/l*. The target solids discharge limit from the clarifiers was required to be $X_E = 40$ *mg/l*.

In order to meet the requirement of the projected AMP4 flows and loads, two new 35*m* diameter clarifiers were proposed to be built alongside the existing tanks. These clarifiers were of a modified design with a 3m side wall depth and a 4.5° floor slope. The original stilling well proposed for this design was to be oversized at 31.4% of the tank diameter and 2.1*m* deep from top water which was the standard design practice for Southern Water. The effluent zone of the tank was also modified to include an inboard launder with a side wall weir baffle following the design of McKinney (MWH, 2003) as shown in Figure 1.6. The $SSVI_{3.5}$ for the site was expected to be maintained between 100 and 130 *ml/g*.

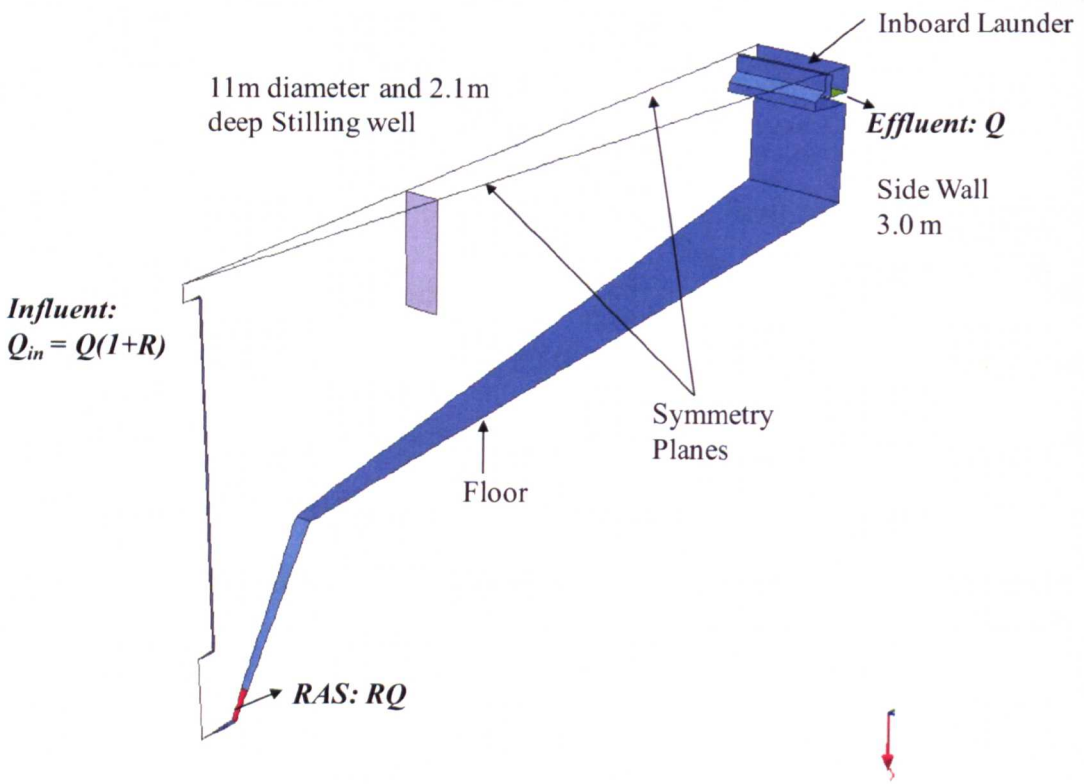

Figure 7.2: Geometry of the two new build clarifiers at Budds Farm STW. Note that oversized or flocculating stilling well, this size of stilling well would normally incorporate an EDI around the influent (Ekama et at, 1997). The design also features a novel inboard launder design (MWH, 2003) with a McKinney wall baffle.

7.2.1 Mass Flux Theory and comparisons with CFD

In order to assess the performance of these tanks for the anticipated AMP4 process conditions, a number of representative state points were defined as shown in Table 7.1. For each state point the value of %1DFT, equation (3.27), indicates the expected performance from the mass flux theory (MFT). These are the percentages of the maximum limit on hydraulic loading that could be achieved where a value under 80% of 1DFT might be considered as safe operation.

Table 7.1: State points for testing the process performance of the Budds Farm clarifiers. D and E are highlighted to emphasise that these are hydraulically over-loaded.

	Flow Rate	Q		RAS		R, Recycle Ratio	X_F	$SSVI_{3.5}$	1 DFT
		[m³/hr]	*[l/s]*	*[m³/hr]*	*[l/s]*		*[mg/l]*	*[ml/g]*	%
A	Current Max	1080.00	300.00	427.50	118.75	0.3958	2000	120	63.88
B	Current Ave	540.00	150.00	216.00	60.00	0.4000	2000	120	31.94
C	Future Ave	496.44	137.90	360.00	100.00	0.7252	3500	125	67.46
D	Future Max	911.16	253.10	416.88	115.80	0.4575	3500	125	*123.82*
E	Future Max	911.16	253.10	416.88	115.80	0.4575	3300	125	*112.01*
F	Future Max	911.16	253.10	416.88	115.80	0.4575	3500	100	75.66

The key CFD results that may be compared with MFT for all designs at all process conditions are the effluent suspended solids value X_E (ESS) and the sludge blanket depth. The ESS is simply recorded transiently from the CFD result as a trace of the concentration of solids at the weir exit boundary condition for the full duration of the transient calculation (usually 8 to 12 hydraulic retention times at the end of which the ESS value is stable or periodically oscillating). The sludge blanket depth is recorded as the position of the 850 *mg/l* solids contour below the top water level (TWL) at the end of the simulation following Matko (1998). These two values are referred to as

the clarifier performance parameters in Chapter 6 and are illustrated for the Crofton clarifier study in Figure 6.22 and Table 6.5. The concept for the comparison is that the ESS will increase and the sludge bed depth will reduce as %1DFT increases and these performance parameters may be plotted against %1DFT to show this trend. A similar concept was used by Ekama and Marais in their work with the SettlerCAD software, (Ekama and Marais, 2004).

7.2.2 A new McKinney Baffle Design

A modified McKinney baffle influent was proposed for installation in the eight existing and two new tanks. It was anticipated that the McKinney baffle influent would allow the clarifier to achieve best performance at the highest flow rates as discussed in Chapter 1. This influent was designed according to the guidance on the McKinney plate slot height (Krebs, 1998) discussed in Chapter 1 but with some significant additional modifications recommended by the author. These were,

- A steep sloping (Chinese hat) arrangement near to the influent riser to prevent the build up sludge in the quiescent flow region.
- The inclusion of a deflection ring around the influent riser designed to maintain a sweeping or cleaning flow over the McKinney plate.
- A fall in the McKinney plate to aid drain down of the tank.
- An overhang of the plate extending beyond the diameter of the stilling drum intended to straighten the radial flow that enters into the settling region of the tank. This last feature was included as a direct result of the observed flow behaviours in the Witney trial discussed in Chapter 6.

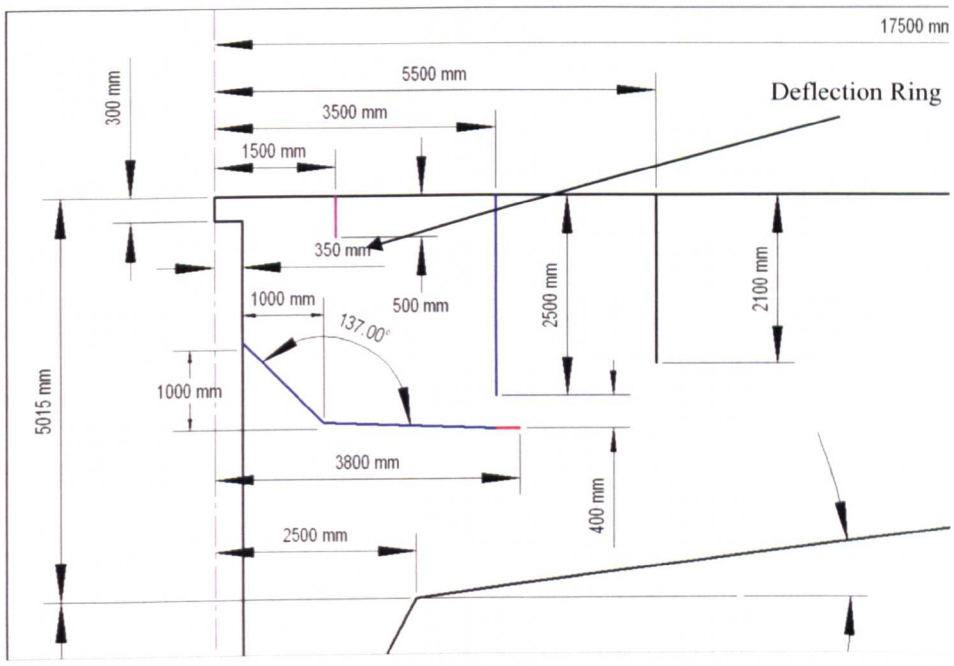

Figure 7.3: Influent modifications applied to all of the Budds farm clarifiers.
The McKinney baffle was extensively remodelled from the simple plate applied at the Witney site (Burt, 2005a) to promote a sweeping flow across the floor and recirculation within the drum.

The effect of these design modifications can be seen in Figure 7.4 where the CFD solution for the flow in the new clarifier is compared at state point F (or 76% of 1DFT) with and without an internal deflection ring.

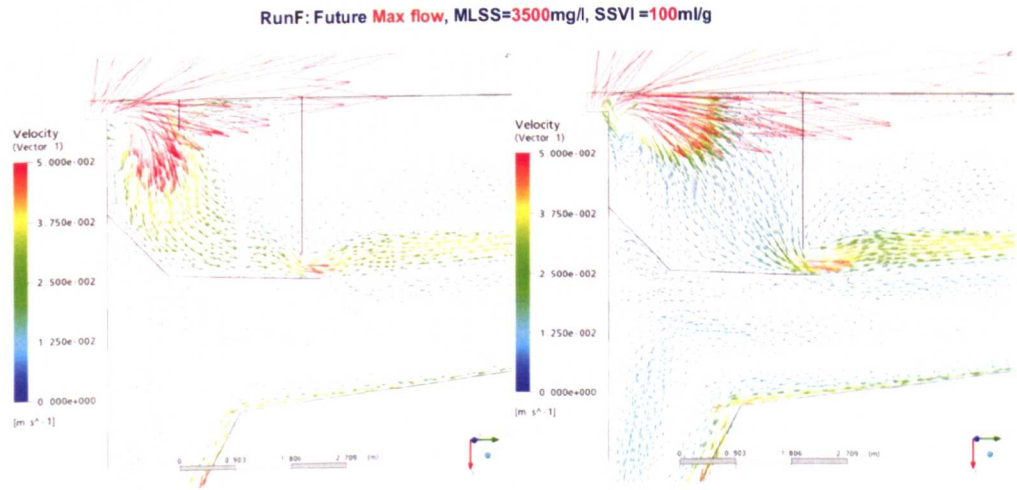

Figure 7.4: Velocity vectors in the Budds Farm new build clarifier at statepoint F, or 76% of 1DFT, with and without a deflection ring.
The addition of the deflection ring promotes a sweeping flow over the top surface of the McKinney baffle.

7.2.3 Side Weir Modification with a Baffled Inboard Launder

The addition of an inboard launder with an overhanging baffle, also originally proposed by McKinney (MWH, 2003), is intended to limit the carry-over of suspended solids (ESS) to the effluent weir by retaining the rising effluent at the side wall (Anderson, 1945). Figure 7.5 shows the velocity distributions and the solids concentration distributions at the side wall for state point F, which is significantly below the mass flux limit for the model, with and without the inboard launder. It can be seen that the shear layer separation that breaks away from the settled bed, and convects solids towards the effluent weir, is not influenced by the presence of the inboard launder. The observation that baffling at the effluent weir has little or no influence on the ESS value has been observed in many modelling studies, including the Crofton study (Burt, 2005c) discussed in Chapter 6, where a larger inclined Stamford wall baffle was installed.

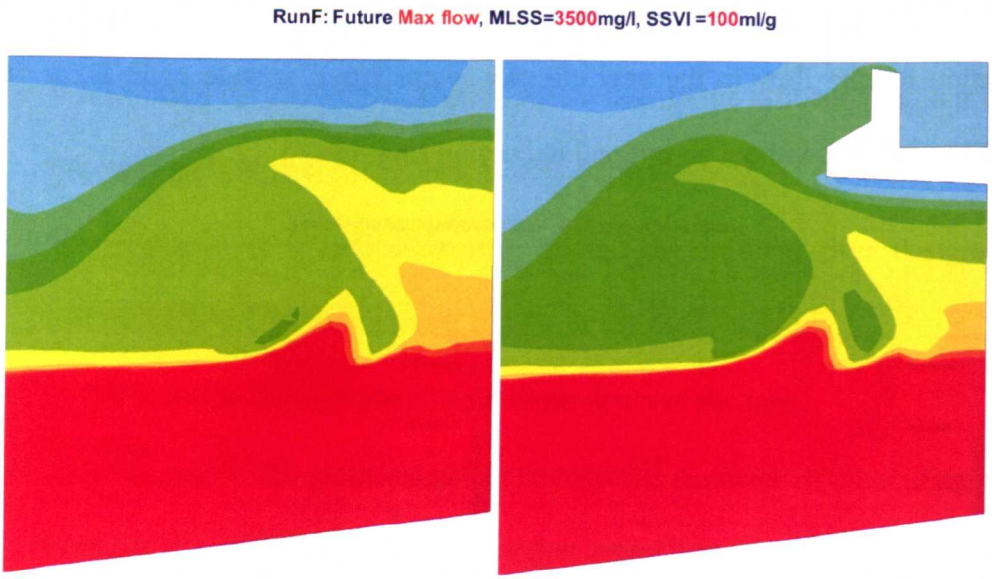

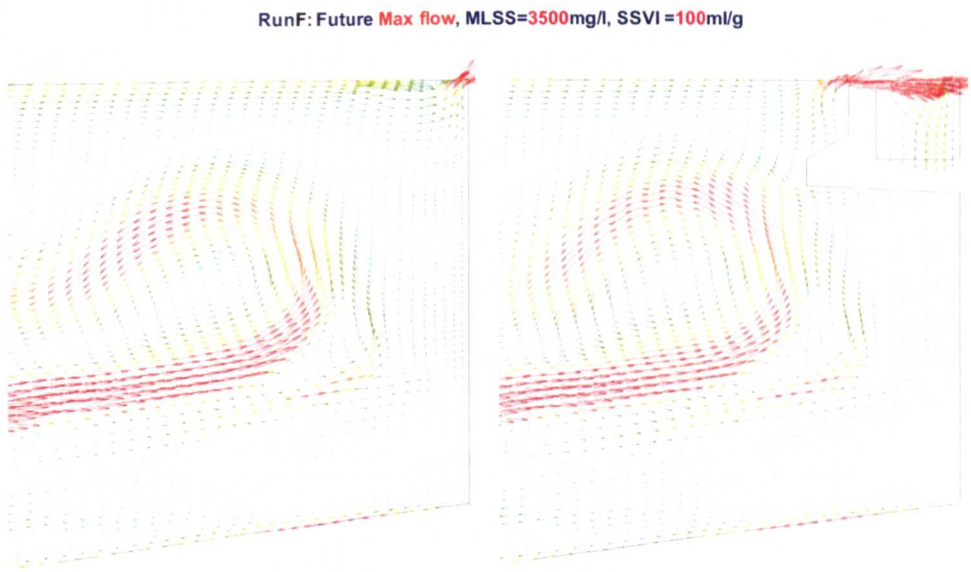

Figure 7.5: Concentration profiles in the range of 0 to 100 *mg/l* and velocity vectors for the Budds Farm new build clarifier at statepoint F, or 76% of 1DFT, with and without the baffled inboard launder.
The presence of the launder does not reduce the effluent solids value X_E.

7.3 Results of Mass Flux and CFD predictions.

CFD analyses were carried out for the new and existing clarifiers, with and without the influent McKinney modification for the original six state points in Table 7.1 and for ten additional state points presented in Appendix E. A sample result is shown in Figure 7.6 for state point X1 which is 73% of the 1DFT limit. The result shows that the proposed design of tank is overloaded and there is carry-over of solids at the weir indicating a sludge blanket spill. When the diameter of the stilling well is reduced to 20% of the tank diameter and a McKinney baffle is included to further control the influent mixed liquors, following Figure 7.3, an improvement in performance is achieved. The results shown in Figure 7.6 are for the same state point and the improvement in sludge blanket retention may be attributed to the revised influent geometry. This is a particularly significant observations and demonstrates that the use of a McKinney baffle to break the influent density current, and therefore control

the local mixing of the sludge bed near the influent, has a strong influence on the overall capacity of the tank.

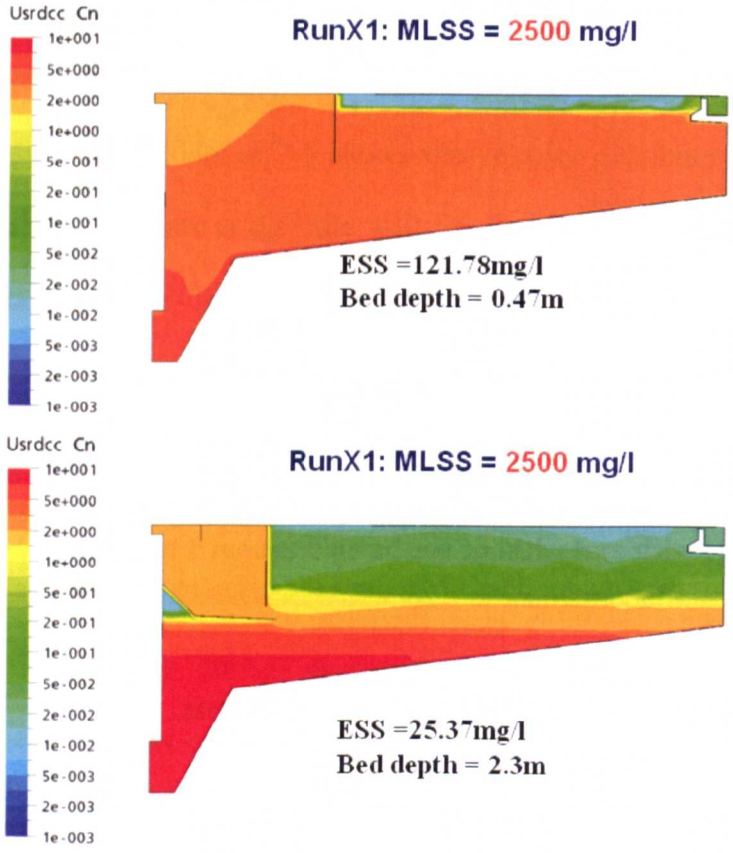

Figure 7.6: An axi-symmetric section of the new 35m diameter circular tank showing concentration gradients between 1 and 10,000 mg/l on a log scale. Both plots are at state point X1 or 73% of 1DFT. This shows the unmodified tank failing while the tank with the smaller stilling drum and McKinney plate modification is operating successfully.

The results for the clarifier performance parameters, ESS and sludge blanket depth, are plotted against the dimensionless parameter for mass flux theory defined in Chapter 3 as %1DFT; where 100% is considered to be the hydraulic limit of the tank. Note that this differs from Ekama and Marais (2004) who chose 100% of criterion I, the solids flux limit, as the absolute limit of 1DFT.

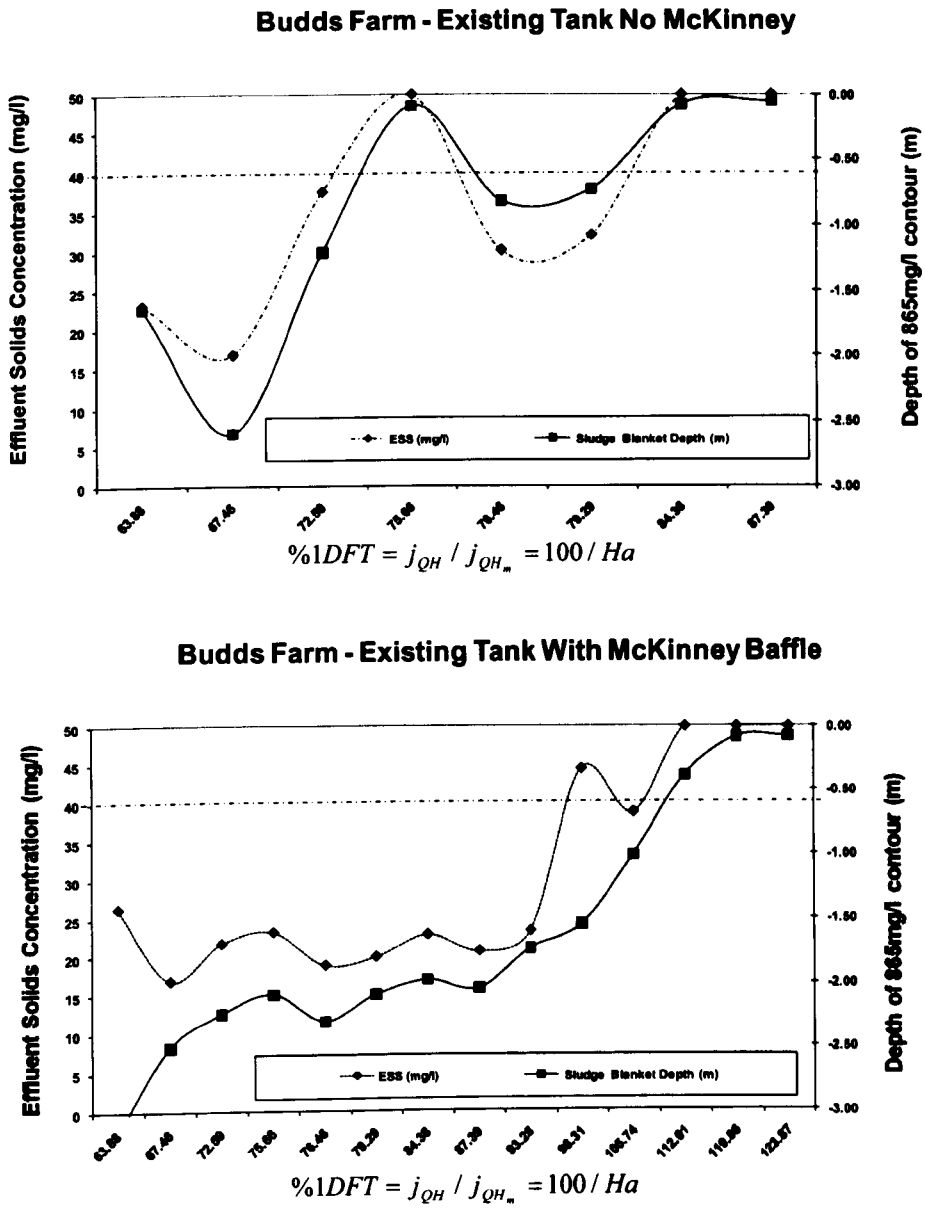

Figure 7.7: CFD results for the exiting tanks plotted against %1DFT.
The value of X_E is required to stay below the solids discharge limit of 40 *mg/l*. Effluents that have exceeded 50 *mg/l* are shown at 50 *mg/l*.

Figure 7.7 shows the performance parameter trend plotted against %1DFT, results are compared with and without the modified influent design for the existing tank design. Note that the failure limit is shown on the graph for effluent suspended solids exceeding 40 *mg/l*. The performance without the modification is erratic and some state points show failure (blanket spill) as low as 76% of 1DFT. The performance

with the modified influent is much better and the X_E is below the required solids discharge limit of 40 *mg/l* even at 98% of 1DFT.

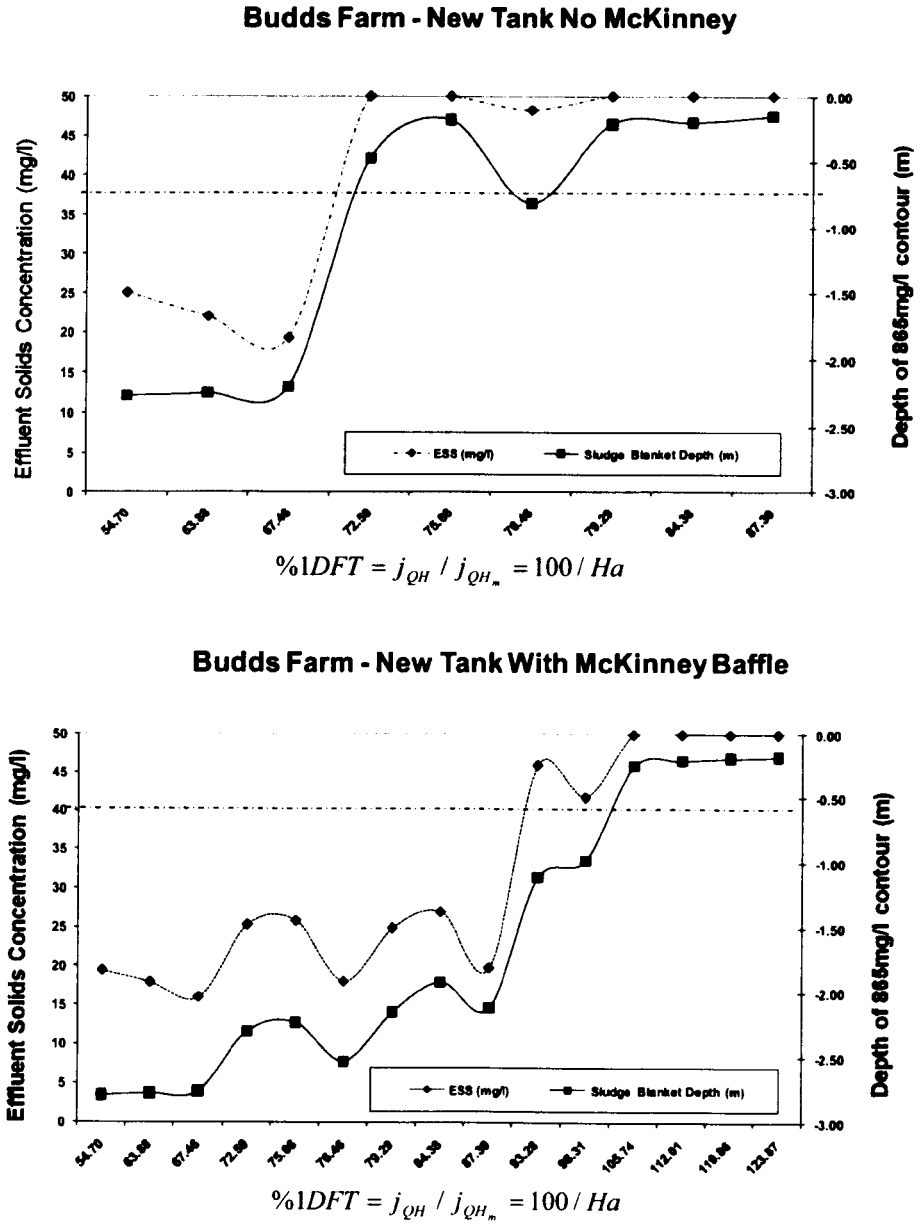

Figure 7.8: CFD results for the new tanks at Budds Farm plotted against %1DFT.

Figure 7.8 shows the performance parameter trend plotted against %1DFT, results are compared with and without the modified influent design for the new tank design. The performance without the modification shows failure (blanket close to spill) at

73% of 1DFT. The performance with the modified influent is much better and the ESS, X_E is below the required limit at up to 90% of 1DFT.

This method of representing the results is a helpful way of comparing designs but the function 1DFT does not necessarily follow a continuous trend. This is because the value of 1DFT is constructed from the four mass flux process variables Q, X_F, R and $SSVI_{3.5}$ and the clarifier system responds differently to variations in each of these parameters. So, in Figure 7.7a, the unmodified tank has failed at 1DFT of 75.66% which is state point F, but operates successfully at state points Y1 and Z2 (see Table E1) with higher 1DFT values. It is interesting to note that for the modified designs, with a McKinney influent, the performance variations are less erratic.

7.4 Conclusions

By testing the design limits with a combination of MFT and CFD and optimising the internal geometry of both tanks it was demonstrated that the required flows and loads could be carried by the Budds Farm clarifiers. The method of plotting the clarifier performance parameters, ESS and sludge blanket depth, against the mass flux index %1DFT is a useful way of comparing designs and demonstrating whether one system is more robust than another. Following on from this study, all of the tanks at Budds Farm were modified to include McKinney baffle influents and these have now been operating successfully since the middle of 2007.

Figure 7.9: The modified McKinney baffle influent as installed at Budds Farm in 2007. Photograph courtesy of A. Nair, MWH and Southern Water.

CHAPTER 8: Discussion

Summary

In this chapter, observations made during the work are developed further. The discussion focuses on the two areas critical to the thesis: modelling and design. The modelling work has focussed on the validation and testing of the various constitutive relationships which make up the new extended drift flux (EDF) model for clarifiers. The limitations of these models are discussed here and potential modifications and improvements are suggested for low and high concentration settling zones (Type 1, 2 and 4) as further work. A new suggestion is made for linking the multiple and extended drift flux models together in order to overcome the need to fit the Takács (1991) parameters at concentrations X <500 *mg/l*. The connection between mass flux theory and the EDF model is also discussed as the two modelling methods may be used together to assist in the design process. The idea for linking the clarifier performance process parameters, effluent suspended solids, X_E and sludge bed depth, h_{850} to the mass flux limits is extended to all of the mass flux criteria. The design work has focussed on changes to clarifier internal structures in order to optimise tank performance. A new generalised McKinney baffle influent is presented for use in shallow circular clarifiers throughout the UK. Explanations of other potential design improvements and the motivations for implementing them are also discussed here.

8.1 The Mass Flux Model

In this work, comparisons have been made with mass flux theory and CFD predictions which consistently show that tank failure can occur well before the mass

flux limit of 100% 1DFT. The serious limitation, that mass flux theory is a 1D model being used for the design of a 3D hydraulic system, cannot be escaped but it can be shown, as in the Crofton and Budds Farm studies of chapters 6 and 7, that where good design practices are followed, the performance of the tank can approach the 1DFT limit. Therefore, the use of mass flux theory in design must always be predicated by a safe working limit and typically values of 80% for the solids flux limit, Criterion I (Ekama and Marais, 2004) are quoted. Where the hydraulic load, Criterion II is used for the 1DFT limit, as shown in Figure 7.7 and 7.8, failure is not uncommon in poorly designed tanks below 75% of the hydraulic limit and so this is suggested here as a conservative limit. All UK water companies continue to use mass flux theory for first pass sizing of tank surface area and the choice of the mass flux limit depends on the design standard being used. It is always incumbent on the designer to produce a combination of tank shell and internals that will behave as close to the ideal 1D limit as can be achieved with good hydraulic design. This thesis provides many points of guidance on this, and some of these have been incorporated into water company standards (Burt et al, 2007). It is worth noting here that 1DFT as it is proposed in chapter 3, equation (3.27) is simply the ratio of the surface over flow rate to the settling velocity at the influent solids concentration. The Hazen (1904) number is given by Stamou (2007) for a circular clarifier as

$$Ha = \frac{A_{st} V_s}{Q} \qquad (8.1)$$

where V_s is a vertical settling velocity. Therefore, the 1DFT ratio j_{QH} / j_{QH_m}, equation (3.27), is simply the reciprocal of the Hazen number in a circular clarifier but because the settling velocity V_s based on the influent concentration X_F it is probably better to say that 1DFT is the reciprocal of the influent Hazen number.

8.1.1 Additional Mass Flux Limits

In order to support this idea of a defendable mass flux limit the use of a ratio of actual value to permissible value may be extended to all of the mass flux criteria. This has been done in a mass flux calculator which has been developed alongside this work for general use within the water industry (ClariSim, 2007).

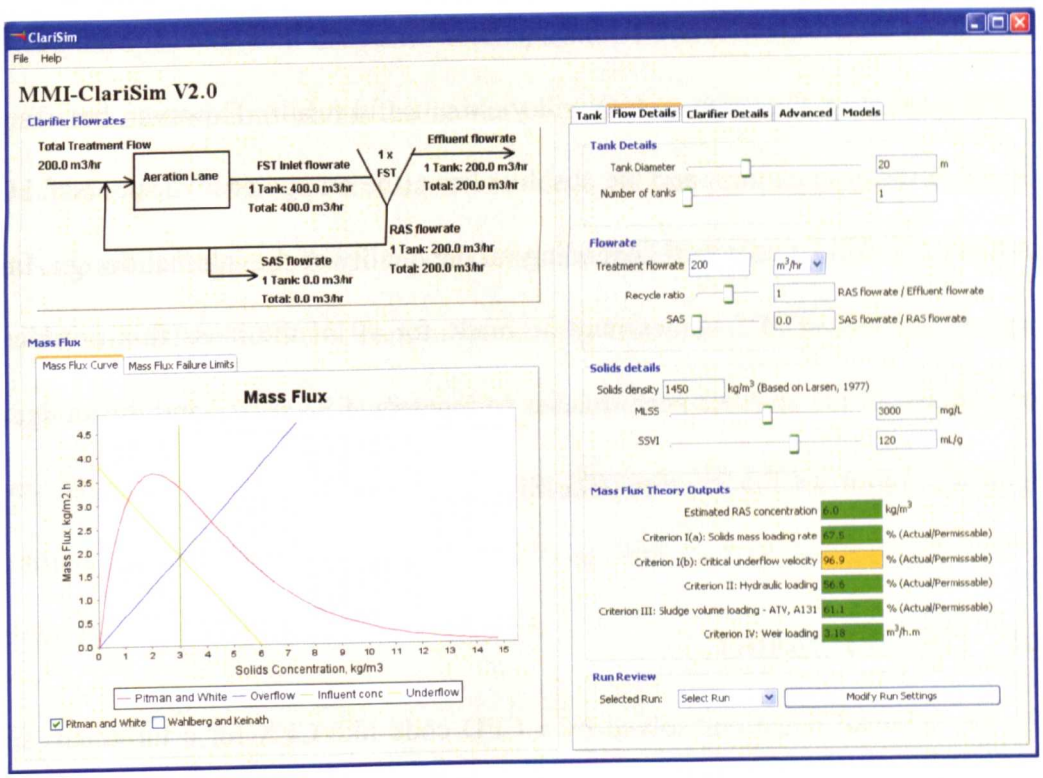

Figure 8.1: Screenshot from the MMI-ClariSim interface which includes a facility to set the mass flux limits.
When a state point exceeds this limit the output box is highlighted in orange. If 100% of 1DFT is exceeded the highlight changes to red.

The operating state point of a clarifier has four parameters (The influent MLSS or X_F, the flowrate Q, the RAS ratio R and the settling index $SSVI_{3.5}$); the ClariSim tool can be used to check whether variations in these parameters will put a tank at risk of failure. An important feature is that the user may set arbitrary limits for the mass flux criteria, because these values are not fixed and different water companies define these limits differently. The parameters of the model are varied through the use of slider bars (Figure 8.1), the state point automatically updates on

the main mass flux graph and the various criteria are highlighted in green, orange or red. Green is shown when the actual/permissible value is less than the specified limit. Orange is set if the chosen limit is exceeded and the output will switch to red if the absolute 100% 1DFT limit is exceeded. By checking the state point for a model system in this way it can be decided whether to proceed to a full CFD analysis of the tank. When the absolute %1DFT limit has been exceeded then it is very unlikely that a CFD solution of the same system will yield a useful result. However, between the bounds of the defined limit and the absolute limit (the orange zone) a successful CFD solution may still be achieved depending on the quality of the internal design. In this way, a table of %1DFT values may be made for all of the mass flux criteria and compared with the clarifier performance parameters (ESS or X_E and the sludge bed depth h_{850}) from a CFD solution (ClariSim, 2007).

8.2 The CFD Model

The fundamental equations solved by a CFD code like CFX for a turbulent, single phase Newtonian flow are very well known (Tennekes, 1972). The limitations on accuracy for the solutions produced by a CFD code are presented by the fundamental discretisation in terms of the grid applied and the numerical differencing scheme used within that grid (Patanker, 1980). For time dependent flows the accuracy of solution is also a function of the time discretisation, which requires that a small enough time step be chosen to resolve the large scale flow frequencies (the small scale turbulent frequencies being averaged by the turbulence model). These issues were considered in Chapter 4 where a grid dependency study was performed to demonstrate that axi-symmetric grids of around 10,000 cells in a single radial plane were generally sufficient for a numerical CFD solution using a 2^{nd} order accurate

differencing scheme and time steps of $\Delta t > 10s$, were achievable when using a transient model to approach a steady state solution (for true transients time steps of $0.5s$ were required).

Beyond these basic rules, the accuracy of the solution is determined by the validity of the physical models. These are the constitutive relationships for density, settling velocity and rheology all discussed in chapter 3. All of these physical models make significant assumptions about the nature of activated sludge in order to model the solid phase as a single species equation which influences the mixture density and rheology according to its local concentration and settles within the fluid mixture at a rate determined by its local concentration. In this thesis the modelling studies in chapters 4, 5 and 6 were all performed as validation of the constitutive relationships. These studies have demonstrated that only the Bokil and Bewtra (1972) and the modified Herschel Bulkley model of de Clercq (2003) worked consistently well for the classes of flow considered.

8.2.1 Density function

The density function (equation, 2.36) is the fundamental extension to the model that captures the physical effects of density currents generated by the solid species mixing in the background fluid. The model contains only one empirical coefficient for the specific gravity of dried activated sludge measured by Larsen (1977) to be 1.445. Because of the variability of activated sludge, this is not a definitive number and for any particular site and on any day this could vary between 1.3 and 1.6. (Tchobanoglous, 1991). This sensitivity is generally not considered in the modelling studies. It is also important to note that where a density model is used, then the overall mass of the clarifier system can change throughout the course of the

numerical calculation (the system may be thought of as compressible). Density gradients also influence the production and dissipation of turbulence and these are included in the model through buoyancy production terms for the turbulent quantities k and ω.

8.2.2 The Standard Settlement Model

The fundamental hindered settling model for activated sludge is given by the Vesilind (1968) equation (3.3). The empirical coefficients for this model can be readily measured for any site using the WRc SSVI test equipment. An experimental procedure for determining these coefficients was described in chapter 3 and the connection with the index $SSVI_{3.5}$ through the Pitman (1980), White (1975), Wahlberg and Keinath (1988) correlations was discussed.

The Vesilind model is limited to the hindered settling range, as shown in Figure 3.5, and in order to provide a complete model for the settlement Types 1 to 4, described in chapter 1, the double exponential function of Takács (1991) was used. This model is particularly appealing as it reconciles all of the low concentration settling behaviour, discrete and flocculent, into a function continuous with the Vesilind hindered settling model.

Two of the Takács parameters, V_o, the free settling velocity, and r_h, the hindered settling coefficient, follow directly from the Vesilind model and are deduced in the same way. The concentration of non-settleables X_{ns}, can be measured directly by drying out and weighing a sample of clarified supernatant on a filter paper, or, for design studies it can be set to a value close to the target effluent solids (ESS) limit. The remaining Takács parameter r_p, the colloid or floc settling coefficient is less

easily determined. In the original work of Takács (1991), r_p is set around 5.0 m^3/kg and the terminating or peak settling velocity for a free floc $V_{s,\max}$ is in the range of 2.0 to 4.6 *mm/s* (Li, 1987). It is stated in the Takács (1991) paper that "parameters of the settling velocity were adjusted to reflect more closely the actual behaviour of the secondary clarifier". In the design studies performed in this work $V_{s,\max}$ is always set to 2.0 *mm/s* following Lakehal (1999) in order to "suppress unrealistically high settling velocities" (Takács, 1991), and r_p is set from 3.0 up to 15.0 m^3/kg depending on the sludge $SSVI_{3.5}$ such that the peak settling velocity occurs at the flocculent (type 2) to hindered (type 3) transition concentration, X_{23}, following Matko (1998). Sensitivity to the value of r_p was tested for a number of clarifier design studies and it was observed that the ESS value could be made to vary by a few *mg/l* by changing this value between the limits of 3.0 and 15.0 but the overall effect on the rest of the model solution was minimal. The uncertainty associated with the Takács parameters for the low concentration regions of the settlement curve suggests that alternative models for free and flocculent settling might be needed based on a free settling model with a known particle size distribution for activated sludge.

8.2.3 Settling in the Low Concentration Zone (Type 1)

A new idea for improving on the Takács model for the low concentration regions is to return to the use of multiple drift fluxes (MDF) to model a range of solid size groups, each settling independently at a free settling velocity. It was demonstrated that this approach could be used for free particles of sand settling in water as part of the Krebs (1998) laboratory clarifier model study in chapter 4. Figure 8.2 shows concentration gradient plots for three selected size groups from the total range of ten.

a) ASM4, V_o = 1.0 mm/s

b) ASM7, V_o = 3.45 mm/s

c) ASM10, V_o = 7.38 mm/s

Figure 8.2: Comparison of settling behaviour for independent size groups for the multiple drift flux model of the Krebs (1998) laboratory clarifier.
The heavier solids easily settle out but for solids with settling velocity of less than 1.0 *mm/s*, a proportion is carried to the effluent weir.

In this model, each size group has a contribution to the total solids concentration but for the low concentration regions, it is appropriate to allow each size class to settle independently. In the case of the laboratory clarifier study of chapter 4, the particles in size group 4 and below, all contribute to the effluent solids while the heavier particles from groups 7 to 10, all settle out in the tank. In order to use such a method for activated sludge flocs, a settling velocity for each size class of a discretised PSD would be required. A new method for providing such a settling velocity distribution (SVD) is now presented.

8.2.4 A Settling Velocity Distribution for SLS

In a parallel study to this work Nakielny (2004) measured the settling time for synthetic latex sludge (SLS) as a sample of N=1382 discrete flocs falling through a 1.8m column of water. From this, a settling time distribution plot was produced for

direct comparison with a particle size distribution produced for the same SLS (Burt and Lim, 2003).

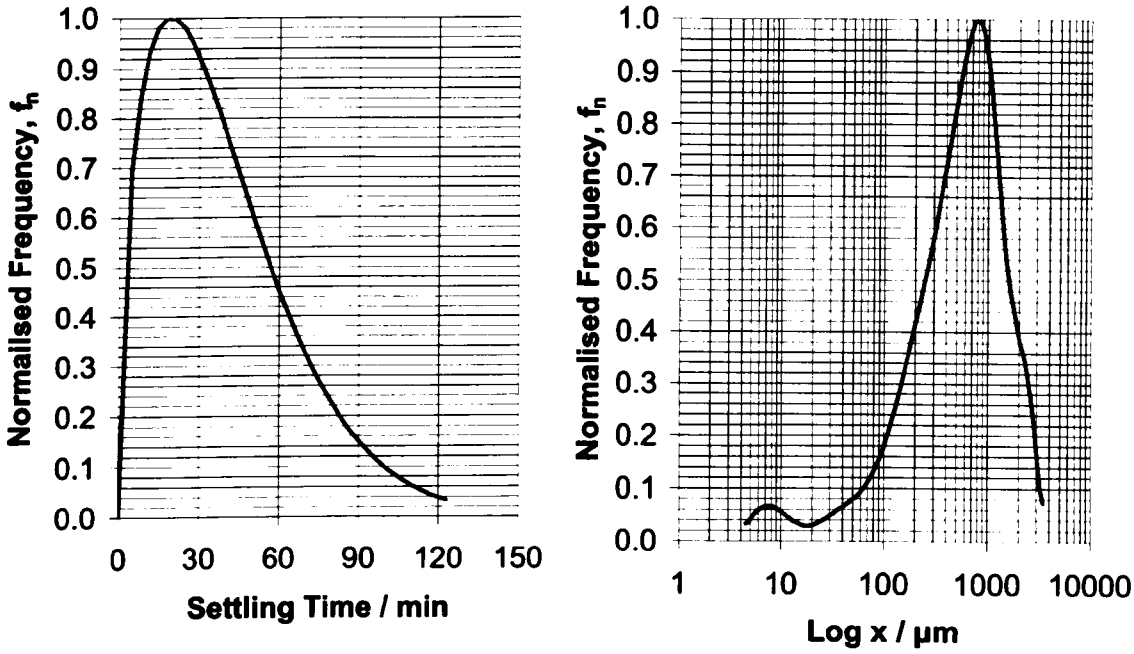

Figure 8.3: Settling time distribution (Nakielny, 2004) and particle size distribution (Burt and Lim, 2003) produced for synthetic latex sludge (SLS).

Using the data contained in Figure 8.3, Nakielney (2004) mapped settling velocity to size distribution and, using the assumption of a spherical floc in an infinite medium, was able to produce a drag law for SLS. Where C_D was found to be constant at 170.0 for particle Reynolds numbers < 0.5, and

$$C_D = 63.881 \times Re_p^{-1.0736} \qquad (8.2)$$

for $Re_p > 0.5$.

The definition of a drag coefficient for an idealised spherical floc is an un-necessary step for use in the CFD model as it is possible to form a settling velocity distribution for SLS, similar to that defined in Table 4.1 for glass beads, by directly interpolating from Figure 8.3. This new idea for producing an MDF model of low concentration activated sludge in the same way as was done for SLS by Nakielney (2004) is

suggested as further work. This is a particularly important concept as it may be used to remove the uncertainty associated with the definition of the value of r_p in the Takács (1991) settling model.

8.2.5 Thickening Functions for the Compression Zone (Type 4)

In the validation studies of Chapter 6, the predictions for the Crofton study, where there is limited thickening of the bed, are well represented by the CFD model. For the Witney site, where the measurements show significant thickening in the lower reaches of the tank (particularly table D3), the model does not produce a good representation of the concentration gradients through the settled beds. The CFD predictions only approached 20,000 mg/l near the floor, as observed in experimental samples, when the Herschel Bulkey rheology model of de Clerq (2003) was applied. The Witney results highlight a weakness in the settling model at higher concentrations in the transition from hindered to compressive settlement. This can be well observed in the settlement data obtained for the Witney site where only the gradients of the settlement curves for the hindered zone were used to construct the Vesilind coefficients for use in the settling model.

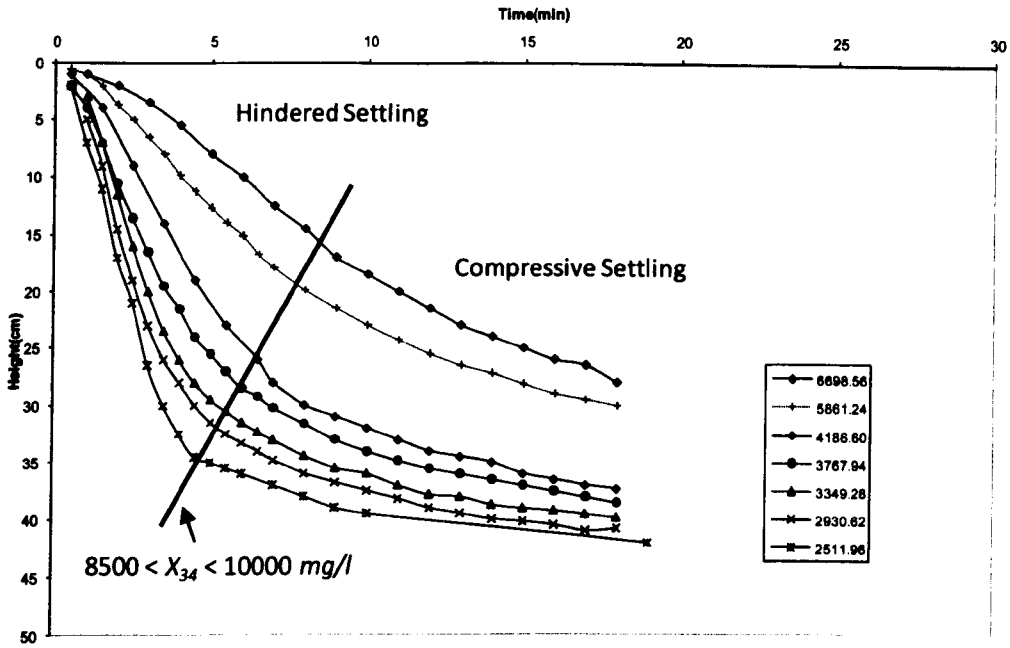

Figure 8.4: Data for the Witney SSVI settling tests marked with the approximate transition X_{34} between hindered and compressive settling.
Only the gradients in the hindered zone were used to construct the Vesilind coefficients.

It can be seen in Figure 8.4, that there is a transition from hindered settling at a constant gradient into compressive settling and for the Witney data, this is occurring when the concentration of the settled bed is between $8{,}500 < X_{34} < 10{,}000$ *mg/l*. The Vaccari (1989) model uses this concept of a transition point to indicate the onset of compressive settlement where the settling rate rapidly reduces following a separate exponential curve discontinuous to the Vesilind curve (figure 3.1). The implementation of a thickening function based on Vaccari (1989), or a similar model, may improve the Witney validation results and this is suggested as further work. The concept of a thickening function for the compressive settling (Type 4) is currently an active area of research (de Clercq, 2006) and a model for this would be an essential addition for studies of clarifier systems where significant thickening is thought or known to occur.

8.2.6 Rheology Models

In modelling the lock exchange experiment of chapter 5, invoking the different rheological models, it was observed that the side wall, having initial contact with high sludge concentration, retained a significant sludge residue within the near wall fluid boundary layer (see Appendix C). Also, when modelling the Rye Meads clarifier with the Bingham Plastic rheology model and no slip wall at the floor (but with momentum sources for the scraper), the model initially predicted very high apparent viscosity near the floor. These high values could only be restrained by bounding the shear rate value to a minimum of 1.0E-3 s^{-1} and the apparent viscosity to a maximum of 20 *Pa.s*.

These modelling artefacts are thought to have two origins. For the plastic viscosity models (Bokil, 1972, Dahl, 1993 and Armbruster, 2003), the viscosity predicted in the static sludge is so high that the sludge becomes bonded to the stationary wall so that convection is restricted. Whereas, real activated sludge at high concentration appears to immediately slump away from the wall suggesting that once disturbed, the connection to the wall is not strong (see the arguments for scraper modelling below). The difficulties with the Bingham plastic model were assumed to be manifestations of the near wall plastic viscosity behaviour but with the additional symptom of the model predicting near infinite apparent viscosity when starting from a stationary initial condition as the magnitude of strain rate becomes very small near the wall (de Clercq, 2003).

These problems were not observed for the Herschel Bulkley model (de Clercq, 2003) modified with the smoothing function of Papanstasiou (1987). This is because a

strain rate term is introduced as a multiplier for the plastic viscosity, allowing this to become small at low strain, and the smoothing function keeps the contribution to apparent viscosity from the yield stress term in a realistic range, even at very low strain. Therefore, the Herschel Bulkley model of de Clercq (2003) gives the most physically representative results in the collapsing column lock exchange test described in Chapter 5.

In the various clarifier studies, where comparisons between rheological models were made, it was noticeable that the standard model (Bokil and Bewtra, 1972) tended to predict the highest sludge bed level and this also agreed well with the experimental measurement of sludge bed depth (where the sludge bed depth, following Matko (1998), is taken to be the position of the 850 mg/l contour below TWL). These observations are consistent with the observations of Lakehal (1999) and Armbruster (2001). The standard model also gave a reasonable representation of the dynamic behaviour in the lock exchange (Appendix C).

In conclusion, there are still some considerable levels of uncertainty associated with the use of these various rheological functions. They are all improvements on modelling without rheology as the sludge dynamics are better captured, as illustrated in the lock exchange model of chapter 5 (figures for no rheology are compared with the experimental data in Appendix C), however interaction with the wall, behaviour at low shear, and the connection between turbulence and rheology are all poorly understood. Obtaining site data for rheology is particularly difficult, because of the complexity associated with developing rheometers for settling slurries, and the apparent thixotropic behaviour of activated sludge (Dick and Ewing, 1967). Hence,

in this work, all of the rheology data used has come from literature and no attempt was made to obtain site specific properties.

The Herschel Bulkley (generalised Bingham Plastic) model of de Clercq (2003) does seem to provide the most complete representation for apparent viscosity in activated sludge. However, until yield stress and plastic viscosity measurements are done for a wide range of sites (in order to obtain a rheology correlation for all sites) it cannot be assumed that the limited rheology data available for this model is applicable to all sites. Therefore, for the purposes of design studies at least, it seems more appropriate to use the standard model of Bokil and Bewtra (1972) which simplifies the rheological relationship to a function of concentration only. It has been fitted for a wide range of site samples (sixty-five) and, for the cases tested in this work, gave good approximation to the sludge bed depth for 2D axi-symmetric clarifier models.

8.2.7 Turbulence

The modelling of turbulence has been given only limited mention in this work. This is because the standard two equation turbulence models have been investigated extensively by others for flow in clarifiers (Adams and Rodi, 1990). The use of the standard $k-\varepsilon$ model (Launder, 1972) was not possible with the versions of CFX used, as modifications to rheology to include an apparent and a turbulent viscosity were only allowed in the code when using a low Reynolds Number $k-\omega$ turbulence model (Wilcox, 1990). This use of a low Reynolds number model makes sense as the flow in a clarifier is dominated by the apparent viscosity of the sludge in the settling zone and turbulent viscosity is only high in the stilling region. The influence of buoyancy on turbulence was also investigated, following the arguments of Lakehal

(1999) but it was concluded that the value of C_3 made no material difference to the results. This contradicted the work of Lakehal and was investigated further. It was noted that while the standard CFX implementation of the turbulent eddy frequency ω (equation 2.31) included the following term on the RHS,

$$C_1 \frac{\omega}{k}(P_b + C_3 \max(G_b, 0)) \tag{8.3}$$

it was written in the Lakehal (1999) paper for epsilon as,

$$C_1 \frac{\varepsilon}{k}(P_b + G_b(1 - C_3)) \tag{8.4}$$

making it possible for the whole term to go negative when the buoyancy production term, G, becomes negative. This difference in implementation is probably the origin of the variable results quoted by Lakehal (1999).

In some of the most recent work published on the modelling of settling tanks the RANS turbulence models have been replaced by the use of Large Eddy Simulation (LES) predictions where the grid is made small enough to resolve the large scale turbulent eddies (Al-Sammarraee, 2009) and a detailed turbulence closure is not required. The comparison of LES solutions and low Reynolds Number $k-\omega$ solutions for flows in circular clarifiers is suggested as further work.

8.2.8 The Floor Boundary and the Influence of the Scraper

In the comparative study of chapter 4 for the Rye Meads clarifier, little difference was observed between the different wall boundary conditions used to represent the scraper at the floor of the tank and it was concluded that the model was relatively insensitive to this floor boundary condition. Experimental observations with activated sludge at Swindon showed that a settled sludge bed is highly cohesive even

to a smooth surface and a significant force is required to overcome the plastic yield of the settled bed. Once in motion, however, compacted sludge moved easily but not in the manner of a fluid, rather the sludge was observed to slide as a solid body on a thin liquid film with little or no shearing near the wall (this is shown in Figure 5.6). These observations supported the idea that flow to RAS is gravity driven and the only role of the scraper is to overcome the yield stress of the sludge and lift it away from the floor (Deininger, 1998). This conclusion was also reached by Armbruster (2001) by comparing a range of numerical predictions. Hence, for a 2D axisymmetric model, the tank floor may be best modelled with the free slip condition to simulate the behaviour of the scraper action without imparting any momentum from the scraper motion. For 3D modelling it is possible to represent the direct action of a scraper with a moving mesh (Winkler, 1999) and ideally comparisons would be made between this and other floor boundary options in any future work.

8.3 Flow Behaviour and its Influence on Design

The early observation of Anderson (1945) that the flow in a clarifier is dominated by the influent density current is demonstrated in all of the CFD modelling studies that have been performed in this work. Where there is only a stilling well at the influent, the density current impinges into the sludge bed and then spreads out into a radial shear layer. This process is the initiating mechanism for solids carryover at the effluent weir .

For shallow circular clarifiers, which use a scraper mechanism to assist in the return of sludge to the RAS hopper, this work identifies some other flow features which influence the performance of the tank. The re-entrainment of the return flows in the upper reaches of the tank can allow clarified supernatant back into the stilling well.

This enhances the density current within the stilling well and hence creates further re-suspension of the sludge blanket. High velocity gradients within the shear layer promote sludge re-suspension and the point at which the shear layer separates is where the first signs of solids lifting occur, as can be seen in Figure 7.5. Where the side wall is too shallow, or in the unusual case where the stilling well is the same depth as the side wall (this can occur when the tank floor slope is at greater than 10°) then shear layer separation can occur earlier than desired through interaction with the floor of the tank. This can be seen in the Rye Meads results, Figure 4.8. In these circumstances the bed depth may still sit well within the tank but effluent quality can still be poor.

The final flow feature that warrants discussion is the sludge bed conveyor; this appears to occur in all of the CFD simulations and is best illustrated in the solids phase streamline plot of Figure 4.16. Where the density influent impinges into the bed and then flows out radially, it meets a return flow to the RAS hopper which runs at highest velocity near to the tank floor. The shearing action of these opposed flow streams induces a strong recirculation within the sludge bed which then coalesces around a slow moving, or dead spot, of higher concentration activated sludge. Where the sludge ages too much, there is the potential for a biochemical process known as denitrification (Siegrist, 1995) to accelerate to the point where excessive nitrogen production can lift off portions of the sludge blanket.

8.4 Performance of the Design Modifications

Mass flux theory only gives guidance on the likely surface area required to effect clarification and this can be a significant underestimate. The modelling techniques applied in this work have largely been used to find the limits of performance for shallow clarifiers with floor slopes in the range 0 to 20° with various forms of RAS

removal system. From these studies, a number of observations have emerged that have provided guidance on internal baffling that can improve effluent quality and allow the tank performance to approach the mass flux limit.

8.4.1 The Stilling Well

One of the first things to consider in internal clarifier design is the diameter and depth of the stilling well. Many modern designs (up to the AMP4 period) embraced the concept of a 'flocculating stilling well' (Parker, 1996) which relied on the idea that the stilling well had to be of large volume, sized up to 30% of the tank diameter, in order to promote orthokinetic flocculation and therefore aid settlement. In this design it is thought that the value of G can be held in the correct range, within the well, by the inclusion of an energy dissipating influent (EDI), or even through the addition of local mixers (Ekama et al, 1997).

In this work, it has been noted that a large stilling well is likely to generate significant re-entrainment from the settling region of the tank, back into the stilling pond, as shown for the Rye Meads study in Chapter 4, and this re-entrainment behaviour can persist even when an EDI is included. These observations are supported by descriptions in Ekama et al. (1997) where it is stated that for large flocculating stilling wells, "Further, mixing was not limited to the centre well itself but occurred in the projected volume below the centre well. This seemed to be caused by density currents owing to the waterfall effect of the downward currents near the inlets, causing currents of clear diluting supernatant to flow under the flocculation well skirt and through scum ports at the top of the skirt". In all cases,

where this re-entrainment behaviour is present, it has been found that the hydraulic limit of the tank is compromised. This is clearly illustrated in the Budds Farm study of chapter 7 where the proposed design for a new tank, which included a large flocculating centre well, was unable to exceed 70% of the 1DFT limit.

The idea that the stilling well plays a key role in the flocculation process is also in question. The work of Biggs (2000) highlighted that a G of around 19.4 s^{-1} would enhance the flocculation of activated sludge whereas $G > 113$ s^{-1} would break up flocs. Indeed, Parker et al (1972) originally suggested that flocculating centre wells should include mixers promoting values of G in the range of 30 to 70 s^{-1}. However, the calculation of G scalar history for Rye Meads, presented in chapter 4, states that the G value is only in the range where orthokinetic flocculation might be promoted (> 20 s^{-1}) within the first few seconds of entry into the tank. Other recent CFD modelling work by Shaw et al (2005) confirms that the volume integrated values of G within a variety of different flocculating centre wells are generally in the range of 1.0 s^{-1} which is consistent with Ekama et al. (1997) where it is stated that "Without mechanical mixing, the calculated G values in the flocculation well due to headloss at the inlets is very low ($G < 5$ s^{-1})". In the work of de-Clerq (2003) extensive on line measurements of the PSD within a stilling well were made and it was noted that there was very little variation in this PSD for all of the locations tested. In other words, there was no evidence of breakup or reformation of flocs within the stilling well. This is further illustrated for the examples of Rye Meads in chapter 4 and Crofton in Chapter 5 where the computational equivalent of the Camp number $G.T$ was calculated by integrating the G scalar histories for flocs passing through the stilling zones. This result showed that not only was G too low in the stilling well but, T was

also far too low and a typical Camp number for a circular clarifier stilling well (size independent) is $G.T \approx 200$. This is two orders of magnitude lower than is considered to be required for a good flocculator (Twort, 2000).

It is concluded form this work, and the other references, that a large stilling well does not promote flocculation, G within the stilling well is always too low, with or without the inclusion of an EDI, and there is experimental evidence that the PSD of activated sludge is constant within any stilling well. The oversize flocculating stilling well also provides an opportunity for re-entrainment to occur which leads to an intimate mixing of the stilling zone with the settling zone and when this mixing occurs the density current is enhanced which always promotes poor hydraulic performance. Therefore, a large flocculating stilling well is most definitely a bad design.

Similarly, it is also noted that if the stilling pond is too small then the down flux of momentum from the influent can be sufficiently large to disrupt the settled bed which can also lead to early failure (Burt, 2005c) and therefore, too small a stilling well is also a bad design.

8.4.2 Modifying the Influent

In all studies, a stilling well diameter of 20%D was found to be most effective with depth set to half of water depth at the radius of the stilling well (Burt et al, 2007), Figure 1.4. Any shallow tank which has an influent based on a 'stilling well only' design will inevitably suffer from strong density current effects at certain state points, which was the initial reason for exploring the influent modifications at Witney, Crofton and Budds Farm discussed in chapters 6 and 7 of this work.

It is apparent from these CFD studies that the central EDI improves performance not because it promotes flocculation but because it spreads the load out uniformly near the top of the stilling well thus reducing the density variation in the stilling pond. If it is designed well, it can limit the influence of flow re-entrainment into the stilling pond and can give good performance across a range of state points. Studies on the influence of vanes, including the Crofton EDI (Burt, 2005b) suggest that these are largely inconsequential except when the combination of slot size and vane angle gives rise to excessive swirl and promote re-suspension of the sludge below the stilling pond. The important requirement is to keep the momentum exiting the EDI ports at a level high enough to promote homogenisation but not so high as to produce re-suspension and experience suggests that aiming for a port velocity of about 0.1 *m/s* will achieve this.

The McKinney baffle cuts the density current and if designed correctly, with $0.5 > Fr' > 0.7$ completely separates the stilling and settling zones (N.B. this cannot be maintained for the whole operating range of the tank and so it is appropriate to calculate Fr' at the full flow to treatment and size the McKinney gap for this state point). However, the McKinney design shows sensitivity to bed depth as it operates most effectively when the baffle sits at the same level as the sludge blanket; in this way the flow exiting the influent forms a level radial jet across the top of the settling bed. For low flow or low SSVI situations a second density current can form at the end of the McKinney baffle which also has a degrading effect on tank performance. Ideally, a McKinney baffle would track the bed height in operation or the bed height would be maintained (perhaps through RAS control) at the level of the McKinney. When including a McKinney baffle it is sometimes necessary to increase the depth of the stilling pond to suit the required slot height.

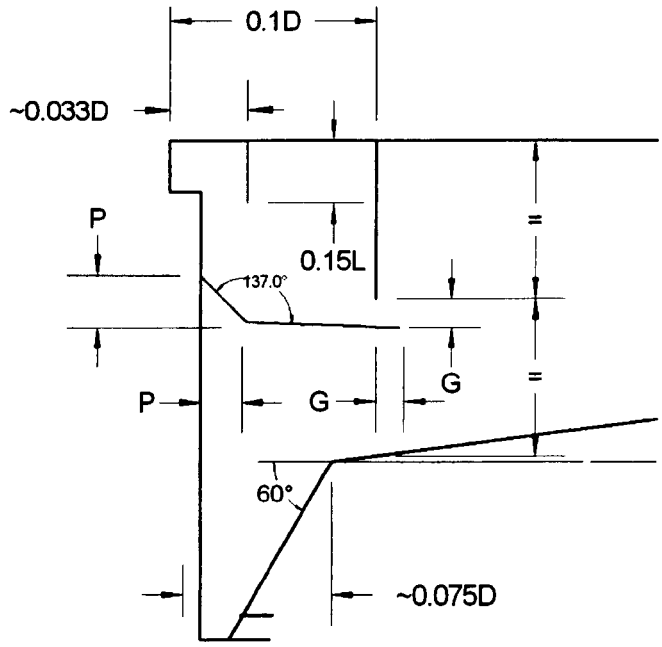

Figure 8.5: A parameterised baffled influent based on an adapted McKinney influent baffle for use in UK shallow circular clarifiers (Burt et al, 2007).

Following many studies of shallow circular clarifiers, a new adapted McKinney influent design is recommended for use in the UK. This parametric design is shown in Figure 8.5. Note that the dimensions P, G and L are tank specific.

8.4.3 Modifying the Effluent Weir

In the Crofton and Budds Farm design studies, modifications to the influent were augmented by a variety of side wall baffling options. In shallow tanks with low floor angles, no clear benefit from using a Stamford or McKinney wall baffle was observed and this is consistent with observed flows in Figure 7.5. The CFD predictions indicate that shear layer separation always occurs before the flow reaches the side wall in such a way that the effluent flow effectively by passes the location of the wall baffle. It is noted however that in flat bottomed deep tanks, with low beds, the shear layer tends to persist all the way to the side wall and the wall baffle can

have a much more significant influence on the effluent quality in these circumstances.

8.5 Summary of Further Work

The discussion has focused on the two key elements of modelling and design that have been explored in depth in this thesis. The limitations of mass flux theory and the extended drift flux model have been explored and some recommendations for further work on the EDF model are proposed as follows,

1. Improved models are required for discrete and flocculent (differential sedimentation) settling and further work representing the low concentrations of activated sludge with multiple drift fluxes may be considered following the characterization work of Nakielney (2004). This could overcome the lack of data available for the Takács parameter, r_p.
2. The transition from hindered settling into compressive settling is not well represented by the Takács (1991) settling model. Further extensions of the model to include a thickening function based on Vaccari (1989), or similar (de Clercq, 2006), are required.
3. Comparisons between 2D models and fully 3D representation of the scraper are required to confirm, or otherwise, that the only role of the scraper is to overcome the yield stress of the sludge and lift it away from the floor (Deininger, 1998), Armbruster (2001).
4. High resolution models of clarifiers may be developed using LES based turbulence models for comparison with the two equation turbulence model solutions produced in this work.

CHAPTER 9: Conclusions

Summary

This chapter concludes the work by returning to the research questions that were presented in the introduction. These questions have been developed throughout the thesis and, where possible, definitive conclusions are drawn. There are still some considerable uncertainties with the physical models and constitutive relationships that are used to in the extended drift flux (EDF) model and these were highlighted with the potential for further work in chapter 8. The first research question about optimising clarifier performance was extended during the work, in particular with regard to influent modifications and two new influent designs were developed for implementation at industrial sites.

9.1 Performance and Design

1. What are the correct CFD modelling approaches for calculating the performance of a clarifier and can the model be used to optimise existing and new designs?

The modelling options available were explored in chapter 2 and it was concluded that any representation of clarifier flow with CFD should be based on extension of the drift flux multiphase frame. This extended drift flux (EDF) model included constitutive relationships for density, settling velocity, apparent viscosity and a turbulence closure based on the low Reynolds Number $k-\omega$ turbulence model of Menter (1994). In chapter 4, an alternative multiple drift flux model (MDF) for discrete particle settling of a larger number of particle size classes was also developed. Neither of these models gave a complete representation of all settling regimes within a clarifier and the limitations of the Takács (1991) settling model in the low and high concentration settling zones were discussed in Chapter 8. The

rheological models presented in Chapters 2 and 3 are based on data from a limited number of sites and, given the large variations that might be expected across sites, it is suggested in chapter 8, that correlations for yield stress and plastic viscosity may need to be developed. However, even with these model limitations, it was demonstrated that the performance of a clarifier could be well assessed using the EDF model and that this model could capture all of the major flow features within the tank observed by Anderson (1945) and others (Ekama et al, 1997).

The initial study of the Rye Meads clarifier in chapter 4, was extended to cover sensitivity to modelling parameters such as spatial and temporal resolution and it was concluded that two dimensional axi-symmetric grid sizes of around 10,000 cells using 2^{nd} order differencing were sufficient to show a level of grid independence and, where state point solutions were required, a time step of around 10 seconds was appropriate.

Following the initial verification of the EDF model against the Rye Meads data (Richardson, 1998), further validation was performed at two operational waste water treatment works Witney (Burt, 2005a) and Crofton (Burt, 2005b) as discussed in chapter 6, before finally applying the model to design, optimisation and performance assessments. The use of the model for design comparison yielded substantial information about best internal configurations and two new influent baffling arrangements were developed alongside the site trials discussed in Chapter 6. The McKinney (Ekama et al, 1997) deflection plate and a counter current energy dissipating influent (EDI) were trialled at Witney and Crofton and these designs were developed further for application in industry. A final implementation study for the Budds Farm site (Burt et al, 2006) presented in Chapter 7 demonstrates how the

combination of mass flux and EDF modelling can be used to optimise new and existing designs.

A summary of the design lessons learnt from using the EDF model for many industrial studies may be reduced to the following concluding remarks.

- Flows in circular secondary clarifiers are characterised by a strong density current, arising from the influent, which drives a radial shear layer above the settling sludge bed. Several flow features exist that must be 'designed out' to optimise the tank performance.

- The flow is far from one dimensional but it can be considered as close to two dimensional and a circular clarifier can therefore be modelled in a 2D axi-symmetric co-ordinate system (x, r, θ in CFX-4).

- The stilling well dimensions are important: if the diameter is too large or the depth too shallow, then the density current momentum is enhanced through re-entrainment. Too small a diameter causes additional down flux into the settling bed, increasing the likelihood of blanket spill. Two influent options may be used to break the fall of the density current: an EDI or a McKinney baffle.

- A central EDI helps to diffuse the density current by spreading the load uniformly near the top of the stilling well and reduces the density gradients within the stilling well. The EDI does not contribute in any way to the process of orthokinetic flocculation within the stilling well.

- The McKinney baffle cuts the density current and, if designed with $0.5 < Fr' < 0.7$, it distinctly separates the stilling zone from the settling zone introducing the flow as a direct radial jet into the settling zone of the clarifier.

- The McKinney design tends to favour a limited operating range as it provides maximum benefit only when the baffle sits slightly above the settling sludge bed (the 850 *mg/l* contour). In its best operating range it will tend to outperform an EDI.

- Sidewall baffling has only a limited influence on shallow circular clarifiers and has not been observed, in any of the model results, to make any material difference to the magnitude of the effluent suspended solids (ESS) reaching the clarifier side weir. However, in deeper tanks, where the shear layer tends to persist all the way to the side wall, then wall baffling can positively influence the effluent quality.

9.2 Validation of the Model

2. How do CFD results compare with experimental data?

Comparisons between experimental results and CFD predictions were provided for the Krebs (1998) laboratory clarifier and for the lock exchange rig developed as part of this work. For the Krebs (1998) laboratory clarifier it was demonstrated that a ten size class MDF model representing the discrete settling of glass particles could give a good representation of the solids distribution throughout the tank. Most usefully, the MDF model can calculate the carryover of solid suspensions to the effluent weir.

This facility is discussed further in Chapter 8 where a new idea is suggested in which an MDF formulation might be used to model the low concentration zones in an activated sludge clarifier where there is uncertainty in the Takács (1991) model. The lock exchange model was used to compare the dynamic behaviour of a collapsing sludge column with predictions based on all of the available rheology models discussed in chapters 2 and 3. From this work it was apparent that the Herschel Bulkley (generalised Bingham Plastic) model of de Clercq (2003) gave the best results.

Validation at an industrial scale was performed using the Rye Meads data (Richardson, 1998) and for new data obtained at the Witney and Crofton sites. For the Rye Meads data the comparisons with the EDF model show that good predictions of bed height and effluent solids can be achieved with the model and that tracer tests for short circuit time were also well predicted by the model. However, there was no data available for comparing the concentration gradients through the settled bed. The Rye Meads rig was therefore re-designed to include a solids point sample unit and higher resolution data for velocity and concentration was obtained at Witney and Crofton.

The comparisons between experimental measurement and the EDF predictions are discussed in Chapter 6 and it is apparent that where the bed is high and diffuse within the tank, as with the Crofton trial, then the EDF predictions give good representation of the velocity field and solids distribution, consistently predicting the radial shear layer just above the settling bed. However, where the bed is very low in the tank, and thickening to high concentrations exceeding 20,000 *mg/l*, as was observed for the Witney trials, then the concentration profile predicted by the EDF model do not

match the data as well. These differences, attributed to the lack of a compression function in the settling model, are discussed in Chapter 8.

9.3 Comparisons between CFD and Mass Flux Theory

3. *Is it possible to calculate the capacity of different clarifier designs with CFD and compare these calculations with flux procedure predictions?*

The concept of total failure for a clarifier is defined as the point at which the sludge blanket within the clarifier can no longer be retained and high concentration sludge flows over the effluent weir. This is observed in practice, and in CFD modelling, to occur below the ultimate mass flux limit of 100% 1DFT. In chapter 3, the mass flux limit was discussed as both a solids load limit following mass flux criterion I (Ekama and Marais, 2004) and as a hydraulic load limit following mass flux criterion II. Exceeding either of these limits can be considered as failure of the tank. The direct connection between the mass flux criteria and CFD modelling was made for the Budds farm study in Chapter 7 where sixteen different state points were compared for four different designs of tank all of the same diameter. By plotting the effluent solids value X_E, and the bed depth h_{850}, for each CFD solution against the hydraulic 1DFT limit it was possible to see that some designs failed much earlier than others. In the extreme cases the poorly designed Budds farm tank failed at 73% of 1DFT while the best design of tank was seen to retain the solids blanket at up to 98% of 1DFT[5].

[5] The index chosen for hydraulic loading, Criterion II, was found to be the reciprocal of the Hazen number (and %1DFT = 100/*Ha.*)

The linkage between the apparent mass flux limits and the CFD solution was found to be a very useful way of normalising all CFD solutions for all tanks and makes direct comparisons between design solutions possible.

9.4 The Production and Use of Synthetic Latex Sludge (SLS)

4. Is it possible to manufacture a simulant for activated sludge and is this simulant useful for experimental validation studies of clarifier systems?

The production and characterisation of SLS was presented in chapter 5. Initial characterisation of the SVI was disappointing as it was a lot lower than would be expected for activated sludge and suggested that SLS would not be a good surrogate. However, further experiments with SLS in a lock exchange rig and direct comparisons with activated sludge, Figure 5.7, demonstrated that there was an unexpected dynamic similarity between the two materials. The reason became apparent when the analysis method used by Larsen (1977) to determine the specific gravity of dried sludge, was applied to the results of the SLS lock exchange test. This revealed that the specific gravity of dried SLS was 1.15, and therefore, equal volumes of SLS with SVI of 35 *ml/g* were equivalent in mass to activated sludge with $SSVI_{3.5}$ of 60 to 65 *ml/g*.

The PSD for SLS was measured as part of a detailed study into shear sensitivity of SLS, (Burt and Lim, 2003) and this showed that the individual floc dimensions and densities for SLS were similar to activated sludge (Table 5.4). Therefore, it would not be unreasonable to use the data generated by Nakielny (2004) as discussed in

chapter 8, as the basis of a multiple drift flux (MDF) model for real activated sludge when representing discrete, Type 1, settlement in a CFD model.

In terms of extending the use of SLS for larger scale trials of dynamic systems, it was noticed that the material did exhibit strong shear sensitivity and tended to break up when over worked and would not reform. However, with careful application and attention to the material differences highlighted in Chapter 5, SLS might be successfully used as a surrogate for activated sludge in the scale modelling of clarifier units for example.

9.5 Flocculation

5. *Is flocculation an important physical process in the performance of a clarifier and, if so, can it be modelled?*

One of the more significant conclusions from this work, also confirmed by Shaw (2005), is that orthokinetic flocculation does not appear to occur in the stilling well of a clarifier. It was shown in chapter 4 that the value of G only exceeded the value required to promote orthokinetic flocculation (>19.4 s^{-1}) in the first few seconds following entry into the stilling well. Beyond this time, the G value quickly falls away to below 10 s^{-1}. This observation has a significant implication to the design of clarifier influents and, following the discussion in chapter 8, it is concluded that there is no benefit in designing a clarifier influent that attempts to promote orthokinetic flocculation. A new modelling method for calculating the Camp number $G.T$ in the stilling well showed that, with or without an EDI, the value of $G.T$ is generally two orders of magnitude lower than required to enhance flocculation.

There is still significant flocculation occurring within a clarifier in the form of differential sedimentation, or type 2 settling. In the current implementation of the EDF model this differential sedimentation process is captured only by the Takács (1991) settling model. Given that the CFD model results seem relatively insensitive to the value of the Takács parameter r_p, it is unlikely that any modification to incorporate flocculation through differential sedimentation will affect the overall hydraulics of the tank. However, this still warrants further investigation with particular regard to the possible influence that differential sedimentation may have on the effluent solids value.

9.6 Final Comments

The extended drift flux models developed and validated during this work have been successfully applied to the design of new influents for shallow circular clarifiers used throughout the UK. There are undoubtedly limitations in the EDF models that may be resolved by further work but the methods developed here are still a significant improvement on the one dimensional flux theory that is most commonly used for waste water plant site assessments.

As a postscript to all of those who have gone before and to all those who may seek to perform further study in the area of Clarifier design: it is the densimetric Froude number Fr' which indicates the extent to which a gravity current will dominate the flow, the influent densimetric Froude number Fr'_{in} which defines the correct influent dimension, the Camp number $G.T$ which shows the presence (or lack) of flocculation in the stilling well and the reciprocal of the Hazen number $1/Ha$ which bounds the absolute limit of hydraulic performance.

References

Abdel-Gawad, S.M. and McCorquodale, J.A.(1984), *Strip Integral Method applied to Settling Tanks*, J. Hydr. Eng., ASCE, 110(1).

Acheson, D.J., (1990), *Elementary Fluid Dynamics*, 1st Ed, Oxford University Press.

Adams, E.W. and Rodi, W. (1990) *Modelling flow and mixing in sedimentation tanks*, J. Hydr. Eng., ASCE, 116(7).

Al-Sammarraee, M., Chan, A., Salim, S.M., Mahabaleswar, U.S.(2009), *Large-eddy simulations of particle sedimentation in a longitudinal sedimentation basin of a water treatment plant. Part I: Particle settling performance*, J. Chem Eng, 152, 315–321

Anderson, N.E. (1945), *Design of Settling Tanks for Activated Sludge*, Sewage Works J., 17(1), 50-63.

ANSYS (2007), *In the Works, Using Simulation to Model Wastewater Plants Effectively,* Ansys Advantage, Volume 1, Issue 3.

Ardern, E. and Lockett, W.T. (1914), *Experiments on the Oxidation of Sewage without the aid of Filters*, J. Soc. Chem. Ind. 33(10)

Argaman, Y. and Kaufman, W.J. (1970), *Turbulence and Flocculation*, J. San. Eng. Div., ASCE, Vol 96 (SA2), 223-241.

Armbruster, M., Krebs, P. And Rodi, W. (2001), *Numerical Modelling of Dynamic Sludge Blanket Behaviour in Secondary Clarifiers*, Water. Sci. Tech, Vol 43 (11), 173-180.

Armbruster, M. (2003), *Untersuchung der möglichen Leistugssteigerung von Nachklärbeken mit Hilfe numerischer Rechungen*, PhD thesis, University of Karlesruhe.

ASF (2003), *University of Sheffield Activated Sludge Forum*, personal communication with Bob de-Clercq, July 2003.

ATV-DVWK, (2000), *Dimensioning of Single Stage Activated Sludge Plants,* German Association for Water, Wastewater and Waste, Standard ATV-DVWK-A 131E

Biggs, C. A. (2000) *Activated Sludge Flocculation: Investigating the Effect of Shear Rate and Cation Concentration on Flocculation Dynamics.* PhD Thesis, Dept of Chem Eng, University of Queensland, Australia.

Bokil, S.D. and Bewtra, J.K. (1972) *Influence of Mechanical Blending on Aerobic Digestion of Waste Activated Sludge.* Proc., 6th Int. IAWPRC Conf. on Water Pollution Res., Int. Assoc. on Water Pollution and Control, London, 421-438.

Burt, D.J., Corton, M., Hetherington, D. and Balmforth, D. (2002) *Multiphase Modelling and the Prediction of Retention Efficiency in a Side Weir CSO,* presented at the ASCE 9th International Conference on Urban Drainage, Oregon, USA, 8th to 13th September 2002.

Burt, D.J., and Lim, M. (2003), *Characterisation of an Activated Sludge Simulant,* Particle Systems Analysis, Harrogate, UK, 10th to 12th Sept 2003.

Burt, D.J., Gilbertson, M. and Pearce, P., (2004) *A Lock Exchange study of Activated Sludge and an equivalent Synthetic Simulant,* ParTEC 2004, International Congress for Particle Technology, Nürnberg Messe, March 2004.

Burt, D.J. (2004a) '*Design of an EDI for use with the Modified Snarrows Clarifier, 3D Model comparisons of EDI port areas and Orientations*', MMI Report, MMU032-R-02_Issue2, August 23rd 2004.

Burt, D.J. and Ganeshalingam, J. (2005a), *Validation Study for the Witney Clarifier,* MMI Engineering Report, MMU033-R-01, Issue 1, February 2005

Burt, D.J. and Ganeshalingam, J. (2005b), *Validation Study for the modified Crofton-Walton Clarifier,* MMI Engineering Report, MMU035-R-01, Issue 1, July 2005.

Burt, D.J. and Ganeshalingam, J., (2005c) *Design and Optimisation of Final Clarifier Performance With CFD Modelling,* Presented at the CIWEM / Aqua Enviro

joint conference on Design and Operation of Activated Sludge Plants, Leeds, UK, 19th April 2005

Burt, D.J. and Gilbertson, M., (2005), *Extended Drift Flux Models for Waste Water Sludges*, Particulate Systems Analysis, Stratford-Upon-Avon, UK, 21st to 23rd Sept 2005.

Burt, D.J., Ganeshalingam, J. and Grand, A. (2006), *Design Assessments with CFD Modelling for the Budds Farm STW Final Clarifiers* MMI Engineering Report, MMU074-R-01, Issue 1, August 2006.

Burt, D.J., Ganeshalingam, J., Robinson, C. and Syred, C. (2007), *Design Guidelines for a New Final Settlement Tank*, MMI Engineering Report, MMU043-R-13, Issue 1, January 2007.

Camp, T. (1945), *Sedimentation and the design of Settling Tanks*, Trans ASCE, 2285, 895-936.

Camp, T. and Stein, P.C. (1943), *Velocity Gradients and Internal Work in Fluid Motion*. J. Boston Soc. Civ. Engrs, Vol 30 (4), 219-237.

Camp, T. (1953), *Flocculation and Flocculation Basins*, Trans ASCE, 2722, 1-16.

Celik, I. and Rodi, W. (1988), *Modelling Suspended Sediment Transport in Non-Equilibrium conditions*, J. Hydr. Eng., ASCE, 114(10).

CFX. (1997), *CFX-4.2 Solver Manual*, AEA Technology, 8.19 Harwell, Oxon.

CFX. (2001), *CFX-4.4 Solver Manual*, Vols 1,2 and 3, AEA Technology, Harwell, Oxon.

Cho, S.H., Colin, F., Sardin, M. and Prost, C. (1993), *Settling Velocity model of Activated Sludge*, Water Res, 27(70), 1237-1242

CIWEM. (1997), *Activated Sludge Treatment*. Chartered Institution of Water and Environmental Management, Handbooks of UK Wastewater practice, London.

ClariSim. (2007), http://www.clarisim.net

Clark, M.M. (1985), *Critique of Camp and Stein's RMS velocity gradient*, J. Environ. Eng., ASCE, Vol 111 (6), 741-754.

Cleasby, J.L. (1984), *Is Velocity Gradient a valid turbulent flocculation parameter?*, J. Environ. Eng., ASCE, Vol 110(5), 875-897.

Clift, R., Grace, J.R. and Weber, M.E. (1978) *Bubbles, Drops and Particles*, Academic Press, London.

Coulson, J.M. and Richardson, J.F. (1968) *Chemical Engineering Vol 2: Unit Operations*, 2nd Edition, Pergamon Press.

Dahl, C.P. (1993), *Modelling of flow field and Settling in Secondary Settling Tanks*, PhD Thesis, University of Aalborg, Denmark.

Dawson, M., Harrison, D., Rafique, S. and Firmansyah, T. (2006), *The use of Computational Fluid Dynamics in the Optimisation of Sludge Processes*, IChemE Sludge 14 Conference, University of Surrey January 13th 2006

De Clercq, B. (2003), *Computational Fluid Dynamics of Settling Tanks: Development of Experiments in Rheological, Settling and Scraper Sub Models*, PhD Thesis, Dept of Applied Math, Biometrics and Process Control (BIOMATH), University of Ghent, Belgium.

De Clercq, J. (2006), *Batch and Continuous Settling of Activated Sludge: In depth Monitoring and 1D Compression Modelling*, PhD Thesis, Faculteit Bio-Ingenieurswetenschappen, University of Ghent, Belgium.

Deininger, A., Holthausen, E. and Wilderer, P. (1998), *Velocity and Solids Distribution in Circular Secondary Clarifiers: Full scale Measurements and Numerical Modelling*, Water Res, 32(10).

Dick, R.I. and Ewing, B. (1967), *The Rheology of Activated Sludge*, J. Water. Pollution Control Fed., 39(4), 543-560.

Egarr, D. (2010), *An iterative method for calculating particle relaxation time*, MMI Engineering Ltd.

Ekama, G.A., Barnard, J.L., Gunthert,F.W., Krebs,P., McCorquadale, J.A., Parker, D.S. and Wahlberg, E.J. (1997), *Secondary Settling Tanks, Theory, Modelling, Design and Operation*, International Association of Water Quality, Scientific and Technical Report No 6.

EnviroSim. (2007), *BioWin 3.0: Software Manuals*, EnviroSim Associates, Ontario, Canada.

Ergun, S. (1952) *Flow through Packed Columns*, Chemical Engineering Progress, Vol 48 (2), 89-94.

Ekama, G. A. and Marais, P. (2004), *Assessing the Applicabililty of the 1D flux Theory to Full-Scale Secondary Settling Tank Design with a 2D hydrodynamic model*, Water Research, 38, 495-506.

Ganeshalingam, J., (2006), *Knostrop WwTW Hydraulic Modelling & Analysis of the New □40m FSTs*, MMI Engineering Report, MMU035-R-08-01, Issue 1, January 2007.

Gidaspow, D. (1994*), Multiphase flow and fluidization, Continuum and kinetic theory descriptions*, Academic Press, Boston.

Härtel, C., Eckart, M. and Necker, F. (2000), *Analysis and direct numerical simulation of the flow at a gravity-current head. Part 1. Flow topology and front speed for slip and no-slip boundaries*, J. Fluid. Mech.,

Hazen, A. (1904), *On Sedimentation*, Trans ASCE, 53, 45-71.

Ishii, M. and Zuber, N. (1979), *Drag Coefficient and Relative Velocity in Bubbly, Droplet and Particulate flow*. J. AIChE., Vol 25, 843-854

IWA. (2000), *Activated Sludge Models ASM1, ASM2, ASM2D and ASM3*, International Association of Water Quality, Scientific and Technical Report, No 9.

IWA. (2008), *Biological Waste Water Treatment, Principles, Modelling and Design*, 1st Edition, IWA Publishing, London UK.

Krebs, P. (1991) *The hydraulics of Final Settling Tanks*, Water. Sci. Tech. 23(4-6), 1037-1046.

Krebs, P., Ambruster, M. and Rodi, W. (1998), *Laboratory Experiments of Buoyancy Influenced Flow in Clarifiers*, J. Hydr. Res., 36(5), 831-851.

Kynch, G.J. (1952), *A Theory of Sedimentation*, Trans. Faraday Soc, 48, pp. 166 – 176.

Lakehal, D., Krebs, P., Krijgsman, J. and Rodi, W. (1999), *Computing Shear Flow and Sludge Blanket in Secondary Clarifiers*, J. Hydr. Eng., ASCE, 125(3), 1999.

Larsen, P. (1977), *On the hydraulics of rectangular settling basins, experimental and theoretical studies*, Dept of Water Resources Engineering: Lund Institute of Technology, Lund University.

Launder, B.E. and Spalding, D.B. (1972) *Lectures in Mathematical Models of Turbulence*, Academic Press, London

Lo, S. (1999), *Application of population balance to CFD modeling of bubbly flows via the MUSIG model*, Proc. 4th Int. Conf. Gas-Liquid and Gas-Liquid-Solid Reactor Eng, Delft, Aug 23-25.

Li, D. and Ganczarczyk, J. J. (1987), *Stroboscopic determination of Settling Velocity. Size and Porosity of Activated Sludge Flocs*, J. Wat. Res., 21, 257-262

Lyn, D.A., Stamou, A.I. and Rodi, W. (1992), *Density Currents and Shear Induced Flocculation in Sedimentation Tanks*, J. Hydr. Eng., ASCE, 118(6).

Matko, T. (1998), *Two Phase flow in Circular Sedimentation Tanks*, Cranfield University School of Water Sciences, Ph.D. Thesis.

McCorquodale, J.A. and Zhou, S. (1993) *Effects of Hydraulic and Solids loading on Clarifier performance*, J. Hydr. Res. 31(4), 461-478.

Menter, F. R., (1994) *Two-Equation Eddy-Viscosity Turbulence Models for Engineering Applications*, *AIAA Journal*, Vol. 32, No. 8, 1994, pp. 1598–1605.

Mohlmann, F.W., (1934), *The Sludge Index*, J. Sewage Wks., 6, 119-122.

Monash University, (2003), Civil Engineering Resources, Lecture 16.

Mironer, A., (1979), Engineering fluid mechanics, McGraw Hill, New York.

MWH (2003), *Training Notes for Final Clarifier Design*, Montgomery Watson Harza.

Nakielny, R., (2004), *Investigation into the Design and Modelling of Secondary Sedimentation Tanks: Ch 5, Settling Characteristics,* MEng Dissertation, June 2004.

Örmeci, B. and Vesilind, A. (2000), *Development of an improved synthetic sludge and a possible surrogate for studying activated sludge dewatering characteristics*, Wat Res, 34(4), pp 1069-1078, Pergamon.

Papanastasiou, T.C. (1987), *Flow of materials with yield.* J. Rheol., Vol 31, pp. 385-404

Parker, D.S., Kaufman, W.J. and Jenkins, D. (1972), *Floc breakup in turbulent flocculation processes*, J. San. Eng. Div., ASCE, Vol 98 (SA1), 79-99.

Parker, D.S. (1996), *Design and Operations Experience with Flocculator Clarifiers in Large Plants*, Water. Sci. Tech, Vol 33 (12), 163-170.

Patanker, S.V. (1980), *Numerical Heat Transfer and Fluid Flow*, Hemisphere Publications, 1st Ed.

Pitman, A.R. (1980), *Settling Properties of Extended Aeration Sludge*, J. Wat. Pollut. Control Fed. 52(3), 524-536.

Richardson, D.S. (1998), *Hydraulic Considerations of Final Settlement Tank Design*, Cranfield University School of Water Sciences, M.Sc. Thesis.

Richardson, J.F., and Zaki, W.N. (1954), *Sedimentation and Fluidisation: part 1*, J. Trans. IChemE, Vol 32, 35-53.

Robinson, C.M.E., Burt, D.J., Egarr, D.E. and Nair, A.K. (2008), *Development and Application of an Automated CFD tool for Modelling Wastewater Clarifiers*, WEFTEC, Chicago, Illinois, Oct 18-22.

Scriven, R. and Richardson, D.S. (1998), *Rye Meads STW – Stage 1 – Final Settlement Tanks Process Investigation*, Thames Water Technical Report, R19808, August 1998.

Shaw, A., McGuffie, S., Wallis-Lage, C. and Barnard, J. (2005), *Optimizing Energy Dissipating Inlet (EDI) Design in Clarifiers Using and Innovative CFD Tool*, WEFTEC, Washington DC, Oct 29-Nov 2.

Siegrist, H., Krebs, P., Bühler, R., Purtschert, I., Röck, C. and Rufer, R. (1995) *Denitrification in Secondary Clarifiers,* Water. Sci. Tech, Vol 31 (2), 205-214

Simpson, J.E., (1982), *Gravity Currents in the Laboratory, Atmosphere, and Ocean,*

Annual Review of Fluid Mechanics, Vol. 14, 213-234

Smoluchowski, M. (1917), *Versuch einer Mathematischen Theorie der Koagulationskinetik Kolloider Losungen*, Z. Phys. Chem., 92, 129-168.

Stamou, A.I., Adams, E.W. and Rodi, W. (1989), *Numerical Modelling of flow and Settling in Primary Recatangular Clarifiers*, J. Hydr. Res. 27 (5), 665-682.

Stamou, A.I, Giokas, D.L., Kim, Y. and Paraskevas, P.A. (2007), *Validation and Application of a Simple Model for Circular Secondary Settling Tanks* J. Global NEST, 10(1), 62-72.

Stovin, V.R. and Saul, A. (1998), *A Computational Fluid Dynamics (CFD) Particle Tracking Approach to Efficiency Prediction*, Wat. Sci. Tech., Vol 37, No 1, pp 285-293.

Takács, I., Patry, G.G., and Nolasco, D. (1991), *A Dynamic Model of the Clarification Thickening Process., Water Res*, 25(10).

Tennekes, H. and Lumley, J.L. (1972), *A First Course in Turbulence*, MIT Press, 1st Ed, 1972.

Tchobanoglous, G. and Burton, F.L. (1991), *Wastewater Engineering: Treatment Disposal and Reuse*, 3rd Ed, Metcalf and Eddy Inc, McGraw Hill.

Thomas, D.N., Judd, S.J. and Fawcett, N. (1999), *Flocculation Modelling: A review*, Water Res, 33(7).

Twort, A.C., Patnayaka, D.D. and Brandt, M.J. (2000), *Water Supply*, Butterworth-Heinmann

Vanderhasselt, A. and Vanrolleghem, P.A. (2000), *Estimation of Sludge Sedimentation parameters from single Batch Settling curves*, Water Res, 34(2), 395-406.

Van Wachem, B.J.D, Schouten, J.C., Krishna, R. and van den Bleek, C.M. (1998) *Eulerian Simulations of Bubbling Behaviour in Gas-Solid Fluidissed Beds*, J. Comp. chem. Eng., Vol 22, 299-306

Vesilind, P.A. (1968), *Theoretical considerations: Design of prototype thickeners from batch settling tests,* Water and Sewage Works, 115 (July), 302-307

Von Sperling, M. (1994), *A new unified solids flux-based approach for the design of final clarifiers: description and comparison with traditional criteria.* Wat. Sci. Tech. 30(4), 57-66

Wahlberg, E.J. and Keinath, T.M. (1988), *Development of settling flux curves using SVI.* J. Wat. Pollut. Control Fed. 60 (12), 2095-2100

Wahlberg, E.J., Keinath, T.M., and Parker, D.S. (1994), *Influence of Activated Sludge Flocculation time on Secondary Clarification.* Water Environmental Research, 66(6), 779-786, Sept/Oct 1994

Wallis, G.B. (1969), *One-Dimensional Two Phase Flow*, McGraw-Hill, 1st Ed.

Weiss, M., Plósz, B. G., Seemiani, K., and Meinhold, J. (2007), *Suction-lift sludge removal and non-Newtonian flow behaviour in circular secondary clarifiers: Numerical modelling and measurements.* J. Chem. Eng., Vol 132, 241-255

Winkler, K., Hermann, F. And Baumer, P. (1999), *Strömungsberechnung für ein rundes Nachklärbecken mit Schildräumer*, GWA 99(2), 137-147

Wu, R.M., and Lee, D.J. (1998), *Hydrodynamic drag force exerted on a moving floc and its implication to free settling tests, Water Research*, Vol 32, 7600-7681.

White, M.J.D. (1975), *Settling of Activated Sludge*, Technical Report TR11, Water Research Centre, Stevenage, UK.

White, M.J.D. (1976), *Design and control of Secondary Settling Tanks*, Wat. Pollut. Control, 75(4), 459-467.

Wilcox, D. W., (1994) *Turbulence Modelling For CFD*, 1st ed., DCW Industries, La Canada.

Witt, P.J. and Perry, J.H., (1995) *A Study in Multiphase Modelling of Fluidised Beds*, Computational Techniques and Applications, CTAC95, Swinburne, Australia, Jul 3-5, 1995.

Zhou, S. and McCorquodale, J.A. (1992), *Modelling of Rectangular Settling Tanks*, *J. Hydr. Eng.*, ASCE, 118(10).

APPENDIX A

APPENDIX A:

The following tensor notations are used in Chapter 2.

Index Tensor Notation	Coordinate Free Tensor Notation	Expanded
x_i	$\boldsymbol{x}$	$\{x_1, x_2, x_3\}$
u_i	$\mathbf{U}$	$\{u_1, u_2, u_3\}$
σ_{ij}	$\boldsymbol{\sigma}$	$\begin{Bmatrix} \sigma_{11}, \sigma_{12}, \sigma_{13} \\ \sigma_{21}, \sigma_{22}, \sigma_{23} \\ \sigma_{31}, \sigma_{32}, \sigma_{33} \end{Bmatrix}$
δ_{ij} $\delta_{ij} = 1$ *for* $i = j$, $\delta_{ij} = 0$ *for* $i \neq j$	δ	$\begin{Bmatrix} 1,0,0 \\ 0,1,0 \\ 0,0,1 \end{Bmatrix}$
$u_i u_j$	$\mathbf{U} \otimes \mathbf{U}$	$\begin{Bmatrix} u_1u_1, u_1u_2, u_1u_3 \\ u_2u_1, u_2u_2, u_2u_3 \\ u_3u_1, u_3u_2, u_3u_3 \end{Bmatrix}$
$\frac{\partial \phi}{\partial x_i}$	$\nabla \phi$	$\frac{\partial \phi}{\partial x_1}, \frac{\partial \phi}{\partial x_2}, \frac{\partial \phi}{\partial x_3}$
$\frac{\partial u_i}{\partial x_i}$	$\nabla \bullet \mathbf{U}$	$\left\{ \frac{\partial u_1}{\partial x_1} + \frac{\partial u_2}{\partial x_2} + \frac{\partial u_3}{\partial x_3} \right\}$

$\frac{\partial u_i}{\partial x_j}$	$\nabla \mathbf{U}$	$\begin{Bmatrix} \frac{\partial u_1}{\partial x_1}, \frac{\partial u_1}{\partial x_2}, \frac{\partial u_1}{\partial x_3} \\ \frac{\partial u_2}{\partial x_1}, \frac{\partial u_2}{\partial x_2}, \frac{\partial u_2}{\partial x_3} \\ \frac{\partial u_3}{\partial x_1}, \frac{\partial u_3}{\partial x_2}, \frac{\partial u_3}{\partial x_3} \end{Bmatrix}$
$\frac{\partial u_j}{\partial x_i}$	$(\nabla \mathbf{U})^T$	$\begin{Bmatrix} \frac{\partial u_1}{\partial x_1}, \frac{\partial u_2}{\partial x_1}, \frac{\partial u_3}{\partial x_1} \\ \frac{\partial u_1}{\partial x_2}, \frac{\partial u_2}{\partial x_2}, \frac{\partial u_3}{\partial x_2} \\ \frac{\partial u_1}{\partial x_3}, \frac{\partial u_2}{\partial x_3}, \frac{\partial u_3}{\partial x_3} \end{Bmatrix}$
$\nabla \bullet \sigma_{ij}$	$\nabla \bullet \boldsymbol{\sigma}$	$\begin{Bmatrix} \frac{\partial \sigma_{11}}{\partial x_1} + \frac{\partial \sigma_{12}}{\partial x_2} + \frac{\partial \sigma_{13}}{\partial x_3} \\ \frac{\partial \sigma_{21}}{\partial x_1} + \frac{\partial \sigma_{22}}{\partial x_2} + \frac{\partial \sigma_{23}}{\partial x_3} \\ \frac{\partial \sigma_{31}}{\partial x_1} + \frac{\partial \sigma_{32}}{\partial x_2} + \frac{\partial \sigma_{33}}{\partial x_3} \end{Bmatrix}$

APPENDIX B

APPENDIX B:

A User Manual for the ClariSim (2007) Implementation in CFX 4.2 (1997) and CFX 4.4 (2001)

Usage of CFX-4 for standard CFD modelling is not discussed here, full details of this code are available in the manual for the software (CFX, 2001). The additional code for Clarifier modelling, referred to in this thesis as ClariSim (2007), is compiled into the CFX-4 Fortran libraries in order to make a new executable code, `f3dCS.exe`. The features available in the ClariSim module are then controlled through the use of a *model.dat* file. A typical execution line on a Windows machine at the CFX-4 command prompt might be,

```
runsolve4 -c m04.fc -geom coarse.geo -restart m03.dmp -exec
../f3dCS.exe -enviro 04
```

where the command file `.fc` controls many aspects of the CFD model, the Clarifier geometry and grid is contained in the `.geo` file, in this case the model restarts from an earlier result set stored in the `.dmp` file and the code itself is stored one directory up as the `f3dCS.exe` file. The Command files, Fortran fragments, solution sequence and post processing steps described in this appendix are all based around the RyeMeads Clarifier example discussed in chapter 4 of this thesis.

B.1 Command File Modifications.

A typical command file for the analysis of a clarifier and the associated Fortran routines are listed in full at the end of this Appendix for the RyeMeads Clarifier and this text should be read with reference to the command file and the Fortran fragments. The command file is largely a standard CFX-4 script with some additions

as follows. The modified routines for effective viscosity are invoked in the command file with the use of the following keywords in CFX 4.4,

```
>>OPTIONS
  TURBULENT FLOW WITH WILCOX MODEL
>>TURBULENCE PARAMETERS
  >>TURBULENCE MODEL
    TURBULENCE MODEL 'MENTER MODIFIED K-OMEGA'
  >>TURBULENCE CONSTANTS
    C3 0.0
```

And in CFX 4.2 which does not include the Menter (1994) modification, just as,

```
>>OPTIONS
  TURBULENT FLOW WITH WILCOX MODEL
>>TURBULENCE PARAMETERS
  >>TURBULENCE CONSTANTS
    C3 0.0
```

Additional user Fortran routines were written to implement the physical models described in this thesis. The fluid molecular viscosity was modified in a non standard user routine `USRMVS.f` according to the model options detailed in chapter 3 (section 3.4.2) this does not need to be selected in the command file . Other standard user Fortran routines do need to be selected in the command file as follows,

```
  >>USER FORTRAN
    USRSLP
    USRDEN
    USRTRN
    USRINT
    END
```

`USRSLP.f` implements the Takács (1991) equation (3.6) or applies fixed settling velocities for a maximum of three drift flux scalars for the MDF model. `USRDEN.f` invokes the equation of state according to Zhou (1992) equation (2.37). `USRTRN.f` controls the model and implements several post processing options. `USRINT.f` sets up many of the model parameters. A fixed naming convention for additional scalars was established for general application to clarifiers as follows,

```
>>OPTIONS
  USER SCALAR EQUATIONS 12
>>VARIABLE NAMES
  USER SCALAR1 'ASM SLUDGE1'
  USER SCALAR2 'ASM SLUDGE2'
  USER SCALAR3 'ASM SLUDGE3'
  USER SCALAR4 'USRDCC_CN'
  USER SCALAR5 'USRDCC_VS'
  USER SCALAR6 'USRDCC_STREAM'
  USER SCALAR7 'USRDCC_LAMVIS'
  USER SCALAR8 'YPLUS'
  USER SCALAR9 'SHEAR RATE'
  USER SCALAR10 'USRDCC_VISP'
  USER SCALAR11 'USRDCC_YLDT'
  USER SCALAR12 'USRDCC_GSCAL'
```

The first three user scalars are used with the Takács EDF model or for a 3 scalar MDF model. Scalar 4 carries concentration which is used by many of the empirical relationships and is a useful parameter to plot. Scalar 5 is the settling velocity from Takács and scalar 7 carries the molecular viscosity based on whichever model is invoked for calculation in USRMVS. Scalar 10 is the Dahl (1993) plastic viscosity calculated from equation (3.12) and Scalar 11 is the Dick and Ewing (1967) plastic yield stress from equation (3.14).

Rest of the command language structure is standard but note the fact that the model is defined as weakly compressible with the standard equation of state selected. This is required in order to force the code to make a call to the USRDEN routine for density modification as a function of sludge concentration.

B.2 Description of the User Fortran

The key components of the model were applied in user Fortran routines, these may be edited along with the command file. For ease of application the parameters and variables required for the model are collated in USRINT and passed to other routines through common blocks. For the clarifier application the user need only modify the USRINT routine as the rest of the coding is general.

B.2.1 Common Blocks

/UCPROP/ holds the phase properties for liquid and sludge.

/UCGEOM/ holds overall tank dimension data

/UCASM/ holds terminal settling velocity constants for the MDF model

/UCTAK/ holds the empirical constants for the Takács relationship.

/UCOUT/ holds only the RAS exit volume flow rate.

/UCVIS/ holds the viscosity model switch and bounds

/UCBBV/ holds the constants for the Bokil Bewtra (1972) non-Newtonian model

/UCDDE/ holds the constants for the Dahl (1993), Dick and Ewing (1967) non-Newtonian model.

/UCPWR/ holds constants for the Armbruster (2003) power law models

/UCHBVS/ holds constants for the de-Clercq (2003), Herschel Bulkley non-Newtonian model.

B.2.2 USRINT

In this sub-routine the constants and variables for the models are defined. A convention is established that allows the key model parameters to be held in a separate file *model.dat.* The user may modify this file to turn the various clarifier models on and off. The *model.dat* file holds only those constant that need to be modified by the user during the course of the analyses.

Table B.1: Model parameters in the order they appear in USRINT.

Variable	Common Block	Default Value	Comments
QRAS	UCOUT	(m^3/s)	The RAS volume flowrate only needed if USRBCS is used.
CNCIN	Local	(kg/m^3)	Influent MLSS concentration
TDIAM	UCGEOM	(m)	Tank diameter
TRn	UCGEOM	Ratio	Positions of output profiles.
IBL	Local	1	Toggle to initialize blanket on or off.
XSLG	Local	2 (m)	Initial guess of sludge blanket depth from free surface.
IVIS	UCVIS	0,1,2,3,4 or –1	Select a Non-Newtonian relationship for viscosity. -1 is constant viscosity.
ISET	UCTAK	0,1,2	Takacs is standrdad Vaccari model is not implemented yet.
DENWAT	UCPROP	1000.0 (kg/m^3)	Water density
DENSLG	UCPROP	1450.0 (kg/m^3)	This is the value suggested by Larsen (1977)
VISMIN	UCVIS	1.0e-3 (Ns/m^2)	Lower bound for viscosity
VISMAX	UCVIS	20.0 (Ns/m^2)	Upper bound for viscosity
SHTINY	UCDDE	1.0E-3 9 ($1/s$)	Lower bound for shear strain rate
SHENOR	UCDDE	1.0E+3($1/s$)	Upper bound for shear strain rate
USn	USASM	1.0E-3 (m/s)	Constant settling velocity for MDF scalars.
USFREE	UCTAK	2.0E-3 (m/s)	Free settling velocity for Takacs
USLIM	UCTAK	2.0E-3 (m/s)	Fixed maximum settling velocity.
RH	UCTAK	0.5 (m^3/kg)	Constant for Takacs
RP	UCTAK	1 to 9 (m^3/kg)	Constant for Takacs
RI	Local	0.005	Defines start of zone 1
CMIN	UCTAK	RI*CNCIN	Concentration of non-settleables for Takacs
CBB1	UCBBV	0.00327 (Ns/m^2)	Coefficient for BB relationship eqn (3.11)
CBB2	UCBBV	0.132 (m^3/kg)	Exponential coefficient for BB eqn (3.11)
CXMIN	UCBBV	0.1 (kg/m^3)	Lower bound of concentration for straight line fit BB
CXMAX	UCBBV	0.7 (kg/m^3)	Upper bound of concentration for straight line fit BB
UYMIN	UCBBV	0.001 (Ns/m^2)	Lower bound of viscosity for straight line fit BB
UYMAX	UCBBV	0.004 (Ns/m^2)	Upper bound of viscosity for straight line fit BB
CPL	UCDDE	2.473E-4($m^5/kg{\cdot}s^2$)	Dahl plastic viscosity coefficient.
BETA1	UCDDE	1.1E-4 ($kg/m{\cdot}s^2$)	Plastic yield stress coefficient for Dick and Ewing see Table 3.5
BETA2	UCDDE	0.98 (m^3/kg)	Exponential coefficient for Dick and Ewing see Table 3.5
CPSA	UCPWR	25.0 (-)	Exponential coefficient for Armbruster see Table 3.4
CPSCCT	UCPWR	4.5 (kg/m^3)	Exponential coefficient for Armbruster see Table 3.4
CPRA	UCPWR	550.0 (-)	Exponential coefficient for Armbruster see Table 3.4
HBA	UCHBVS	9.0364E-4($kg/m{\cdot}s^2$)	Exponential coefficient for DeClerq see Table 3.6
HBB	UCHBVS	2.493E-4($m^5/kg{\cdot}s^2$)	Exponential coefficient for DeClerq see Table 3.4
HBM	UCHBVS	169.47(s)	Exponential coefficient for DeClerq see Table 3.6
HBP	UCHBVS	0.7748 (-)	Exponential coefficient for DeClerq see Table 3.6

B.2.3 USRDEN

In this sub-routine the mixture density, based on equation (2.36) is calculated at each cell centre, at inlet boundaries and at all walls.

B.2.4 USRSLP

In this sub-routine the slip velocity, based on the Takács (1991) equation (3.6) is calculated at each cell center and applied to the U component of velocity for the slip scalar. The routine may be modified to account for slippage in other directions

B.2.5 USRBCS

In this sub-routine selected boundary conditions are updated at each time step. The mass flow boundary `OUTLET_RAS` is modified to give constant volume flowrate and the scraper wall boundary `WALL_FLOOR` can have constant angular and radial velocity components applied. This routine is not always used.

B.2.6 USRMVS

The user chooses in `USRINT` a value for `IVIS` which controls the the fluid mixture viscosity model. In `USRMVS` the shear rate and G scalar are computed and the selected viscosity model is applied at each cell centre.

B.2.7 USRTRN

A number of standard outputs are calculated in this routine. The mass averaged concentration at `RAS` and at effluent, a stream function distribution and profiles of concentration and velocity with depth at key radial distances.

B.2.8 Mapping 'G' back to Streamlines.

Several source routines in CFX-4 were adapted to allow the mapping of additional User Scalars, including 'G' back to particle tracks. These routines are `GASPRO.f`, `PARCAL.f`, `PARMOD.f`, `PRINTD.f` and `VARVRT.f`. A description of this

coding is not included here. The source routines have been commented to allow understanding of the modifications made.

B.2.9 Modifying the Wilcox turbulence model for variable apparent viscosity.

In most turbulent flows the viscosity is dominated by the turbulent component. Therefore, the standard CFX-4 code does not allow for variation in molecular viscosity in a turbulent flow. Additional arrays for carrying all components of viscosity are made to the code to allow the viscosity variable to be made up of both a turbulent and an apparent component for the low Reynolds number turbulence models only.

Many source routines in CFX-4 were adapted to allow this, in the 4.2 version (CFX,1997) these are, `CMVSFN.f` (a new routine), `CVIS.f`, `CVISFN.f`, `DFTVIS.f`, `DIFENG.f`, `DIFFUS.f`, `DIFVFT.f`, `GENBSQ.f`, `GENBUO.f`, `GENSHR.f`, `GRASET.f`, `OUTBCS.f`, `SCED.f`, `SCEDTB.f`, `SCMVST.f`, `WALDIS.f`, `WALSTR.f`, `WALVIS.f` and `WALVST.f`. A particular problem was noted in the routine `WALDIS.f` where source terms had to be initialized to zero at adjacent interior nodes otherwise old values were carried through to the next iteration causing failure of the run.

B.3 Model Set Up and Solution

In order to understand how the CFX-4 code is used for the analysis of a clarifier system it is important to understand the how the boundary and initial conditions are defined for the solver and how the equations sets are subsequently solved. An important part of this work has been the experience developed in the use of the code to obtain accurate and fully converged solutions for density driven stratification in Clarifer flows. Generally, calculations are performed in the axi-symmetric co-ordinate system (X,r,θ) for 2D segments of the tank. The U velocity field is positive

in the positive x axis. The V velocity field is positive in the positive y axis and the swirl velocity W is positive in the positive z (θ) axis.

B.3.1 Boundary Conditions

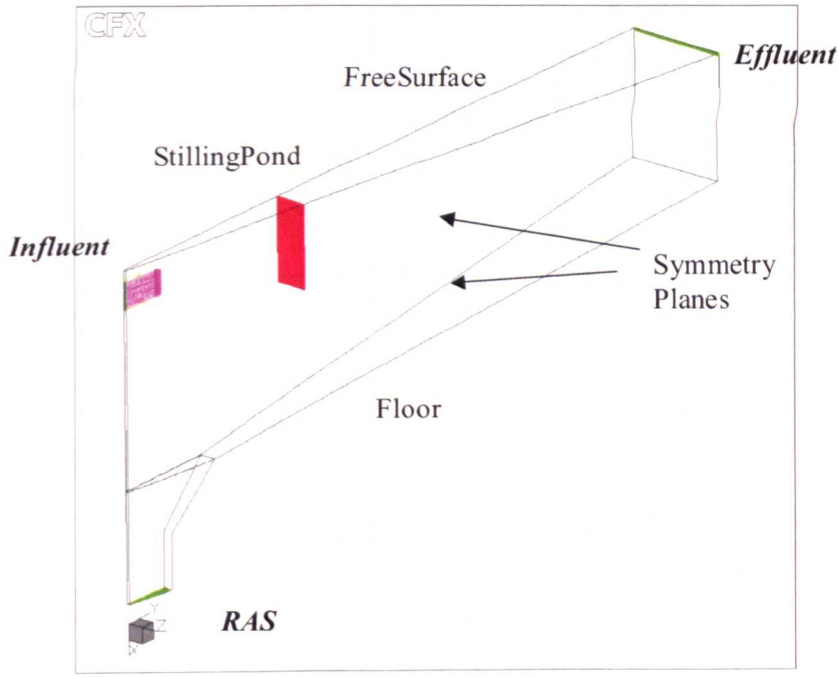

Figure B.1: Typical boundary conditions for an axi-symmetric clarifier model.

Table B.2: Patch naming conventions as used for a standard clarifier.

Boundary	CFX-4 PATCH TYPE	PATCH NAME (These labels are used by the code)	Routines that use the patch name	Comments
Influent	INLET	INLET_INFLUENT	CMD, USRTRN	Always constant velocity
Free Surface	WALL	WALL_FREESURFACE	CMD	Always a slipping wall set in CMD
Floor	WALL	WALL_FLOOR	CMD, USRBCS	Free slip or Idealised scarper
Symmetry Planes	SYMMET or BLKBDY	KPER*n*	CMD	Symmetry or Periodic can be adjusted in the CMD file.
Effluent	OUTLET or PRESS	PRESS_EFFLUENT	CMD, USRTRN	
RAS	OUTLET	OUTLET_RAS	USRTRN, USRBCS	Always an outlet. Can be adjusted in USRBCS to give constant volume flow.
Axis	SYMMET	SYMMET_AXIS	CMD	Not always needed. Can replace with a solid pipe.
Stilling Pond	WALL	WALL_STILLING		Double sided thin surface

For this code implementation it is important to use a naming convention for the boundary conditions as these are referred to in the sub-routines. The patch names are defined in Table B.2.

Table B.3: Boundary conditions calculated for the Rye Meads Clarifier model discussed in chapter 4.

	INFLUENT		EFFLUENT		RAS	
Diameter (m)	0.76		28.00		2.76	
Area (m^2)	1.1938		0.8796		5.529203	
Height (m)	0.5		0.01			
Velocity (m/s)	0.167531517		0.1137		0.0181	
Kinetic Energy	5.61336E-05					
Epsilon	2.80378E-06					
Omega	0.0499					
	Qin = Q(1+R)		Q		R.Q	
	(m^3/hr)	(m^3/s)	(m^3/hr)	(m^3/s)	(m^3/hr)	(m^3/s)
Flowrate	720.00	0.2	360.00	0.1	360.00	0.1
	MLSS					
	(mg/l)	(kg/m^3)	(mg/l)	(kg/m^3)	(mg/l)	(kg/m^3)
Conc	2825.00	2.83	16.5	0.02	8613	8.61
Mixture Density		1000.876724		1000.005121		1002.673
Mass Fraction (kg/kg)		0.002822525		1.64999E-05		0.00859
Volume Fraction (m^3/m^3)		0.001948276		1.13793E-05		0.00594
TOTAL MASS FLOW (kg/s)	200.1753448		100.0005		100.2673	
Mass flow ratios	1		0.499565		0.500897	

The data shown in Table B.3 is from a boundary condition calculator spreadsheet produced as an input sheet for defining the input parameters to a generic clarifier model. The input for the sheet are shaded light grey, the darker grey inputs may be used for estimating effluent and RAS conditions.

B.3.2 Symmetry Planes and Axisymmetry

Circular clarifiers may be modeled with a 2D axisymmetric configuration with an arbitrary theta dimension (usually 2π is used for clarity in the output boundary conditions). For radial flow only, the high and low θ planes may be defined as symmetry to all variables. If the influent is used to direct a tangential flow, similar to the Energy Dissipating Inlet (EDI) designs discussed by Richardson (1998) , then the high and low θ planes must be defined as periodic and the full set of momentum equations including a swirl component W should be solved.

B.3.3 Influent

At this boundary the user defines a constant normal velocity, the turbulence quantities k and ω, and the solids loading. The solids may be expressed as a mass fraction or a volume fraction depending on how the equation of state is modelled.

B.3.4 Effluent

The exit weir may be set at constant reference pressure or with a proportion of the total mass flow. The height of the weir free surface at the sidewall can be calculated from the side weir equation. Flow should not enter through this boundary but in order to account for any numerical instability, which may result in a temporary flow reversal, the ambient conditions downstream of the weir should also be defined.

B.3.5 Return Activated Sludge (RAS)

The exit volume flow rate is fixed, as in a real plant controlled by varying a downstream bell-mouth or where a pump is used to draw off the RAS. Most CFD codes do not support a constant volume boundary but do provide a constant mass flow boundary. This is an important issue for Clarifier modeling where the solids hold up, and hence the total mass of the system, is varying with time. In these models the boundary is initially defined with a mass flux estimated from the likely solids concentration present in the RAS. In this implementation the exit mass flow can be updated at each time step in `USRBCS` to account for the concentration above the RAS exit. Convergence of the model is apparent when updates to this value are no longer significant and the exit density approaches a constant.

B.3.6 Water free surface

The water free surface is modeled as a fixed slipping wall. That is the flow is confined by the wall but there is no shear stress at the wall. This is a common approach applied for modelling a water free surface where there is known to be little

disturbance. This approximation is invalid for strong wind cross flows or any other asymmetric sources of momentum.

B.3.7 Tank Floor and Scraper Source Terms

In a 2D axi-symmetric model it is not possible to represent the periodic action of the scraper. There are various ways of modelling the floor boundary condition to approximate the scraper, de Clerq (2003) describes several approaches in his thesis, these include,

- Slip floor
- No slip floor
- Fixed velocity on the wall.
- Momentum source terms near the wall.

Several of these approaches are implemented through USRBCS and are compared in the verification and validation study, chapter 4. Some sludge withdrawal systems replace the conventional scraper with a rotating suction manifold referred to as either a Simplex or Tow-Bro mechanism. Modelling of these systems requires the use of sink boundary conditions at the floor tuned either to keep velocity of withdrawal constant (Tow-Bro) or constant mass flux per unit area of withdrawal pipe (Simplex).

B.4 Solution sequence

There is discussion in the literature with regard to the unsteady nature of the flow in clarifiers. Of the tanks studied in the course of this work some were seen to exhibit transient behaviour whilst others settled to a steady state. In terms of approaching the solution numerically a scheme has been developed which has been shown to work for all cases. This scheme has been encoded in a series of batch files to allow a quick initialization of any clarifier model. There is no need to compile the additional fortran routines into the code as the ClariSim version of CFX has been compiled as a stand alone *.exe* file. The various models and parameter switches are enabled through the *model.dat* file referring to the initialization routine `USRINT`. Table B.4 below

shows the content of the model.dat file for the following sequence used to obtain a converged solution for the Ryemeads clarifier discussed in chapter 4.

1. **Laminar start**. Establish a steady state, single phase laminar flow solution in the tank with the inlet mass flow, RAS and effluent boundaries correctly defined. This calculation uses a standard command and geometry file and no Fortran is invoked.

```
runsolve4 -c m01.fc -geom coarse.geo -exec ../f3d42.exe -
enviro 01
```

2. **Make Blanket**. Restart the model as transient, laminar and first order but with the density relationship and the settling relationship enabled and a bed height initiated. This converges readily with the main flow features formed and a sediment bed established. The exit mass flow rate can be defined as constant with an assumed exit concentration (likely to be between 5000 and 8000 mg/l). This solution represents a good initial guess for the more detailed models. Notice that the viscosity is kept constant and the routine USRMVS is not used at this stage.

```
runsolve4 -c m02.fc -geom coarse.geo -exec ../f3dCS.exe -
restart m01.dmp -enviro 02
```

3. **Make turbulent**. Restart the model transient, first order with turbulence but still with a constant apparent viscosity for the fluid mixture.

```
runsolve4 -c m03.fc -geom coarse.geo -restart m02.dmp -exec
../f3dCS.exe -enviro 03
```

4. **Viscous high order**. Restart from 3 as transient, second order with turbulence and the Bokil Bewtra rheology relationship enabled. This simple viscosity model is more robust than the Bingham plastic model and provides a stable viscosity field through the settled bed. At this stage the modifications to the k-ω model for varying molecular viscosity are also invoked.

```
runsolve4 -c m04.fc -geom coarse.geo -restart m03.dmp -exec
../f3dCS.exe -enviro 04
```

5. **Herschel Bulkley**. Restart from 4 as transient, second order with turbulence and a high order viscosity model if required.

```
runsolve4 -c m05.fc -geom coarse.geo -restart m04.dmp -exec
../f3dCS.exe -enviro 05
```

B.4.1 The *model.dat* file

The *model.dat* file holds only those constant that need to be modified by the user during the course of the analyses. The table below shows the content and a sequence used to obtain the converged solution for the Rye Meads coarse grid described in chapter 4.

Table B.4: The file *model.dat* is updated for each run in the sequence.

Parameters	Run 2 Make Blanket	Run 3 Make Turbulent	Run 4 Viscous High Order	Run 5 Herschel Bulkley
IVIS	-1	-1	1	4
ISET	0	0	0	0
CNCIN	2.825	2.825	2.825	2.825
USFREE	2.0e-3	2.0e-3	2.0e-3	2.0e-3
RH	0.3785	0.3785	0.3785	0.3785
RP	7.1464	7.1464	7.1464	7.1464
TDIAM	28	28	28	28
TR1	0.15	0.15	0.15	0.15
TR2	0.3	0.3	0.3	0.3
TR3	0.5	0.5	0.5	0.5
TR4	0.64	0.64	0.64	0.64
TR5	0.78	0.78	0.78	0.78
TR6	0.96	0.96	0.96	0.96
US1	0.001	0.001	0.001	0.001
US2	0.005	0.005	0.005	0.005
US3	0.002	0.002	0.002	0.002
IBL	1	0	0	0
XSLG	1.9	1.9	1.9	1.9

B.5 Post processing steps.

In addition to the standard data generated by the postprocessor it is also useful to obtain additional plots showing clarifier performance. These additional steps are as follows.

1. Switch off all of the equations for flow, solids and turbulence, and calculate the passage of a tracer pulse through the tank over several hydraulic retention times. Data is used to construct response curves at discreet points and CRTD curves for the tank.

2. Restart and track mass-less particles from the influent through the domain following the liquid velocity field. These tracks can be coloured with time to give indicative residence.
3. Restart and track mass less particles from the influent through the domain following the solid / slipped velocity field. These tracks can be coloured with time to give indicative residence and with G (through the use of additional fortran routines to give a G-t history.

The residence data is of particular interest with respect to sludge lifetime. High age may be indicative of de-nitrification processes occurring in the tank.

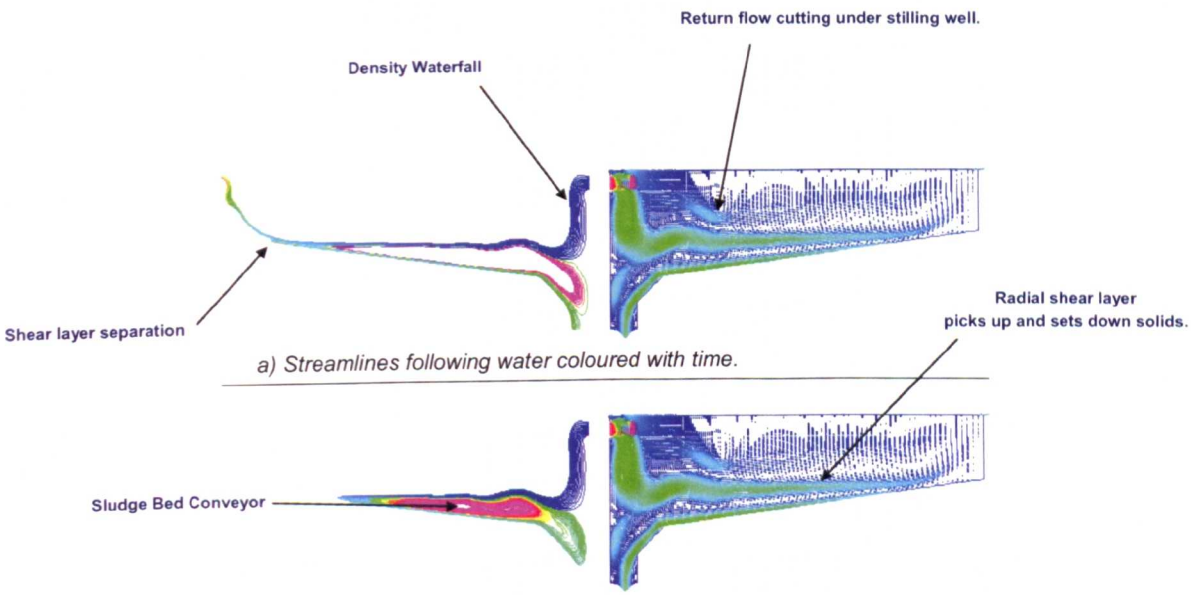

Figure B.2: Plotting of stream function following the flow and following the flocs.

```
/*-------------------------------------------------------------------*/
/* Ryemeads Final Run 4.2                                            */
/*  - Fine Grid                                                      */
/* SLIP VELOCITY SET AS A FUNCTION OF CONCENTRATION IN USRSLP        */
/* USES MODEL OF TAKACS ET AL.                                       */
/* DENSITY SET AS A FUNCTION OF CONCENTRATION IN USRDEN.             */
/* RHEOLOGY SET AS A FUNCTION OF CONCENTRATION IN USRMVS.            */
/*  - Turbulent flow                                                 */
/*  - Variable viscosity                                             */
/*  - Second order                                                   */
/*                                                                   */
/*-------------------------------------------------------------------*/
/* DJB 14 June 2005                                                  */
/*-------------------------------------------------------------------*/

/* Model is set as weakly compressible but alternative form
   of equation of state applied */

#CALC
 R     = 8314.0;          /* UNIVERSAL GAS CONSTANT */
 PREF  = 1.01325E+5;      /* REFERENCE PRESSURE (Pa)*/
 TREF  = 300;             /* REFERENCE TEMPERATURE IN (K) */
 W     = 18.0;            /* MOL WEIGHT (kg/kmol)   */
#ENDCALC

>>CFX4
/*
  >>SET LIMITS
    TOTAL INTEGER WORK SPACE 2000000
    TOTAL CHARACTER WORK SPACE 10000
    TOTAL REAL WORK SPACE 8000000
    MAXIMUM NUMBER OF BLOCKS 100
    MAXIMUM NUMBER OF PATCHES 500
    MAXIMUM NUMBER OF INTER BLOCK BOUNDARIES 300
    END
*/
 >>OPTIONS
    TWO DIMENSIONS
    BODY FITTED GRID
    CYLINDRICAL COORDINATES
    AXIS INCLUDED
    TURBULENT FLOW WITH WILCOX MODEL
    BUOYANT FLOW
    COMPRESSIBLE FLOW
    TRANSIENT FLOW
    USER SCALAR EQUATIONS 12
    END

/* Do not need to include USRMVS here, automatically called by
   modifications to k-w model in supplied object code */

  >>USER FORTRAN
    USRSLP
    USRDEN
    USRTRN
    USRINT
    END

  >>VARIABLE NAMES
    USER SCALAR1 'ASM SLUDGE1'
    USER SCALAR2 'ASM SLUDGE2'
    USER SCALAR3 'ASM SLUDGE3'
    USER SCALAR4 'USRDCC_CN'
    USER SCALAR5 'USRDCC_VS'
    USER SCALAR6 'USRDCC_STREAM'
    USER SCALAR7 'USRDCC_LAMVIS'
    USER SCALAR8 'YPLUS'
    USER SCALAR9 'SHEAR RATE'
    USER SCALAR10 'USRDCC_VISP'
    USER SCALAR11 'USRDCC_YLDT'
    USER SCALAR12 'USRDCC_GSCAL'
    END
/*-------------------------------------------------------------------*/
>>MODEL TOPOLOGY
  >>INPUT TOPOLOGY
    READ GEOMETRY FILE
    END
  >>CREATE PATCH
    PATCH NAME 'KPER'
    PATCH TYPE 'SYMMETRY PLANE'
    BLOCK NAME 'BLOCK-NUMBER-1'
    HIGH K
    LOW K
    END
  >>CREATE PATCH
    PATCH NAME 'KPER'
```

```
    PATCH TYPE 'SYMMETRY PLANE'
    BLOCK NAME 'BLOCK-NUMBER-2'
    HIGH K
    LOW K
    END
/*-------------------------------------------------------------*/
/* INLET PATCHES AND FREE SLIP DEFINED IN CFX-BUILD            */
/*-------------------------------------------------------------*/
>>MODEL DATA
  >>TITLE
    PROBLEM TITLE 'SST, TRANSIENT RUN'
    END
  >>SET INITIAL GUESS
    >>INPUT FROM FILE
      READ DUMP FILE
      FORMATTED
      END
  >>DIFFERENCING SCHEME
    U VELOCITY 'HIGHER UPWIND'
    V VELOCITY 'HIGHER UPWIND'
    ASM SLUDGE1 'HIGHER UPWIND'
    ASM SLUDGE2 'HIGHER UPWIND'
    ASM SLUDGE3 'HIGHER UPWIND'
    END
  >>PHYSICAL PROPERTIES
    >>FLUID PARAMETERS
      VISCOSITY 1.0E-3
      DENSITY 1000.0
      END
/* Total run is at least 4 hydraulic retention times */
    >>TRANSIENT PARAMETERS
      TIME STEPS 1000*10
      END
    >>COMPRESSIBILITY PARAMETERS
      WEAKLY COMPRESSIBLE
      UNIVERSAL GAS CONSTANT #R
      REFERENCE PRESSURE #PREF
      FLUID MOLECULAR WEIGHT #W
      MINIMUM TEMPERATURE 273.0
      END
    >>BUOYANCY PARAMETERS
      GRAVITY VECTOR 9.81 0.0 0.0
      BUOYANCY REFERENCE DENSITY 1000.0
      END
    >>SCALAR PARAMETERS
      >>DIFFUSIVITIES
        ASM SLUDGE1 1.0E-15
        ASM SLUDGE2 1.0E-15
        ASM SLUDGE3 1.0E-15
    >>TURBULENCE PARAMETERS
/*
      >>TURBULENCE CONSTANTS
        C3 0.0
        END
*/
      >>LOGLAYER CONSTANT
        ASM SLUDGE1 1.0
        ASM SLUDGE2 1.0
        ASM SLUDGE3 1.0
      >>SUBLAYER THICKNESS
        ASM SLUDGE1 1.0
        ASM SLUDGE2 1.0
        ASM SLUDGE3 1.0
      >>TURBULENCE MODEL
        PHASE NAME 'WATER'
        TURBULENCE MODEL 'LOW REYNOLDS NUMBER K-OMEGA'
        END
/*-------------------------------------------------------------*/
>>SOLVER DATA
  >>PROGRAM CONTROL
    MAXIMUM NUMBER OF ITERATIONS     20
    MINIMUM NUMBER OF ITERATIONS     2
    INTERMEDIATE PRINTING INTERVAL  1001
    OUTPUT MONITOR BLOCK 'BLOCK-NUMBER-1'
    OUTPUT MONITOR POINT  10 4 1
    MASS SOURCE TOLERANCE 1.0E-7
    END
  >>UNDER RELAXATION FACTORS
    U VELOCITY 0.7
    V VELOCITY 0.7
    ASM SLUDGE1   0.4
    ASM SLUDGE2   0.4
    ASM SLUDGE3   0.4
    DENSITY 0.3
    K 0.1
    OMEGA 0.1
```

```
    END
  >>DEFERRED CORRECTION
    K START        5001
    K END          5002
    OMEGA START    5001
    OMEGA END      5002
    END
/*-------------------------------------------------------------*/
>>CREATE GRID
  >>INPUT GRID
    READ GRID FILE
    END
/*-------------------------------------------------------------*/

/* Expected velocity & Turbulence */

#CALC
 PICNST   =  3.14159;
#ENDCALC

/* SST DIMENSIONS */
#CALC
 DTANK    =  28.0;
 DIN      =  0.84;
#ENDCALC

/* TURBULENCE */
#CALC
 UIN      = 0.3609;
 H        = DIN;
 TE       = 0.002*UIN*UIN;
 EPS      = TE**1.5/(0.3*H);
 OMEG     = EPS/TE;
#ENDCALC

>>MODEL BOUNDARY CONDITIONS
  >>INLET BOUNDARIES
    PATCH NAME 'INLET_INFLUENT'
    NORMAL VELOCITY #UIN
    K               #TE
    OMEGA           #OMEG
    ASM SLUDGE1 0.002822
    ASM SLUDGE2 0.000001
    ASM SLUDGE3 0.000001
    END
  >>MASS FLOW BOUNDARIES
    >>FLUXES
      FRACTIONAL MASS FLOW SPECIFIED
      FLUXES 0.5 0.5
      END
   >>WALL BOUNDARY CONDITIONS
    PATCH NAME 'WALL_FREESURFACE'
    TAUX 0.0
    TAUY 0.0
    TAUZ 0.0
    END
   >>WALL BOUNDARY CONDITIONS
    PATCH NAME 'WALL_FLOOR'
    TAUX 0.0
    TAUY 0.0
    TAUZ 0.0
    END
>>OUTPUT OPTIONS
  >>PRINT OPTIONS
    >>WHAT
      ALL VARIABLES
    >>WHEN
      FINAL SOLUTION
      END
  >>DUMP FILE FORMAT
    FORMATTED
    END
  >>LINE GRAPH DATA
    XYZ  0.01 14.0 1.0
    EACH TIME STEP
    FILE NAME 'EXITC'
    USRDCC_CN
    END
  >>LINE GRAPH DATA
    XYZ  0.01 14.0 1.0
    EACH TIME STEP
    FILE NAME 'EXITV'
    V VELOCITY
    END
>>STOP
```

USRINT.f User areas only.

```
C
C+++++++++++++++++ USER AREA 1
++++++++++++++++++++++++++++++++++++++++
C---- AREA FOR USERS EXPLICITLY DECLARED VARIABLES
C
C+++++++++++++++++ END OF USER AREA 1
++++++++++++++++++++++++++++++++++
C
C
C+++++++++++++++++ USER AREA 2
++++++++++++++++++++++++++++++++++++++++
C---- AREA FOR USERS TO DECLARE THEIR OWN COMMON BLOCKS
C     THESE SHOULD START WITH THE CHARACTERS 'UC' TO ENSURE
C     NO CONFLICT WITH NON-USER COMMON BLOCKS
C
      COMMON
     + /UCPROP/ DENSLG,DENWAT
     + /UCGEOM/ TDIAM,TR1,TR2,TR3,TR4,TR5,TR6
     + /UCASM/ US1,US2,US3
     + /UCTAK/ ISET,USFREE,USLIM,RH,RP,CMIN
     + /UCOUT/ QRAS
     + /UCVIS/ IVIS,VISMIN,VISMAX
     + /UCBBV/ DYDX,CVIS,CBB1,CBB2,CXMIN,CXMAX
     + /UCDDE/ SHTINY,SHENOR,CPL,BETA1,BETA2
     + /UCPWR/ CPSA,CPSCCT,CPRA
     + /UCHBVS/ HBA,HBB,HBM,HBP
C
C+++++++++++++++++ END OF USER AREA 2
++++++++++++++++++++++++++++++++++
C
C
C+++++++++++++++++ USER AREA 4
++++++++++++++++++++++++++++++++++++++++
C---- TO USE THIS USER ROUTINE FIRST SET IUSED=1
C
      IUSED=1
C
C+++++++++++++++++ END OF USER AREA 4
++++++++++++++++++++++++++++++++++
C
C
C+++++++++++++++++ USER AREA 5
++++++++++++++++++++++++++++++++++++++++
C
C-----------------------------------------------------------------------
-
C  INITIALISE ALL MODEL VARIABLES FIRST
C-----------------------------------------------------------------------
-
C
C  The RAS volume flow rate is known but the RAS mass flow rate
C  is not. Have to use USRBCS to correct the RAS mass flow for
C  each time step as the mixture density varies at exit.
C
      QRAS = 0.1
C
C Influent MLSS concentration (kg/m^3)
C
      CNCIN  = 2.825
C
C Tank diameter (m)
C
      TDIAM  = 28
      TR1 = 0.15
      TR2 = 0.35
      TR3 = 0.5
      TR4 = 0.64
      TR5 = 0.78
      TR6 = 0.96
C
C  Initial blanket depth from surface
C     IBL = 1 : initialise the blanket to depth XSLG
C     IBL = 0 : don't initialise the blanket to depth XSLG
C
      IBL = 1
      XSLG = 1.9
C
C  Choose a viscosity law here
C     IVIS = 0 : Dahl Dick and Ewing (DDE)
C     IVIS = 1 : Bokil Bewtra Model (BB)
C     IVIS = 2 : Quadratic approach following Armbruster 2003
C     IVIS = 3 : Parabolic approach following Armbruster 2003
C     IVIS = 4 : Herschel Bulkley following deClerq 2003
```

```
C     IVIS = -1 : Set a constant velocity = VISMIN
C
      IVIS = -1
C
C  Choose a settling law here
C     ISET = 0 : Takacs
C     ISET = 1 : Vaccari
C     ISET = 2 : Constant settling velocity for each scalar
C
      ISET = 0
C
C-----------------------------------------------------------------
-
C  STANDARD FLUID PROPERTIES
C-----------------------------------------------------------------
-
C
C  Water and dry solid density kg/m^3
C
      DENWAT = 1000.0
      DENSLG = 1450.0
C
C  Bounds for viscosity Ns/m^2,
C  VISMIN is molecular viscosity for clear water
C
      VISMIN = 1.0E-3
      VISMAX = 20
C
C  Bounds for rate of shear strain,
C
      SHTINY = 1.0E-03
      SHENOR = 1.0E+03
C
C-----------------------------------------------------------------
-
C  COEFFICIENTS FOR SETTLING
C-----------------------------------------------------------------
-
C
C Constant settling for three slip scalars
C
      US1 = 1.0E-3
      US2 = 0.5E-3
      US3 = 0.2E-3
C
C  CONSTANTS FOR FOUR ZONE TAKACS SETTLING VELOCITY FORMULA
C  Appear in FAST2D as
C
C     RH = cset1
C     RP = cset2
C     RI = cset0     : Defines start of Zone 1
C     USFREE = vset0 : Free settling velocity of a floc
C     USLIM = vset1i : Limit on settling velocity Zone 2
C
C  Ryemeads values for 80 SSVI, 28 Feb 2004
C
      USFREE = 2.0E-3
      USLIM = 2.0E-3
      RH = 0.3785
      RP = 7.1464
      RI = 0.005
      CMIN = RI*CNCIN
C
C-----------------------------------------------------------------
-
C  FIXEC PARAMETERS FOR VISCOSITY MODEL
C-----------------------------------------------------------------
-
C
C  CONSTANTS FOR BOKIL AND BEWTRA (BB), 1972
C
C  Appear in FAST2D as
C  CBB1 = cpba : NB I don't divide by density
C  CBB2 = cpbb
C
      CBB1 = 0.00327
      CBB2 = 0.132
C
C  CONSTANTS FOR BB LINEAR INTERPOLATION SECTION
C  This bit doesn't seem to be in Fast2D
C
      CXMIN = 0.1
      CXMAX = 0.7
      UYMIN = 0.001
      UYMAX = 0.004
      DYDX = (UYMAX-UYMIN)/(CXMAX-CXMIN)
```

```
      CVIS = UYMAX-DYDX*CXMAX
C
C  CONSTANTS FOR BINGHAM PLASTIC MODEL (DDE)
C  DAHL, 1993, FOR PLASTIC VISCOSITY
C  DICK & EWING, 1967, FOR YIELD STRESS
C
C  Dahl Coefficient, 1993
C  Appears in Fast2D root and square laws
C
C     CPL = cpsb in square law
C     CPL = cprb in root law
C
      CPL = 2.473E-4
C
C  Dick and Ewing Coefficients, 1967
C  Appear in Fast2D Bingham law
C
C     BETA1 = cbma
C     BETA2 = cbmb
C
      BETA1 = 1.1E-4
      BETA2 = 0.98
C
C  Power law coefficients from Armbruster, 2003
C
      CPSA = 25.0
      CPSCCT = 4.5
      CPRA = 550.0
C
C  Herschel Bulkley coeeficients from de Clerq, 2003
C
      HBA = 9.0364E-4
      HBB = 2.49338e-4
      HBM = 169.47
      HBP = 0.7748
C
C-----------------------------------------------------------------
-
C  NOW READ IN ALL MODEL VARIABLES
C-----------------------------------------------------------------
-
C
      OPEN (UNIT=41,FILE='../MODEL.DAT',STATUS='OLD')
C
C READ THE DATA FROM FILE
C
      READ (41,FMT=*) IVIS
      READ (41,FMT=*) ISET
C
      READ (41,FMT=*) CNCIN
      READ (41,FMT=*) USFREE
      READ (41,FMT=*) RH
      READ (41,FMT=*) RP
C
      READ (41,FMT=*) TDIAM
      READ (41,FMT=*) TR1
      READ (41,FMT=*) TR2
      READ (41,FMT=*) TR3
      READ (41,FMT=*) TR4
      READ (41,FMT=*) TR5
      READ (41,FMT=*) TR6
C
      READ (41,FMT=*) US1
      READ (41,FMT=*) US2
      READ (41,FMT=*) US3
C
      READ (41,FMT=*) IBL
      READ (41,FMT=*) XSLG
C
      CLOSE (UNIT=41)
C
C
C    WRITE NUMBERS TO OUTPUT FILE
C
      WRITE(NWRITE,*)'*** MODEL INPUT DATA ***'
      WRITE(NWRITE,*)' '
      WRITE(NWRITE,*)'TANK DIAMETER (m)                =',TDIAM
      WRITE(NWRITE,*)'MLSS CONCENTRATION (kg/m^3)      =',CNCIN
      WRITE(NWRITE,*)'TAKACS Uso (m/s)                 =',USFREE
      WRITE(NWRITE,*)'TAKACS RH  (m^3/kg)              =',RH
      WRITE(NWRITE,*)'TAKACS RP  (m^3/kg)              =',RP
      WRITE(NWRITE,*)'TAKACS RP  (m^3/kg)              =',RP
      WRITE(NWRITE,*)'IVIS =',IVIS
      WRITE(NWRITE,*)'ISET =',ISET
      WRITE(NWRITE,*)' '
C
```

```
C-----------------------------------------------------------------
-
C  If requested, initialise the sludge blanket for x > XSLG to have
C  a mass fraction approaching the value expected
C-----------------------------------------------------------------
-
C
      IF (IBL.EQ.1) THEN
C
         FULL = CNCIN/1000.0
         EMPTY = 1.0E-10
         CALL GETSCA('ASM SLUDGE1',JSP1,CWORK)
C
         CALL IPALL('*','*','BLOCK','CENTRES',IPT,NPT,CWORK,IWORK)
C
C----    SET UP SLUDGE EVERYWHERE AS EMPTY
C
         DO 100 I = 1,NPT
            INODE = IPT(I)
            SCAL(INODE,1,JSP1) = EMPTY
  100    CONTINUE
C
C---- SET UP SLUDGE BLANKET
C
         CALL IPALL('*','*','BLOCK','CENTRES',IPT,NPT,CWORK,IWORK)
         DO 120 I = 1,NPT
            INODE = IPT(I)
            IF (XP(INODE).GT.XSLG) THEN
               SCAL(INODE,1,JSP1) = FULL
            ENDIF
  120    CONTINUE
C
      ENDIF
C
C+++++++++++++++++ END OF USER AREA 5
++++++++++++++++++++++++++++++++++
C
```

USRTRN.f User areas only.

```
C
C+++++++++++++++++ USER AREA 2
++++++++++++++++++++++++++++++++++++++++
C---- AREA FOR USERS TO DECLARE THEIR OWN COMMON BLOCKS
C     THESE SHOULD START WITH THE CHARACTERS 'UC' TO ENSURE
C     NO CONFLICT WITH NON-USER COMMON BLOCKS
C
      COMMON
     + /UCGEOM/ TDIAM,TR1,TR2,TR3,TR4,TR5,TR6
C
C+++++++++++++++++ END OF USER AREA 2
++++++++++++++++++++++++++++++++++
C
C
C+++++++++++++++++ USER AREA 3
++++++++++++++++++++++++++++++++++++++++
C---- AREA FOR USERS TO DIMENSION THEIR ARRAYS
C
      DIMENSION PSIV(100000),PSIP(100000)
      PARAMETER (NPROF=6)
      DIMENSION RPROF(NPROF),JPROF(NPROF)
C
C---- AREA FOR USERS TO DEFINE DATA STATEMENTS
C
C+++++++++++++++++ END OF USER AREA 3
++++++++++++++++++++++++++++++++++
C
C
C+++++++++++++++++ USER AREA 4
++++++++++++++++++++++++++++++++++++++++
C---- TO USE THIS USER ROUTINE FIRST SET IUSED=1
C
      IUSED=1
C
C+++++++++++++++++ END OF USER AREA 4
++++++++++++++++++++++++++++++++++
C
C
C+++++++++++++++++ USER AREA 5
++++++++++++++++++++++++++++++++++++++++
C
      IF (KSTEP.EQ.NSTEP) THEN
C
      CALL GETSCA('USRDCC_CN',JCNC,CWORK)
C
C========VELOCITY AND CONCENTRATION
PROFILES==========================
C
C  This code is not general and relies on BLOCK 1 being the main
tank.
C  Also relies on J in block 1 being the radial direction.
C
        CALL IPREC('BLOCK-NUMBER-1','BLOCK','CENTRES',
     +             IPT,ILEN,JLEN,KLEN,CWORK,IWORK)
C
C------ POSITION OF PROFILES
C
        TRAD = TDIAM/2.0
        RPROF(1) = TR1*TRAD
        RPROF(2) = TR2*TRAD
        RPROF(3) = TR3*TRAD
        RPROF(4) = TR4*TRAD
        RPROF(5) = TR5*TRAD
        RPROF(6) = TR6*TRAD
C
C------ FIND J LOCATION OF PROFILES
C
        WRITE(NWRITE,*) 'PROF  I  J  K '
        I=1
        K=1
        DO 10 L=1,NPROF
          DO 13 J=1,JLEN
            INODE=IP(I,J,K)
            IF(YP(INODE).GE.RPROF(L)) GO TO 14
 13       CONTINUE
 14       CONTINUE
          JPROF(L)=J
          WRITE(NWRITE,17) L,I,JPROF(L),K
 10     CONTINUE
 17     FORMAT(4I5,I10)
C
        K=1
        DO 30 L=1,NPROF
```

```
          WRITE(44,*) 'PROFILE ',L
          WRITE(44,*) 'X      Conc (g/l)'
          WRITE(45,*) 'X      Radial Vel (m/s)'
          WRITE(46,*) 'X      Axial Velocity (m/s)'
          J = JPROF(L)
          DO 20 I=1,ILEN
             INODE=IP(I,J,K)
             CONC = SCAL(INODE,1,JCNC)
             VVEL = V(INODE,1)
             UVEL = U(INODE,1)
             WRITE(44,50) XP(INODE),CONC
               WRITE(45,50) XP(INODE),VVEL
             WRITE(46,50) XP(INODE),UVEL
 20       CONTINUE
 30     CONTINUE
C
 50     FORMAT(2E12.4)
C
C===STRUCTURE FUNCTION CODE=============================================
C-----------------------------------------------------------------------
C  CALCULATE THE STREAM FUNCTION FOR A MULTI BLOCK MESH
C  AS LONG AS THE LOW J FACE OF EACH BLOCK IS A WALL OR SYMMETRY
C
C  DJB, 11/4/97
C-----------------------------------------------------------------------
C
      CALL GETSCA('USRDCC_STREAM',IUS1,CWORK)
C
      DO 150 I = 1,100000
         PSIV(I) = 0.0
         PSIP(I) = 0.0
 150  CONTINUE
C
      DO 200 IBLOCK=1,NBLOCK
C
C---- GET SIZE FOR THE BLOCK
C     NI = NUMBER OF CELLS IN I + DUMMIES (+2)
C     NJ = NUMBER OF CELLS IN J + 2
C     NK = NUMBER OF CELLS IN K + 2
C
         NI = IBLK(1,IBLOCK)
         NJ = IBLK(2,IBLOCK)
         NK = IBLK(3,IBLOCK)
         IPNBLK = IBLK(4,IBLOCK)
         NIJ = NI*NJ
C
         WRITE(NWRITE,*) 'NI ',NI
         WRITE(NWRITE,*) 'NJ ',NJ
         WRITE(NWRITE,*) 'NK ',NK
C
C---- SET THE STREAM FUNCTION TO BE ZERO ON THE LOW J WALL
C
         DO 100 I = 1,NI-1
            PSIV(I) = 0.0
 100     CONTINUE
C
C---- LOOP OVER VERTICES
C
         K = 2
         DO 102 I = 1,NI-1
            DO 103 J = 2,NJ-1
               INODE = IPNBLK-1+I+(J-1)*NI+(K-1)*NIJ
               INODC = INODE+1
               IFACE = IPFACN(INODC,4)
               IF (INODE.GE.100000) THEN
                  WRITE(NWRITE,*) 'DIMENSION OF PSIV EXCEEDED'
                  CALL F3DSTP('USRTRN')
               ENDIF
C
C---- ONLY WORKS BECAUSE CONV IS ON THE LOW I FACE
C
               PSIV(INODE) = PSIV(INODE-NI)+CONV(IFACE,1)
C              WRITE(NWRITE,*) I,J,INODC,IFACE,PSIV(INODE)
 103        CONTINUE
 102     CONTINUE
C
C---- NOW INTERPOLATE TO THE CELL CENTRES
C
         WRITE (NWRITE,*) 'NOW INTERPOLATE TO THE CELL CENTRES'
         K = 2
         DO 120 I=2,NI-1
            DO 110 J=2,NJ-1
               INODE = IPNBLK-1+I+(J-1)*NI+(K-1)*NIJ
               PSIP(INODE) = 0.25*(PSIV(INODE)+PSIV(INODE-1)
     +                           +PSIV(INODE-NI)+PSIV(INODE-NI-1))
C              WRITE(NWRITE,*) INODE,PSIP(INODE)
```

```
            SCAL(INODE,1,IUS1) = PSIP(INODE)
 110        CONTINUE
 120      CONTINUE
C
 200   CONTINUE
C
       DO 300 IBDRY=1,NBDRY
          ICELL=IPNODB(IBDRY,1)
          IBNODE=NCELL+IBDRY
          IDUM=IPNODB(IBDRY,2)
C SET BOUNDARY NODE
C
          SCAL(IBNODE,1,IUS1)=SCAL(ICELL,1,IUS1)
C SET DUMMY CELL
C
          SCAL(IDUM,1,IUS1)=SCAL(ICELL,1,IUS1)
   300 CONTINUE
C
C
C===MASS FLOW INFLUENT=========================================
C
       IPHASE=1
C
       CALL IPALL('INLET_INFLUENT','INLET','PATCH','CENTRES',
      +           IPT,NPT,CWORK,IWORK)
       FLIN=0.0
       ARIN=0.0
       DO 900 I=1,NPT
          INODE = IPT(I)
          IBDRY = INODE-NCELL
          IFACE = IPFACB(IBDRY)
          NWL = IPNODB(IBDRY,3)
          SGN = SGNWL(NWL)
          AREAX = AREA(IFACE,1)
          AREAY = AREA(IFACE,2)
          AREAZ = AREA(IFACE,3)
          AREAM = SQRT(AREAX**2+AREAY**2+AREAZ**2)
          AMDOT=CONV(IFACE,IPHASE)*SGN
          FLIN=FLIN+AMDOT
          ARIN=ARIN+AREAM
   900 CONTINUE
C
C===MASS FLOW RAS==============================================
C
       CALL IPALL('OUTLET_RAS','*',
      +           'PATCH','CENTRES',IPT,NPT,CWORK,IWORK)
       FLRAS=0.0
       ARRAS=0.0
       DO 905 I=1,NPT
          INODE = IPT(I)
          IBDRY = INODE-NCELL
          IFACE = IPFACB(IBDRY)
          NWL = IPNODB(IBDRY,3)
          SGN = SGNWL(NWL)
          AMDOT=CONV(IFACE,IPHASE)*SGN
          AREAX = AREA(IFACE,1)
          AREAY = AREA(IFACE,2)
          AREAZ = AREA(IFACE,3)
          AREAM = SQRT(AREAX**2+AREAY**2+AREAZ**2)
          FLRAS=FLRAS+AMDOT
          ARRAS=ARRAS+AREAM
   905 CONTINUE
C
C===MASS FLOW EFFLUENT=========================================
C
       CALL IPALL('PRESS_EFFLUENT','*',
      +           'PATCH','CENTRES',IPT,NPT,CWORK,IWORK)
       FLEFF=0.0
       AREFF=0.0
       DO 910 I=1,NPT
          INODE = IPT(I)
          IBDRY = INODE-NCELL
          IFACE = IPFACB(IBDRY)
          NWL = IPNODB(IBDRY,3)
          SGN = SGNWL(NWL)
          AMDOT=CONV(IFACE,IPHASE)*SGN
          AREAX = AREA(IFACE,1)
          AREAY = AREA(IFACE,2)
          AREAZ = AREA(IFACE,3)
          AREAM = SQRT(AREAX**2+AREAY**2+AREAZ**2)
          FLEFF=FLEFF+AMDOT
          AREFF=AREFF+AREAM
   910 CONTINUE
C
C===MASS AVERAGE CONCENTRATION AT INFLUENT ===============
C
```

```
      CALL IPALL('INLET_INFLUENT','INLET',
     +           'PATCH','CENTRES',IPT,NPT,CWORK,IWORK)
      CNCIN=0.0
      DO 915 I=1,NPT
         INODE = IPT(I)
         IBDRY = INODE-NCELL
         INODE1 = IPNODB(IBDRY,1)
         IFACE = IPFACB(IBDRY)
         NWL = IPNODB(IBDRY,3)
         SGN = SGNWL(NWL)
         AMDOT=CONV(IFACE,IPHASE)*SGN
         CNCIN=CNCIN+AMDOT*SCAL(INODE,1,JCNC)/FLIN
  915 CONTINUE
C
C====MASS AVERAGE CONCENTRATION AT RAS ====================
C
      CALL IPALL('OUTLET_RAS','*',
     +           'PATCH','CENTRES',IPT,NPT,CWORK,IWORK)
      CNCRAR=0.0
      DO 920 I=1,NPT
         INODE = IPT(I)
         IBDRY = INODE-NCELL
         INODE1 = IPNODB(IBDRY,1)
         IFACE = IPFACB(IBDRY)
         NWL = IPNODB(IBDRY,3)
         SGN = SGNWL(NWL)
         AMDOT=CONV(IFACE,IPHASE)*SGN
         CNCRAS=CNCRAS+AMDOT*SCAL(INODE,1,JCNC)/FLRAS
  920 CONTINUE
C
C
C====MASS AVERAGE CONCENTRATION AT EFFLUENT ============
C
      CALL IPALL('PRESS_EFFLUENT','*',
     +           'PATCH','CENTRES',IPT,NPT,CWORK,IWORK)
      CNCEFF=0.0
      DO 930 I=1,NPT
         INODE = IPT(I)
         IBDRY = INODE-NCELL
         INODE1 = IPNODB(IBDRY,1)
         IFACE = IPFACB(IBDRY)
         NWL = IPNODB(IBDRY,3)
         SGN = SGNWL(NWL)
         AMDOT=CONV(IFACE,IPHASE)*SGN
         CNCEFF=CNCEFF+AMDOT*SCAL(INODE,1,JCNC)/FLEFF
  930 CONTINUE
C
C    WRITE NUMBERS TO OUTPUT FILE
C
         WRITE(NWRITE,*)'*** MASS BALANCE ***'
         WRITE(NWRITE,*)' '
         WRITE(NWRITE,*)'AREA IN (m^2)                    =',ARIN
         WRITE(NWRITE,*)'INFLOW (kg/s)                    =',FLIN
         WRITE(NWRITE,*)'CONCENTRATION INFLUENT (mg/l)
=',CNCIN*1000
         WRITE(NWRITE,*)'AREA RAS (m^2)                   =',ARRAS
         WRITE(NWRITE,*)'OUTFLOW RAS(kg/s)                =',FLRAS
         WRITE(NWRITE,*)'CONCENTRATION RAS (mg/l)
=',CNCRAS*1000
         WRITE(NWRITE,*)'AREA EFFLUENT (m^2)              =',AREFF
         WRITE(NWRITE,*)'OUTFLOW EFFLUENT(kg/s)           =',FLEFF
         WRITE(NWRITE,*)'CONCENTRATION EFFLUENT (mg/l)
=',CNCEFF*1000
         WRITE(NWRITE,*)' '
C
      ENDIF
C
C---- END OF POST PROCESSING
C
C+++++++++++++++++ END OF USER AREA 5
++++++++++++++++++++++++++++++++++++
C
```

USRDEN.f User areas only.

```
C
C+++++++++++++++++ USER AREA 2
++++++++++++++++++++++++++++++++++++++++
C---- AREA FOR USERS TO DECLARE THEIR OWN COMMON BLOCKS
C     THESE SHOULD START WITH THE CHARACTERS 'UC' TO ENSURE
C     NO CONFLICT WITH NON-USER COMMON BLOCKS
C
      COMMON
     + /UCPROP/ DENSLG,DENWAT
C
C+++++++++++++++++ END OF USER AREA 2
++++++++++++++++++++++++++++++++++
C
C
C+++++++++++++++++ USER AREA 4
++++++++++++++++++++++++++++++++++++++++
C---- TO USE THIS USER ROUTINE FIRST SET IUSED=1
C
      IUSED=1
C
C+++++++++++++++++ END OF USER AREA 4
++++++++++++++++++++++++++++++++++
C
C
C+++++++++++++++++ USER AREA 5
++++++++++++++++++++++++++++++++++++++++
C
C     Modify density according to Zhou - McCorquadale model
C
C     Changes in density expected to be small but these
C     have a significant effect on the flow.
C
      CALL GETSCA('ASM SLUDGE1',JSP1,CWORK)
      RREF = DENWAT
      PSG = DENSLG/DENWAT
C
C-----FOR INCOMPRESSIBLE OR WEAKLY COMPRESSIBLE MODELS IT IS
C     GENERALLY SUFFICIENT TO SET THE DENSITY ON INTERNAL NODES
C     AND INLET BOUNDARY NODES ONLY.
C     FOR WEAKLY COMPRESSIBLE FLOWS BUT NOT INCOMPRESSIBLE FLOWS
C     DRHODP SHOULD BE SET TO ZERO AT THESE NODES.
C     FOR WEAKLY COMPRESSIBLE BUOYANT FLOWS IT IS NECESSARY TO SET
C     THE DENSITY AT WALL NODES.
C
      DO 400 IPHASE=1,NPHASE
C
         CALL IPALL('*','*','BLOCK','CENTRES',IPT,NPT,CWORK,IWORK)
         DO 300 I=1,NPT
            INODE=IPT(I)
            DENN(INODE,IPHASE) =
     +        RREF+SCAL(INODE,1,JSP1)*DEN(INODE,IPHASE)*(1-(1/PSG))
            DRHODP(INODE,IPHASE) = 0.0
300      CONTINUE
C
         CALL
IPALL('*','INLET','PATCH','CENTRES',IPT,NPT,CWORK,IWORK)
         DO 310 I=1,NPT
            INODE=IPT(I)
            DENN(INODE,IPHASE) =
     +        RREF+SCAL(INODE,1,JSP1)*DEN(INODE,IPHASE)*(1-(1/PSG))
            DRHODP(INODE,IPHASE) = 0.0
310      CONTINUE
C
C OUTLETS AND PRESSURE BOUNDARIES ARE CORRECTED AUTOMATICALLY UNLESS
C FLOW IS ENTERING THE DOMAIN THROUGH SUCH BOUNDARIES. IN THAT CASE
C THE EQUIVALENT OF THE INLET METHOD DESCRIBED ABOVE SHOULD BE USED.
C
C FOR WEAKLY COMPRESSIBLE BUOYANT FLOWS, THE EQUIVALENT OF THE INLET
C METHOD DESCRIBED ABOVE SHOULD BE USED AT WALLS. WALL VALUES ARE NOT
C USED IN BUOYANT CALCULATIONS BUT ARE USED FOR GRAPHICS.
C
         CALL IPALL('*','WALL','PATCH','CENTRES',IPT,NPT,CWORK,IWORK)
         DO 320 I=1,NPT
            INODE=IPT(I)
            DENN(INODE,IPHASE) =
     +        RREF+SCAL(INODE,1,JSP1)*DEN(INODE,IPHASE)*(1-(1/PSG))
            DRHODP(INODE,IPHASE) = 0.0
320      CONTINUE
400   CONTINUE
C
C
C+++++++++++++++++ END OF USER AREA 5
++++++++++++++++++++++++++++++++++
```

USRSLP.f User areas only.

```
C
C+++++++++++++++++ USER AREA 1
++++++++++++++++++++++++++++++++++++++++
C---- AREA FOR USERS EXPLICITLY DECLARED VARIABLES
C
      LOGICAL LFIRST
C
C+++++++++++++++++ END OF USER AREA 1
++++++++++++++++++++++++++++++++++
C
C
C+++++++++++++++++ USER AREA 2
++++++++++++++++++++++++++++++++++++++++
C---- AREA FOR USERS TO DECLARE THEIR OWN COMMON BLOCKS
C     THESE SHOULD START WITH THE CHARACTERS 'UC' TO ENSURE
C     NO CONFLICT WITH NON-USER COMMON BLOCKS
C
      COMMON
     + /UCPROP/ DENSLG,DENWAT
     + /UCTAK/ ISET,USFREE,USLIM,RH,RP,CMIN
     + /UCASM/ US1,US2,US3
C
C+++++++++++++++++ END OF USER AREA 2
++++++++++++++++++++++++++++++++++
C
C
C+++++++++++++++++ USER AREA 3
++++++++++++++++++++++++++++++++++++++++
C---- AREA FOR USERS TO DIMENSION THEIR ARRAYS
C
C---- AREA FOR USERS TO DEFINE DATA STATEMENTS
C
      DATA LFIRST /.TRUE./
C
C+++++++++++++++++ END OF USER AREA 3
++++++++++++++++++++++++++++++++++
C

C
```

```
C+++++++++++++++++ USER AREA 4
++++++++++++++++++++++++++++++++++++++++
C---- TO USE THIS USER ROUTINE FIRST SET IUSED=1
C
      IUSED=1
C
C+++++++++++++++++ END OF USER AREA 4
++++++++++++++++++++++++++++++++++
C

C
C+++++++++++++++++ USER AREA 5
++++++++++++++++++++++++++++++++++++++++
C
C--SET SLIP VELOCITY FOR ALL ALGEBRAIC SLIP SCALARS
C
C  SCALAR EQUATION NUMBERS FOR SLIP MODEL SPECIES
      CALL GETSCA('ASM SLUDGE1',JSP1,CWORK)
      CALL GETSCA('ASM SLUDGE2',JSP2,CWORK)
      CALL GETSCA('ASM SLUDGE3',JSP3,CWORK)
      CALL GETSCA('USRDCC_CN',JCNC,CWORK)
      CALL GETSCA('USRDCC_VS',JVS1,CWORK)
C
C  LOOP OVER ALL ASM SPECIES
      DO 300 ISP = 1,NASMSP
C
C  SCALAR NUMBER OF SPECIES
        ISC = IWORK(JASMSP+ISP-1)
C
C---- Simple model with constant fall velocity on each scalar
C
        IF (ISET.EQ.2) THEN
          IF(ISC.EQ.JSP1) UMAX = US1
          IF(ISC.EQ.JSP2) UMAX = US2
          IF(ISC.EQ.JSP3) UMAX = US3
          DO 10 INODE = 1,NCELL
            SLIPX(INODE,ISP) = UMAX
            SLIPY(INODE,ISP) = 0.0
            SLIPZ(INODE,ISP) = 0.0
 10       CONTINUE
C
C---- Vaccari model goes here, currently Takacs
C
```

```
        ELSE IF (ISET.EQ.1) THEN
C
           DO 50 INODE = 1,NCELL
C
              CONC = SCAL(INODE,1,JSP1)*DEN(INODE,1)
              CDIFF = CONC-CMIN
              AA = EXP(-RH*CDIFF)
              BB = EXP(-RP*CDIFF)
              US = USFREE*(AA-BB)
              UMAX = MIN(US,USLIM)
              SLIPX(INODE,ISP) = UMAX
              SLIPY(INODE,ISP) = 0.0
              SLIPZ(INODE,ISP) = 0.0
C
C  Set graphic scalars for viewing in post processor.
C
              SCAL(INODE,1,JCNC) = CONC
              SCAL(INODE,1,JVS1) = US
   50       CONTINUE
C
C---- Takacs model
C
        ELSE IF (ISET.EQ.0) THEN
C
           DO 100 INODE = 1,NCELL
C
              CONC = SCAL(INODE,1,JSP1)*DEN(INODE,1)
              IF (CONC.GT.CMIN) THEN
                 CDIFF = CONC-CMIN
                 AA = EXP(-RH*CDIFF)
                 BB = EXP(-RP*CDIFF)
                 US = USFREE*(AA-BB)
                 UMAX = MIN(US,USLIM)
                 SLIPX(INODE,ISP) = UMAX
                 SLIPY(INODE,ISP) = 0.0
                 SLIPZ(INODE,ISP) = 0.0
C
C  Set graphic scalars for viewing in post processor.
C
                 SCAL(INODE,1,JCNC) = CONC
                 SCAL(INODE,1,JVS1) = US
              ELSE
                 SLIPX(INODE,ISP) = 0.0
                 SLIPY(INODE,ISP) = 0.0
                 SLIPZ(INODE,ISP) = 0.0
                 SCAL(INODE,1,JCNC) = CMIN
                 SCAL(INODE,1,JSP1) = CMIN/1000
                 SCAL(INODE,1,JVS1) = 0.0
              ENDIF
C
  100       CONTINUE
C
        ENDIF
C
  300 CONTINUE

C
C+++++++++++++++++ END OF USER AREA 5
++++++++++++++++++++++++++++++++++
C
```

USRMVS.f User areas only.

```
C
C+++++++++++++++++ USER AREA 2
++++++++++++++++++++++++++++++++++++++++
C---- AREA FOR USERS TO DECLARE THEIR OWN COMMON BLOCKS
C     THESE SHOULD START WITH THE CHARACTERS 'UC' TO ENSURE
C     NO CONFLICT WITH NON-USER COMMON BLOCKS
C
      COMMON
     + /UCPROP/ DENSLG,DENWAT
     + /UCVIS/ IVIS,VISMIN,VISMAX
     + /UCBBV/ DYDX,CVIS,CBB1,CBB2,CXMIN,CXMAX
     + /UCDDE/ SHTINY,SHENOR,CPL,BETA1,BETA2
     + /UCPWR/ CPSA,CPSCCT,CPRA
     + /UCHBVS/ HBA,HBB,HBM,HBP
C
C+++++++++++++++++ END OF USER AREA 2
++++++++++++++++++++++++++++++++++
C
C
C+++++++++++++++++ USER AREA 3
++++++++++++++++++++++++++++++++++++++++
C---- AREA FOR USERS TO DIMENSION THEIR ARRAYS
C
      DIMENSION RMW(5),RMF(5),RMU(5),PHI(5,5)
      DIMENSION TC(5),PC(5),ETA(5)
C---- AREA FOR USERS TO DEFINE DATA STATEMENTS
C
C+++++++++++++++++ END OF USER AREA 3
++++++++++++++++++++++++++++++++++
C
C
C+++++++++++++++++ USER AREA 4
++++++++++++++++++++++++++++++++++++++++
C---- TO USE THIS USER ROUTINE FIRST SET IUSED=1
C
      IUSED=1
C
C+++++++++++++++++ END OF USER AREA 4
++++++++++++++++++++++++++++++++++
C
C
C+++++++++++++++++ USER AREA 5
++++++++++++++++++++++++++++++++++++++++
C
      CALL GETSCA('USRDCC_LAMVIS',ILMV,CWORK)
      CALL GETSCA('ASM SLUDGE1',JSP1,CWORK)
      CALL GETSCA('USRDCC_CN',JCNC,CWORK)
      CALL GETSCA('SHEAR RATE',JSHEAR,CWORK)
       CALL GETSCA('USRDCC_VISP',JVISP,CWORK)
       CALL GETSCA('USRDCC_YLDT',JYLDT,CWORK)
      CALL GETSCA('USRDCC_GSCAL',JTCG,CWORK)
C
      URF=0.2
C
C  USE IPALL TO FIND 1D ADDRESSES OF ALL CELL CENTRES
      CALL IPALL('*','*','BLOCK','CENTRES',IPT,
     +     NPT,CWORK,IWORK)
C
C  LOOP OVER ALL INTERIOR CELLS
      DO 110 I=1,NCELL
C  USE ARRAY IPT TO GET ADDRESS
         INODE=IPT(I)
C
C---- GET AND BOUND THE RATE OF SHEAR STRAIN, SHRATE
C
         SHRATE = SCAL(INODE,1,JSHEAR)
         SHRATE = MAX(SHRATE,SHTINY)
         SHRATE = MIN(SHRATE,SHENOR)
C
C---- ED stores OMEGA for the k-w model
C
C---- CORRECTION 25/9/03 EPSILON = K * OMEGA
C
         EPSILON=TE(INODE,1)*ED(INODE,1)
         SCAL(INODE,1,JTCG) =
     +      SQRT(DEN(INODE,1)*EPSILON/MAX(VISMOL(INODE,1),VISMIN))
C
C---- Set cell viscosity according to chosen relationship
C
         CONC = SCAL(INODE,1,JSP1)*DEN(INODE,1)
C
C---- Herschel Bulkley law following de Clerq 2003
C
```

```
        IF (IVIS.EQ.4) THEN
            CNCV = MIN(CONC,30.0)
          COEFK = VISMIN+HBB*CNCV**2
          YLDT = HBA*CNCV**2
          AA = (YLDT/SHRATE)*(1-EXP(-HBM*SHRATE))
          VISC = AA + COEFK*SHRATE**(HBP-1)
           SCAL(INODE,1,JYLDT) = YLDT
           SCAL(INODE,1,JVISP) = COEFK
C
C---- Square law following Armbruster 2003
C
        ELSE IF (IVIS.EQ.3) THEN
           IF (CONC.GT.CPSCCT) THEN
              VISC = CPSA*CPL*(CONC-CPSCCT)**2
           ELSE
              VISC = VISMIN
           ENDIF
C
C---- Square root law following Armbruster 2003
C
        ELSE IF (IVIS.EQ.2) THEN
           IF (CONC.GT.CPSCCT) THEN
              VISC = CPRA*CPL*(CONC-CPSCCT)**0.5
           ELSE
              VISC = VISMIN
           ENDIF
C
C---- Bokil and Bewtra
C
        ELSE IF (IVIS.EQ.1) THEN
           IF (CONC.LE.CXMIN) THEN
              VISC = VISMIN
           ELSE IF (CONC.LE.CXMAX) THEN
              VISC = DYDX*CONC+CVIS
           ELSE
              VISC = CBB1*10**(CBB2*CONC)
           END IF
C
C---- Bingham Plastic followind Dahl, Dick and Ewing, Lakehal 1999.
C
        ELSE IF (IVIS.EQ.0) THEN
            CNCV = MIN(CONC,30.0)
          COEFK = VISMIN+CPL*CNCV**2
          YLDT  = BETA1*EXP(BETA2*CNCV)
          VISC = YLDT/SHRATE + COEFK
           SCAL(INODE,1,JYLDT) = YLDT
           SCAL(INODE,1,JVISP) = COEFK
        ELSE
          VISC = VISMIN
        ENDIF
C
C---- Under relax the viscosity if needed
C
         VISNEW=MIN(VISC,VISMAX)
          VISOLD=SCAL(INODE,1,ILMV)
         VISMOL(INODE,1)=URF*VISNEW+(1-URF)*VISOLD
          SCAL(INODE,1,ILMV) = VISMOL(INODE,1)
C
  110 CONTINUE
C
C---- END OF EXAMPLE




C+++++++++++++++++ END OF USER AREA 5
++++++++++++++++++++++++++++++++++++
C
```

APPENDIX C

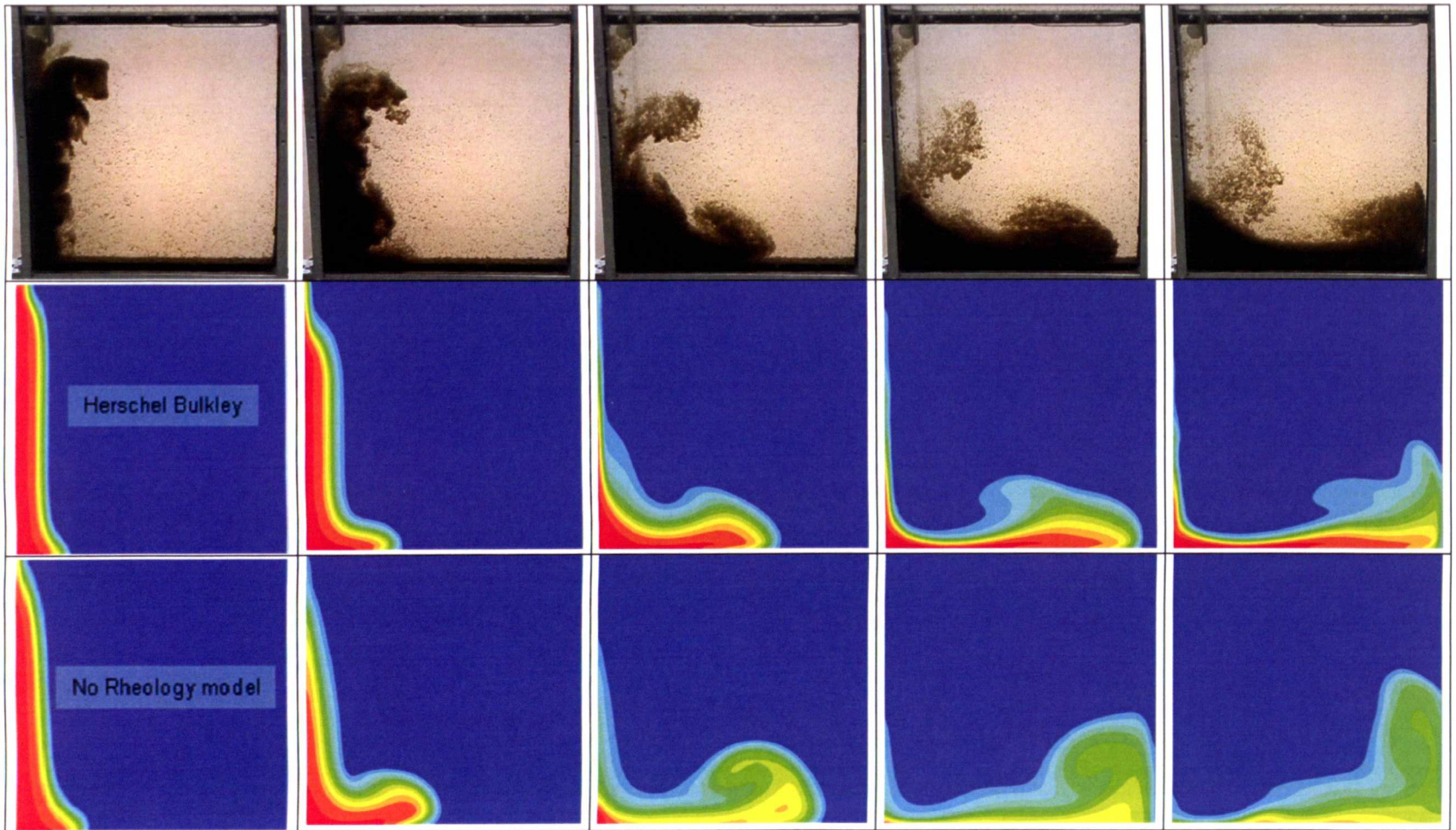

2 Seconds	6 Seconds	10 Seconds	14 Seconds	18 Seconds

Figure C1: Comparison of the Herschel Bulkley and No Reheology models for the Lock Exchange Experiment, Chapter 5.

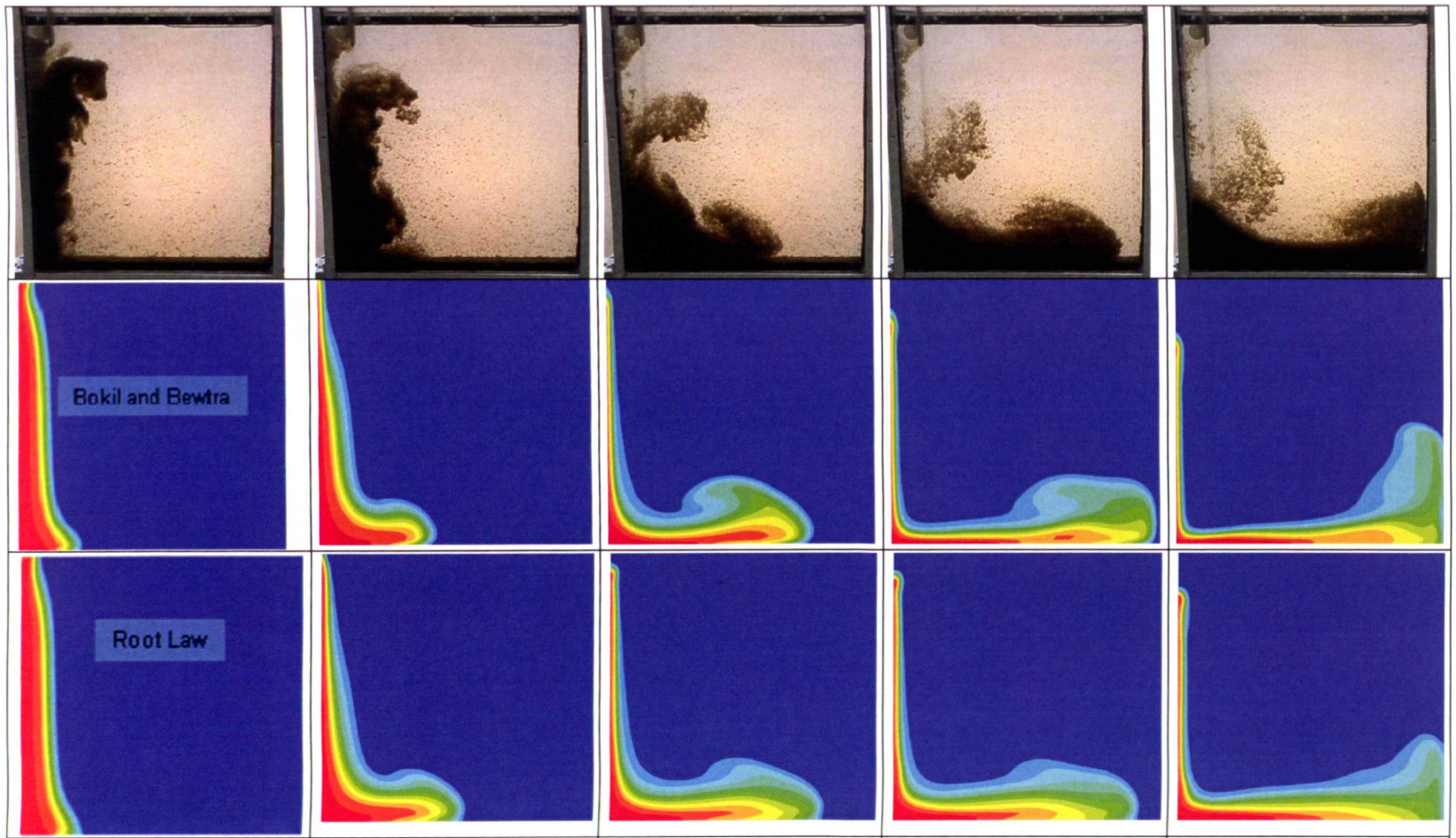

Figure C2: Comparison of the Bokil Bewtrea and Power Law Reheology models for the Lock Exchange Experiment, Chapter 5

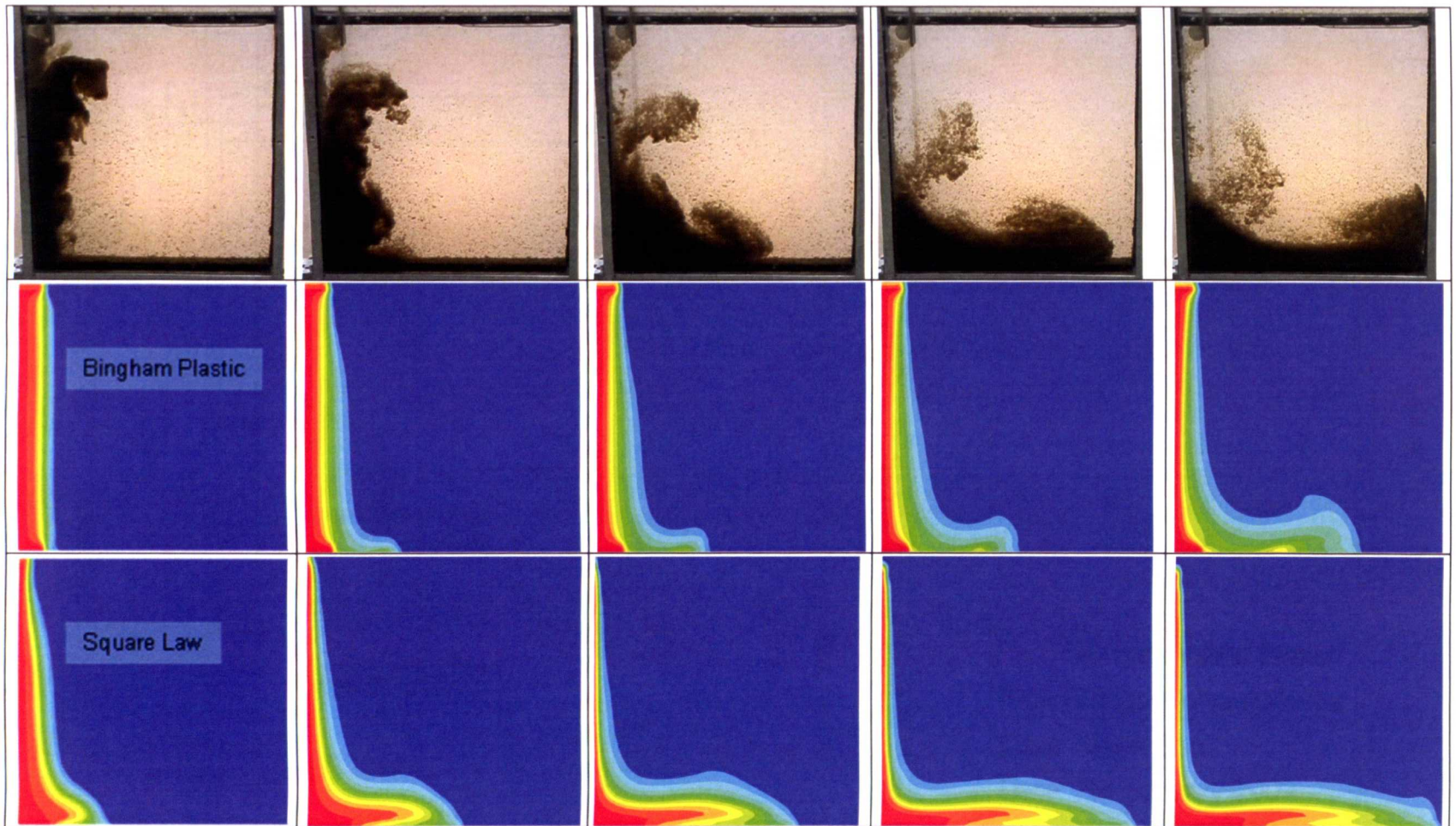

Figure C3: Comparison of the Bingham Plastic and Square Law Rheology models for the Lock Exchange Experiment, Chapter 5. The Bingham model causes the sludge to stick to the stationary wall because of unrealistic viscosity at very low shear.

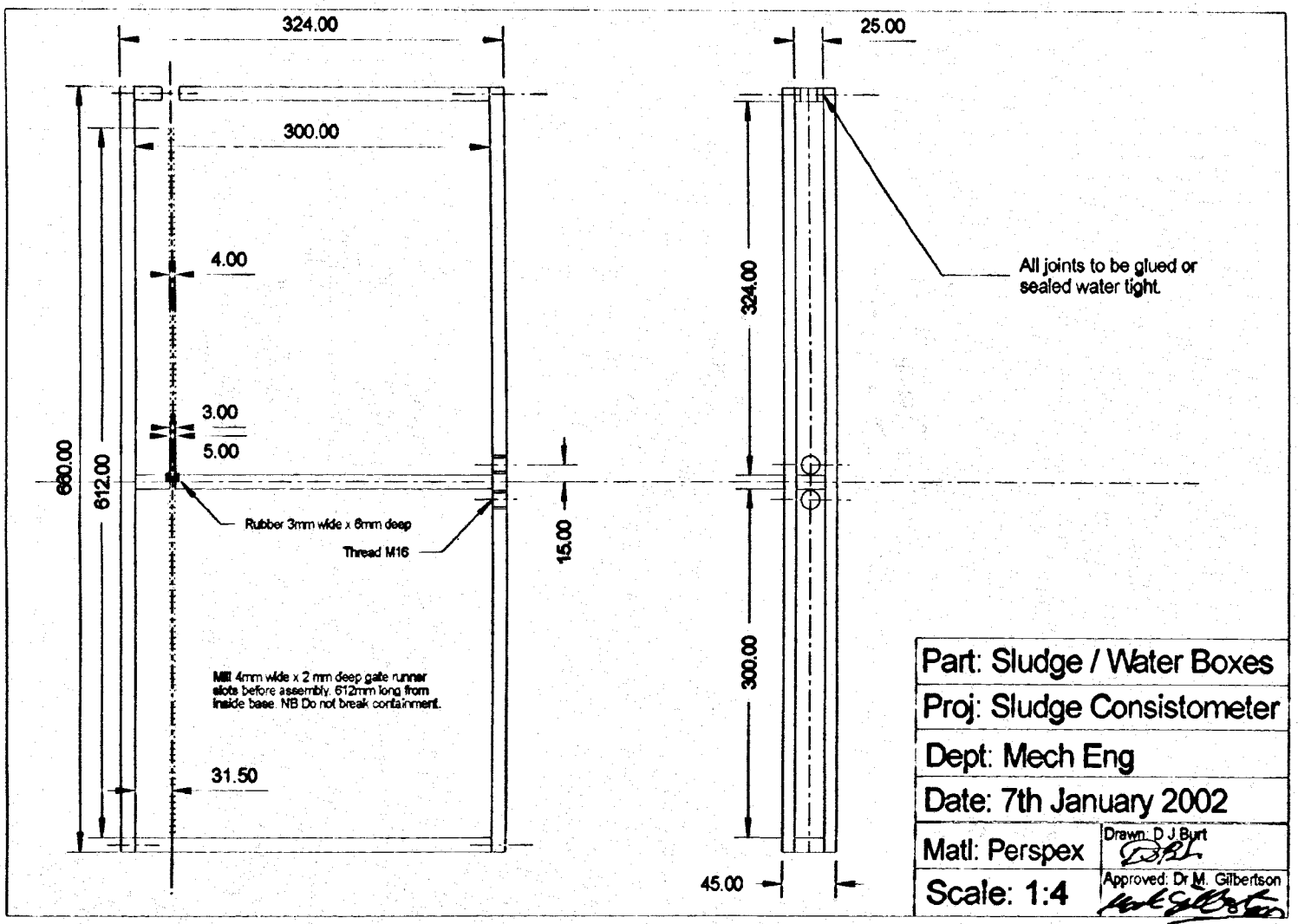
324.00
300.00
4.00
3.00
5.00
680.00
612.00
Rubber 3mm wide x 6mm deep
Thread M16
15.00
Mill 4mm wide x 2 mm deep gate runner slots before assembly. 612mm long from inside base. NB Do not break containment.
31.50
25.00
324.00
All joints to be glued or sealed water tight.
300.00
45.00
Part: Sludge / Water Boxes
Proj: Sludge Consistometer
Dept: Mech Eng
Date: 7th January 2002
Matl: Perspex
Drawn: D J Burt
Scale: 1:4
Approved: Dr M. Gilbertson

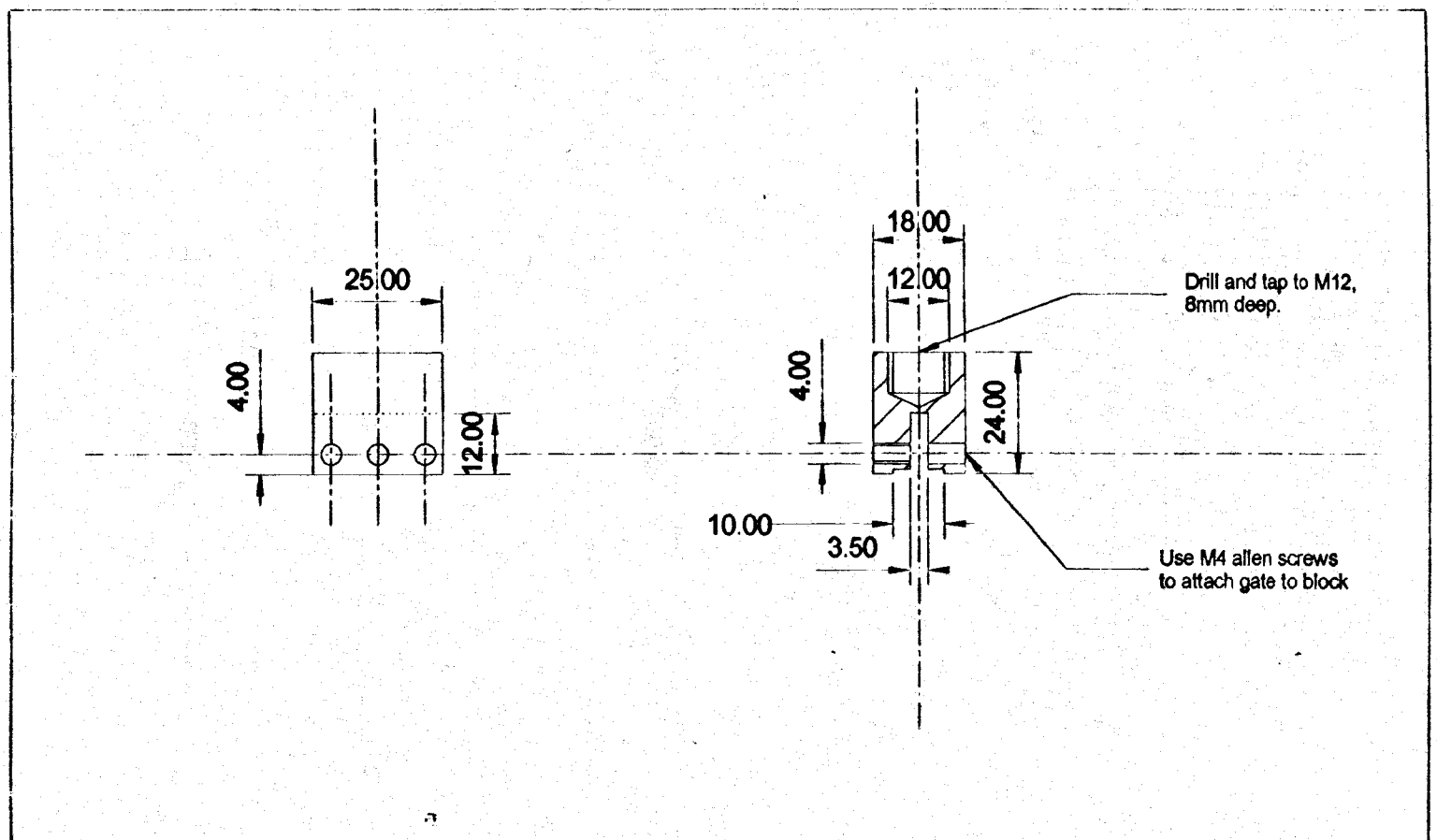

Drawn: D J Burt	Matl: Brass	Dept: Mechanical Engineering	Proj: Sludge Consistometer
Approved: Dr M Gilbertson	Scale: 1:1	Part: Gate Block	Date: 7th January 2002

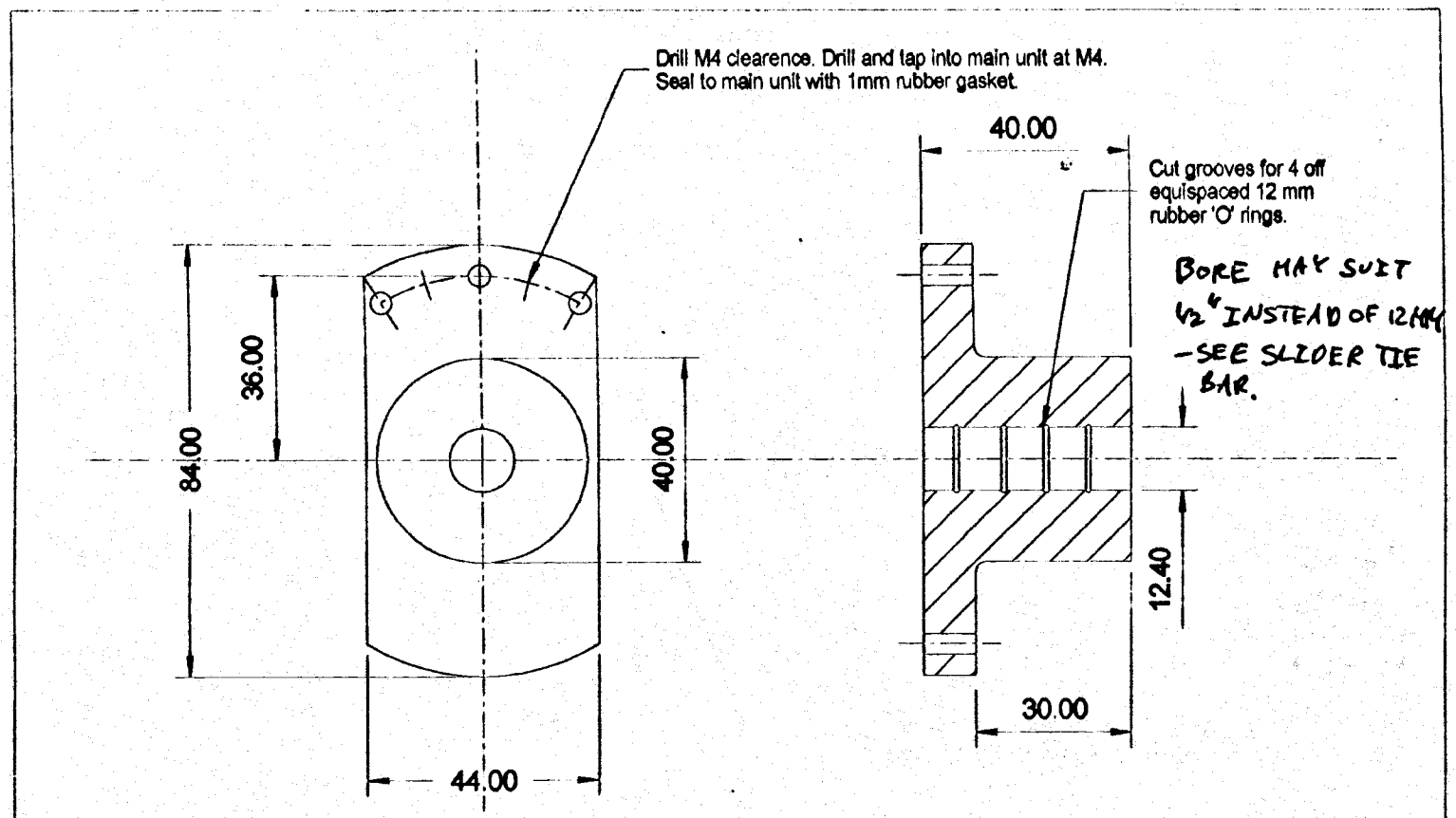
Drill M4 clearence. Drill and tap into main unit at M4.
Seal to main unit with 1mm rubber gasket.
40.00
Cut grooves for 4 off equispaced 12 mm rubber 'O' rings.
BORE MAY SUIT ½" INSTEAD OF 12MM -SEE SLIDER TIE BAR.
84.00
36.00
40.00
12.40
30.00
44.00
Aluminium
Drawn: R J Burt
Approved: Dr M Gilbertson
Matl: ~~S.Steel~~
Scale: 1:1
Dept: Mechanical Engineering
Part: Slider Seal Block
Proj: Sludge Consistometer
Date: 7th January 2002

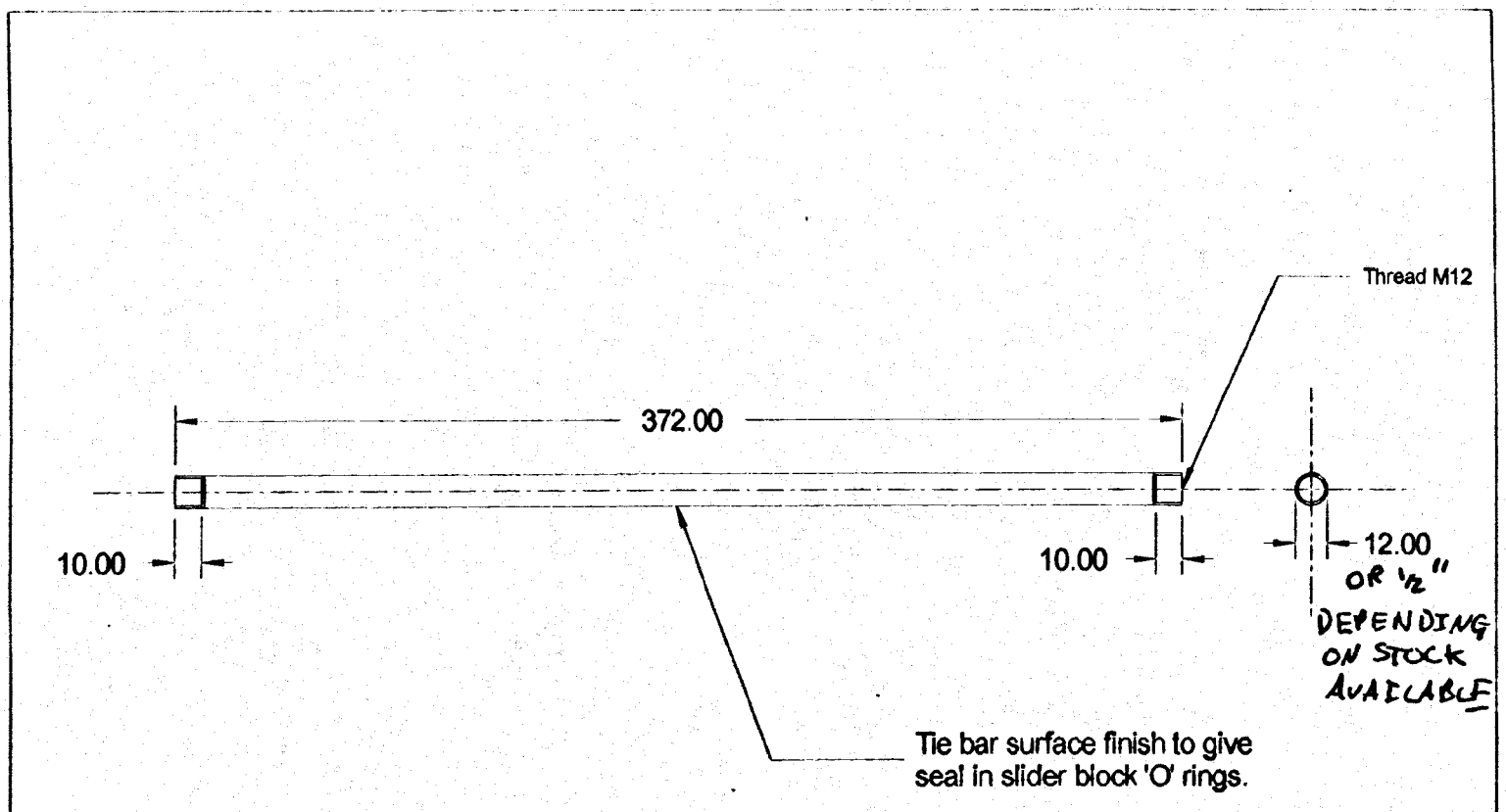

Drawn D J Burt	Matl: S.Steel	Dept: Mechanical Engineering	Proj: Sludge Consistometer
Approved Dr M Gilbertson	Scale: 1:2	Part: Slider Tie Bar	Date: 7th January 2002

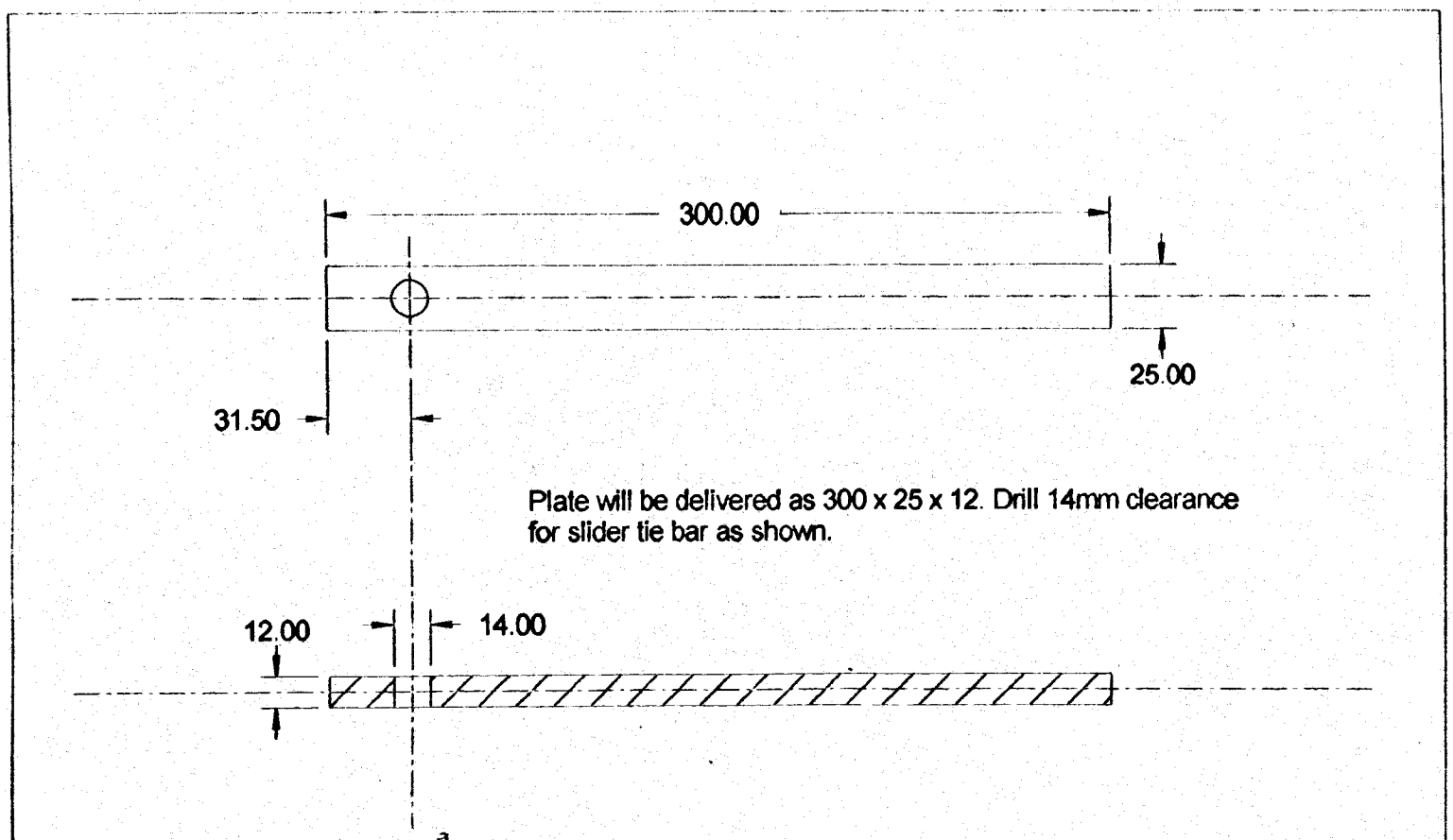
300.00
25.00
31.50
Plate will be delivered as 300 x 25 x 12. Drill 14mm clearance for slider tie bar as shown.
12.00
14.00
Drawn: D J Burt
Approved: Dr M. Stephenson
Matl: Perspex
Scale: 1:2
Dept: Mechanical Engineering
Top plate
Proj: Sludge Consistometer
Date: 7th January 2002

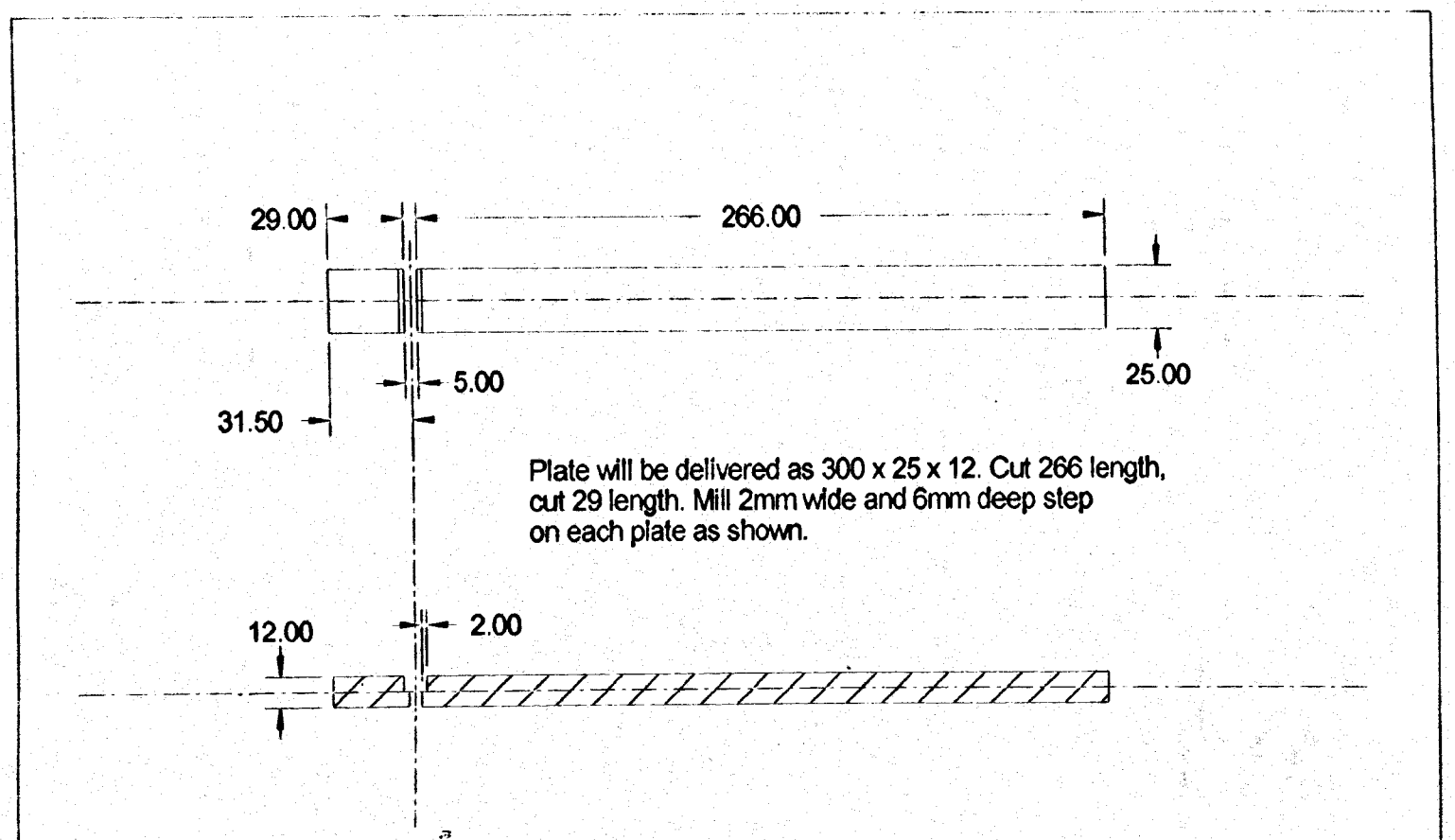
29.00
266.00
25.00
5.00
31.50
Plate will be delivered as 300 x 25 x 12. Cut 266 length, cut 29 length. Mill 2mm wide and 6mm deep step on each plate as shown.
12.00
2.00
Drawn: D J Burt
Approved: Dr M Gilbertson
Matl: Perspex
Scale: 1:2
Dept: Mechanical Engineering
Dividing plate
Proj: Sludge Consistometer
Date: 7th January 2002

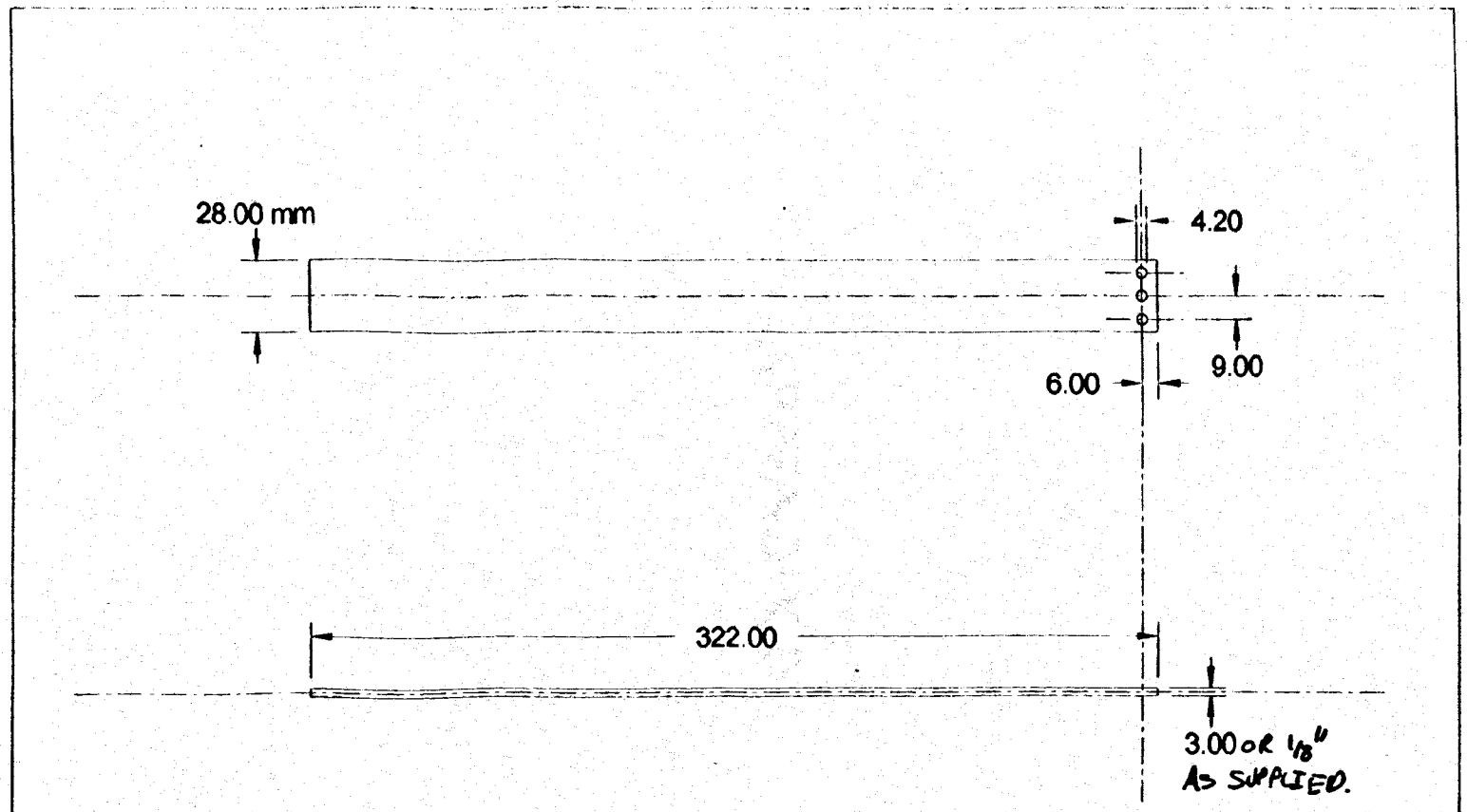

Drawn: D.J.Burt	Matl: Brass	Dept: Mechanical Engineering	Proj: Sludge Consistometer
Approved: Dr.M.Gibertson	Scale: 1:2	Part: Sliding Gate	Date: 7th January 2002

APPENDIX D

Depth measured below TWL (mm)	Location [mm], U veocity [cm/s] and standard deviation (STDEV)											
	Stilling Well		A		B		C		D		E	
	U [cm/s]	STDEV	U [cm/s]	STDEV	U [cm/s]	STDEV	U [cm/s]	STDEV	U [cm/s]	STDEV	U [cm/s]	STDEV
200	-4.1884	1.2529	-0.3590	0.2559	-0.4317	0.4083	-0.0124	0.3871	0.5208	0.4123	-0.0588	0.3201
400	0.7973	1.3625	0.0050	0.3032	-0.3660	0.2372	-0.1290	0.3243	0.1330	0.2808	-0.3833	0.3136
600	2.4031	1.1814	-0.2504	0.4246	-0.4916	0.2113	-0.2991	0.3593	-0.1581	0.3023	-0.4759	0.3357
800	1.6053	1.3999	-0.4725	0.5052	-0.5043	0.2549	-0.4651	0.2149	-0.0626	0.2647	-0.0437	0.3339
1000	0.9557	1.6270	-1.3646	0.3860	-0.8121	0.2103	-0.9963	0.2975	0.1642	0.3554	0.2078	0.2228
1100									1.1763	0.6574	0.4760	0.4420
1200	2.8146	1.4023	-1.7412	0.3221	-1.5128	0.2569	0.3599	0.8002	0.2312	0.5238	0.8600	0.4083
1300									-0.0473	0.4477	0.6257	0.5117
1400	3.5460	1.4300	-1.2594	0.6682	-1.8315	0.2905	-0.0807	0.4437	-0.4402	0.4860	0.8754	0.7065
1500									-0.5235	0.4893	0.0551	0.5178
1600	3.5606	1.4939	1.6898	1.3064	-1.3812	0.3801	-0.0786	0.7113	1.3471	0.6275	0.2742	0.5886
1700									1.7620	1.1346	-1.2296	0.4437
1800	4.3930	1.0310	2.3894	0.9221	2.2163	1.4363	1.6280	0.8057	0.2541	0.6495	-0.6588	0.4787
1900									0.0058	0.2276	-0.0134	0.1456
2000	4.5274	1.2385	2.3471	1.0857	2.9396	1.0272	-0.0184	0.1703	-0.0031	0.1455		
2100			-2.0297	0.3844	3.3597	1.3277	-0.0118	0.1953				
2200	5.4357	1.5569	-0.0263	0.1298	-0.2021	0.9542	0.0090	0.2683				
2300					-0.0150	0.1343						
2400	4.6411	1.3318			-0.0171	0.1996						
2500					0.0068	0.1758						
2600	1.0044	2.1802										

Table D1: Radial velocity profile data for the Witney Trial number 1. Recorded by the Nortek ADV probe, 28/06 to 02/07/2004.

Depth measured below TWL (mm)	Location [mm], U veocity [cm/s] and standard deviation (STDEV)											
	Stilling Well		A		B		C		D		E	
	U [cm/s]	STDEV	U [cm/s]	STDEV	U [cm/s]	STDEV	U [cm/s]	STDEV	U [cm/s]	STDEV	U [cm/s]	STDEV
200	3.3215	1.3916	-0.0449	0.3329	0.2703	0.2755	0.0693	0.4192	-0.0024	0.3789	0.3703	0.3451
400	3.7864	1.4574	-0.0581	0.3061	0.0912	0.2960	-0.1962	0.2948	-0.1607	0.2802	0.1990	0.3198
600	2.1649	1.9984	-0.0936	0.3084	-0.1856	0.2610	-0.1703	0.2439	-0.0660	0.2491	-0.1865	0.3083
800	0.8862	1.6415	-0.2421	0.2980	0.0279	0.2511	-0.0061	0.2445	-0.1628	0.2693	-0.1297	0.2618
1000	0.7125	1.7303	-0.0306	0.2867	0.2049	0.2491	-0.2692	0.2444	0.4362	0.2519	-0.0032	0.3022
1100											-0.1374	0.2433
1200	-2.9207	2.0473	-0.2910	0.2869	-0.0405	0.2572	-0.1222	0.2602	0.3848	0.2956	0.2493	0.2128
1300											0.2020	0.2216
1400	-5.0319	2.3852	-0.5679	0.2869	-0.4836	0.2644	0.2221	0.5127	0.6798	0.3280	0.2048	0.2469
1500											0.3062	0.2496
1600	-6.8553	2.3429	-0.7224	0.2612	-0.5630	0.3845	0.0745	0.7412	0.1573	0.3888	-0.0113	0.2354
1700											-0.2538	0.2696
1780	-2.8935	4.0988										
1800			-0.8628	0.2871	-0.3788	0.4686	0.5654	0.6556	-0.0715	0.2285	0.0003	0.7009
1900											-0.1459	0.3017
1955											-0.6337	0.2677
2000			0.4510	1.1842	2.0305	0.6060	0.9940	0.5588	0.2806	0.3490		
2100			2.4008	0.9160	-0.6463	0.1963	0.0497	0.4511	-0.2522	0.3393		
2200			1.8944	0.9866	-0.0127	0.1745	0.2250	0.5597				
2280							-0.0009	0.2175				
2300			-1.0355	0.2333	-0.0020	0.2983						
2400			-0.0155	0.2675	-0.0086	0.3030						
2500			0.0096	0.2656	0.0073	0.3168						
2540					0.0033	0.4010						
2590			-0.0137	0.3178								

Table D2: Radial velocity profile data for the Witney Trial number 2. Recorded by the Nortek ADV probe, 02/08 to 06/08/2004.

Depth measured below TWL (mm)	Location [mm], U veocity [cm/s] and standard deviation (STDEV)											
	Stilling Well		A		B		C		D		E	
	U [cm/s]	STDEV	U [cm/s]	STDEV	U [cm/s]	STDEV	U [cm/s]	STDEV	U [cm/s]	STDEV	U [cm/s]	STDEV
200			0.4218	0.5717	0.3384	0.4542	0.0464	0.3389	0.1439	0.3922	0.3067	0.5164
400			0.1956	0.5069	0.2610	0.4034	0.0398	0.2859	0.2864	0.2979	0.3497	0.2665
600			0.4597	0.4737	0.0460	0.3430	0.0533	0.2861	0.1218	0.3144	-0.1671	0.2620
800			0.0550	0.4282	-0.2541	0.4031	-0.0331	0.3161	-0.5720	0.2910	0.1513	0.2863
1000			0.0303	0.4799	-0.6212	0.3745	-0.6382	0.2824	-0.5067	0.3248	0.2970	0.2372
1100											0.2327	0.2701
1200			-0.5318	0.4447	-0.3332	0.3939	-0.2981	0.3158	-0.6506	0.3388	0.3431	0.2913
1300											0.2860	0.5224
1400			-0.8010	0.4890	-0.5281	0.4639	-0.3634	0.4594	-0.1620	0.4687	0.3806	0.4616
1500											0.5173	0.4114
1600			-0.8620	0.4569	-0.6656	0.4918	0.7680	0.5765	0.9466	0.5917	0.0445	0.3748
1700											0.4731	0.4058
1800			0.0584	0.7238	2.9695	1.0710	-0.0418	0.2856	0.6681	0.7140	0.2060	0.4697
1900											0.0028	0.2264
1940											-0.0176	0.2143
2000			2.1011	1.1995	1.5093	1.1078	0.0004	0.2179	-0.0037	0.1960		
2100			2.9559	1.5528	-1.0844	0.3052	-0.0079	0.2580	0.0041	0.2377		
2120									-0.0026	0.3076		
2200			3.0635	2.3565	-0.0260	0.2316	-0.0057	0.2770				
2280							-0.0004	0.2917				
2300			-0.9349	1.9450	-0.0439	0.3539						
2400			-0.0630	0.1580	-0.0346	0.3115						
2500			-0.0067	0.3114	-0.0009	0.3033						
2550					-0.0028	0.4330						
2600			0.0049	0.3537								
2640			0.2700	-0.6300								

Table D3: Radial velocity profile data for the Witney Trial number 3. Recorded by the Nortek ADV probe, 09/08 to 13/08/2004.

Depth measured below TWL (mm)	Location and suspended solids (mg/l)					
	Stilling Well	A	B	C	D	E
0						
100						
200	232	18	12	13	22.5	35
300						
400	498				12.5	23.5
500						
600	96				16	24
700						
800	798				69	55
900						
1000	1460	43	44.5	68.5	188	89
1100					155	98
1200	880				120	182
1300					218	218
1400	1150				120.5	213
1500					272	254
1600	1030	82	151	240	201	276
1700					302	232
1800	800	830		329	1198	1140
1900					12320	14820
2000	810	7350	664	15020	18760	
2100		16380	766	21190		
2200	150	23190	2860	23800		
2300			12460			
2400	1100		20320			
2500			23930			
2600	2040					

Table D4: Radial concentration profile data for the Witney Trial number 1. Recorded by direct sampling, 28/06 to 02/07/2004.

Depth measured below TWL (mm)	Location and suspended solids (mg/l)					
	Stilling Well	A	B	C	D	E
0						
100						
200	3380	6	9	11.5	6.5	11.5
300						
400	3280					15
500						
600	3250					13.5
700						
800	3300					14
900						
1000	3450	12.5	14	22	23.5	25.5
1100					22.5	25
1200	3360				29.5	21
1300					41	23.5
1400	3220				42.5	24
1500					41.5	27
1600	4430	18	28	44	19.5	25.5
1700					47	61
1780	5360					
1800		21	35	39	26	28.5
1900					47	25.5
1955						100.5
2000		500	1660	37	85	
2100		900	6760	54.5	63	
2200		1990	15680	79		
2280				686		
2300		6900	20940			
2400		15350	24760			
2500		22070	26610			
2540			25050			
2590		23370				
2600						

Table D5: Radial concentration profile data for the Witney Trial number 2. Recorded by direct sampling, 02/08 to 06/08/2004.

Depth measured below TWL (mm)	Location and suspended solids (mg/l)					
	Stilling Well	A	B	C	D	E
0						
100						
200		15	13	16.5	14.5	15.5
300						
400						22
500						
600						26
700						
800						34
900						
1000		26	26	26.5	29.5	36
1100						44.5
1200						45
1300						53
1400						91.5
1500						105
1600		43	45.5	30	38	112
1700						360
1800		780	2090	5880	83	351
1900						585
1955						1860
2000		4400	3870	17950	14230	
2100		2760	8970	20960	18840	
2120					16570	
2200		2500	16800	22770		
2280				23520		
2300		5490	24060			
2400		12480	26710			
2500		20030	26630			
2550			27840			
2600		25500				
2640		23800				

Table D6: Radial concentration profile data for the Witney Trial number 3. Recorded by direct sampling, 09/08 to 13/08/2004.

Figure D1: ADV Velocity profile measurements. Witney STW. Wednesday June 30th to Friday 2nd July 2004.
FST is 18.2m diameter, 1.9m side wall depth and 6m diameter diffuser drum to depth 0.8m.
Influent flow 182 m^3/hr. RAS flow 95 m^3/hr. R=1.09. MLSS at influent 4187 mg/l. SSVI is 30 ml/g by Wahlberg and Keinath.

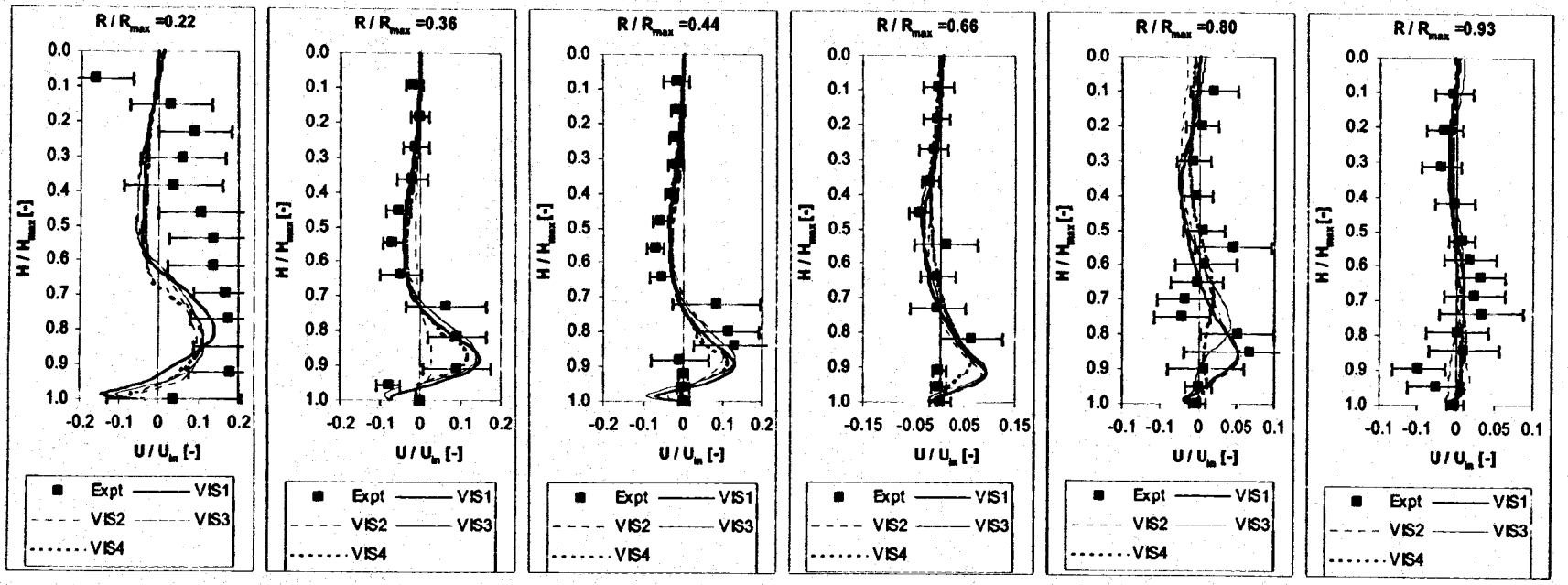

Witney STW Validation study – Radial velocity profile.

- Vis 1 is Bokil and Bewtra Rheology, Vis 2 is Armbruster Square Law, Vis 3 is Armbruster Square Root Law, Vis 4 is DeClerq variant of Herschel Bulkley.
-

These results are for the radial velocity profiles only. X axis normalized to influent velocity. Y axis is normalised to the total depth at the radius measured. The First profile is in the stilling well where there is considerable mixing and possibly bifurcation of influent jet.Velocimetry recorder at 200mm intervals except through shear layer where 100mm intervals used. Error bars are 2 standard Deviations.

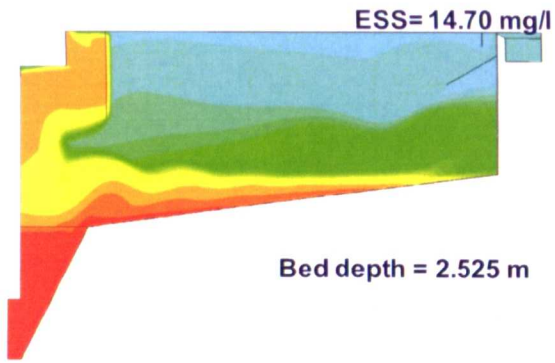

a) Q_DesignMax at SSVI = 80

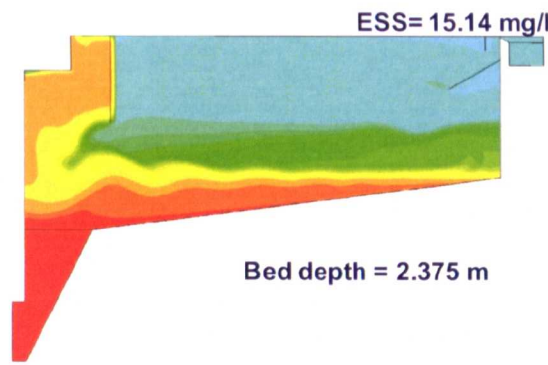

b) Q_DesignMax at SSVI = 100

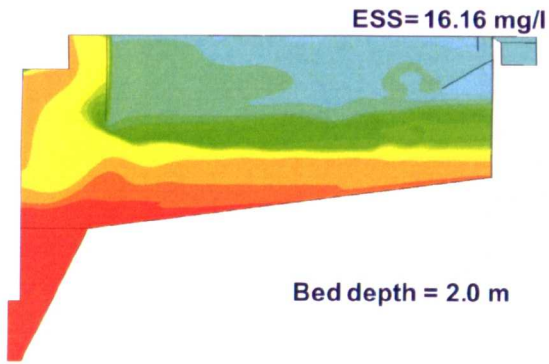

APPENDIX E

Process Conditions	A	X1	B	Z1	C	Y1	X2	Y2	Z2	X3	F	Y3	X4	E	X5	D
Tank Diameter	35	35	35	35	35	35	35	35	35	35	35	35	35	35	35	35
SST Area (m^2)	923.63	923.63	923.63	923.63	923.63	923.63	923.63	923.63	923.63	923.63	923.63	923.63	923.63	923.63	923.63	923.63
Tank Floor Angle	4.75	4.75	4.75	4.75	4.75	4.75	4.75	4.75	4.75	4.75	4.75	4.75	4.75	4.75	4.75	4.75
Forward Flow (Q, l/s) per Tank	300.00	245.00	150.00	245.00	137.90	177.17	245.00	202.48	245.00	245.00	253.10	227.79	245.00	253.10	245.00	253.10
SSVI (ml/g)	120	125	120	90	125	125	125	125	110	125	100	125	125	125	125	125
Influent MLSS (kg/m^3)	2.00	2.50	2.00	3.25	3.50	3.25	2.80	3.25	3.25	3.00	3.50	3.25	3.25	3.30	3.50	3.50
RAS Flow (RQ, l/s), per Tank	118.75	115.80	60.00	115.80	100.00	115.80	115.80	115.80	115.80	115.80	115.80	115.80	115.80	115.80	115.80	115.80
RAS ratio	0.3958	0.4727	0.4000	0.4727	0.7252	0.6536	0.4727	0.5719	0.4727	0.4727	0.4575	0.5084	0.4727	0.4575	0.4727	0.4575
Estimated RAS Conc. (kg/m^3)	7.05	7.79	7.00	10.13	8.33	8.22	8.72	8.93	10.13	9.35	11.15	9.64	10.13	10.51	10.91	11.15
Criterion I - Solids mass loading rate - WRc																
Actual Flux - JQFm ($kg/m^2.hr$)	3.30	3.55	1.65	4.62	3.28	3.75	3.98	4.07	4.62	4.26	5.09	4.40	4.62	4.79	4.97	5.09
Permissible Flux - JL ($kg/m^2.hr$)	4.59	4.37	2.88	5.63	3.96	4.37	4.37	4.37	4.82	4.37	5.19	4.37	4.37	4.37	4.37	4.37
Actual / Permissible, (%)	72	81	57	82	83	86	91	93	96	98	98	101	106	110	114	116
Criterion II - Hydraulic loading																
Actual Overflow Rate, (m/h)	1.12	0.92	0.56	0.92	0.52	0.66	0.92	0.76	0.92	0.92	0.95	0.85	0.92	0.95	0.92	0.95
Permissible Overflow Rate, (m/h)	1.83	1.32	1.83	1.75	0.80	0.90	1.13	0.90	1.20	1.02	1.30	0.90	0.90	0.88	0.80	0.80
Actual / Permissible, (%)	64	73	32	55	67	76	84	87	79	93	76	98	106	112	120	124
Criterion III - Sludge volume loading - ATV, A131																
Volumetric loading rate, (l/m^2h)	359.21	381.97	179.60	357.53	300.99	359.09	427.81	410.38	436.98	458.37	441.95	461.68	496.56	520.87	534.76	552.44
Actual Volumetric loading rate, (l/m^2h)	500	500	500	500	500	500	500	500	500	500	500	500	500	500	500	500
Actual / Permissible, (%)	72	76	36	72	60	72	86	82	87	92	88	92	99	104	107	110
BuddsFarm - Existing Tank																
Basecase (As built) Design																
ESS Conc. (mg/l)	23	38	16	16	17	30	792	898	32	-	829	-	-	1430	-	1680
Bed Depth (m)	1.64	1.20	3.00	2.60	2.59	0.82	0.08	0.06	0.73	-	0.09	-	-	0.07	-	0.06
McKinney Design																
ESS Conc. (mg/l)	26	22	17	16	17	19	23	21	20	23	23	44	39	50	845	931
Bed Depth (m)	3.15	2.25	2.98	2.64	2.51	2.31	1.99	2.05	2.10	1.74	2.10	1.55	1.01	0.39	0.09	0.08
BuddsFarm - New Tank																
Basecase (As built) Design																
ESS Conc. (mg/l)	-	122	-	25	19	48	617	524	583	-	740	-	-	1355	-	1574
Bed Depth (m)	-	0.47	-	2.27	2.20	0.81	0.20	0.15	0.21	-	0.18	-	-	0.11	-	0.08
McKinney Design																
ESS Conc. (mg/l)	-	25	-	20	16	18	27	20	25	46	26	42	450	742	747	946
Bed Depth (m)	-	2.30	-	2.79	2.76	2.53	1.92	2.12	2.15	1.11	2.23	0.98	0.25	0.21	0.19	0.18

Table E1: State Points analysed for the Budds Farm STW Clarifier Design Study compared with CFD predictions of bed height and ESS.